Profilin 1 and profilin 2-dependent actin dynamics shape neuronal morphology and are involved in brain development

Dissertation

zur Erlangung des Doktorgrades

“Doctor rerum naturalium”

der Mathematisch-Naturwissenschaftlichen Fakultät

der Rheinischen Friedrich-Wilhelms Universität Bonn

Vorgelegt von

Marina Di Domenico

Aus Cava de‘ Tirreni, Italien

Bonn, 2021

Diese Arbeit wurde mit Genehmigung der Mathematischen-Naturwissenschaftlichen Fakultät der Rheinischen Friedrich-Wilhelms-Universität Bonn angefertigt.

1. Gutachter: Prof. Dr. Walter Witke
2. Gutachter: Prof. Dr. Valentin Stein

Tag der Promotion: 20-10-2022
Erscheinungsjahr: 2023

Eidesstattliche Erklärung

Hiermit versichere ich, dass ich die vorliegende Arbeit selbstständig angefertigt und keine anderen als die angegebenen Hilfsmittel und Quellen benutzt habe. Ebenfalls erkläre ich, dass die vorliegende Arbeit an keiner anderen Universität als Dissertation eingereicht wurde.

Bonn, den 20. Januar 2021

Summary

The actin cytoskeleton is an important structure at the synaptic terminals and controls key parameters in synaptic physiology and plasticity. Actin binding proteins (ABPs) regulate cytoskeletal remodeling and actin dynamics at the synapse affecting synaptic transmission. Among all the different ABPs, profilin 1 (PFN1) and profilin 2 (PFN2) are part of a family of proteins that bind monomeric actin and promote filament polymerization. It has been previously shown that the mouse model lacking PFN2 exhibits an alteration of synaptic activity, due to increased excitability of glutamatergic transmission in the cortico-striatal pathway, while the mouse model lacking PFN1 in the brain displays mild neuronal migration defects but no synaptic function alterations.

In the first part of this thesis are reported evidences suggesting that *Pfn2* loss in mice produces an autistic-like behavior, caused by an imbalanced glutamatergic/GABAergic transmission in the Schaffer collaterals. The maintenance of the excitation-inhibition balance is critical for normal brain development and for its regular functioning.

In the second part of the thesis, studies on *Pfn1;Pfn2* double knockout mouse lines were performed at both developmental and adult age in order to properly dissect the specific and redundant functions of the two profilin isoforms. PFN1 appears most relevant for patterning brain structures during early development of the CNS and, for the first time, PFN2-redundant functions are also uncovered. Moreover, the function of profilins, especially PFN1, in regulating cell cycle progression supports the existence of an actin cytoskeleton checkpoint preceding phase G2/M transition of the cell cycle. In the adult brain both profilins are necessary for the maintenance of dendritic complexity of cortical and hippocampal pyramidal neurons. Since PFN2 is higher expressed compared to PFN1, PFN2 loss has higher impact on neuronal structural integrity.

In conclusion, this work shows that PFN1 and PFN2 play different functions in the developing and adult brain.

Table of contents

Abbreviations

+/+ or wt	Wildtype
+/-	Heterozygous
-/- or ko	Knockout, mutant
ABI	Abl interactor
ABP	Actin-binding protein
ACSF	Artificial cerebrospinal fluid
ADHD	Attention-deficit hyperactivity disorder
ADP	Adenosine diphosphate
ALS	Amyotrophic lateral sclerosis
AMPA	Amino-3-hydroxy-5-methylisoxazole-4- propionic acid
AP	Action potential
ARP2/3	Actin-related protein 2/3
ASD	Autism spectrum disorder
ATP	Adenosine triphosphate
Bp	Base pair
BSA	Bovine serum albumin
CA1/2/3	Cornu ammonis regions 1, 2 or 3, part of the hippocampus
CAMKIIα	Calcium/calmodulin-dependent protein kinase II alpha
CAZ	Cytomatrix at the active zone
CDK1	Cyclin-dependent kinase 1 or Cdc2 kinase
CNV	Copy number variation
C_c	Critical concentration
CGN	Cerebellar granular neuron
CYFIP	Cytoplasmic FMRP Interacting Protein
CNS	Central nervous system
C-T	Carboxy-terminal
DG	Dentate gyrus, part of the hippocampus
DMSO	Dimethylsulfoxide
DNA	Deoxyribonucleic acid
dNTP	Deoxyribonucleoside triphosphate
E	Embryonic day
EC	Enthorhinal cortex
ECL	Enhanced chemical luminescence
EDTA	Ethylenediaminetetraacetic acid
EGTA	Ethyleneglycoltetraacetic acid
EIF4E	Eukaryotic initiation factor 4E
EPSC	Excitatory post-synaptic current
EPSP	Excitatory post-synaptic potential
F-actin	Filamentous actin
fEPSP	Field excitatory post-synaptic potential
Flx	Floxed allele
Fmr1	Fragile X mental retardation 1 (gene)

FMRP	Fragile X mental retardation protein
FV	Fiber volley
FXS	Fragile X syndrome
G-actin	Globular actin
GABA	Gamma-aminobutyric acid
GC	Glial cell
GTP	Guanosine triphosphate
H&E	Hematoxylin and eosin
HEPES	4-(2-hydroxyethyl)-1-piperazineethanesulfonic acid
HRP	Horseradish peroxidase
I-O	Input-Output
ID	Intellectual disability
IEI	Inter-event interval
IPSC	Inhibitory post-synaptic current
IPSP	Inhibitory post-synaptic potential
KA	Kainate
KS	Kolmogorov-Smirnov
LTD	Long-term depression
LTP	Long-term potentiation
mEPSC	Miniature excitatory post-synaptic current
mGLUR	Metabotropic glutamate receptor
mIPSC	Miniature inhibitory post-synaptic current
mRNA	Messenger ribonucleic acid
NAP1	Nck-associated protein 1
NESTIN	Neuroepithelial stem cell protein
NLGN	Neuroligin
NMDA	N-methyl-D-aspartate
NPC	Neuronal progenitor cell
NPF	Nucleation-promoting factor
NRXN	Neurexin
N-T	Amino-terminal
Nt	Nucleotide
NT	Neurotransmitter
O/N	Overnight
P	Postnatal day
Pi	Inorganic Phosphate
PAGE	Polyacrylamide gel electrophoresis
PBS	Phosphate buffered saline
PC	Purkinje cell
PCR	Polymerase chain reaction
PCL	Purkinje cell layer
PFN	Profilin
PIP_2	Phosphatidylinositol-4,5-bisphosphate

PLP	Poly-L-Proline
PPF	Paired-pulse facilitation
PPR	Paired-pulse ratio
PSD	Post-synaptic density
PTX	Picrotoxin
PVDF	Polyvinylidene difluoride
QX-314	N-(2,6-Dimethylphenylcarbamoylmethyl)triethylammonium bromide
RG	Radial glial
RHOA	Transforming protein RhoA
RNA	Ribonucleic acid
ROCK	Rho-associated protein kinase
RRP	Readily releasable pool
RP	Releasable pool
RT	Room temperature
SAR	Same arm return
SDS	Sodium dodecylsulfate
SHANK	SH3 and multiple ankyrin repeat domains protein
SI	Social interaction
SMA	Spinal muscular atrophy
SMN	Survival of motor neurons protein
SNAP25	Synaptosomal-associated protein 25 kDa
SNARE	SNAP (soluble NSF attachment protein) receptor
SNP	Single nucleotide polymorphism
SNV	Single nucleotide variant
SPA	Spontaneous alternation
SV	Synaptic vesicle
TCM	Trichlormethiazide
TTX	Tetrodotoxin
USV	Ultrasound vocalization
VAMP	Vesicle-associated membrane protein/Synaptobrevin
VPA	Sodium valproate
VZ	Ventricular zone
WAVE	ABI family verprolin-homologous protein
WASP	Wiskott-Aldrich syndrome protein
WRC	WAVE regulatory complex

Units of measurement

˚C	Degree Celsius
GΩ	Gigaohm
h	hour
kDa	Kilodalton
kHz	Kilohertz
M	Molar
mA	Milliampere
mg	Milligram
MHz	Megahertz
min	Minute
ml	Milliliter
mM	Millimolar
ms	Millisecond
mV	Millivolt
MΩ	Megaohm
N	Newton
nA	Nanoampere
nm	Nanometer
pA	Picoampere
RPM	Revolutions per minute
s	Second
µg	Microgram
µl	Microliter
µm	Micrometer
µM	Micromolar
V	Volt

List of figures

List of tables

A mio padre,

in te il mio pensiero si rifugia
nei momenti di confusione,

con te il mio pensiero corre
quando devo ritrovare la forza,

a te la mia mente sempre torna
nei momenti di Gioia.

Introduction

1.1 The cytoskeleton

The cytoskeletal network of eukaryotic cells is composed principally of three types of protein filaments -actin microfilaments, microtubules and intermediate filaments - each one of them having unique biophysical and biochemical properties. The remodeling of these protein filaments, by multiple intrinsic and extrinsic cues, allows the cytoskeleton to control the diversity of eukaryotic cell shapes, to provide structural and mechanical support to the cell and, moreover, to modify dynamic cellular behaviors in order to generate cell movement (Dillon & Goda, 2005). The cytoskeleton is a dynamic structure, ready to adapt to cell demands.

Microtubules are hollow fibers of 25 nm diameter, formed by 13 protofilaments of polymerized α- and β- tubulin heterodimers. Microtubules contribute to cell stability and during cell division are involved in spindle formation. In neurons, microtubules serve as a scaffold for organelle transport and are structural components of neurites, playing an important role in their elongation (Fukushima, 2011).

Intermediate filaments assembly begins with the folding of the proteins into a conserved alpha-helical rod shape, followed by a series of polymerization and annealing events that lead to the formation of filaments of roughly 8 to 12 nm in diameter. The primary function of intermediate filaments is to provide structural support and to create cell cohesion.

1.1.1 Actin cytoskeleton

The evolutionarily highly conserved actin molecules assemble reversibly into filaments of 7 nm diameter (Pollard *et al.*, 2016). Actin is a crucial component of the cellular scaffold, essential for sculpting and maintaining cell shape. Actin dynamics also support a myriad of processes ranging from cell motility, cell division and cell

morphogenesis to endocytosis, exocytosis and intracellular proteins/vesicles trafficking.

Actin function is critical during embryonic development and in the plasticity of the nervous system. In the developing CNS the actin cytoskeleton is needed for all migration processes and in neurons it has a crucial role in neurite formation, extension and branching as well as synaptogenesis. In mature neurons, actin is the most prominent cytoskeletal protein at synapses, being present in both pre- and post-synaptic terminals, with structural and physiological functions (Dominguez & Holmes, 2011; Cingolani & Goda, 2008).

Due to its important functions, it is not surprising that the 42 kDa actin monomer is one of the most abundant proteins in the majority of cells, from amoebas to human, often accounting for 10 % or more of total protein content (Kron *et al.*, 1992).

Bacteria, archaea, and eukaryotes all have actin-related molecules structurally and functionally similar to each other. In bacteria, actin-like proteins (MreB, FtsA, and ParM) can be found. All eukaryotes have one or more genes for actin. Sequence comparisons have established that actin is one of the most conserved gene families, varying by only a few amino acids between algae, amoeba, fungi and animals. This conservation is attributed to constraints imposed by the interactions of actin with itself to polymerize, with motors and with a large number of regulatory proteins (Gunnin *et al.*, 2015).

Actin in higher eukaryotes is represented by several isoforms that differ by only a few amino acids, with most variations occurring in the N-terminal region. Vertebrates express three main actin isoforms: α-isoform, exclusively in muscles cells, and the β- and γ- isoforms in both non-muscle and muscle cells.

Actin exists in two different forms, globular actin (G-actin) is the monomeric form that can assemble into a polar double-stranded right–handed helical filamentous form (F-actin). As all actin subunits point to the same direction, the filament is polar and based

on the arrowhead pattern created when myosin binds to F-actin, the fast-growing end of the filament is called 'barbed' or (+) end, whereas the slow growing end is denoted 'pointed' or (-) end (Pollard & Cooper, 2009).

The actin monomer consists of two major domains each of which contains two subdomains; the four subdomains are organized to form a rather flat molecule of 42 kDa. The nucleotide (ADP or ATP) and the associated divalent cation (Mg^{2+} or Ca^{2+}) bind in a deep cleft, interacting more strongly with subdomains 3 and 4, but also with residues in subdomains 1 and 2. The lower hydrophobic cleft, between subdomains 1 and 3, changes conformation depending on the state of the nucleotide and constitutes the binding site for most actin-binding proteins (ABPs) (Dominguez, 2004) (Fig 1.1).

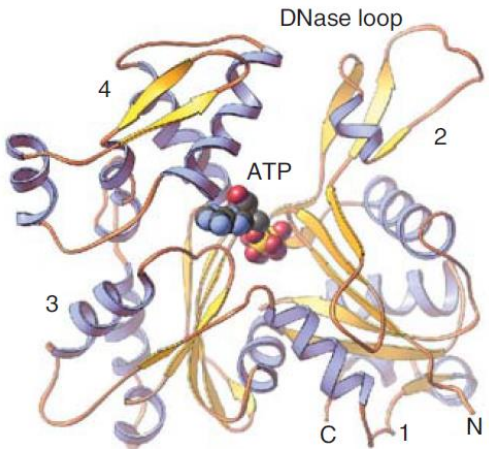

Figure 1.1 **| Ribbon structure of uncomplexed actin in the ATP state.** Numbers 1, 2, 3 and 4 label the four subdomains (protein data bank [PDB]: 1ATN). ATP is bound at the center where subdomains 2 and 4 meet. Subdomains 2 and 4 mark the (-) end of filaments, while 1 and 3 represent the (+) end (figure from Pollard, 2016).

The "nucleation phase" starts the actin polymerization process. It is a highly unfavorable and slow event (Sept & McCammon, 2001), which consists in the initial formation of a dimer and the addition of a third subunit to form a trimer. However, *in vitro*, once oligomers are formed, spontaneous actin filament elongation can occur if the concentration of actin monomers is above the "critical concentration" (C_c) at the barbed ends. The C_c is reached when the net rates of filament assembly and disassembly at one end of the filament are identical. Owing to the difference in the polymerization rates at the two ends, the C_c of G-actin at the pointed end is higher (0.8 µM), than that at the barbed end (0.1 µM). This difference, at the G-actin

concentration lying between the two C_c, leads to a net loss of actin molecules at the pointed end and a simultaneous gain of monomers at the barbed end.

Actin filaments therefore extend when ATP-bound G-actin monomers are preferentially incorporated at the barbed end. As the filament matures, the ATP is hydrolyzed into ADP and inorganic phosphate (P_i). The phosphate is released, and the resulting ADP-actin filament is disassembled by loss of monomers from the pointed end. The released ADP-actin monomers can then undergo nucleotide exchange to generate ATP-actin monomers that can be used for new rounds of polymerization at the barbed end (Pantaloni *et al.*,1984; Pollard *et al.*, 2000; Pantaloni *et al.*, 2001). Importantly, this phenomenon, known as actin treadmilling, creates a net flow of newly incorporated actin monomers through the filament, allowing dynamic turnover of the actin filament itself (Pollard *et al.*, 2000; Kovar & Pollard, 2004) (Fig 1.2).

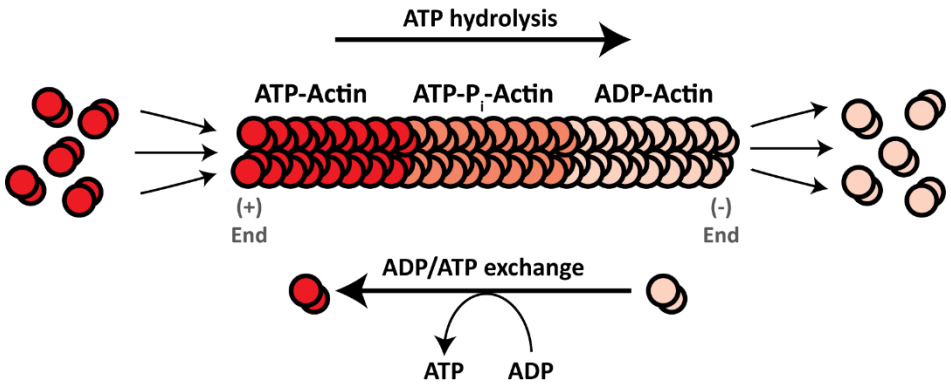

Figure 1.2 **| Actin treadmilling process**. *In vitro*, the filament length is maintained in a state of equilibrium as a result of the constant binding of new monomers of ATP-G-actin (red) and the constant dissociation of monomers of ADP-G-actin (pink). On the actin filament the association of monomers of G-actin proceeds quickly, with one end ((+) end), growing much faster than the other ((-) end). Since the affinity between the actin monomers is higher in the ATP-bound state rather than in the ADP-bound state, the (+) end contains mainly associated ATP-actin monomers, whereas on the (-) end a higher concentration of ADP-actin is formed. The ATPase activity of actin strongly increases on incorporation into the filament. After the binding of ATP-actin to the filament, the hydrolysis of ATP and the dissociation of P_i destabilize the filament. Dissociated ADP-actin undergoes nucleotide exchange, which, *in vivo*, is strongly facilitated by profilin.

1.1.2 Actin binding proteins

In order to carry on cytoskeletal based functions, cells are required to regulate polymerization and depolymerization processes, to obtain a rapid remodeling of the actin cytoskeleton in response to diverse environmental cues. Actin-binding proteins (ABPs) are regulatory proteins responsible for the fine control of actin cytoskeleton dynamics (dos Remedios *et al.*, 2003; Winder, 2005). Collectively, ABPs maintain a large pool of actin monomers available for polymerization, nucleate assembly of new filaments, promote elongation and depolymerization, cap barbed or pointed ends to terminate or stabilize elongation, sever and crosslink filaments (Pollard, 2016).
ABPs are classified according to their functions into distinct groups, even though their activity is often not limited to a specific class (dos Remedios *et al.*, 2003) (Fig 1.3).

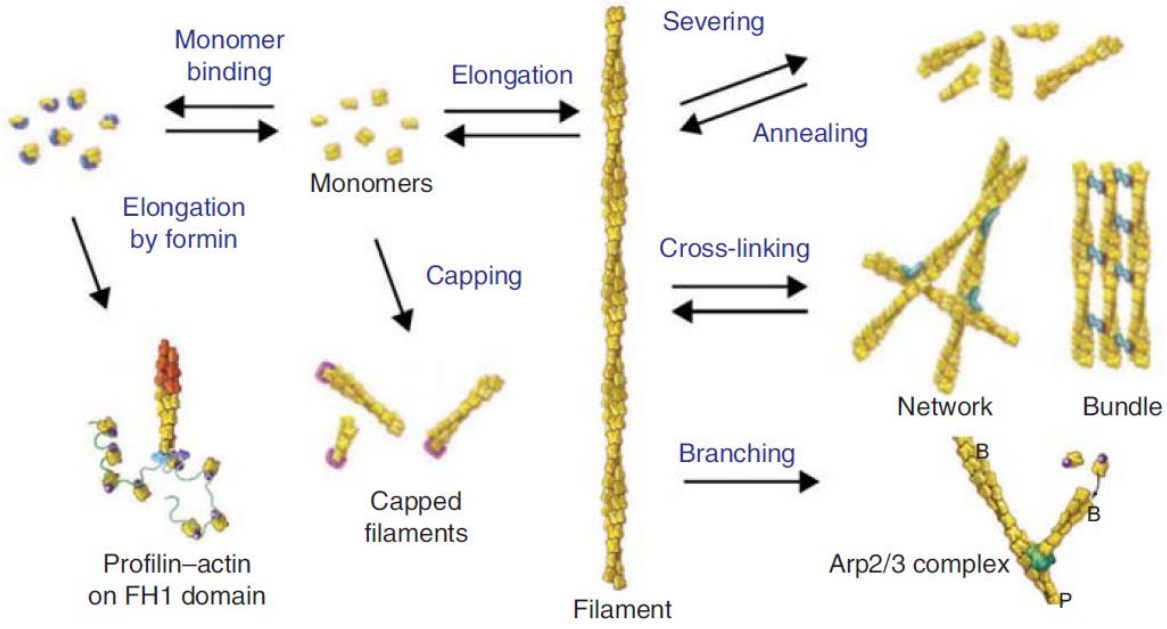

Figure 1.3 **| Actin binding proteins.** Actin binding proteins regulate actin dynamics and organize actin structures. ABPs are involved in many aspects of actin dynamics, including monomer binding (*e.g.* profilin), filament polymerization (*e.g.* formins), filament end capping (*e.g.* CapG, CapZ), filament severing (*e.g.* gelsolin) and depolymerizing (*e.g.* ADF/cofilin), filament bundling and cross-linking (*e.g.* fascin, filamin) and filament branching *(e.g.* ARP2/3) (figure from Pollard, 2016).

1.1.2.1 Monomer binding proteins

In many higher eukaryotic cells, there are two major actin monomer sequestering proteins: profilin and thymosin β4. These proteins provide G-actin-buffering capacity and have opposite functions in promoting or inhibiting actin polymerization in cells.
The binding of actin to thymosin β4 blocks all actin assembly reactions, including nucleation and growth at the end of the filament. Instead, the binding of profilin to an actin monomer allows to elongate the barbed end of a filament. Profilin maintains a pool of actin ready for filament elongation at the barbed ends, while thymosin β4 holds the rest of the monomers in reserve. Profilin, competing with thymosin β4 for binding to actin monomers, offers a pathway for actin monomers sequestered by thymosin β4 to re-enter the elongation process (Pollard & Borisy, 2003; Pollard, 2016).
The topic of this thesis is the study of profilin function during mouse brain development and in the adult brain.

1.2 Profilin

About four decades ago, profilin (PFN) was first described as a small 14-15 kDa protein (125-139 amino acid residues) that copurifies with monomeric actin from calf spleen and inhibits actin polymerization *in vitro.* The name of the protein derives from its ability to keep actin in a "profilamentous" state (Carlsson *et al.*, 1977). Profilins are among the most highly expressed proteins in eukaryotic cells, with concentrations ranging from 5 to 100 µM (Buss F *et al.,* 1992; Pollard *et al.,* 2000); they were initially isolated based on their ability to bind to G-actin in a 1:1 stoichiometric complex, called profilactin (Carlsson *et al.*, 1977; Schlüter *et al.*, 1997).
Profilins have been well conserved during evolution and can be found throughout the entire animal and plant kingdoms. In particular, profilins have been discovered in lower eukaryotes, like protozoa, slime molds and fungi (Haugwitz *et al*., 1991; Ozaki *et*

al., 1983; Reichstein & Korn, 1979; Tilney *et al.*, 1983; Wilkes & Otto, 2000 and 2003), plants (Valenta *et al.*, 1993), invertebrates (Cooley *et al.*, 1992; Polet *et al.*, 2006; Somboonwiwat *et al.*, 2006) and vertebrates (Braun *et al.*, 2002; Honoré *et al.*, 1993; Witke *et al.*, 1998 and 2001). There is even a viral isoform of profilin whose gene organization is homologous to the mammalian profilins (Blasco *et al.*, 1991; Butler-Cole *et al.*, 2007). Plant profilins expression is strictly regulated during development and can be ubiquitous or restricted to reproductive tissues (Kandasamy *et al.*, 2002), specifically to pollen (Hussey *et al.*, 2006).

The number of profilin genes per organism correlates roughly with its complexity. While lower eukaryotes contain one or two, occasionally three genes (Dictyostelium discoideum - Arasada *et al.*, 2007; Caenorhabditis elegans - Polet *et al.*, 2006), higher eukaryotes display higher numbers, with plants expressing up to ten different profilin genes (Jockusch *et al.*, 2007).

1.2.1 Profilin function in F-actin polymerization

In vivo, profilin supports actin filament polymerization. Profilin is able to bind ADP-loaded G-actin and catalyze the exchange of ADP to ATP (on the bound G-actin), with 1000-fold higher efficiency then spontaneous exchange. The ATP-loaded G-actin constitutes the pool of monomeric actin ready for polymerization, since only the ATP-loaded form of G-actin is incorporated at the barbed end of uncapped filaments (Pring *et al.*, 1992; Pantaloni & Carlier, 1993). Upon binding of the profilin-actin complex to the barbed end, profilin's affinity for actin diminishes tremendously because the profilin binding domain of G-actin is partially overlapping with its barbed end binding region (Gutsche-Perelroizen *et al.*, 1999).

Profilin also binds to a number of actin nucleators. The function of actin nucleators is to facilitate the stable formation of an actin nucleus (G-actin trimer), which is an essential step for the growth of a new filament. Actin nucleators are divided into three classes: formins, WH2-domain containing actin nucleators (Spire, Cordon-bleu and Leiomodin) and the ARP2/3 complex regulated by nucleation promoting factors (the

WASP and the WAVE families) (Ahuja *et al*., 2007; Campellone & Welch, 2010; Chesarone & Goode, 2009; Kunda *et al.*, 2003; Winder *et al*., 2005). It was shown that profilin interacts with formins, delivering on growing filaments the ATP-G-actin required for actin polymerization (Kovar *et al.*, 2006), as well as VASP and MENA and WASP and WAVE proteins (Gertler *et al.*, 1996; Reinhard *et al.*, 1995; Miki *et al.*, 1998; Suetsugu *et al.*, 1998).

1.2.2 Profilin structure and binding domains

All studied profilin isoforms share common structural and biochemical properties, although the amino acid sequences, among distantly related species, show less than 25 % homology (Schlüter *et al.*, 1997). Numerous studies on profilins from different species demonstrate that they have highly similar tertiary structures (Metzler *et al.*, 1993; Schutt *et al.*, 1993; Thorn *et al.*, 1997; Vinson *et al.*, 1993). Therefore, the conservation of the protein folds seems to be more important than the conservation of the primary sequence (Witke, 2004). In fact, all profilin structures that have been resolved to date are similar, for example human profilin 1 and profilin 2 are almost superimposable even with only 61 % amino acid identity (Odalman *et al.*, 1999).

Profilins of *Acanthamoeba*, mammalian or birch origin display a similar polypeptide fold: a compact center composed of seven β-strands packed into a β-sheet, surrounded by four α-helices (Domke *et al.*, 1997; Fedorov *et al*., 1997; Schutt *et al*., 1993). On one side, this core is flanked by N- and C-terminal regions, both being part of an α-helix and adjacent to each other (Fig 1.4).

Profilins share biochemical properties, characterized by the ability to interact with three classes of ligands: (i) G-actin and actin related proteins (Machesky *et al.*, 1994; Schutt *et al.*, 1989; Tobacman *et al.*, 1983) (ii) phosphatidylinositol-4,5-bisphophate (PIP_2) (Lassing & Lindberg, 1985) (iii) poly-L-proline (PLP) stretches (Fig 1.4).

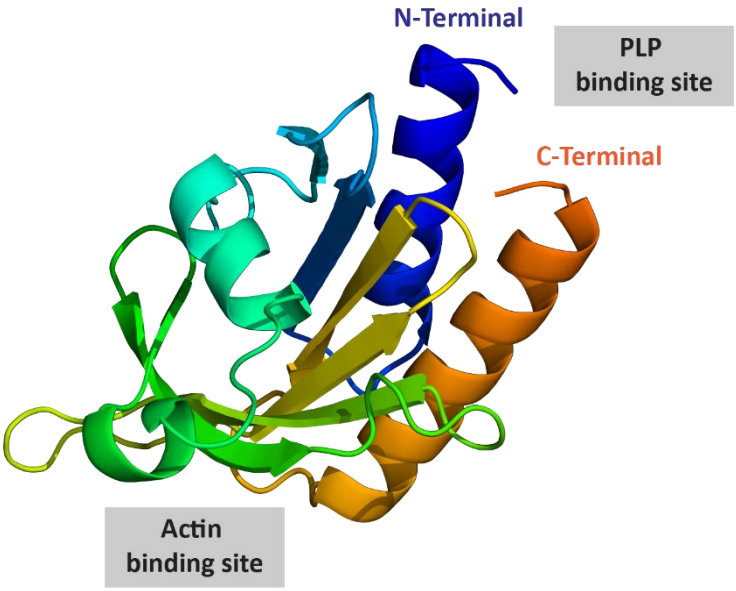

Figure 1.4 **| Crystal structure of rat PFN2.** Four α-helices surround a β-sheet structure. The blue and orange helices form the PLP-binding domain. On the opposite region, the actin binding domain is localized. The PIP_2 binding domain overlaps with the other two (figure modified from Haikarainen *et al.*, 2009).

Not surprisingly, the amino acid sequences defining these domains are relatively well conserved throughout different kingdoms. The affinity for distinct ligands may differ among species and even isoforms. Extreme examples are a minor mouse splice form (PFN2b) (Di Nardo *et al.*, 2000) and Vaccinia virus profilin (Machesky *et al.*, 1994), that have been reported not to bind to G-actin and to poorly interact with PLP stretches.

The binding motif for PIP_2 has been described as a hydrophobic patch within the actin-binding site. The physiological role of this PIP_2-profilin interaction is unclear and requires further investigations, nevertheless it seems to function as a negative regulator of actin-binding (Skare & Karlsson, 2002). It has been reported that these ligands compete with each other for profilin binding (Lassing & Lindberg, 1985; Machesky *et al.*, 1990). Binding of PIP_2 results in a conformational change in profilin that disrupts the profilin-actin complex (Raghunathan *et al.*, 1992). PIP_2- and actin-binding sites partially overlap on the surface of the profilin molecule, providing an explanation for the inhibition of actin binding by phospholipids (Skare & Karlsson, 2002). A second binding site for PIP_2 has been described as overlapping with the PLP-binding site (Lambrechts *et al.*, 2002; Skare & Karlsson, 2002; Witke, 2004), demonstrating that there could also be competition between PIP_2 and PLP-stretch

containing ligands at the C-terminal region (Gareus *et al.*, 2006; Lambrechts *et al.*, 1997). Both PIP_2 binding sites are part of a broad band of surfaced-exposed hydrophobic residues (Witke, 2004).

PLP-stretches interact with a distinct binding site on the profilin molecule, formed by both the N- and C-terminal α-helices (Lambrechts *et al.*, 2002; Skare & Karlsson 2002; Witke, 2004). Thus, the binding of PLP to profilins has no effect on the interaction with G-actin (Archer *et al.*, 1994; Kaiser *et al.*, 1989). PLP binding might be involved in localizing the profilin-actin complex close to the barbed end of polymerizing filaments (Schluter *et al.*, 1997). This suggestion is supported by profilins interaction with the PLP rich sequences of several proteins that are intimately involved in F-actin elongation. These proteins include formins (Watanabe *et al.*, 1997), MENA/VASP (Gertler *et al.*, 1996; Reinhard *et al.*, 1995), WASP/WAVE (Miki *et al.*, 1998; Suetsugu *et al.*, 1998) and ARP2/3 (Mullins *et al.*, 1998; Kelleher *et al.*, 1995; McCollum *et al.*, 1996; Machesky *et al.*, 1994).

Proteins interacting with the PLP-binding domain of profilin are referred to as profilin ligands and are important in the regulation of both the cytoskeleton and also other processes, which are not directly linked to actin.

Different organisms employ multiple isoforms of profilins with diverse ligands specificities and binding abilities.

1.2.3 Profilin isoforms

In mammals four profilin genes have been identified: *Pfn1* to *4.* Both *Pfn1* and *Pfn2* genes consist of 3 exons, with introns of varying length in between the coding regions (Fig 1.5 A). The *Pfn2* gene additionally contains a fourth alternative exon embedded in the 3' UTR. The alternative exon 4 can be included in the open reading frame (ORF) of *Pfn2* instead of exon 3, leading to two alternative splice variants, *mRNA Pfn2a* and *mRNA Pfn2b* (Fig 1.5 B). The two isoforms differ in their C-terminal structure; in this study I will refer to PFN2a as PFN2, as it is the more prominent isoform expressed in

the brain and since PFN2b has only reduced binding affinity to actin and PLP-stretches (Di Nardo *et al.*, 2000; Lambrechts *et al.*, 2000).

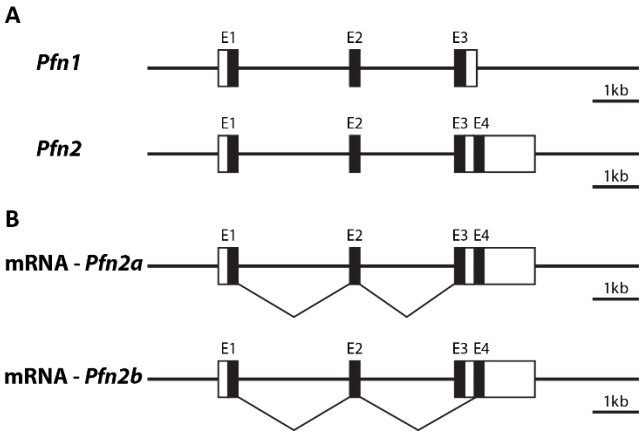

Figure 1.5 **| Exon-intron organization of the mouse *Pfn1* and *Pfn2* genes and alternatively spliced transcripts *Pfn2a* and *Pfn2b*. A.** The mouse genomic sequence of *Pfn1* and *Pfn2* genes is shown as a thin horizontal line. Exons (E) are indicated by boxes: filled boxes represent coding sequences, and open boxes represent untranslated regions (UTR). *Pfn2* E4 is located within the 3' UTR of the gene. **B.** The alternative E4 can be included in the ORF of *Pfn2* instead of E3, leading to two alternative splice variants, *Pfn2a* and *Pfn2b* (figure modified from Lambrechts *et al.,* 2000).

The amino acid sequence is not very well conserved among the paralogs, for example PFN1 and PFN2 in human and mouse are only 61 % identical. Nevertheless, their structural domains and basic functions are well conserved (Gieselmann *et al.*, 1995; Lambrechts *et al.*, 1997).

In mice and humans, the expression of PFN2, PFN3 and PFN4 is restricted to specific tissues, while PFN1 is ubiquitously expressed, except for adult skeletal muscle. PFN2 is a neuronal specific isoform, which is also expressed at low levels in some other tissues (Witke *et al.*, 1998; 2001; Witke, 2004). Studies on tissue-specific abundance show that PFN1 accounts for 0.2-0.4 % of total protein in non-neuronal tissues and only for 0.05 % of total protein in the brain; on the contrary PFN2 accounts only for 0.01-0.02 % of total protein in tissues where it is expressed, except for the brain where the content is 15-fold higher (Witke *et al.*, 1998; Ding *et al.*, 2012). PFN3 and PFN4 main expression is restricted to testis, where they have a key role in acrosome biogenesis and sperm morphogenesis (Hu *et al.*, 2001; Braun *et al.*, 2002; Obermann *et al.*, 2005; Behnen *et al.*, 2009).

PFN1 and PFN2 have distinct functions in regulating actin dynamics and although they share a few ligands, even though with different binding affinities, they mostly interact with specific sets of ligands (Witke, 2004). PFN1 has a higher binding efficiency to G-actin compared to PFN2; on the contrary, PFN2 has more affinity for MENA/VASP, mDIA and piccolo/aczonin. Only PFN2 specifically binds to ROCK, dynamin 1, synapsins and the WRC complex (CYFIP, NAP1, ABI, WAVE and BRICK) (Witke *et al.*, 1998; Witke, 2004; Pilo Boyl *et al.*, 2007). Both isoforms can bind to some formins and drebrin.

1.3 Development of the mouse brain

The complete architecture of the adult brain is the result of the interplay between inductive signals, already defined genetic instructions and the generation of specific cell types in the embryo. The development of the nervous system proceeds in five major steps: (i) generation of a primordial nervous system (neural plate and neural tube), (ii) partitioning of the neural tube in major brain subdivisions (iii) specification of glial cells and distinct neuronal subtypes, (iv) migration of post-mitotic neurons from sites of generation to their final positions, and (v) establishment of neuronal connections (Purves *et al.*, 2001; Kandel *et al.*, 2012).

1.3.1 Gastrulation, neurulation and formation of the major brain subdivisions

The establishment of basic body axes is critical for proper generation of organs, including brain. There are 3 main body axes: anterior–posterior (mouth–anus), dorsal–ventral (back–belly) and medial–lateral (midline–periphery). The primitive embryo consists of three germ layers of cells: an outer ectoderm/neuroectoderm, which gives rise to the nervous system; a middle mesoderm for muscle, connective tissues and the majority of the vascular system; and an inner endoderm, which gives rise to lungs,

pancreas, liver and gut tube (Purves *et al.*, 2001; Kandel *et al.*, 2012). The layers and the axes of symmetry of the entire body are formed as a result of the gastrulation process, which begins as a local invagination of a subset of cells in the early embryo (Purves *et al.*, 2001; Kandel *et al.*, 2012).

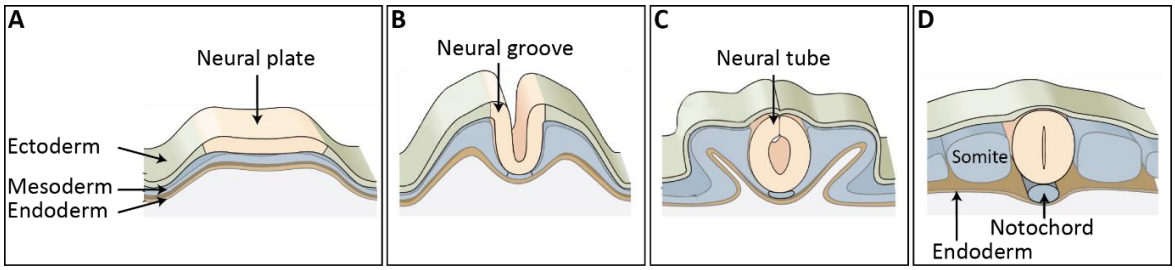

Figure 1.6 | **The neural plate folds to form the neural tube. A**. The three germ cell layers—the ectoderm, mesoderm, and endoderm—lie close together. The ectoderm gives rise to the neural plate, the precursor of the central and peripheral nervous systems. **B.** The neural plate buckles at its midline to form the neural groove. **C.** Closure of the dorsal neural folds to form the neural tube. **D.** The neural tube lies over the notochord and is flanked by somites, a group of mesodermal cells that give rise to muscle and cartilage (figure modified from Kandel *et al.*, 2012).

After gastrulation the first event in the generation of the nervous system, is the thickening of the midline dorsal ectoderm, called neural plate (Fig 1.6 A). During early neurulation, the notochord forms by invagination of the mesoderm. The notochord is a transient structure required for early neuronal differentiation; it specifies the axis of symmetry of the embryo, determining the position of the nervous system. Through a neurulation process, the neural plate begins to fold into a tubular structure forming the neural groove (Fig 1.6 B) and later the neural tube, which is complete when the two neural folds fuse together (Fig 1.6 C). The neural tube lies above the notochord, which sends inductive signals to the ectoderm that lies above differentiating a subset of cells into neuroectodermal precursor cells. During neurulation, a population of precursors produce the neural crest (Fig 1.6 D). Neural crest cells give rise to a variety of progeny, including neurons and glia of the sensory and visceral motor (autonomic) ganglia, the neurosecretory cells of the adrenal glands and the neurons of the enteric nervous system (Purves *et al.*, 2001; Kandel *et al.*, 2012).

For all rodents the day after mating is counted as day 0.5. In mice the neural tube starts to close along the ventral midline around E9 (Embryonic day 9), and the process of neurulation is complete approximately at E10 (Lomaga *et al.*, 2000; Gurniak *et al.*, 2005).

Differences in the rate of proliferation of cells in the anterior neural tube result in the formation of three brain vesicles: the forebrain (or prosencephalic vesicle), the midbrain (or mesencephalic vesicle), and the hindbrain (or rhombencephalic vesicle) (Fig 1.7 A). Each of these three major regions acquires diverse neuronal fates and identities. The first and the third primary embryonic vesicles divide further to form a

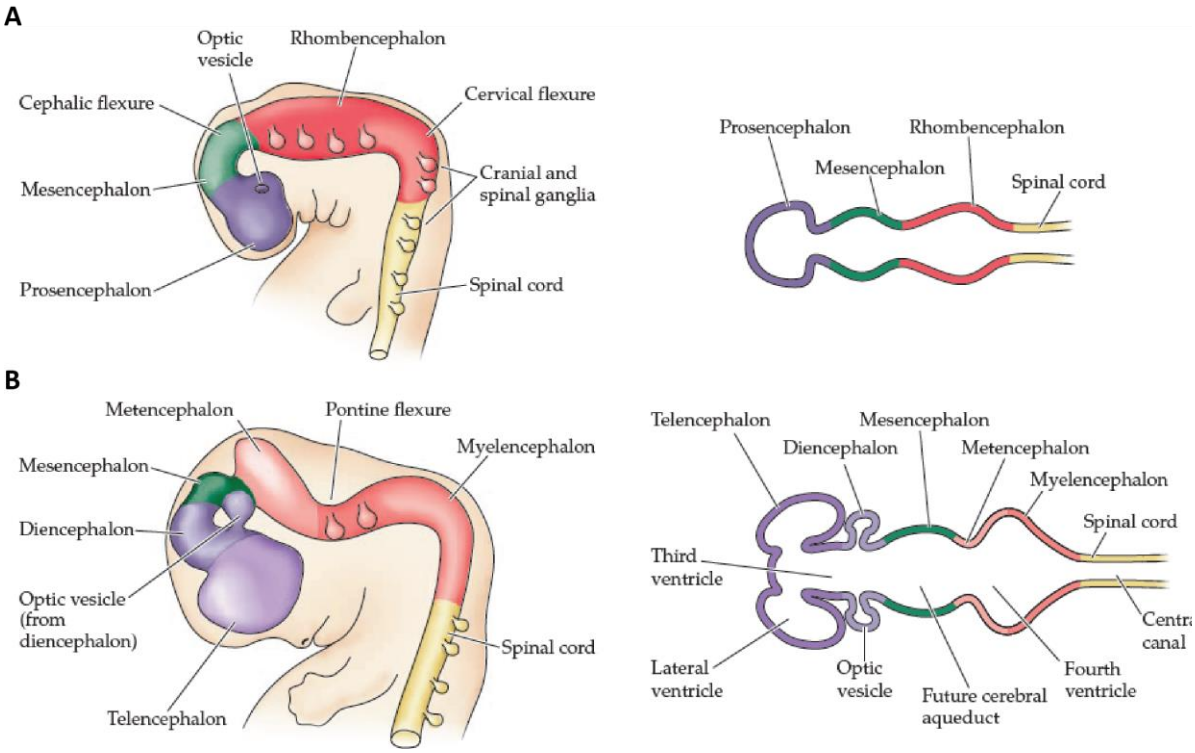

Figure 1.7 **| Sequential stages of neural development**. **A.** Schematic picture of a whole mouse embryo and a horizontal section at an early stage of neural tube development. Three brain vesicles are visible: prosencephalon (at the anterior end of the embryo), mesencephalon and rhombencephalon. The spinal cord differentiates from the more posterior region of the neural tube. **B.** Schematic picture of a whole mouse embryo and a horizontal section further in the development. Additional regions are formed: from the prosencephalon, telencephalon and diencephalon; from the rhombencephalon, metencephalon and myelencephalon (figure from Purves *et al.*, 2001).

five-vesicle stage. In detail, the rostral part of the forebrain forms the telencephalon, which will give rise to the cerebral cortex, hippocampus, basal ganglia, basal forebrain nuclei and olfactory bulbs. The caudal portion of the forebrain forms the diencephalon, which originates thalamus, hypothalamus, pineal gland and optic vesicles. The rostral part of the hindbrain becomes the metencephalon and originates the cerebellum and pons; instead the caudal part becomes the myelencephalon and gives rise to the medulla (Fig 1.7 B) (Purves *et al.*, 2001; Kandel *et al.*, 2012).

Specifically in the mouse embryo, the development of Purkinje cells (PC) and deep cerebellar nuclei have their peak at E10.5; the dopaminergic neurons of the substantia nigra start their development around E8.5-10.5 (Prakash & Wurst, 2006); whereas the development of subiculum, parasubiculum and hippocampal CA1/CA2 regions occurs around E13-E15 (Finlay & Darlington, 1995).

1.3.2 Cortical neurogenesis and neuronal migration

Neurogenesis begins right after the neural tube structure is complete. Neural progenitor cells (NPCs), also known as radial glial (RG) cells, have their cell bodies in the ventricular zone (VZ - the inner/apical cell layer surrounding the lumen of the neural tube) and extend their processes radially to the basal membrane on the pial surface (Fig 1.8 A).

Particularly in the mammalian forebrain, RG cells can generate additional copies of themselves, with a process of self-renewing symmetric division, or give rise to differentiated neurons or glial cells, with an asymmetric division. When neurogenesis is complete, many RG cells differentiate into astrocytes, a subclass of glial cells (GC) (Purves *et al.*, 2001; Kandel *et al.*, 2012).

A balance between cell lineage inductive factors and receptors promote the differentiation of embryonic stem cells into neural progenitor cells and later to different classes of glial or neuronal cells. Inductive factors are signaling molecules that can be either secreted by nearby cells or be already available in the extracellular

matrix. Receptors respond to inductive factors, triggering specific patterns of gene expression in neurons (Purves *et al.*, 2001; Kandel *et al.*, 2012).

During cell division RG cells in the VZ undergo stereotyped pattern of cell movements as they progress through the mitotic cycle, leading to the formation of post-mitotic neurons that leave the VZ, using RG projections as a guide and migrate to their final positions (Fig 1.8 A). In the developing brain, RG cells have a dual function, acting as stem cells and as migration guides of newly generated neurons, which wrap around the shaft of the RG cell and translocate (Purves *et al.*, 2001; Kandel *et al.*, 2012) (Fig 1.8 B).

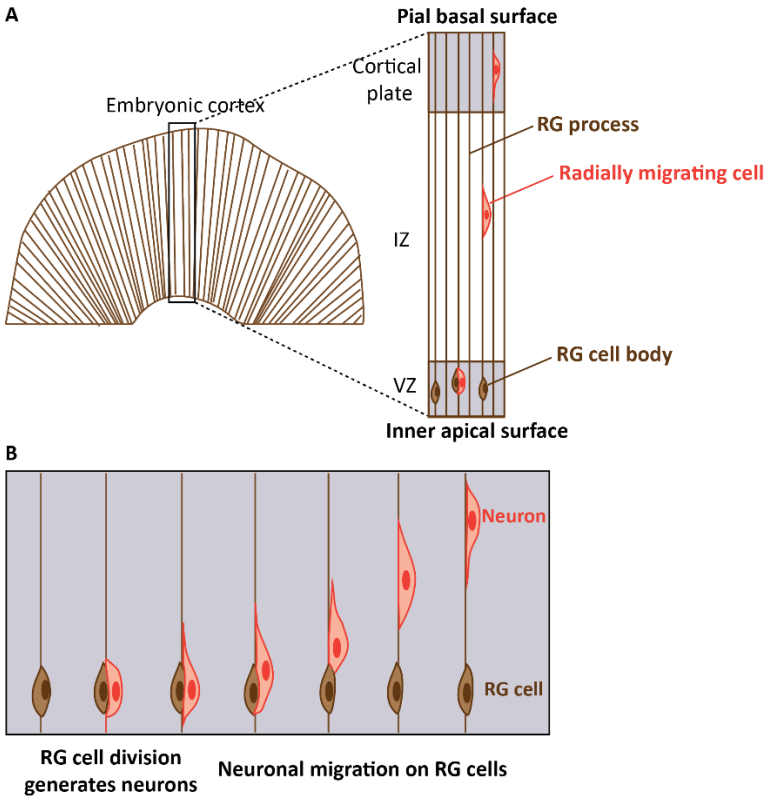

Figure 1.8 **| Radial migration in the developing cortex. A.** Section of the developing forebrain showing RG processes from the inner surface of the VZ to the pial surface. Migrating neurons are apposed to RG cells, which guide them to their final position in the cortex. **B.** RG cells serve as precursors to neurons in the CNS and also provide a scaffold for radial neuronal migration. Progenitor cells, in the VZ of the developing cerebral cortex, have nuclei that migrate along the apical-basal axis as they progress through the cell cycle. During cell division, RG cells give rise to postmitotic neurons. Newly generated neurons, in the embryonic cerebral cortex, extend a leading process that wraps around the shaft of the RG cell, thus using the RG cells as scaffolds during their migration from the VZ to the pial surface of cortex (figure modified from Purves *et al.*, 2001 and from Kandel *et al.*, 2012).

RG scaffolds are especially important in the development of the primate cortex, where neurons organize in a six-layer structure created in an inside-out manner. Each layer is formed by diverse types of neurons generated in distinct times. The early born neurons are located in the deepest layers, whereas later generated neurons migrate from the subventricular zone through the older cells and settle in more superficial cortical layers. The innermost layers (VI-V-IV) are established during embryonic days 11.5-14.5 of the mouse development; whereas the more superficial layers of the cortex (III, II), develop last, appearing at mouse E13.5-E16.5 (Germain *et al.*, 2010). Only exception are the Cajal Retzius cells, which are born first, around E10–E11.5, but immediately migrate to form the outmost layer I.

Another crucial mechanism of cell translocation in the developing nervous system is tangential migration, a non-radial mode of neuronal translocation that does not require specific interactions with RG cell processes (Ghashghaei *et al.*, 2007). Tangential migration is defined by neurons migrating parallel to the pial surface and orthogonal to the basal process of RG (Barber & Pierani, 2015). In mice, tangential migration begins around E11 and peaks at E13.5 (Bellenchi *et al.*, 2007).

1.3.3 Hippocampal formation

The structures that line the edge of the cortex form the so-called limbic system (Latin *limbus* = *edge*). This includes hippocampus, amygdala, thalamus and hypothalamus. The limbic structures represent the neural basis of emotion.

The hippocampus was first anatomically and physiologically studied in murine models. The murine hippocampus is an elongated C-shaped structure extending symmetrically from the septal nuclei to the rostral-dorsal-medial end, bending over and around the diencephalon, into the temporal lobe to the caudal-ventral-lateral end (Deshmukh & Knierim, 2012).

The term hippocampus derived from the similarity of the shape of the human hippocampus to the seahorse (Latin: hippocampus), from the description of the

anatomist Julius Ceasar Aranzi (Bir *et al.,* 2015). The hippocampus is characterized by three main histological divisions CA1, CA2 and CA3; these abbreviations derive their names from the Latin *Cornu Ammonis* (ram's horn). CA1, CA2, CA3 areas together with the dentate gyrus (DG) and para-hippocampal regions, including the subiculum and the entorhinal cortex (EC), form the hippocampal formation (Fig 1.9).

The hippocampus plays a role in the consolidation of episodic memory, spatial learning and context-dependent learning processes (Deshmukh & Knierim, 2012; Andersen, 2007). The fundamental role of the hippocampus was revealed by studies on Henry Gustav Molaison (known as patient H.M.). H. M. suffered of severe epilepsy and underwent experimental surgery involving bilateral removal of both hippocampi. After treatment H.M. had a severe anterograde amnesia (deficit in the creation of new long-term memories) (Scoville & Milner, 1957).

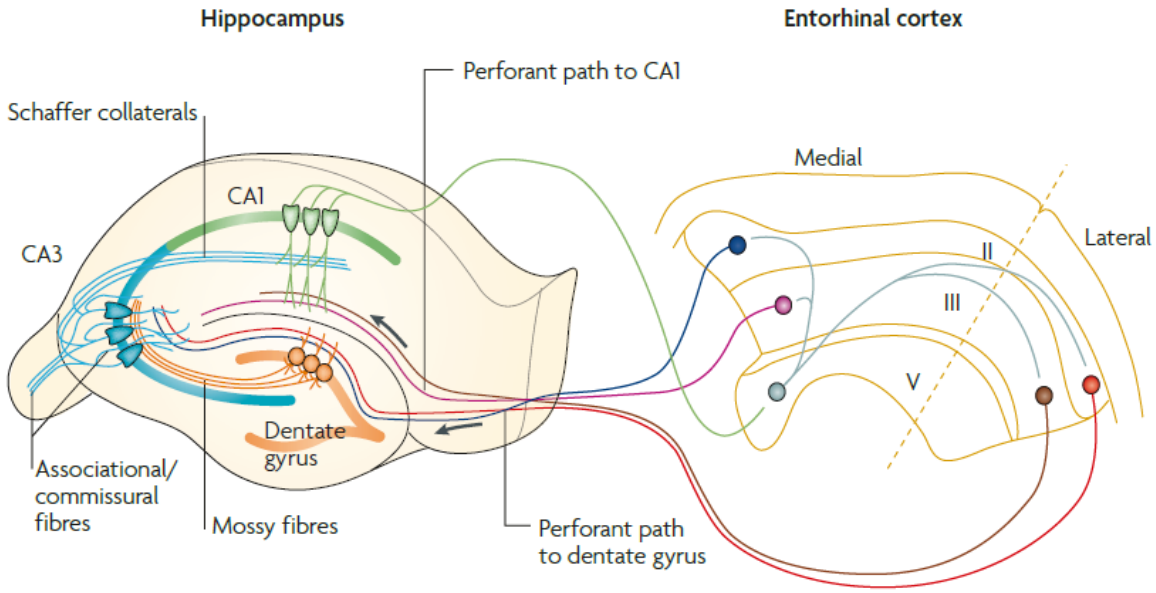

Figure 1.9 **| Schematic illustration of the hippocampal trisynaptic pathway.** The wiring diagram of the hippocampus is traditionally presented as a trisynaptic circuit. From the EC the lateral perforant path projects to granular cells of the DG (blue, red). DG neurons send mossy fibers onto CA3 pyramidal neurons (orange). CA3 neurons connect through Shaffer collaterals to the CA1 area (light blue). In turn, CA1 pyramidal neurons project to the subiculum, the main output of the hippocampus and then back to the EC (green) (figure from Neves *et al.*, 2008).

The EC is the main "interface" between the brain and the hippocampus. The deep layers of the EC receive the most prominent output from many other parts of the brain, while the superficial layers provide the input into the hippocampus, in particular projecting to granular cells of the DG (perforant path). In turn granular cells of the DG project mossy fibers onto CA3 pyramidal cells, whose Schaffer collaterals axons innervate CA1 pyramidal neurons. Finally, CA1 cells project to the subiculum, the main output region of the hippocampus and back to the EC (Fig 1.9). In addition to the sequential trisynaptic circuit, there is also a dense associative network interconnecting CA3 cells on the same side. CA3 pyramidal cells are also innervated by a direct input from layer II cells of the EC (not shown in figure 1.9). Furthermore, the distal apical dendrites of CA1 pyramidal neurons receive a direct input from layer III cells of the EC. The DG granule cells also project to the mossy cells in hilus and hilar interneurons, which send excitatory and inhibitory projections, respectively, back to the granule cells (Fig 1.9) (Neves *et al.*, 2008).

The hippocampus is an ideal model to study the functionality of the synapse, since synaptic connections are well characterized, and they are mostly found on the same layer. In this study, the canonical synapse formed by CA3-Shaffer collaterals onto dendrites of CA1 pyramidal neurons is used to further characterize the role of PFN2 in synapse physiology.

1.3.4 Neuritogenesis: dendrites and axon specification

The establishment of the neuronal structure is an essential step to allow the formation of synaptic connections among different neurons and their integration within a circuit. Neurons are polarized cells where distinct processes with different functions can be recognized (Fig 1.10). Dendrites are the input area of the neuron; they serve as collectors of synaptic inputs from axons of other neurons and are specialized in signal transduction. Dendrites are highly branched processes, which emerge from the soma.

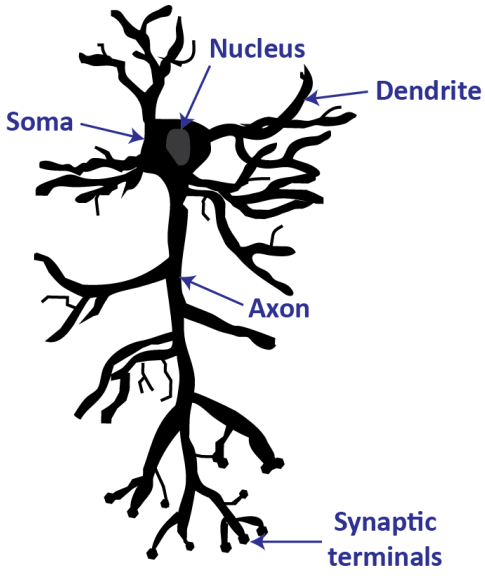

Figure 1.10 **| Schematic structure of a neuron**. Most neurons in the vertebrate nervous system have several main features in common. The soma contains the nucleus and gives rise to two types of cell processes: dendrites and axon. The dendrites and the cell body constitute the input area of the neuron, receiving signals from other neurons. The axon is the transmitting element of the neuron; it is a thin projection, varying greatly in the length among different types of neurons, and it is often branched. The axon is insulated by a sheath of myelin that is regularly interrupted at gaps called the nodes of Ranvier (not shown). The action potential, the cell's conducting signal, is initiated in the initial segment of the axon and propagates to the pre-synaptic terminals, the sites where signals flow from one neuron to another.

In addition, small membranous protrusions called spines extend from the dendritic branches. These structures are responsible for collecting the excitatory post-synaptic potentials. Although the core features of dendritic formations are common to many neurons, they differ in their complexity of branching. The axon is considered to be the output structure of a neuron. Normally an axon is a single thin long protrusion where action potentials propagate in order to reach the pre-synaptic sites. Like dendrites, also axons show high variability in the branching pattern and in their extension depending on the neuronal type (Purves *et al.*, 2001; Kandel *et al.*, 2012) (Fig 1.10).

Once neurogenesis is complete and the round-shaped post-mitotic neuron is produced, neuritogenesis begins with the outgrowth of neuronal processes. Initially several short neurites, processes of equivalent length, extend form the immature neuron. One of these equally long neurites starts to grow rapidly to become the axon while the remaining processes acquire dendritic features. The axonal specification is a key event in the establishment of neuronal polarity, since signals coming from the new-born axon suppress the generation of other axons and promote dendrites formation (Purves *et al.*, 2001; Kandel *et al.*, 2012). When the growing axon reaches the appropriate and specific target neuron, the synaptic contacts are formed. The

assembly of a functional neuronal circuit often requires major rearrangements, such as synapses elimination, a process also known as pruning (Purves *et al.*, 2001; Kandel *et al.*, 2012).

The growth cone is a specialized compartment at the tip of the extending neurites, formed by microtubules and actin. Growth cones are particularly important for axon growth and guidance. The axonal growth cone has a highly dynamic behavior: it explores the surrounding environment and determines the direction of axon growth depending on the presence of attractive/chemotropic or repulsive/chemorepellent molecular signals. The actin and tubulin cytoskeletons have an important function in establishing and maintaining neuronal polarity (Witte & Bradke, 2008), since they are able to perform structural changes affecting cell morphology following external molecular cues. The neurite that becomes the axon shows enhanced growth cone dynamics, due to elevated actin turnover, and therefore elongates rapidly (Bradke & Dotti, 1999; Witte & Bradke, 2008). On the contrary, in an initial stage future dendrites have a stable growth cone and actin cytoskeleton and, as a result, they grow slowly (Witte & Bradke, 2008).

1.3.5 Function of profilins in brain development and neuronal migration

In mice, deletion of *Pfn1* leads to embryonic lethality at pre-implantation stage because of defects in cytokinesis (Witke *et al.*, 2001). Instead embryos with *Pfn1* haploinsufficiency survive but are disadvantaged in development being also frequently lost in utero. Mice completely lacking *Pfn2* are viable.

PFN1 seems to have an important function during embryonic development and the reason for the different impact of *Pfn1* and *Pfn2* deletion could be rooted in their different embryonic expression pattern. In mice, PFN1 is ubiquitously expressed and it is present at all stages of embryonic development at high levels. Instead, PFN2 is not expressed in early mouse development and its expression starts around embryonic day 12 mostly in the developing CNS, therefore cannot compensate for the early loss of PFN1 (Witke *et al.* 2001). A more detailed analysis on PFN1 and PFN2 expression will

be shown in this study.

Conditional embryonic brain-specific knockout (ko) of P*fn1* shows cerebellar hypoplasia (Fig 1.11 A), aberrant layering of cerebellar cortex and ectopic localization of cerebellar granular neurons (CGNs). These defects are due to impairment of radial migration of CGNs (Fig 1.11 B), due to the essential role of PFN1 for normal adhesion between CGNs and GCs (Kullmann *et al.*, 2011). Although PFN1 is important for cerebellar radial migration, it seems to be dispensable for cortical radial migration and only mildly affects tangential migration.

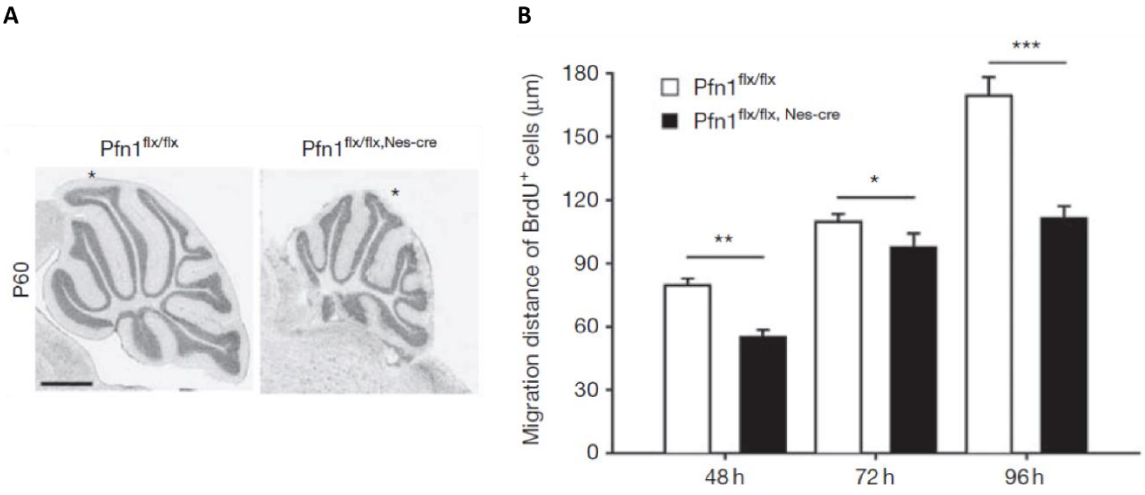

Figure 1.11 **| Cerebellar hypoplasia and impaired radial migration in *Pfn1* conditional ko. A.** Cerebellar hypoplasia in *Pfn1* CNS-specific embryonic ko. Nissl-stained parasagittal sections of a control and a mutant mouse brain at P60 show that the cerebellum is smaller in mutant mice. **B.** Impaired radial migration of CGNs in *Pfn1* ko. Animals injected at P8 with BrdU were analyzed 48, 72 and 96 hours after injection; mean migration distance of BrdU labelled neurons was reduced at all three time points in *Pfn1* ko mice (figure from Kullmann *et al.*, 2011).

Mice completely lacking PFN2 (*Pfn2*$^{-/-}$) show normal brain anatomy, indicating that neither tangential migration nor radial migration was altered (Pilo Boyl *et al.*, 2007). It has been shown that profilins localize to the leading edge of growth cones; and that PFN2, through the RhoA/ROCK pathway, is a negative regulator of neurite sprouting and elongation. In fact, *Pfn2* deletion in neurons results in the destabilization of the actin cytoskeleton, which in turn produces increased neurite length and number during very early *in vitro* neuronal development (Da Silva *et al.*, 2003) (Fig 1.12 A).

PFN2 has been suggested to play a role in the maintenance of dendritic structure in mature hippocampal neurons in organotypic cultures, exerting PFN1-independent as well as redundant functions (Michaelsen *et al.*, 2010) (Fig 1.12 B). Conversely, it has been demonstrated in *Pfn2*$^{-/-}$ mice that PFN2 is not essential for neurite extension and neuronal polarization, suggesting a different role of PFN2 *in vivo*, specifically in synaptic plasticity (Pilo Boyl *et al.*, 2007).

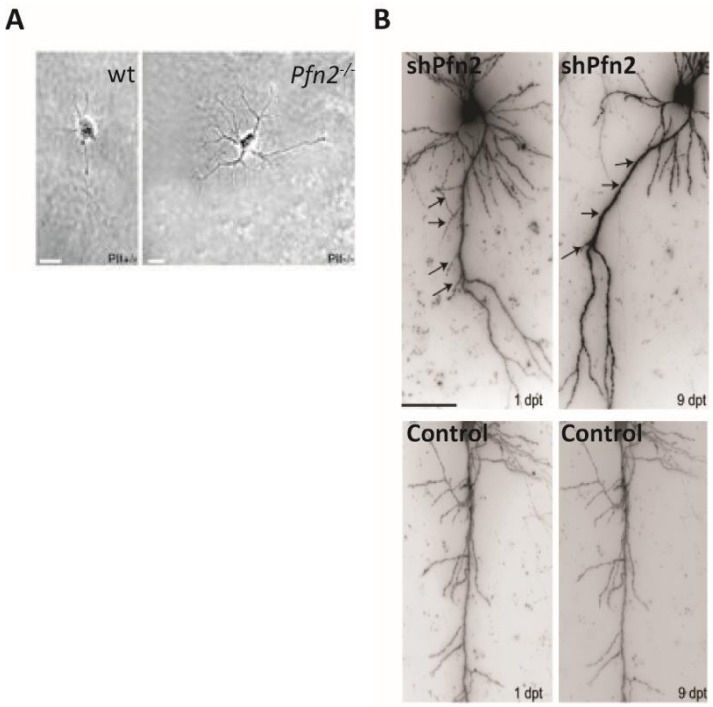

Figure 1.12 **| PFN2 function in neurite development. A.** Pfn2 is a negative regulator of neurite sprouting. Neurons from *Pfn2*$^{-/-}$ mice 24 hrs after plating display increased number of highly branched neurites, with higher mean lengths. Scale bar: 10 mm (figure modified from Da Silva *et al.*, 2003). **B.** In organotypic hippocampal cultures, 9 days after *Pfn2* knockdown by transfection of a *Pfn2*-specific short hairpin RNA, it was observed pruning of already existing dendrites (top part - arrows). No pruning was detectable in control neurons transfected with GFP (bottom). Scale bar: 50 µm (figure modified from Michaelsen *et al.*, 2010).

1.4 Synaptic transmission

A fundamental task of the nervous system is to communicate and process information in order to generate behavior. The human nervous system is composed of hundreds of billions of neurons. Synapses are the principal sites for communication among

neurons; typically, the axon terminal of the pre-synaptic neuron lies adjacent to a specialized region of the target cell rich in post-synaptic receptors. Synapses are divided into two types: electrical and chemical. Electrical synapses are direct connections between cells that allow passage of ions and that play important roles in fast cell-to-cell communication, especially among glial cells and among neurons during development. In chemical synapses, the pre- and post-synapse are separated by a synaptic cleft and communicate via the secretion of molecules, called neurotransmitters (NTs) and their specific receptors (Johnston & Wu, 1995; Kandel *et al.*, 2012). Chemical synapses are divided into excitatory and inhibitory, depending on the molecules used as NTs.

1.4.1 The excitatory synapse

Glutamate is the most used excitatory NT. Upon an action potential (AP), glutamate is released from pre-synaptic vesicles into the synaptic cleft and binds to specific receptors localized on the post-synaptic membrane. The activation of post-synaptic receptors gives rise to an excitatory post-synaptic current (EPSCs) due to cations entry. Therefore, an excitatory synapse is characterized by the depolarization of the post-synaptic membrane. This event will increase the likelihood to fire a post-synaptic AP.

1.4.1.1 Function of the pre-synapse in excitatory transmission

The function of an excitatory pre-synapse is to convert an electrical signal, a current, into a chemical one, the NT release. The NT is stored in synaptic vesicles (SVs), small round membrane compartments, which are located in the pre-synaptic terminal. SVs form pools which are either in direct contact with the pre-synaptic membrane and ready to be released (readily releasable pool - RRP) or they are found at more distant sites and serve as a reserve pool (RP) (Rosenmund & Stevens 1996; Dillon & Goda, 2005). SVs exocytosis is restricted to a small portion of the pre-synaptic plasma membrane called “active zone” containing electron-dense material (Couteaux &

Pecot-Dechavassine, 1970). Thus, the active zone lies at the interface between the pre-synaptic terminal and the synaptic cleft, and its major function is to transform a pre-synaptic AP into a released NT (Fig 1.13).

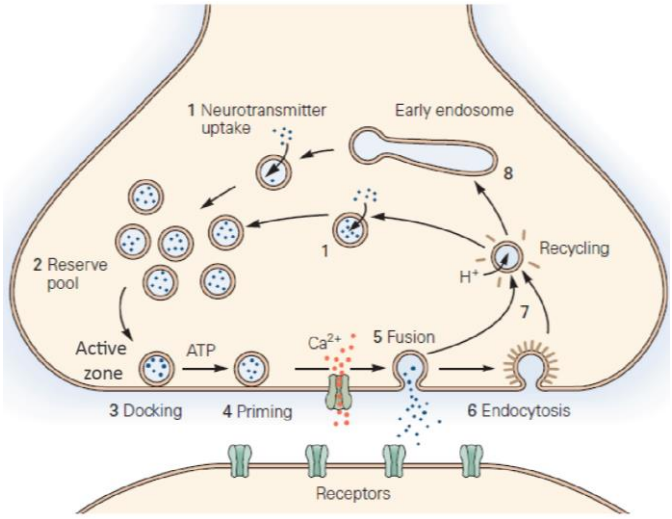

Figure 1.13 **| Synaptic vesicle cycle.** Synaptic vesicles (SVs) are filled with neurotransmitters (NTs) through an active transport system (**step 1**) and join the reserve pool of vesicles (**step 2**). Filled SVs are moved to the readily releasable pool at the active zone (**step 3 - Docking**) and prepared for calcium-triggered exocytosis in an ATP-dependent process (**step 4 - Priming**). The arrival of an AP induces SV fusion with the pre-synaptic membrane and release of the NT in the synaptic cleft (**step 5 - Fusion**). The membrane of the exocytosed vesicles is recycled *via* complex mechanisms; it is first retrieved *via* clathrin-mediated endocytosis (**step 6**) and then it is either recycled directly (**step 7**) or indirectly by endosomal processing (**step 8**) into the reserve pool (figure modified from Kandel *et al.*, 2012).

The active zone is thought to be involved in defining the NT release site, anchoring and localizing pre-synaptic membrane proteins (including Ca^{2+} channels) and organizing the exocytic and endocytic machineries at the transmitter release site. The active zone consists of three different protein groups that perform distinct functions during NT release:

- Voltage-gated calcium channels, as mentioned above, to induce SVs release;
- Structural evolutionarily conserved proteins including RIMs, MUNC13, α-liprin, ELKSs, piccolo and bassoon;

- SNARE complex and associated proteins, crucial for the process of SVs exocytosis (Südhof & Rizo, 2011). The SNARE complex consists of three membrane proteins, the synaptic vesicle protein synaptobrevin 2 (also known as vesicle-associated membrane protein, VAMP2) and the plasma membrane proteins syntaxin 1 and SNAP25 (synaptosome-associated protein of 25 kDa).

Once SVs reach the plasma membrane they are docked and primed for release (Fig 1.13, n. 3-4). During docking, a four-helix bundle is formed between SVs and the pre-synaptic membrane by the SNARE complex, bringing the SVs in close proximity to the pre-synaptic membrane. The arrival of an AP causes the depolarization of the pre-synaptic membrane of the neuron and the opening of voltage-gated Ca^{2+} channels, which in turn allow calcium influx in the pre-synapse. The calcium sensor synaptotagmin is then activated by the Ca^{2+} and in turn disinhibits the SNARE complex, removing the interaction with MUNC18 and allowing the fusion of SVs with the pre-synaptic membrane (Fig 1.13, n. 5). After SVs have emptied their content, they are recycled in the pre-synaptic terminal and refilled with NT (Fig 1.13, n. 6-8).

1.4.1.2 Function of the post-synapse in excitatory transmission

The released glutamate binds to receptors located on the tips of specialized post-synaptic compartments termed dendritic spines. The post-synapse encompasses a complex network of proteins called post-synaptic density (PSD). The PSD sustains, traffics and organizes the glutamate receptors, which detect the release of glutamate from the pre-synaptic terminal and, depending on their nature, allow Na^{+}/Ca^{2+} influx into the post-synaptic terminal or activate associated signaling molecules that transduce glutamate binding into post-synaptic biochemical responses. A great variety of scaffold proteins (e.g. PSD95, SHANK) assemble the in PSD, anchoring glutamate receptors and other post-synaptic membrane proteins, signaling enzymes and cytoskeletal elements. Due to all these interactions the PSD network allows the regulation of receptor trafficking and in particular their exo- and endocytosis (Sheng & Hoogenraad, 2007).

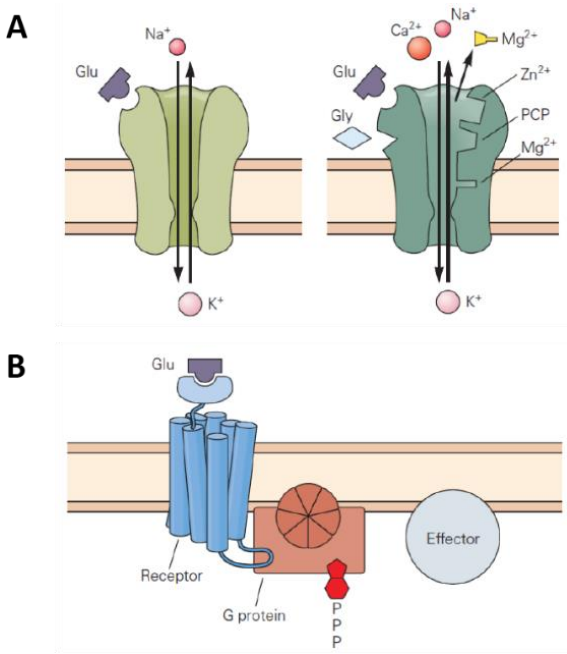

Figure 1.14 **| Glutamate receptors regulate excitatory synaptic transmission between neurons. A.** Ionotropic glutamate receptors are ion channels permeable to cations. The AMPA and KAR receptors (on the left) are distinguished by their binding to the agonists AMPA and kainate, respectively. These receptors consist of a channel permeable to Na^+ and K^+. The NMDA receptors (on the right) are characterized by the binding to the agonist NMDA and are channels permeable to Ca^{2+}, K^+, and Na^+. NMDA receptors have binding sites for glutamate, glycine, D-serine, Zn^{2+} and Mg^{2+}, each of which regulates the functioning of the channel differently. **B.** Metabotropic glutamate receptors indirectly gate ion channels by activating a GTP-binding protein, which in turn interacts with effector molecules that alter metabolic and ion channel activity (figure from Kandel *et al.*, 2012).

Three classes of ionotropic glutamate receptors are known: amino-3-hydroxy-5-methyl-4-isoxazolepropionic acid (AMPA) receptors, N-methyl D-aspartate (NMDA) receptors and kainate (KA) receptors, which are ligand gated ion channels permitting the passage of positively charged ions (Na^+, K^+, Ca^{2+}) (Fig 1.14A).

AMPA receptors mediate fast excitatory transmission between neurons. They are tetramers composed of highly similar subunits GluR1–4, each with a large extracellular N-T domain, three membrane-spanning domains, a hairpin that contributes to the pore, and a cytoplasmic C-T domain. The AMPA receptor subunits differ in the length of their intracellular C-T domain, which is longer for GluR1 and GluR4. In the hippocampal CA1/CA2 region, mainly GluR1/GluR2 and GluR2/GluR3 subunits combinations are found (Keinänen *et al.*, 1990; Hollmann & Heinemann, 1994; Rosenmund *et al.*, 1998; Barry & Ziff, 2002).

NMDA receptors are heteromultimers of NR1, NR2 (A-D) and NR3 subunits; in particular in the hippocampus they assemble into heterodimers or heterotrimers.

Notably, they are characterized by an extremely low kinetic rate, which means once glutamate molecules have become bound to NMDA receptors, they remain bound for a long time, during which the ionotropic channels can undergo repeated openings (Lester *et al.*., 1990; Andersen, 2007).

In addition to their slow kinetics, NMDA receptors have three other important features. First, a second agonist-binding site for glycine (or alternatively D-serine) must be occupied before glutamate is able to activate them (Johnson & Ascher, 1987; Kleckner & Dingledine, 1988). Second, Mg^{2+} ions block the ion channels in a voltage-dependent manner, specifically under negative membrane potential, therefore a depolarization must also occur in order to allow their opening (Nowak *et al.*, 1984). The last important feature is that they are highly permeable to both Ca^{2+} ions and monovalent cations (Ascher & Nowak, 1988; Andersen, 2007). The slow kinetics and Ca^{2+} influx guarantee that NMDA receptors play a central role in several forms of long-term synaptic plasticity, for example long-term potentiation (LTP) or long-term-depression (LTD). Ca^{2+} ions are actually ubiquitous secondary messengers, and NMDA receptor activation has been shown to trigger further release of Ca^{2+} from intracellular stores (Emptage *et al.*, 1999).

AMPA and NMDA receptors cooperate for the functionality of the synapse. For this reason, synapses containing only NMDA receptors and lacking AMPA receptors are termed “silent synapses”. Specifically, at negative membrane potentials (-70 mV) glutamate binding to AMPA receptors results in Na^{+} influx into the post-synapse. NMDA receptors, instead, at negative membrane potentials remain silent due to the Mg^{2+} block. As soon as the sodium enters the post synapse through the AMPA receptors, the membrane potential becomes positive (+40 mV) and the Mg^{2+} block is removed from NMDA receptors, leading to their activation.

While the role of AMPA and NMDA receptors in glutamatergic synaptic transmission is well established, the one of KA receptors is still poorly understood. From different studies it has emerged a role for KA receptors in the mossy fiber synapse, the one between dentate granule cells and CA3 pyramidal cells of the hippocampus. In fact, it

has been shown that KA receptor-mediated synaptic transmission is pathway specific, only KA receptors on CA3 pyramidal cells can be selectively activated by stimulation of the mossy fibers (Epsztein *et al.*, 2017).

Besides the ionotropic glutamate receptors, also metabotropic (G-protein coupled) glutamate receptors (mGluR1-8) are known (Fig 1.14 B). mGluRs are classified into three groups according to sequence homology, G-protein coupling and ligand selectivity. mGluRs activate a multitude of second messenger signaling pathways important for modulating neuronal excitability, synaptic plasticity and feedback regulation of NT release. More specifically, group I mGluRs are often localized post-synaptically and their activation leads to cell depolarization and increase of neuronal excitability. In contrast, group II and III mGluRs are localized on pre-synaptic terminals where they inhibit NT release (Niswender & Conn, 2010).

1.4.2 The inhibitory synapse

The activation of an inhibitory synapse decreases the probability to generate an AP, by creating a more negative post-synaptic membrane potential (hyperpolarization) and preventing in this way the excitation of the neurons.

Inhibitory transmission is mainly mediated by γ-aminobutyric acid (GABA). GABA release from the pre-synaptic terminals, *via* calcium-dependent vesicles fusion to the pre-synaptic membrane, does not differ from glutamate release.
On the post-synaptic side, also GABA receptors are divided into ionotropic ($GABA_A$) and metabotropic ($GABA_B$). $GABA_A$ receptors are heteropentameric complexes formed by different classes of subunits, α (1-6), β (1-3), γ (1-3), δ, ε (1-3), θ, and π (Bormann & Feigenspan, 1995). Most hippocampal $GABA_A$ receptors contain two α-subunits, two β-subunits and one γ-subunit; the last one can be replaced by other variants (Chang *et al.*, 1996; Farrar *et al.*, 1999; Whiting *et al.*, 1999). The clustering and trafficking of $GABA_A$ receptors at inhibitory synapses is mediated by the multifunctional protein gephyrin, which binds to the β-subunit of the receptors (Meyer *et al.*, 1995, Kneussel

et al., 1999) and connects them to microtubules (Kirsch *et al.*, 1991; Ramming *et al.*, 2000) and microfilaments (Mammoto *et al.*, 1998). Activation of ionotropic $GABA_A$ receptors causes a Cl^- influx and triggers hyperpolarizing inhibitory post-synaptic potential (IPSP).

$GABA_B$ receptors are heterodimers, composed of GBR1 and GBR2 subunits (Jones *et al.*, 1998), coupled to G-proteins, which mediate a slow response to GABA. Rather than activating Cl^- selective channels, $GABA_B$ receptors mediate inhibition through activation of K^+ channels, causing a hyperpolarizing K^+ outflow from the neuron.

1.4.3 Functions of the actin cytoskeleton and profilins at the synapse

The actin cytoskeleton has important tasks in the formation and maintenance of synapses as well as in regulating their functionality: actin dynamics in pre- and post-synaptic terminals of neurons is essential for synaptic transmission (Fig 1.15).

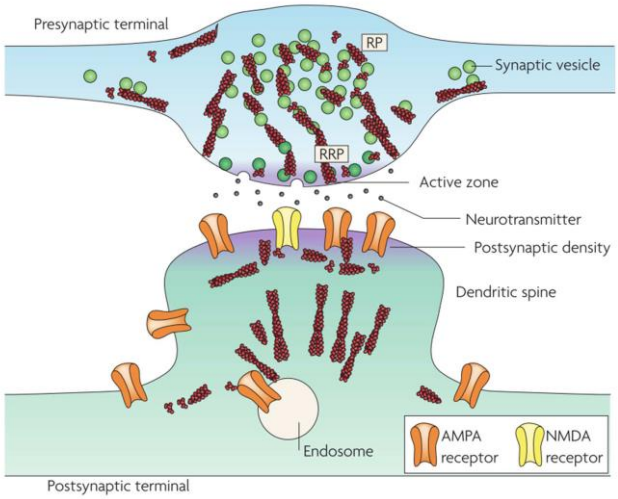

Figure 1.15 **| Actin functions at the pre- and post-synapse.** In the pre-synaptic terminal (top), SVs centrally located belong to the reserve pool (RP, light green) and are confined and interconnected by actin filaments (red). Actin filaments, extending from the RP to the plasma membrane, also guide the vesicles to the region of the readily releasable pool (RRP, dark green) and facilitate their docking. Finally, actin filaments participate in the exocytosis of primed SVs at the active zone, allowing NT release, and in their reuptake and recycling. In the post-synaptic terminal (bottom), actin is a key element for dendritic spines shape and maturation. Actin filaments also organize and interconnect scaffolding proteins of the post-synaptic density (PSD). AMPA and NMDA receptors are localized in the PSD, which lies opposite to the active zone and the actin dynamics regulate their membrane diffusion and their exo–endocytic trafficking (figure from Cingolani & Goda, 2008).

1.4.3.1 Pre-synaptic functions of actin and profilins

Actin in pre-synaptic terminals is involved in maintaining and regulating the synaptic vesicle pools, by serving as a barrier to restrict vesicle mobility and by providing tracks to direct the transfer of vesicles between the RP and the RRP pools. Actin filaments, interacting with synapsins which, in turn, are linked to vesicles, confine them in the RP in the center of the pre-synaptic terminal (Landis *et al.*, 1988; Greengard *et al.*, 1994; Evergren *et al.*, 2007). Upon increased neuronal activity, vesicles from the RP and the recycling pool need to be mobilized, in order to provide the proper amount of NT to sustain stimulation, and actin filaments provide the tracks for the vesicles to reach the active zone. At the active zone, actin has a dual role. On one side, it is able to facilitate the docking of the vesicles, thus promoting vesicles exocytosis of the RRP, while on the other side it holds back SVs of the RP, preventing their uncontrolled fusion (Fig 1.15). Fluorescence microscopy of giant axons of *Lampetra fluviatilis* showed actin localization surrounding the vesicle cluster, and electron micrographs, from rat hippocampal organotypic cultures, revealed actin filaments in the regions where vesicle endocytosis is thought to occur (Shupliakov *et al.*, 2002; Sankaranarayanan *et al.*, 2003). Accordingly, it was also shown that actin, together with myosin VI, facilitates the endocytic retrieval of synaptic vesicles (Bloom *et al.*, 2003; Yano *et al.*, 2006).

Lower eukaryotes have provided evidence for a role of profilins in endocytosis and membrane trafficking (Wolven *et al.*, 2000; Pearson *et al.*, 2003). In mice, PFN1 (Neuhoff *et al.*, 2005) and PFN2 (Pilo Boyl *et al.*, 2007) are both present at pre-synaptic terminals. A screen in mouse brain for profilin ligands revealed that many PFN2-interacting proteins are part of the vesicle cycle machinery (Witke *et al.*, 1998). For example, PFN2 associates with synapsins (Witke *et al*., 1998) and Piccolo (Wang *et al*., 1999) at the active zone. It also associates with dynamin 1, inhibiting its activity and thus the endocytosis of extra-synaptic clathrin-coated SVs, needed in the process of NTs reuptake (Gareus *et al.*, 2006). Moreover, PFN2 restrains glutamatergic vesicle

exocytosis during synaptic activity, by promoting fast F-actin polymerization. *Pfn2*$^{-/-}$ mice show increased number of docked/primed vesicles and increased synaptic excitability of glutamatergic neurons in the cortico-striatal pathway, due to higher vesicle exocytosis (Pilo Boyl *et al.*, 2007).

1.4.3.2 Post-synaptic functions of actin and profilins

In the post-synaptic terminal, actin is also heterogeneously present. The receptor abundance on the membrane is an effective valuable mechanism to regulate the strength of synaptic transmission. Actin participates in the anchoring and trafficking of the receptors, by exo- and endocytosis mechanisms (Fig 1.15).

In excitatory synapses, dendritic spines formation, plasticity and maintenance depend on synaptic activity and are modulated by neurotransmission. Changes in the morphology and density of spines are due to the plastic remodeling of the actin cytoskeleton (Nimchinsky *et al.*, 2002).
In inhibitory synapses, it has been shown that gephyrin, a prominent scaffolding component of the post-synaptic network, interacts with diverse proteins involved in actin dynamics, such as MENA/VASP, PFN1 and PFN2. In particular, it competes with G-actin and PIP_2 for the same binding site on profilins. Profilins have been identified as the molecular linkers between gephyrin and microfilaments that in cooperation with microtubules may regulate the receptor packing densities at inhibitory post-synaptic specializations (Giesemann *et al.*, 2003).
Interestingly also other scaffolding post-synaptic proteins interact with PFN1 and PFN2: drebrin, involved in the process of dendritic spine morphology (Koganezawa *et al.*, 2017), and delphilin, which binds to glutamate receptor δ2 subunit in PCs (Miyagi Y. *et al.*, 2002).

Actin cytoskeleton remodeling at the synapse correlates to electrophysiological changes of synaptic plasticity. The term “plasticity” describes the property of synapses to perform morphological changes in order to strengthen or weaken the neuronal

communication in response to different stimuli in adulthood.

Sustained synaptic activity leads to a form of plasticity called long-term potentiation (LTP). During LTP, the increased F-actin content enlarges both the pre-synaptic bouton and the spine head volume, thus strengthening synaptic contacts. On the contrary, slow repetitive stimulation results in a process of long-term depression (LTD). LTD triggers a change in structural dynamics opposite to the changes induced by LTP: a shift in the spine F-actin/G-actin ratio to G-actin, and a concomitant decrease in spine head volume with the occasional disappearance of some spines (Okamoto *et al.*, 2004).

It remains elusive whether profilins have a post-synaptic function, since studies from different groups lead to divergent results. It was previously shown that the stimulation of NMDA receptors, in murine cultured hippocampal neurons, induced PFN2 redistribution to dendritic spines and the stabilization of their morphology (Ackermann & Matus, 2003). Studies in rats also showed a recruitment of profilin to dendritic spines in the amygdala upon fear conditioning (Lamprecht *et al.*, 2006). *In vitro* studies demonstrated that PFN2 exerts PFN1-independent as well as redundant functions at the post-synaptic level. Specifically, knockdown of PFN2 in cultured hippocampal neurons negatively affects dendritic complexity and spine density. In this study, the concomitant expression of PFN1 could only compensate for the reduction in spine number, whereas the expression of PFN2 completely restored both number of spines and dendritic complexity (Michaelsen *et al.*, 2010). However, in a *Pfn2*$^{-/-}$ mouse model no post-synaptic function was detectable, neither with electrophysiological investigation nor with behavioral studies on associative learning and long-term memory (Pilo Boyl *et al.*, 2007). As previously mentioned, PFN2 has an established pre-synaptic function (Pilo Boyl *et al.*, 2007), instead PFN1 is dispensable for post-mitotic neurons in both pre- and post-synaptic physiology. In fact, *Pfn1* forebrain-specific deficient mice show preserved synapse density and morphology as well as unaltered basal synaptic transmission, pre-synaptic physiology, and post-synaptic plasticity (LTP and LTD) (Görlich *et al.*, 2012). The discrepancy of the data could be explained by a

potential overlap between PFN1 and PFN2 functions; to clarify this, studies on *Pfn1-Pfn2* double mutant mice are required and will be presented in this work.

1.5 Profilins in disease

It has become progressively clear that profilins are important players in cytoskeleton dynamics, and it has been proven their involvement in several cytoskeleton-based processes of clinical importance. Therefore, altered profilins levels are found in different pathological conditions.

Commonly, PFN1 has been described as a tumor suppressor in various invasive adenocarcinomas (breast, hepatic, and bladder) (Janke *et al.*, 2000; Das *et al.*, 2009; Zou *et al.*, 2007; Zoidakis *et al.*, 2012). PFN1 upregulation in cancer cells provides a potential pathway for the elimination of cells expressing the tumorigenic phenotype (Alkam *et al.*, 2017). Conversely, high levels of profilins are found in human gastric cancer (Tanaka *et al.*, 1992). Nevertheless, in our mouse models lacking PFN1 a correlation was not found between reduced PFN1 levels and tumor formation (Witke unpublished).

PFN1 has also been shown to be involved in vascular problems, huntington disease, amyotrophic lateral sclerosis (ALS) and spinal muscular atrophy (SMA) pathogenesis.

Profilin as a molecule involved in plasticity processes, it is expected to be associated to various neurological disorders. It has been demonstrated that, *Pfn1* mRNA is a Fragile X mental retardation syndrome protein (FMRP) target and, accordingly, PFN1 levels are altered in a mouse model for Fragile X syndrome (FXS) (Hinton *et al.*, 1991; Rudelli *et al.*, 1985; Birbach 2008). Moreover, PFN1 overexpression in a *Fmr1* ko mouse model rescues the impairment in spinogenesis, a hallmark of FXS (Michaelsen-Preusse *et al.*, 2016).

SMA is the most common human genetic disease resulting in infantile mortality; it is

caused by mutations or deletions in the ubiquitously expressed survival motor neuron 1 (*Smn1*) gene. Upregulation of PFN2 in a SMA mouse model leads to an inappropriate activation of RhoA/ROCK pathway (Bowerman *et al.*, 2009). In turn, PFN2 regulation by RhoA/ROCK kinases can modulate neuritogenesis (Da Silva *et al.*, 2003) and, furthermore, the *in vivo* inhibition of RhoA has been shown to prolong the survival of a SMA mouse model (Bowerman *et al.*, 2010).

Genetic studies in a group of Finnish families identified a novel gene locus, named AUTS2, linked to autism spectrum disorder (ASD). The AUTS2 locus is localized in the same chromosomal region (3q25-27) encoding for *PFN2* (Auranen *et al.*, 2002).

1.5.1 Autism spectrum disorder

Autism spectrum disorder is a pervasive neurodevelopmental disorder mainly caused by genetic factors, with the contribution of psychological and environmental ones (Kim *et al.*, 2015). Recent studies have reported higher prevalence of ASD in monozygotic twins (from 75 % to 95 %) compared to dizygotic twins (from 0 % to 31 %) (Ronald *et al.*, 2011). Those epidemiological studies show that ASD is one of the most heritable of all neurodevelopmental disorders.

In a subset of patients, a single fully penetrant mutation can be enough to cause ASD, but in others the accumulation of many low-risk gene variants (>1000) could be the origin of the disorder (Huguet *et al.*, 2013; Betancur, 2011). The interplay between mutations in the genes and the genetic background of the individual also play an important role in the heterogeneity of the disease, since the buffering capacity of the genetic background can be sufficient to compensate the impact of certain deleterious mutations (Burgeron, 2016). Among the genetic causes of ASD, heritable mutations represent the majority of syndromic ASD, while recently *de novo* mutations have been identified in 20-30 % of idiopathic cases (De Rubeis & Buxbaum et al., 2015; Pinto *et al.*, 2014).

Besides the genetic basis of ASD, it is argued that the role of epigenetic regulation and the effect of environmental factors should not be excluded from the research of ASD causes. In fact, environmental factors might be responsible for ASD manifestation, by modulating through epigenetic mechanisms already existing genetic factors (Kleijer *et al.*, 2017). Prenatal exposure to maternal infection (Atladóttir *et al.*, 2010; Zerbo *et al.*, 2013), to sodium valproate (VPA) (Christensen *et al.*, 2013) and other toxins increase the risk of having a child with ASD. Exposure to mutagens and toxins can lead to problems during child development causing unbalanced brain connectivity.

Clinically it is referred to as autism spectrum disorder, since the severity and degree of functional impairment is really variable among affected individuals (Burgeron *et al.*, 2015). ASD is typically diagnosed within the first three years of life and affects about 1 % of the population (Varghese, 2017). Nowadays the prevalence of autism is higher than previous estimates (Centers for disease control and prevention 2016 estimates: 16.8 in 1000 children) due to the increased ability in diagnosing younger children (Nassar *et al.*, 2009; Parner *et al.*, 2008).
ASD affects more males than females; this is especially true among individuals with a normal intelligence quotient (>5 males/1 female affected) and the ratio becomes more balanced among ASD individuals with intellectual disability (ID) (2 males/1 female affected - Miles *et al.*, 2005).

Autistic disorder was first described by the psychiatrist Leo Kanner in 1943 (Kanner, 1943). The two ASD core symptoms recently defined in the DSM-5 (American Psychiatric Association, 2013) are: (i) social interaction deficits (ii) repetitive, ritualistic and stereotyped behaviors. During the first year of life ASD infants are often described as “quiet babies”, they do not babble or use any other communicative vocalizations. They fail to develop interest and attachment to their primary caregivers. Later, they eventually develop attachment to their parents, but have little interest in other children and people unknown to them. Older children may prefer to play alone and often do not point things out or use eye contact to share the pleasure of seeing

something with another person. Adults are awkward in their social initiations and greetings and they have difficulty in casual social settings. They might show impairments in the social aspect of communication; this includes eye contact and showing interest in the opinions of other people. In autistic patients, often the use of language is limited to the communication of needs or to provide information, but rarely to exchange information, chat or socialize (Ruttler & Schopler, 1987; Kim, 2015). The second diagnostic criterion are restricted, repetitive, and stereotyped patterns of behavior and interests. Children with ASD can demonstrate atypical behaviors in a variety of areas, including peculiar mannerisms, unusual attachments to objects, obsessions, compulsions, self-injurious behaviors, and stereotypes. Children with autism ask the same question repeatedly, regardless of the reply that is given, or engage in highly repetitive, perseverative games (Ruttler & Schopler, 1987; Kim, 2015).

ASD is often associated with other psychiatric and medical conditions including motor control difficulties, attention deficit and hyperactivity disorder (ADHD), anxiety, sleep disorders, FXS, tuberous sclerosis, Angelman syndrome, Rett's syndrome and others. Epilepsy is highly associated to ASD (Muhle *et al.*, 2004). The presence of cognitive impairments is not a defining criterion for ASD (Gillberg *et al.*, 2010), considering that cognitive abilities in ASD patients range from non-verbal-children with severe mental disability and self-injury (Gillberg & Coleman, 2000; Muhle *et al.*, 2004) to college students with an above average IQ, despite poor social skills (Baron-Cohen et *al.*, 2001).

No therapy is currently available for ASD and present pharmacological treatments do not address the core ASD behaviors, but target comorbid conditions such as seizures, anxiety and ADHD (Gillberg, 1991; Doyle & McDougle, 2012; Varghese, 2017). Different pathways may converge at the molecular, cellular, and systemic level; each of these levels can, thus, provide hints for the identification of drug targets and treatment strategies.

1.5.2 Risk-genes in autism spectrum disorder

A growing number of genes have been associated to ASD, whose mutations are predicted to impair the following molecular pathways: (i) chromatin remodeling and regulation of transcription, (ii) protein translational regulation, and above all (iii) neurodevelopment, (iv) neurotransmission and (v) synaptic function (Burgeron, 2016). Based on the different pathways associated with ASD, two main observations can be made regarding the shared properties of ASD-risk genes. First, these mutations seem to affect neuronal development and network formation. Second, they impair or alter synaptic development, function and plasticity (Courchesne & Pierce, 2005; Just *et al.*, 2007).

Examples of relevant proteins, involved in chromatin remodeling and transcription, are: two X-linked genes, *MECP2* and *FMR1*, involved in autism 'secondary' to Rett and Fragile X syndromes, respectively. MECP2 and other transcription factors, such as CHD8 and CTNNB1, contribute to brain development and function and are risk-genes for ASD (Burgeron, 2015; Kim, 2014).

Many proteins encoded by ASD-risk genes participate in different aspects of neuronal transmission, such as glutamatergic (for example NR2B) and GABAergic (for example, $GABA_A$ receptor subunit α3 and $GABA_A$ receptor subunit β3) transmission (Burgeron 2015).

Neurexins (NRXNs) and neuroligins (NLGNs) are synaptic cell-adhesion molecules that connect pre-synaptic boutons to post-synaptic terminals, mediating essential signaling between pre- and post-synaptic specializations. This signaling is central to the brain's ability to process information. In humans, alterations in genes encoding neurexins or neuroligins have been involved in ASD, linking synaptic cell adhesion to cognition and its disorders (Südhof, 2008). The first evidence that NLGN-NRXN complexes are relevant in ASD was obtained from a study in 2003, identifying mutations in the X-linked genes encoding NLGN3 and NLGN4 in siblings with autism (Jamain *et al.*, 2003).

The positioning of cell-adhesion molecules and NT receptors at the synapse involves a complex architecture of post-synaptic proteins, including scaffolding proteins, signaling molecules and the actin cytoskeleton (Burgeron, 2015). Many of these proteins are encoded by ASD-risk genes; an example is provided by mutations in members of the SHANK gene family (SHANK1, SHANK2, and SHANK3).

As previously explained, actin remodeling is essential in developmental processes and is also involved in signal transduction and neuronal activity. Among ASD-risk genes, there is a notable number of genes encoding proteins involved in actin dynamics. In Finnish families with ASD it was found a link between autism and DISC1 (Kilpinen *et al.*, 2008), a scaffold protein abundant in dendritic spines (Kirkpatrick *et al.*, 2006). Another gene that has been linked to ASD is diaphanous 3 (Vorstman *et al.*, 2011), a nucleation factor interacting with profilin. Cordon-bleau, another actin nucleation factor (Ahuja *et al.*, 2007), has also been proposed as a candidate gene in a unique ASD case (Griswold *et al.*, 2012). Lastly, PFN2 was found to bind to the WAVE regulatory complex, and one of its main components is CyFIP1. CYFIP1 is an mRNA translation regulator in association with FMRP (Napoli *et al.*, 2008) and has been shown to be involved in several neuropsychiatric disorders including ASD and schizophrenia (De Rubeis *et al.*, 2013); moreover genomic deletions affecting the expression of CYFIP1 have been found in ASD patients also carrying mutations in the SHANK2 gene (Leblond *et al.*, 2012) and are associated to ASD phenotypes in patients with the Prader-Willi syndrome (Bittel *et al.*, 2006).Furthermore, it was hypothesized that an alteration of the expression level of the FMRP-EIF4E-CYFIP1 complex creates an imbalance in the level of many synaptic proteins that are associated with ASD (Burgeron, 2015).

Therefore, taking into consideration PFN2 interaction with CyFIP1 in the WAVE complex, it was hypothesized that PFN2 could be an autism susceptibility gene.

1.6 Mouse models

In this work three different mouse models have been used:

- *Pfn2*$^{-/-}$
- *Pfn1*$^{flx/del}$*;Pfn2*$^{-/-}$*;Nes-Cre*$^{cre/wt}$
- *Pfn1*$^{flx/flx}$*;Pfn2*$^{-/-}$*;Camk2a-Cre*$^{cre/wt}$

1.6.1 *Pfn2*$^{-/-}$ mouse model

The *Pfn2*$^{-/-}$ mouse was generated by heterologous gene transfer. The β-galactosidase/neomycin ('geo') cassette was inserted, by homologous recombination, into the coding region of exon 3 of the *Pfn2* gene, thereby disrupting the gene expression (Pilo Boyl *et al.*, 2007) (Fig 1.16).

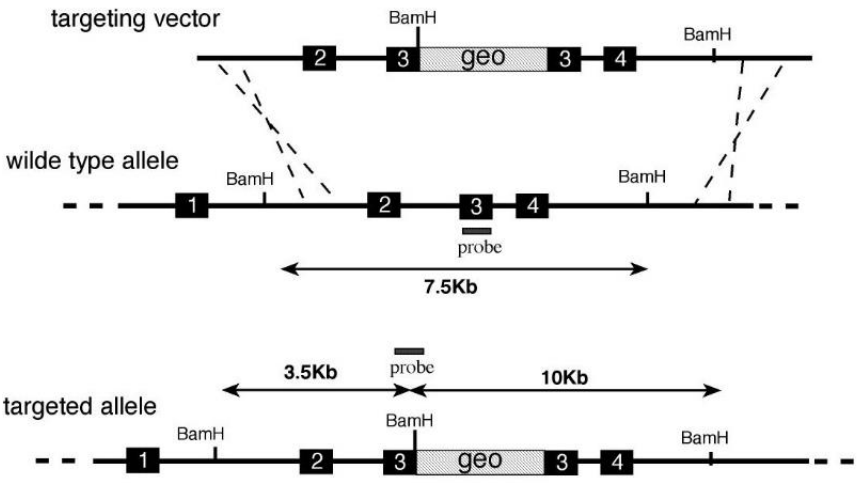

Figure 1.16 **| The *Pfn2*$^{-/-}$ mouse model.** Scheme of the gene targeting strategy in which the geo (β-galactosidase/neomycin) cassette was inserted into exon 3 of *Pfn2* gene. The result is the complete loss of PFN2 expression (figure from Pilo Boyl *et al.*, 2007).

The *Pfn2*$^{-/-}$ mouse model is viable and has an unaltered brain morphology (regular cortical layering, normal organization of the hippocampus and architecture of the cerebellum). The *Pfn2*$^{-/-}$ mouse does not show associative learning and memory deficits but has hyperactivity and increased novelty-seeking behavior in response to changes in the environment. The main physiological problem observed in the *Pfn2*$^{-/-}$

mouse is hyperactivity of glutamatergic neurons due to loss of regulation of glutamatergic vesicle exocytosis, because of altered fast actin polymerization dynamics (Pilo Boyl *et al.*, 2007).

1.6.2 *Pfn1$^{flx/del}$;Pfn2$^{-/-}$;Nes-Cre$^{cre/wt}$* mouse model

This conditional profilin double ko mouse model, *Pfn1$^{flx/del}$;Pfn2$^{-/-}$;Nes-Cre$^{cre/wt}$,* was generated in order to study the function of both PFN1 and PFN2 during the embryonic development of the CNS. In this mouse line, the deletion of *Pfn2* occurs already in the germ line, whereas a brain specific mid-embryonic deletion of *Pfn1* was obtained crossing the *Pfn1 $^{del/wt}$;Nes-Cre$^{cre/wt}$* background, which was already heterozygous for *Pfn1* and carried a transgenic Cre recombinase under the control of the rat *nestin* minimal promoter (Tronche *et al.*, 1999; Kullmann *et al.*, 2011; Kullmann *et al.*, 2012), with the *Pfn1$^{flx/flx}$* background to introduce the *Pfn1* floxed allele in the final mouse genotype.

The intermediate filament protein NESTIN (neuroepithelial stem cell protein) is the major cytoskeletal protein expressed by NPCs in the mammalian CNS, the radial glia cells. Therefore, in this *Pfn1$^{flx/del}$;Nes-Cre$^{cre/wt}$* background, one *Pfn1* allele is deleted already in the germ line, while the deletion of the second allele occurs only in neuronal and astroglial cells, starting from ~E9.5, at the onset of brain development.

1.6.3 *Pfn1$^{flx/flx}$;Pfn2$^{-/-}$;Camk2a-Cre$^{cre/wt}$* mouse model

The second conditional profilin double ko mouse model, *Pfn1$^{flx/flx}$;Pfn2$^{-/-}$;Camk2a-Cre$^{cre/wt}$*, was generated in order to study the function of both PFN1 and PFN2 in the adult brain. As described above, the deletion of *Pfn2* is complete since germ line, while the deletion of *Pfn1* is again temporally and tissue-specifically regulated. In this mouse model *Pfn1* is specifically deleted in the adult forebrain. To obtain this, the *Camk2a-Cre* transgene was used, expressing the Cre recombinase under the control of the Ca^{2+}/calmodulin-dependent protein kinase II-α partial promoter (Minichiello *et al.*, 1999).

CAMKIIα is highly expressed throughout the forebrain, while hindbrain regions express the lowest levels (Burgin *et al.*, 1990). In particular, the *Camk2a-Cre* transgene is active in the pyramidal neurons of the CA and in the granular neurons of the DG of the hippocampus, in the principal neurons of the cortex and in the medium spiny neurons of the striatum (Minichiello *et al.*, 1999; Liu & Murray, 2012).

In this double ko line, therefore, the deletion of *Pfn1* occurs in the forebrain, specifically in the excitatory neurons of cortex and hippocampus starting from P18.5 (post-natal day 18.5).

Results

2.1 A novel molecular pathway in autism spectrum disorder is associated with profilin 2 and actin dynamics in pre-synaptic terminals

It was previously shown that PFN2 has an essential role in restraining vesicle exocytosis during synapse depolarization. Consistent with this function, *Pfn2*$^{-/-}$ mice exhibit hyper-excitability at the physiological and behavioral level (Pilo Boyl *et al.*, 2007). Furthermore, it was observed that *Pfn2* loss in mice caused spontaneous epileptic seizures and affected their breeding behavior, reminding of features typical of an autistic-like phenotype. Therefore, it was investigated weather PFN2 loss could cause autistic-like behavior in mice and the understanding of its etiology was deeply explored.

2.1.1 Protein expression of PFN2 in the *Pfn2* ko mouse line

Many brain regions have been shown to be involved in autistic-like behavior, but it is generally accepted that the hippocampus and the cortex are central in higher brain functions. Therefore, in all this work these two brain regions have been the focus of our studies. Since in ASD often gene dosage appears to play an important role, the effect of gene dosage on PFN2 protein levels in the hippocampus and cortex of the *Pfn2* ko mouse line was studied. Total protein lysates were prepared from wt, *Pfn2*$^{+/-}$ and *Pfn2*$^{-/-}$ tissues and PFN2 levels evaluated by western blot analysis. The calibration of the protein of interest was obtained by Coomassie staining on the membranes (as explained in chapter 4.2.6.4) and the resulting PFN2 levels were normalized to the wt control. PFN2 in both hippocampal and cortical lysates was halved in heterozygous mice and was not detectable in ko mice (Fig. 2.1 A-B). Therefore, the western blot analysis confirms that the protein levels in hippocampus and cortex follow the gene dosage in the mouse model.

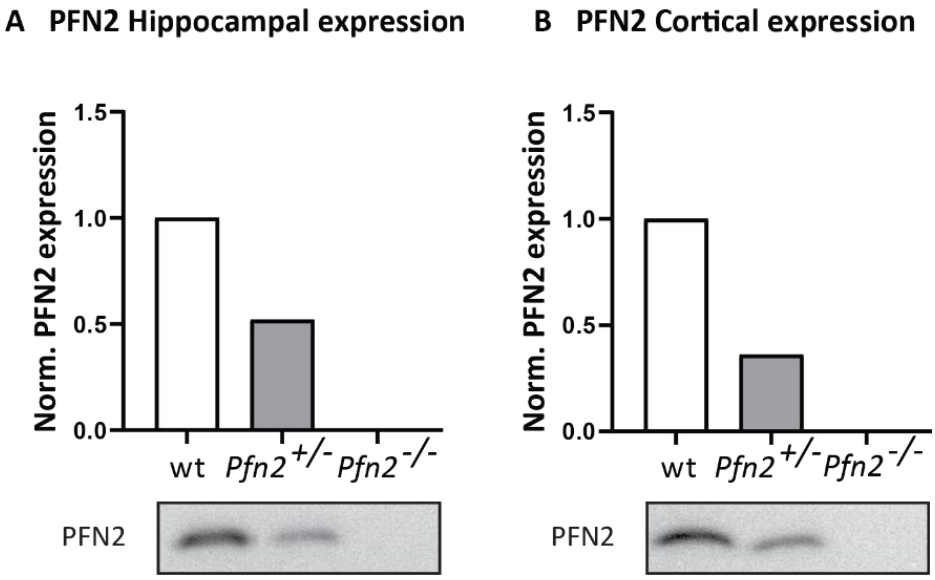

Figure 2.1 **| PFN2 protein expression is halved in *Pfn2*$^{+/-}$ mice and undetectable in *Pfn2*$^{-/-}$ mice. A,B Top.** Relative quantification of PFN2 protein levels in hippocampal (**A**) and cortical (**B**) total lysates from the three indicated genotypes normalized to the wt levels. **A,B Bottom.** Western blot images of hippocampal (**A**) and cortical (**B**) lysates from the same genotypes probed with anti-PFN2 (rb3003) antibody. Coomassie staining of the membranes (not shown) was used to calibrate the PFN2 signals. n=1 per genotype.

2.1.2 Loss of PFN2 increased basal excitatory synaptic transmission in the hippocampus

To study if PFN2 loss would affect basal excitatory synaptic transmission also in the hippocampus, similarly to what was shown in other excitatory circuits (Pilo Boyl *et al*., 2007), input-output (I-O) curves were recorded from the CA3-CA1 synapse in acute hippocampal brain slices of wt and *Pfn2*$^{-/-}$ mice, aged between P16 and P21.

A stimulation electrode was placed in the Schaffer collaterals in the CA3 region, whereas the sum of post synaptic responses (fEPSP) was recorded in the stratum radiatum of the CA1 region. The amount of activated fibers was indicated by the size of the fiber volley (FV) peak. In the I-O graph is reported the intensity of the post-synaptic response upon activation of pre-synaptic neurons with increasing stimulus intensities that were set to obtain 0.05, 0.1, 0.15, 0.2, and 0.25 mV fiber volley peak.

Picrotoxin (PTX), an inhibitor of $GABA_A$ receptors, was added to the bath solution of the hippocampal slice in order to isolate excitatory inputs.

Both wt and *Pfn2*$^{-/-}$ mice showed increasing response to the increasing stimulation intensity. However, the I-O relation was significantly enhanced in *Pfn2*$^{-/-}$ mice compared to wt animals. In fact, while the I-O relation in wildtypes is well interpolated by a linear regression, the I-O relation in mutant mice is better described by a polynomial regression. In addition, *Pfn2*$^{-/-}$ mice show higher responses to increasing stimulation intensities, as also demonstrated by the significant increase of the fEPSP slope at 0.25 mV (Fig 2.2 A). No differences were observed in the excitability of the Shaffer collaterals, meaning that the stimulation intensity applied to evoke the same FV in the two genotypes did not differ (Fig 2.2 B).

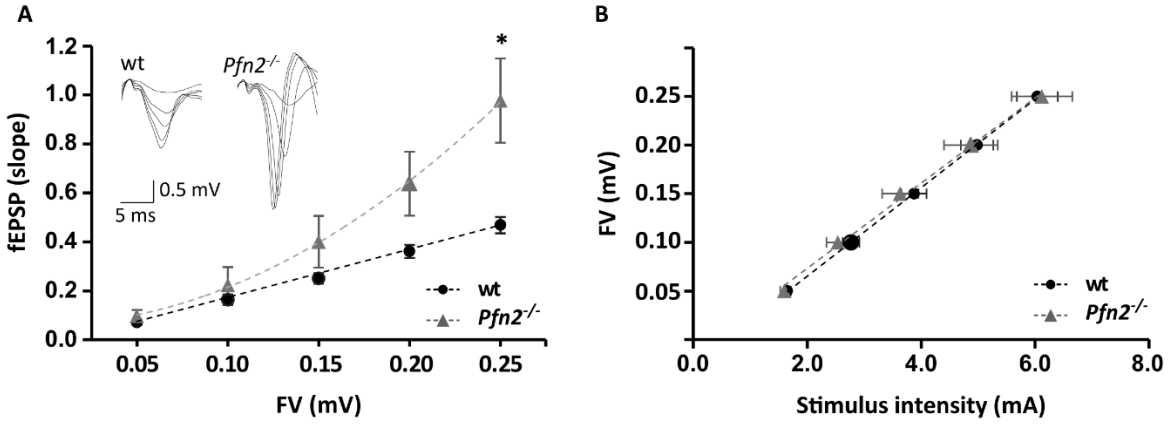

Figure 2.2 **| *Pfn2*$^{-/-}$ mice show increased basal glutamatergic neurotransmission. A.** The graph shows fEPSP slopes (mean ± SEM, with the slope of the fEPSP being a directly proportional measure of the strength of the post-synaptic response) upon activation of pre-synaptic neurons with increasing stimulus intensities that were set to obtain 0.05, 0.1, 0.15, 0.2, and 0.25 mV FV peak. I-O relationship in CA3-CA1 synapses is linear in wt mice while it follows a polynomial relationship in *Pfn2*$^{-/-}$ mice. Synaptic transmission is significantly enhanced in *Pfn2*$^{-/-}$ mice at higher stimulus intensity (two-tailed t-test, P=0.0164). **Inset**: Representative superimposed sample traces of an input-output experiment from a wt and a *Pfn2*$^{-/-}$ slice. **B.** Graph of the average FV intensity obtained at each stimulus intensity for wt and *Pfn2*$^{-/-}$ slices. The stimulus intensities required to generate the different FV amplitudes do not differ in *Pfn2*$^{-/-}$ mice compared to controls. wt n=15 slices/6 mice; P*fn2*$^{-/-}$ n=13 slices/7 mice. *P≤0.05.

The input-output relationship is a measure of synaptic transmission and the experiment shown in Fig 2.2 demonstrates that loss of PFN2 results in increased glutamatergic transmission.

2.1.3 Loss of PFN2 increases pre-synaptic vesicle release probability

Since loss of PFN2 resulted in increased excitatory basal neurotransmission, additional experiments were performed to analyze functional pre-synaptic changes. Paired-pulse facilitation (PPF) was studied on acute hippocampal slices with extracellular field recordings. In PPF experiments two consecutive stimuli are given to the Schaffer collaterals with a definite time interval of 40 ms and post-synaptic responses are recorded in the CA1 area. The term facilitation refers to the effect of Ca^{2+} ions, accumulated in pre-synaptic terminals following the first stimulus, which facilitate vesicle exocytosis upon a second one. For this reason, alterations in PPF reflect changes in vesicle release probability.

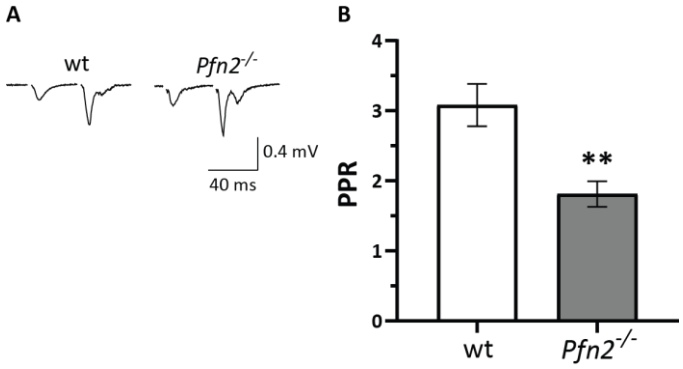

Figure 2.3 **| Pre-synaptic vesicle release probability in excitatory synapses is increased in *Pfn2*$^{-/-}$ mice. A.** Sample traces of PPF in a wt (left) and *Pfn2*$^{-/-}$ (right) slice. **B.** The paired-pulse ratio (PPR) with an inter-stimulus interval of 40 ms was significantly reduced in *Pfn2*$^{-/-}$ mice (by 40 %) compared to wt controls (P=0.0102). wt n=15 slices/6 mice; P*fn2*$^{-/-}$ n=9 slices/5 mice. Two-tailed t-test, ** P≤0.01

A measure of PPF is the paired-pulse ratio (PPR), calculated dividing the slope value of the second fEPSP by the one of the first fEPSP. PPR values for *Pfn2*$^{-/-}$ mice were 40 % lower than in control littermates, indicating a higher vesicle release probability (Fig 2.3).

Therefore, the higher excitatory transmission of *Pfn2*$^{-/-}$ mice can be related to increased release probability of vesicles from the pre-synapse.

2.1.4 Loss of PFN2 increases AP-independent synaptic transmission

In order to support this conclusion, pre-synaptic physiology was further analyzed *via* patch-clamp recordings, by measuring miniature excitatory post-synaptic currents (mEPSC) in CA1 pyramidal neurons.

mPSC are caused by spontaneous (AP-independent) vesicle fusion in the pre-synapse. Their isolation is obtained by bath application of tetrodotoxin (TTX), a voltage gated Na^+-channel blocker. Furthermore, the recording efficiency of mPSCs is increased by blocking potassium channels. With this approach stochastic excitatory vesicle exocytosis events at the active zone of afferent CA3 neurons can be measured from single CA1 patch-clamped neurons.

The frequency and the amplitudes of mEPSC events are normally evaluated. The frequency reflects the vesicle release probability, the amount of functional synapses and the number of release sites. On the other hand, the amplitude is a measurement of the strength of the synapse, reflecting the amount of functional AMPA receptors on the post-synaptic membrane.

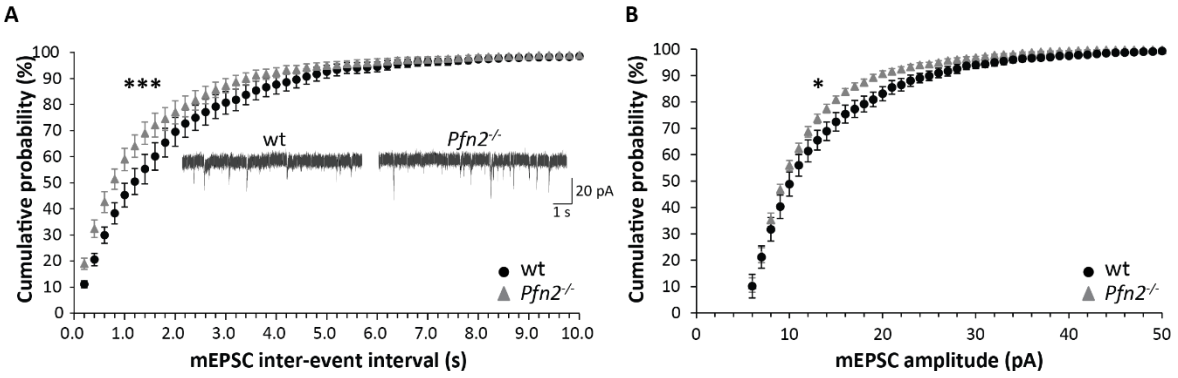

Figure 2.4 **| *Pfn2*$^{-/-}$ mice show increased excitatory synaptic vesicle release. A.** Percentage cumulative distributions of inter-event intervals of mEPSCs recorded from CA1 pyramidal neurons of *Pfn2*$^{-/-}$ and wt control cells. The graph indicates that *Pfn2*$^{-/-}$ neurons have an increased frequency of mEPSCs compared to wt control mice (P=0.001), as shown by the increased percentage of smaller (left shift) inter-event intervals in the cumulative distribution. **In the inset**, sample traces of mEPSC recordings from wt (left) and *Pfn2*$^{-/-}$ (right) cells. **B.** Percentage cumulative frequency distributions of mEPSC amplitudes show a mild decrease of events amplitude in *Pfn2*$^{-/-}$ mice (P=0.025). wt n=7 cells/4 mice; P*fn2*$^{-/-}$ n=8 cells/3 mice. Kolmogorov-Smirnov (KS), *P≤0.05 ,***P≤0.001.

mEPSCs were significantly more frequent in *Pfn2*$^{-/-}$ mice compared to wt controls, as shown by the leftward shift of the cumulative curve (Fig 2.4 A); a mild reduction in mEPSC amplitude was also observed in ko mice (Fig 2.4 B).

The higher frequency of mEPSCs is in line with the PPR findings. Since in a previous work it was shown that in the hippocampus synaptic density is not altered in *Pfn2*$^{-/-}$ mice, while docked vesicles are increased (Pilo Boyl *et al.*, 2007), this change in mEPSC frequency points to an increased pre-synaptic vesicle release probability, resulting in an excessive glutamatergic transmission onto CA1 pyramidal neurons.

2.1.5 Reduced inhibitory transmission in *Pfn2*$^{-/-}$ mice

An imbalance between excitatory and inhibitory transmission has been proposed as a cause of ASD. For this reason, the effects of PFN2 loss on inhibitory transmission were also investigated.

On acute hippocampal slices miniature inhibitory post-synaptic currents (mIPSC) were measured with patch-clamp recordings on CA1 pyramidal neurons. mIPSC were isolated by excluding excitatory transmission with NBQX, a blocker of AMPA and KA receptors.

As for mEPSC recordings, the frequency and the amplitudes of mIPSC events were evaluated. In this case, while the inter-event interval distribution of mIPSCs of *Pfn2*$^{-/-}$ mice did not differ from control, indicating that the number of inhibitory synapses and the mechanisms of GABA release are unaltered in *Pfn2*$^{-/-}$ mice (Fig 2.5 A), the amplitudes of mIPSCs were significantly smaller (leftward shift of the percentage cumulative distribution) in *Pfn2*$^{-/-}$ mice compared to wt littermate controls (Fig 2.5 B). The reduced amplitude of mIPSCs suggests a loss of $GABA_A$ receptor clustering on the post-synapse or an alteration in their trafficking dynamics.

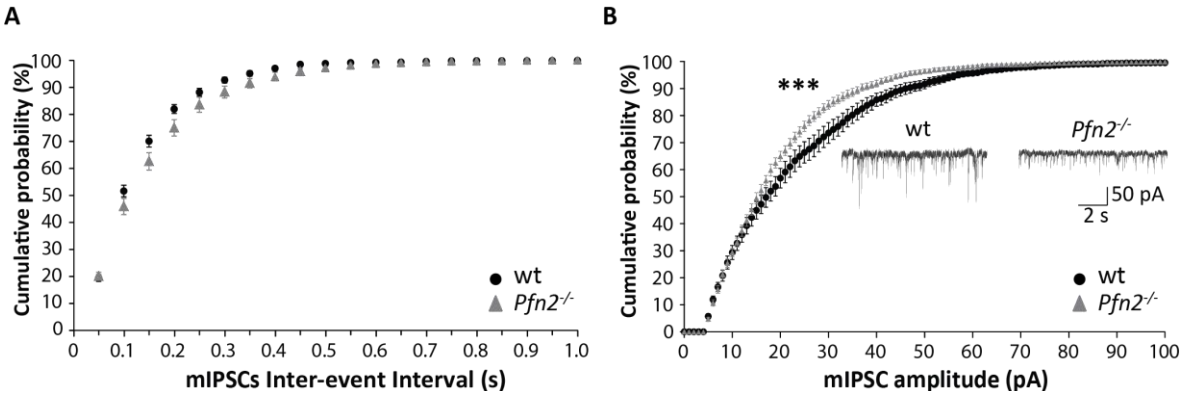

Figure 2.5 **| Decrease in the amplitude of mIPSCs points to impaired inhibitory transmission in *Pfn2*$^{-/-}$ mice. A.** Percentage cumulative distributions plot of mIPSC frequencies shows no difference between *Pfn2*$^{-/-}$ and wt control mice. **B.** Percentage cumulative distributions plot of mIPSC amplitudes shows a significant decrease of the amplitudes in *Pfn2*$^{-/-}$ mice compared to wt control littermates. **In the inset**, sample mIPSC traces from wt and *Pfn2*$^{-/-}$ cells. wt n=10 cells/3 mice; P*fn2*$^{-/-}$ n=10 cells/4 mice. KS, ***P≤0.001.

In order to support this novel finding, I-O curves for inhibitory transmission in single cells with the patch-clamp technique were then recorded. Evoked IPSCs were measured in response to increasing extracellular stimulations, applied ~100 µm away from the soma of the recorded CA1 pyramidal cell. I-O curves revealed a decreased response in Pfn2$^{-/-}$ mice compared to wt controls over a range of stimulus intensities (Fig 2.6 A).

In the end, the PPR of two evoked IPSCs with a 40 ms interval was calculated to exclude possible defects in pre-synaptic release mechanisms in inhibitory neurons. With the small number of cells analyzed no significant difference was detected in the PPR between wt and *Pfn2*$^{-/-}$ animals (Fig 2.6 B), although a tendential PPR increase could suggest either a diminished number of inhibitory synapses on CA1 neurons or altered vesicle exocytosis dynamics in GABAergic neurons.

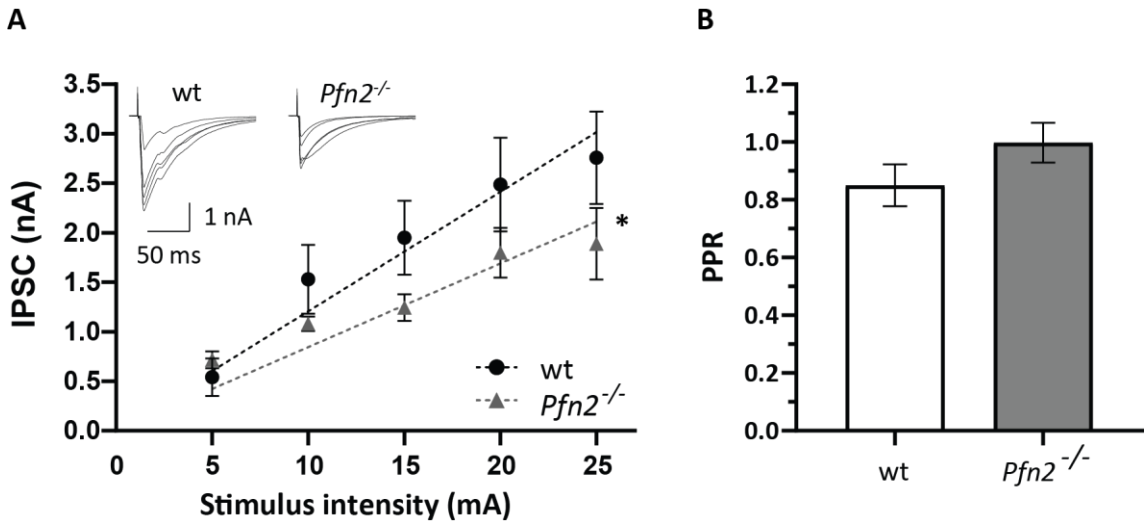

Figure 2.6 **| Evoked IPSCs recordings show reduced inhibitory transmission in *Pfn2*$^{-/-}$ mice.** I-O relationship shows a significant decrease of the inhibitory synaptic transmission in *Pfn2*$^{-/-}$ pyramidal cells compared to wt controls (two-tailed t-test on the angular coefficients of the individual cells linear regressions, P=0.048). Evoked IPSCs were measured as a function of the stimulus strength in patch-clamped CA1 pyramidal cells in acute hippocampal slices. The extracellular stimulation was produced by an electrode positioned in proximity (~100 µm) of the recorded cell. **In the inset**, representative traces of evoked IPSCs in wt and *Pfn2*$^{-/-}$ neurons. wt n=5 cells/3 mice; P*fn2*$^{-/-}$ n=5 cells/3 mice. **B.** Paired-pulse ratio, a measurement of pre-synaptic NT release probability, shows no significant difference between wt (0.85±0.07) and *Pfn2*$^{-/-}$ (1.06±0.03) mice. wt n=5 cells/3 mice; *Pfn2*$^{-/-}$ n=5 cells/3 mice. Two-tailed t-test, * P≤0.05.

In any case, the reduced amplitudes of the evoked IPSCs and the smaller amplitudes of mIPSCs suggest that, in mice, PFN2 is relevant for the appropriate GABA receptors-mediated inhibitory transmission in hippocampal pyramidal neurons. Therefore, loss of *Pfn2* in mice reduces GABAergic transmission, contributing to the excitation to inhibition ratio increase.

2.1.6 Infantile mortality and shorter life expectancy of *Pfn2*$^{-/-}$ mice

Since the electrophysiological properties of *Pfn2* ko neurons in the hippocampus support the hypothesis of an autistic-like phenotype, a phenotypic analysis was undertaken on the mutant mice.

Risk of premature mortality has been reported in autism (Hirvikoski *et al*, 2016). The risk of premature mortality has been estimated to be two-fold to ten-fold higher in

ASD patients. The higher mortality rate in ASD is related to the presence of comorbid medical conditions, rather than ASD *per se* (Bilder *et al.*, 2013). One possible cause is epilepsy, the most frequent medical disorder associated with autism and affecting one third of autistic individuals (Muhle *et al.*, 2004). About 30 % of *Pfn2*$^{-/-}$ mice showed spontaneous seizures, which appeared to be related to increased sensitivity to stressful events or loud stimuli. At weaning age (P21-P25), the expected Mendelian ratio of 25 % mutant mice from heterozygote matings was altered, with only 20 % *Pfn2*$^{-/-}$ animals present (Fig 2.7 A) and a proportional increase of wt and *Pfn2*$^{+/-}$ mice, suggesting a loss of mutants before weaning. When pups were genotyped at P7, the results matched the expected 25 % Mendelian ratio, confirming a small mortality rate of ~15 % of *Pfn2*$^{-/-}$ animals between P7 and P25 (Fig 2.7 B). Survival and life expectancy of *Pfn2*$^{-/-}$ mice was further investigated through a standard survival analysis over the span of a mouse life. The Kaplan-Meier plot showed significantly increased mortality of *Pfn2*$^{-/-}$ mice between 7 and 13 months, with the median survival halved compared to wt controls (Fig 2.7 C). Interestingly, heterozygote mice displayed an intermediate phenotype, significantly different from wt controls, indicating a gene dosage effect of *Pfn2* function on longevity. As a consequence, life expectancy (average life span) of *Pfn2* mutants and heterozygotes was significantly reduced compared to wt controls (Fig 2.7 C, bar graph inset).

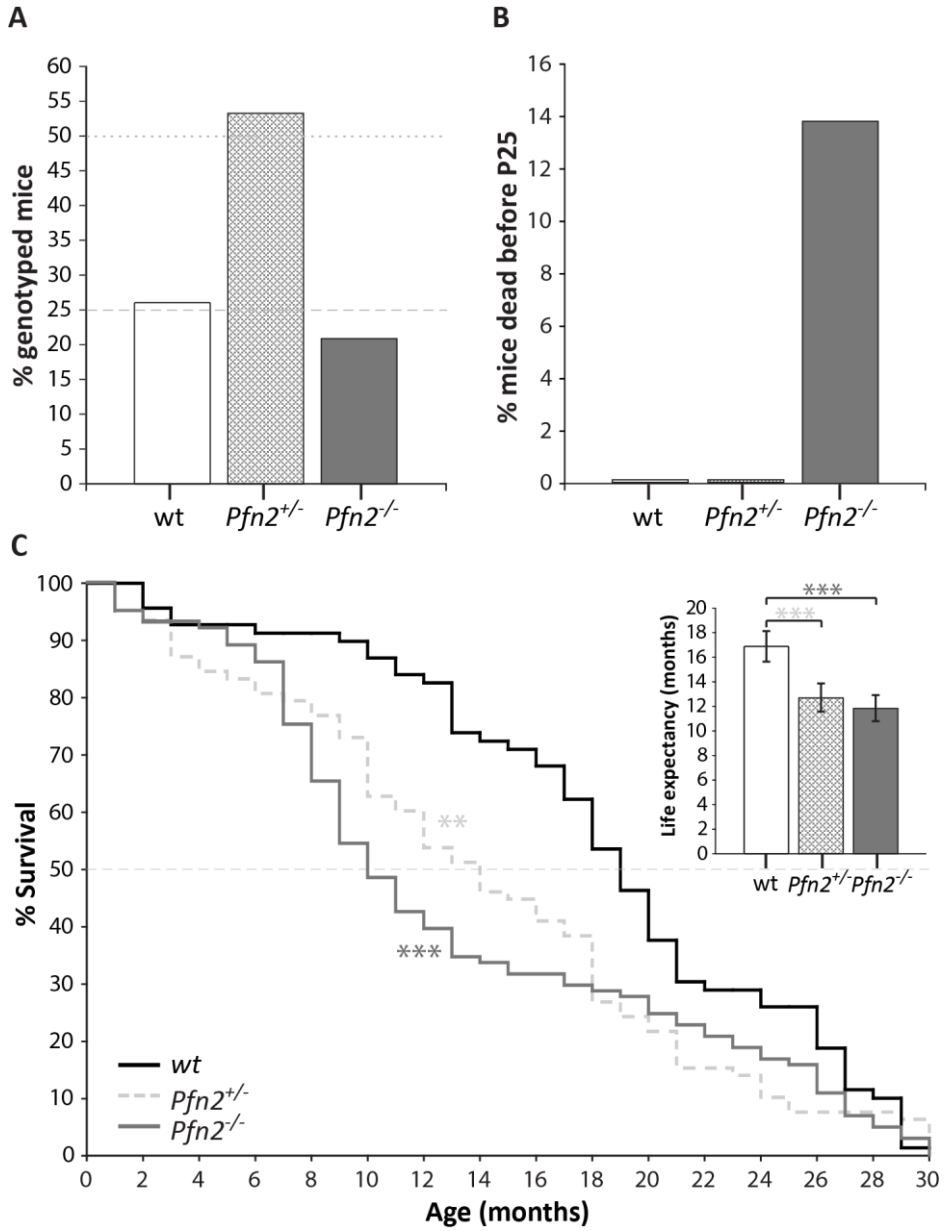

Figure 2.7 **| Reduced survival before weaning and shorter life expectancy of *Pfn2*$^{-/-}$ mice.** **A.** In the offspring of *Pfn2*$^{+/-}$ matings, fewer *Pfn2*$^{-/-}$ and proportionally increased wt and *Pfn2*$^{+/-}$ mice were found than expected from Mendelian ratio (dashed gray line, 25 %, and dotted gray line, 50 %) at weaning (P21-P25). n=47 *wt*, n=97 *Pfn2*$^{+/-}$, and n=38 *Pfn2*$^{-/-}$ genotyped animals from 24 litters. **B.** Pre-weaning loss of *Pfn2*$^{-/-}$ pups. Offspring were genotyped at P7 and followed until weaning (P25): 14 % of *Pfn2*$^{-/-}$ mice were lost in this period but no wt and *Pfn2*$^{+/-}$ mice. n=76 *wt*, n=178 *Pfn2*$^{+/-}$, n=75 *Pfn2*$^{-/-}$ P8 animals. **C.** Kaplan-Meier plot of survival data of mice shows higher mortality rate of *Pfn2*$^{-/-}$ mice between 7 and 13 months of age with an intermediate phenotype for *Pfn2*$^{+/-}$ mice (Peto-Prentice generalized Wilcoxon test: *Pfn2*$^{-/-}$ vs. *wt*, P<0.001; *Pfn2*$^{+/-}$ vs. *wt*, P=0.001). The median survival (dotted line in the graph) is 10 months for *Pfn2*$^{-/-}$ mice, 14 months for *Pfn2*$^{+/-}$ and 19 months for wt controls. **In inset**, life expectancy (average life span, in months) for each genotype (two-tailed t-test: *Pfn2*$^{-/-}$ vs. *wt* mice, P<0.0001; *Pfn2*$^{+/-}$ vs. *wt* mice, P=0.0008). n=69 wt, n=78 *Pfn2*$^{+/-}$, n=101 *Pfn2*$^{-/-}$ animals. **P≤0.01, ***P≤0.001.

2.1.7 Impaired maternal and social behavior of *Pfn2*$^{-/-}$ mice

General cage behavior of *Pfn2*$^{-/-}$ mice appeared evidently altered, with mutant mice ignoring other mice in the cage and spending more time alone. In addition, *Pfn2*$^{-/-}$ males lacked aggressive behavior towards other males and breedings with *Pfn2*$^{-/-}$ females resulted in a frequent loss of their litters. Therefore, two main aspects of social behavior were studied in detail: maternal behavior and social interactions.

Table 2.1 Maternal Behavior

Genotype		Number of litters	Litter survival	Father cohabitation
Mother	**Father**			
Pfn2$^{-/-}$	Wt	7	0 %	x
Pfn2$^{-/-}$	*Pfn2*$^{+/-}$	5	0 %	x
Pfn2$^{-/-}$	*Pfn2*$^{-/-}$	3	0 %	x
Pfn2$^{-/-}$	Wt	5	100 %	✓
Pfn2$^{-/-}$	*Pfn2*$^{+/-}$	3	100 %	✓
Pfn2$^{-/-}$	*Pfn2*$^{-/-}$	7	45 %	✓

Maternal behavior was found severely affected in *Pfn2* mutants. Nest building was almost absent in *Pfn2*$^{-/-}$ females (Fig 2.8 A) and when *Pfn2*$^{-/-}$ mothers were allowed to foster alone their litters, all pups were lost irrespectively of the pups' genotype (Table 2.1, top half). Interestingly, with the cohabitation of a *Pfn2*$^{+/-}$ or wt father, all litters of *Pfn2*$^{-/-}$ mothers survived, while only about half of them survived when both parents were *Pfn2* mutants (Table 2.1, bottom half).

In association to the fostering deficit also the pup retrieval behavior was severely compromised: when asked to retrieve P7 pups dispersed in the cage, wt mothers quickly started to retrieve the first pup, and within 7 minutes the entire litter was collected into the nest (Fig 2.8 B); instead, *Pfn2*$^{-/-}$ mothers never retrieved a single pup within the allowed experimental time (30 min). It is possible that the maternal behavior deficit of *Pfn2*$^{-/-}$ mothers was arising from the stress produced by the novel social context created by the pups, since with helping wt or heterozygous males litter survival was rescued, pointing to normal lactation and rearing abilities. Since *Pfn2*$^{-/-}$

fathers could only partially compensate the behavioral impairment of the mothers, this points to a robust and gender-independent social interaction deficit, which was further investigated.

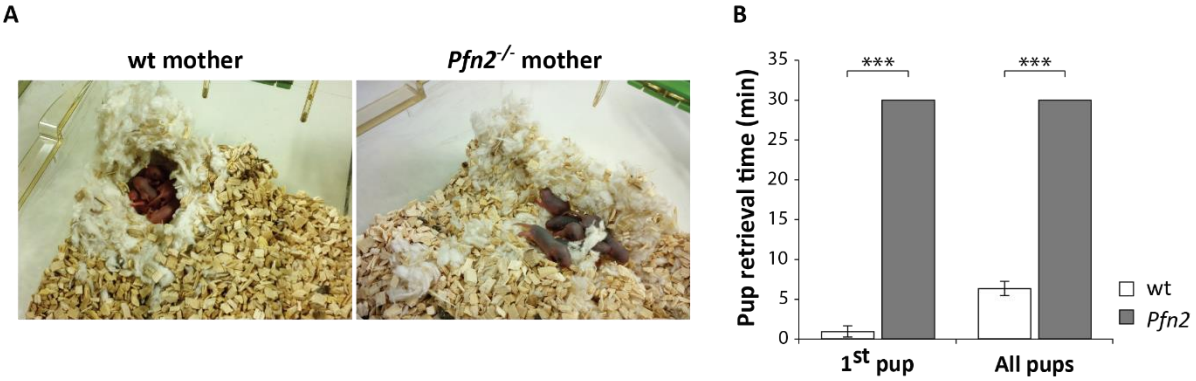

Figure 2.8 **| Maternal behavior is impaired in *Pfn2*$^{-/-}$ mice. A.** Example of nests from wt control and *Pfn2*$^{-/-}$ mothers, as indicated. The *Pfn2* mutant mothers do not build a proper nest, leaving the nesting material and pups sparsely distributed in the cage. **B.** Maternal behavior: pup retrieval by *Pfn2*$^{-/-}$ females is completely missing within the experimental time of 30 min, while on average wt control females retrieve the first pup within 1 min and the entire litter in about 7 min. n=5 wt and n=7 *Pfn2*$^{-/-}$ females. One-tailed t-test, *** P≤0.001

To assess sociability in males in a non-aversive context, the social Interaction paradigm in the 3-chambered maze (Moy *et al.*, 2007) was performed. The sociability is characterized by the tendency of a mouse to spend time interacting with a novel mouse. In this test a mouse is placed in the central compartment of a 3-chambered test box and the time spent in the two lateral compartments, one containing an unfamiliar mouse and the other being empty, is measured. The unfamiliar mouse is placed within a small wire enclosure, to allow exposure to visual, auditory, olfactory and some tactile stimuli, while preventing aggressive interactions. When social interaction between the adult test mouse and a stranger juvenile was assessed, *Pfn2*$^{-/-}$ mice showed reduced sociability. By number of visits, *Pfn2*$^{-/-}$ mice showed no significant preference between the social interaction (SI) zone and the empty zone (Fig 2.9 A). Although *Pfn2*$^{-/-}$ mice still spent more time in the SI zone, like wt controls (Fig 2.9 B), the average visit duration to the stranger mouse was tendentially reduced compared to wt controls (Fig 2.9 C), as well as the average sniffing time (Fig 2.9 D).

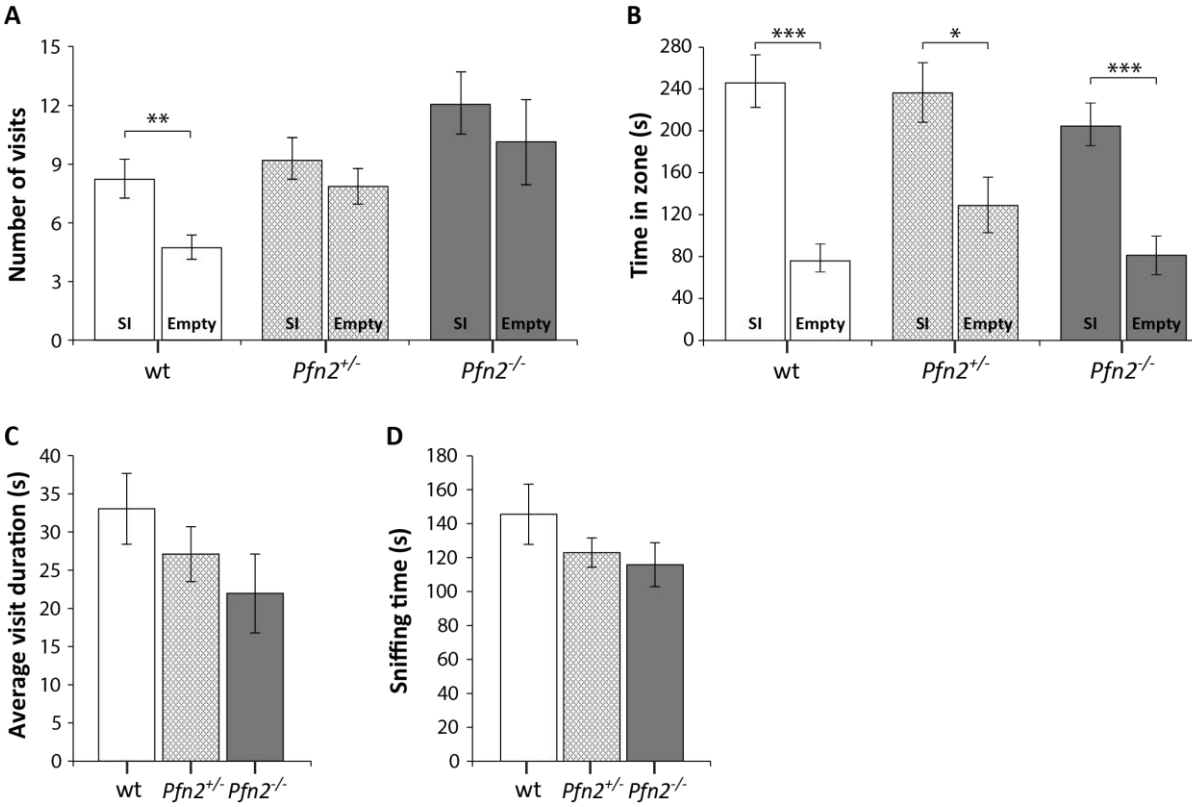

Figure 2.9 **| Social behavior is impaired in *Pfn2*$^{-/-}$ mice. A.** The number of visits of *Pfn2*$^{-/-}$ mice to the SI (Social Interaction) and the Empty zone showed no significant preference (P=0.4683) while wt control mice showed a significant preference for the SI zone (P=0.0098), indicating social interaction impairment in mutant mice. In this experiment heterozygous mice performed similarly to mutant mice. **B.** All tested genotypes spent more time in the SI zone than in the Empty zone, although *Pfn2*$^{-/-}$ mice showed the least interest. **C.** On average *Pfn2* mutant mice spent less time per visit in the SI zone compared to wt mice. Heterozygous mice displayed an intermediate performance. **D.** Sniffing in the SI zone was also reduced in *Pfn2* mutant and heterozygote mice compared to wt controls. n=8 wt, n=7 *Pfn2*$^{+/-}$ and n=9 *Pfn2*$^{-/-}$. Two-tailed t-test, *P≤0.05, **P≤0.01, ***P≤0.001.

Social deficits in autism may appear as inappropriate or indiscriminate approaches to strangers, rather than a complete lack in social approach (Loveland *et al.*, 2001). For this reason, the qualitative interaction of *Pfn2*$^{-/-}$ mice with the stranger juvenile mouse was evaluated and appeared different from control mice. Direct nose contacts between *Pfn2*$^{-/-}$ mice and the stranger mouse were rare, with the mutant mice mostly exploring the metal enclosure and its surroundings, rather than the mouse itself. This finding is in agreement with the previously reported novelty-seeking behavior of *Pfn2*$^{-/-}$ mice (Pilo Boyl *et al*, 2007). Again, heterozygous mice showed an intermediate phenotype in this test, suggesting a gene dosage effect of the mutation.

2.1.8 Increased stereotypic behavior in *Pfn2*$^{-/-}$ mice

Autistic individuals often maintain rigid habits and frequently show a strong insistence on sameness and are upset when their routine is changed (Frith, 1991; Hollander *et al.*, 2003). Ritualistic and repetitive behavior, together with resistance to changes, is in fact the other core symptom of autism. Animal models of autism exhibit spontaneous motor and stereotypic behaviors (Peça *et al*, 2011; Schmeisser *et al*, 2012). Therefore, an array of stereotypic behaviors in *Pfn2* mutant mice was assessed. *Pfn2*$^{-/-}$ animals showed significantly higher occurrence of circling, jerking, and wall leaning stereotypies compared to *Pfn2*$^{+/-}$ and wt control mice, indicating a stronger susceptibility to repetitive behavior. In this context, no significant differences were observed for self-grooming and digging (Fig 2.10).

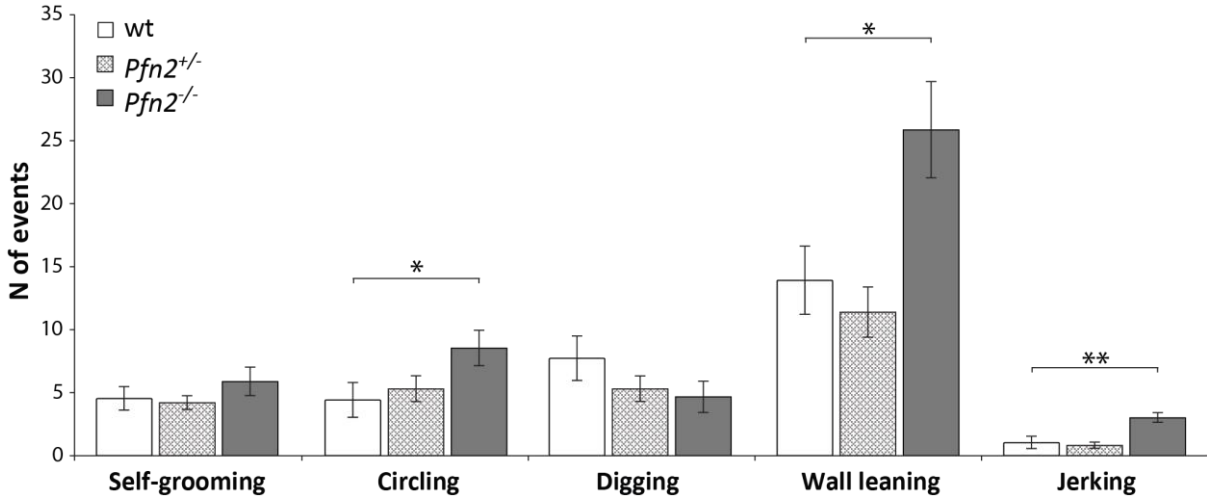

Figure 2.10 **| Stereotypic and repetitive behavior is increased in *Pfn2*$^{-/-}$ mice.** Five stereotypic behaviors were measured after transfer in a novel cage environment. Circling (P=0.0442), wall leaning (P=0.0273) and jerking (P=0.0015) were increased in *Pfn2*$^{-/-}$ mice compared to wt controls, grooming and digging were not changed. n=10 wt, n=11 *Pfn2*$^{+/-}$ and n=15 *Pfn2*$^{-/-}$ mice. Two-tailed t-test, *P≤0.05, **P≤0.01.

The Y- and T-maze have been frequently used to asses spatial working memory and repetitive behaviors. Mice are usually driven by exploratory needs and strategically explore different parts of the surrounding when placed in a novel environment (Chang, Cole & Costa, 2017). In this study the Y-maze setting was used, which provides a more natural turning angle compared to the T-maze (Lainiola *et al.*, 2014). To estimate the

resistance to changes and as a measurement of insistence on the sameness, the returns into the same arm (SAR) were evaluated compared to the spontaneous alternation (SPA) of the entries into the three arms. *Pfn2*$^{-/-}$ mice displayed decreased SPA (Fig 2.11 A) and whereas no control mouse ever returned to the same arm, about 50 % of the tested *Pfn2*$^{-/-}$ mice showed this behavior (Fig 2.11 B). *Pfn2*$^{-/-}$ mutants also showed a marked deficit in decision making, as suggested by the longer latency to initiate exploration (Fig 2.11 C).

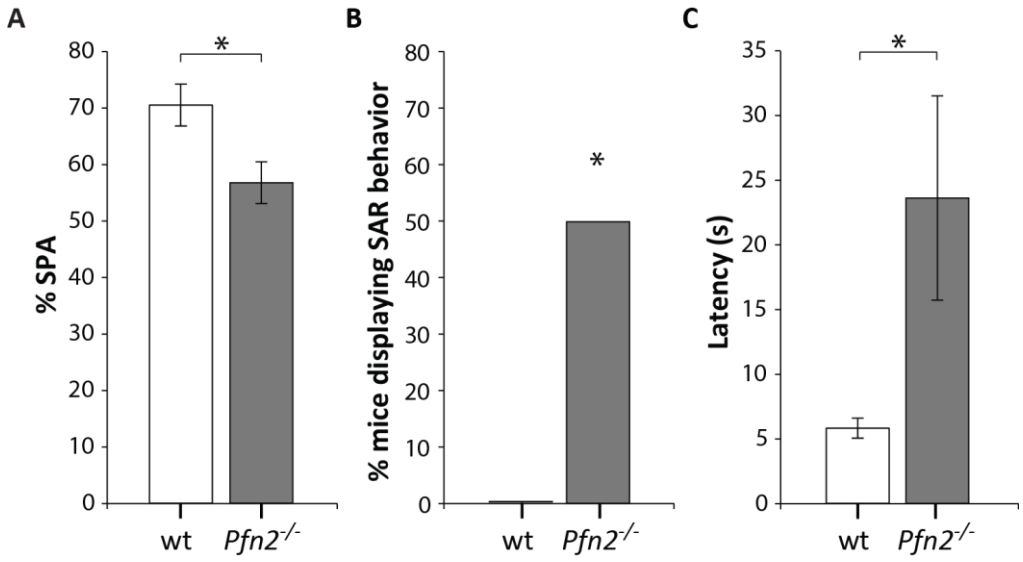

Figure 2.11 **|Insistence on sameness is increased in *Pfn2*$^{-/-}$ mice.** The Y-maze test was used to explore repetitive behavior. **A.** Spontaneous alternation (SPA) exploration strategy is diminished in *Pfn2*$^{-/-}$ mice compared to wt controls (P=0.0159). **B.** Same arm return (SAR) exploration is performed by 50 % of the *Pfn2*$^{-/-}$ mice (P=0.0122), indicative of a repetitive behavior in the mutants. **C.** Latency to start exploring the maze by entering the first arm is higher in *Pfn2*$^{-/-}$ animals compared to wt controls (P=0.0409). n=11 wt, n=10 *Pfn2*$^{-/-}$ animals. Two-tailed t-test, *P≤0.05.

These data point to increased repetitive behavior and resistance to changes in the mutant mice.

2.1.9 Altered vocalization pattern in *Pfn2*$^{-/-}$ pups

Excessive crying has been frequently reported in infants that were later diagnosed with ASD. In newborn mice the crying behavior is an important type of communication

triggered by the separation distress and aimed at eliciting retrieval behavior by the mother. Rodents' communication mainly occurs through ultrasound vocalizations (USVs). Accordingly, in order to obtain the mother's attention, young mouse pups emit high frequency vocalization calls in the 30-110 MHz ultrasonic frequency range when separated from the nest. In 5-7 days old *Pfn2*$^{-/-}$ pups separated from the mother it was observed increased number of ultrasonic vocalizations compared to wt controls (Fig 2.12 A), similarly to what has been observed in other mouse models of autism (Scattoni *et al*, 2009; Tsai *et al*, 2012). Detailed analysis of the USV traces, revealed a more monotonous vocalization pattern in *Pfn2*$^{-/-}$ pups, with long (20-90 ms), sometimes interrupted calls in the lower range of US frequencies (<70-75 kHz) and rather flat in frequency modulation (example in Fig 2.12 B). *Pfn2*$^{-/-}$ male and female pups showed a 5 times median increase of this type of 'flat calls' compared to wt control littermates (Fig 2.12 C). In *Pfn2* mutants the 'flat calls' were often intense (<-50 dB, darker gray tone) and arranged in particularly long trains of uniformly spaced calls (regular inter-call interval of 150±10 ms). *Pfn2*$^{-/-}$ pups exhibited significantly higher number of long trains composed of more than 10 'flat calls' compared to wt control littermates (Fig 2.12 D). Moreover, about 50 % of *Pfn2* mutant pups exhibited one or more trains of more than 20 'flat calls', while none of the control mice showed this behavior. Vocalization patterns are usually complex, with 2-4 closely spaced calls (inter-call interval <50 ms) arranged in a "group", showing frequency variations and harmonics. It was observed increased "group" size and duration in both *Pfn2*$^{-/-}$ males and females compared to wt control littermates (Fig 2.12 E-F), further strengthening a 'despair calling' phenotype.

In summary, male and female *Pfn2*$^{-/-}$ pups showed increased number and monotony of US vocalizations, suggesting a higher level of despair similar to persistent crying of ASD diagnosed infants.

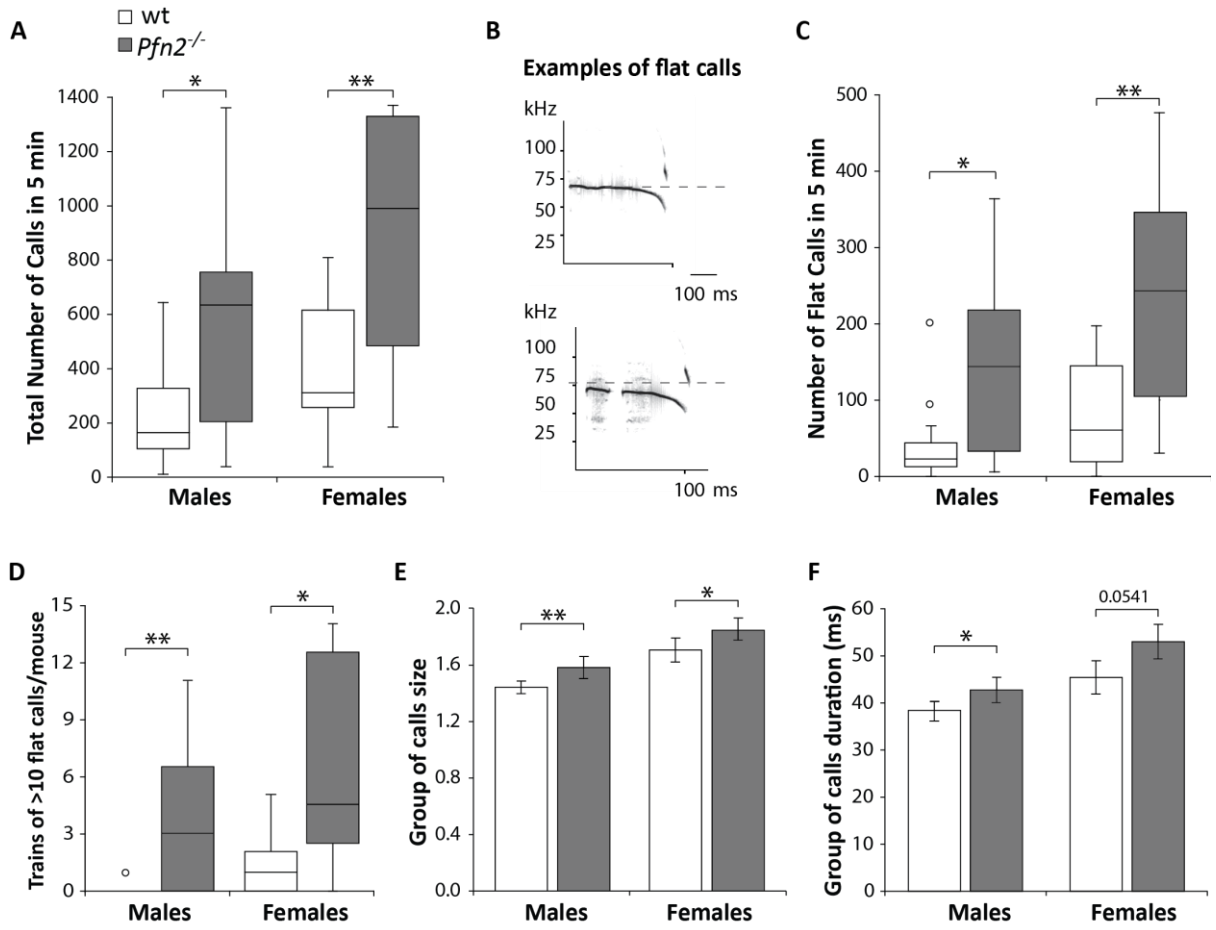

Figure 2.12 **|The ultrasonic vocalization pattern is altered in *Pfn2*$^{-/-}$ pups. A.** Box plot of the total number of US calls from P5-P7 *Pfn2*$^{-/-}$ and wt control pups separated from the nest in 5 min recording time. The median (horizontal black line in the box) for *Pfn2* mutant pups is about 3 times higher compared to wt controls (Rank-sum test, P=0.0390 for males and P=0.0066 for females). **B.** Graphic representation of two sample flat call traces from *Pfn2*$^{-/-}$ pups, one continuous and one interrupted. Note the quite uniform frequency below 70 kHz and the length (90-100 ms). **C.** Box plot of the number of flat calls from *Pfn2*$^{-/-}$ and wt control pups in 5 min recording time. The median for *Pfn2* mutant pups is about 5 times higher compared to controls (Rank-sum test, P=0.0231 for males; P=0.0037 for females). **D.** The number of trains with more than 10 flat calls per mouse is strongly increased in *Pfn2* mutants compared to wt controls (Rank-sum test, P= 0.0062 for males; P=0.0120 for females). **E.** The average size of the group of calls (number of shorter calls with inter-call time <50 ms) is increased in *Pfn2*$^{-/-}$ compared to wt control pups (t-test, P=0.0087 for males; P=0.0298 for females). **F.** The average duration of the group of calls is increased in *Pfn2*$^{-/-}$ compared to wt control pups (t-test, P=0.0351 for males; P=0.0542 for females). n=16 wt and n=11 *Pfn2*$^{-/-}$ males, n=13 wt and n=12 *Pfn2*$^{-/-}$ females. *P≤0.05, **P≤0.01.

2.1.10 Motor and coordination defects in *Pfn2*$^{-/-}$ mice

In addition to the core symptoms, impaired motor coordination is a hallmark of ASD (Fournier *et al*, 2010). *Pfn2*$^{-/-}$ mice showed mild but significant impairment of motor performance and coordination upon daily handling. Additionally, *Pfn2*$^{-/-}$ mice showed from early age (P10) the characteristic coordination deficit of clamping the hind legs when picked up by the tail instead of spreading them out (Supplementary Fig 7.1).

The basic motor performance was tested with a fixed rotation speed RotaRod paradigm, while coordination and motor learning were assessed by constantly increasing the rotation speed. In older *Pfn2* mutants motor performance and coordination were significantly impaired (Fig 2.13 A-B), while motor learning appeared unaffected, in agreement with previous results obtained with different learning paradigms (Pilo Boyl *et al.*, 2007). A mild gene dosage effect was observed in *Pfn2*$^{+/-}$

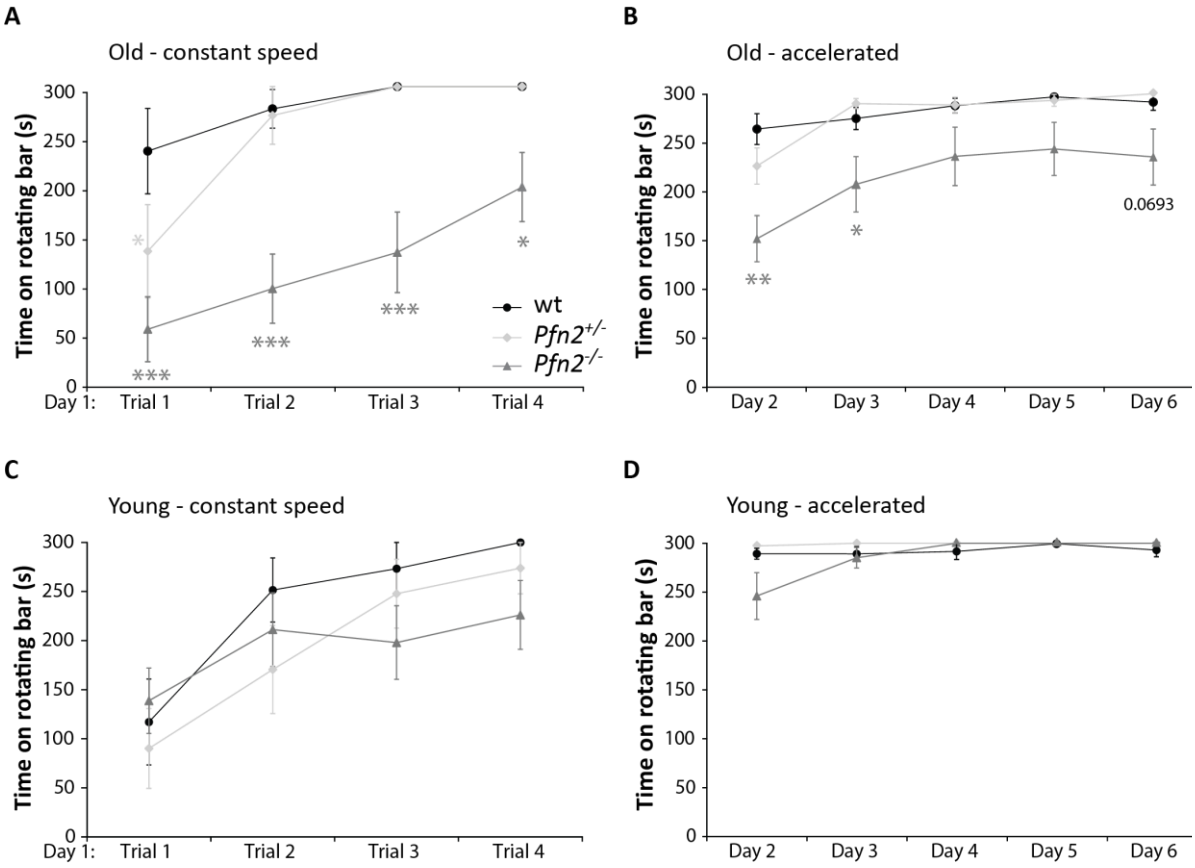

animals only on the first trial/day. Motor impairment of *Pfn2*$^{-/-}$ mice was age-dependent since younger mutant mice did not show significant deficits on the RotaRod (Fig 2.13 C-D). Coordination skills were further addressed with the Hanging test, which requires both muscle strength and coordination between the legs and the body. The Hanging test performance was impaired in both young (Fig 2.14 A) and older *Pfn2* mutant mice (Fig 2.14 B). In the group of older mice, the *Pfn2*$^{+/-}$ animals showed again a gene dosage-dependent intermediate phenotype. To discriminate between muscle strength and coordination, it was measured the grip strength of the forelimbs only and of all four limbs. Both *Pfn2*$^{-/-}$ and *Pfn2*$^{+/-}$ mice showed about 20 % less pulling strength with their forelegs (Fig 2.14 C, left). However, grip strength with all four legs was reduced only in *Pfn2* mutant mice (Fig 2.14 C, right), while *Pfn2*$^{+/-}$ animals were indistinguishable from wt controls. The coordination deficit in *Pfn2*$^{-/-}$ mice reproduces another common trait observed in a significant number of ASD patients.

Figure 2.13 **| Motor performance and coordination decreases with age in *Pfn2*$^{-/-}$ mice. A.** 6-8 months old *Pfn2*$^{-/-}$ mice showed lower performance on a RotaRod (constant speed, 3 rpm) than wt controls (two-way ANOVA with repeated measures, genotype effect $F(2,25)=19.09$, $P<0.0001$; Tukey's post-hoc test for *Pfn2*$^{-/-}$ vs wt control: Trial 1, P=0.0001; Trial 2. P=0.0001; Trial 3, P=0.0004; and Trial 4, P=0.0487). *Pfn2*$^{+/-}$ mice showed a motor deficit only in Trial 1 (P=0.0425). **B.** 6-8 months old *Pfn2*$^{-/-}$ mice showed lower performance on a RotaRod in an accelerated rotation paradigm (3-30 rpm in 300 s); (two-way ANOVA with repeated measures, genotype effect $F(2,25)=6.285$, P=0.0061; Tukey's post-hoc test for *Pfn2*$^{-/-}$ vs wt control: Day 2, P<0.0001; Day 3, P=0.0224; Day 6, P=0.0693). Notably, motor learning remained unaffected (Day effect $F(4,100)=22.68$, P<0.0001). **C.** In young mice (3-5 months) no significant differences were seen in *Pfn2*$^{-/-}$, *Pfn2*$^{+/-}$ and wildtype mice in the performance at constant speed, as well as **D.** in the accelerated Rotarod mode. Represented data are the average of the best of 3 performances of the day. Old mice, n=9 wt and *Pfn2*$^{-/-}$, n=10 *Pfn2*$^{+/-}$; young mice n=11 per genotype. *P≤0.05, **P≤0.01, ***P≤0.001.

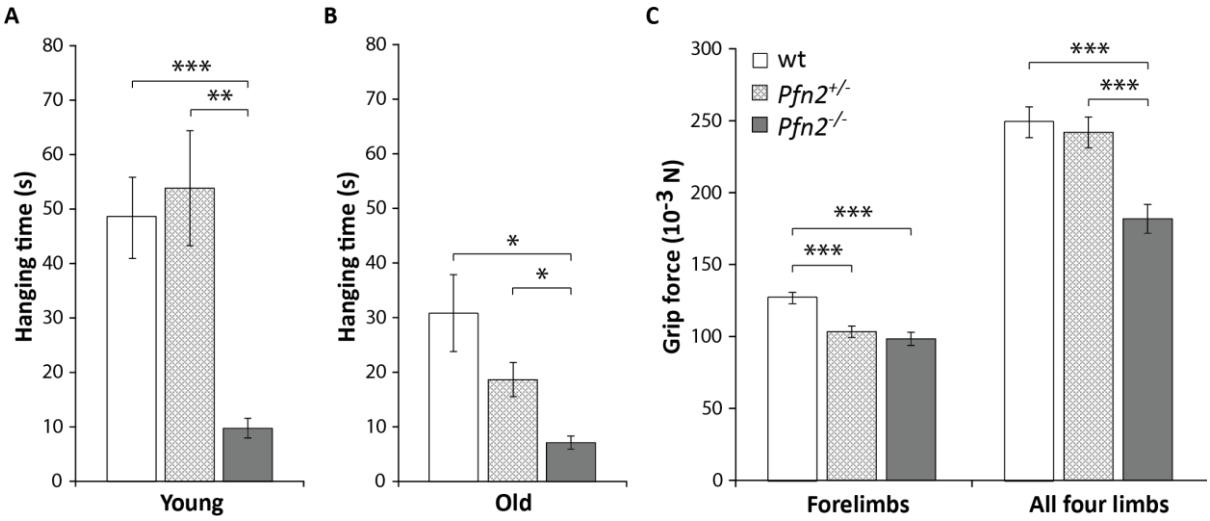

Figure 2.14 **| Limbs coordination and grip strength are reduced in *Pfn2*$^{-/-}$ mice. A.** In the Hanging test young (3-5 months) *Pfn2*$^{-/-}$ mice showed strong deficits compared to wt controls (t-test, P=0.0004) and *Pfn2*$^{+/-}$ mice (t-test, P=0.0018). **B.** Older mice (6-8 months) performed in general less well than young mice, but *Pfn2*$^{-/-}$ mutants again displayed significant coordination impairment compared to wt controls (t-test, P=0.0103) and to *Pfn2*$^{+/-}$ mice (t-test, P=0.0207). Heterozygous mice showed an age dependent loss of coordination ability. **C.** Grip strength with the forelegs was significantly reduced in *Pfn2*$^{-/-}$ mice (t-test, P<0.0001) as well as in *Pfn2*$^{+/-}$ mice (t-test, P<0.0001) compared to wt controls. When all 4 paws were used, only *Pfn2*$^{-/-}$ mice were found impaired (t-test, P=0.0003), while *Pfn2*$^{+/-}$ mice performed similarly to wt controls (t-test, P=0.0002 *Pfn2*+/- vs. *Pfn2*$^{-/-}$ mice). Same animals as in figure 2.13 were used. *P≤0.05, **P≤0.01, ***P≤0.001.

2.2 Distinct functions of profilin 1 and profilin 2 during embryonic brain development

The brain specific single ko of *Pfn1* (*Pfn1*$^{flx/flx}$*;Nes-Cre*$^{Cre/wt}$) highlighted the critical role of PFN1 in radial migration of CGNs but not in other aspects of cerebellar development, such as tangential migration, neuron proliferation or Bergmann glia morphology (Kullmann *et al.*, 2011; Kullmann *et al.*, 2012). On the contrary, the single *Pfn2* ko did not uncover any specific function of PFN2 during brain development, since brain morphology appeared unaltered in adult *Pfn2*$^{-/-}$ mice (Pilo Boyl *et al.*, 2007). In this second part of the thesis a conditional *Pfn1*$^{-/-}$*;Pfn2*$^{-/-}$ CNS double ko mouse line

was employed in order to investigate the specific and common functions of the two PFN isoforms in the development of the embryonic mouse brain.

2.2.1 PFN1 and PFN2 expression patterns differ during embryonic and postnatal brain development and in the adult brain

The brain expression levels of PFN1 and PFN2 were evaluated, by western blotting, in wt animals aged between embryonic day 10.5 and postnatal day 60. For E10.5 and E12.5 embryos the entire head was used, while from E15.5 up to P60 only the cortex was dissected. To facilitate the data visualization, the calibrated PFN1 and PFN2 protein levels at the different ages were normalized to the respective value at P1.

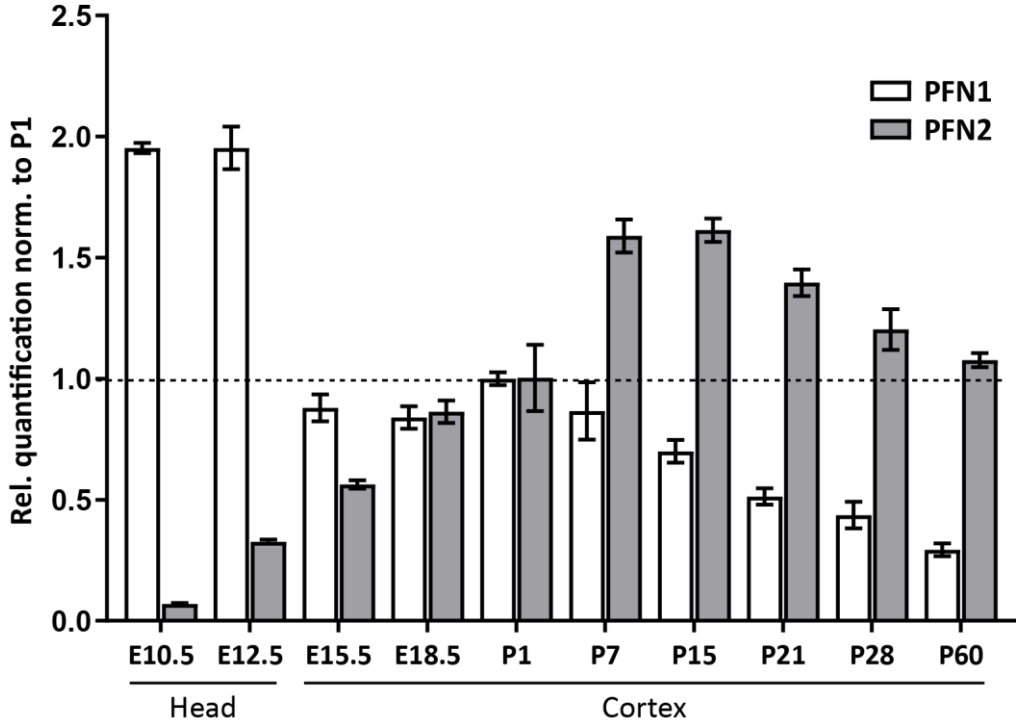

Figure 2.15 **| PFN1 and PFN2 protein expression patterns differ during embryonic-postnatal brain development and in the adult brain.** Relative quantification of PFN1 and PFN2 protein amounts in wt brains at different embryonic and adult ages normalized to post-natal day 1 (P1). PFN1 showed a different expression pattern compared to PFN2, appearing to be mostly needed during early embryonic brain development. On the contrary, PFN2 appears to be mostly required after birth, particularly at the time of synaptogenesis, and also in adulthood. n=3 samples per age. Error bars represent s.e.m.

PFN1 showed an inverse expression pattern compared to PFN2 (Fig 2.15). PFN1 expression was highest during earliest embryonic stages (E10.5 - E12.5), also as a result of the non-neuronal tissue contribution. Its expression remained stable from later embryonic stages (E15.5 - E18.5) until birth, pointing to its need during embryonic brain development. After birth PFN1 expression constantly decreased to lastly reach the lowest levels in adulthood (P60). On the contrary, PFN2 expression was lowest during brain patterning (E10.5), but constantly increased during embryonic brain development (E12.5 - E15.5 - E18.5 - P1) to peak at synaptogenesis (P7-P21). PFN2 expression pattern indicates its requirement for synaptic physiology and synaptic plasticity because, unlike PFN1, its expression stabilizes on quite high levels in adulthood.

2.2.2 Profilin mutants to study embryonic brain development

The differential expression pattern of the two profilins and the diverse phenotype of the single *Pfn1* and *Pfn2* ko mouse models pose many questions on PFNs specific and redundant functions during brain development.

In this section of the thesis, to understand whether brain development could still be preserved in absence of more than two *Pfn* alleles, a $Pfn1^{flx/del};Pfn2^{-/-};Nes\text{-}Cre^{cre/wt}$ brain-specific double ko mouse line was generated. In this mouse model, while the deletion of *Pfn2* was systemic, complete deletion of *Pfn1* occurred only in NPCs (i.e. radial glia) starting around E9.5 (Zimmermann *et al.*, 1994). This mid-embryonic CNS-*Pfn1* and germ line-*Pfn2* concomitant deletion resulted in embryonic lethality, therefore embryos at different gestational stages after the double deletion occurred were analyzed, specifically at E11.5, E14.5, and E16.5.

The genotypes listed in table 2.2, expressing a different allele dosage of *Pfn1* and *Pfn2*, were analyzed.

Table 2.2 *Pfn1-Pfn2* mutants for the study of the developmental function of profilins

Genotype	Given name	*Pfn* allele dosage
$Pfn1^{flx/wt};Pfn2^{+/+};Nes\text{-}Cre^{wt/wt}$	Wt	4 *Pfn* alleles
$Pfn1^{flx/del};Pfn2^{-/-};Nes\text{-}Cre^{wt/wt}$	$Pfn1^{+/-};Pfn2^{-/-}$	1 *Pfn1* allele
$Pfn1^{flx/del};Pfn2^{+/-};Nes\text{-}Cre^{cre/wt}$	$Pfn1^{-/-};Pfn2^{+/-}$	1 *Pfn2* allele
$Pfn1^{flx/del};Pfn2^{-/-};Nes\text{-}Cre^{cre/wt}$	$Pfn1^{-/-};Pfn2^{-/-}$	0 *Pfn* alleles

Deletion of *Pfn1* should occur around E9.5 (Zimmermann *et al.*, 1994), for this reason the earliest developmental stage analyzed was E11.5, expecting a consistent loss of PFN1. Therefore, the expression level of PFN1, as well as of PFN2, was analyzed in E11.5 wt and profilin mutant embryos. At this developmental stage it was not possible to isolate the brain, therefore to obtain an evaluation of the protein content specifically for the cerebral region, the entire head of the embryo was separated from the rest of the body and total tissue lysates were prepared from the four different genotypes: wt, $Pfn1^{+/-};Pfn2^{-/-}$, $Pfn1^{-/-};Pfn2^{+/-}$ and $Pfn1^{-/-};Pfn2^{-/-}$. Consequently, a complete loss of PFN1 was not expected, due to the high contribution of PFN1 from non-neuronal tissue.

In figure 2.16 A and B are reported the relative expression levels of PFN1 and PFN2, respectively, in the different mutant embryos normalized to the wildtype levels. At E11.5, PFN1 expression was lowered to ~40 % in $Pfn1^{+/-};Pfn2^{-/-}$ embryos, bearing one *Pfn1* allele in the CNS, and to approximately 25 % in $Pfn1^{-/-};Pfn2^{+/-}$ embryos and to a similar level in $Pfn1^{-/-};Pfn2^{-/-}$ embryos, the latter two genotypes with a CNS conditional deletion of *Pfn1* (Fig 2.16 A). The residual PFN1 signal still visible in the CNS-restricted *Pfn1* ko embryos likely derives from the cartilage, skin and other tissues present in the embryo head.

PFN2 expression in E11.5 embryos was reduced to ~40 % in $Pfn1^{-/-};Pfn2^{+/-}$ embryos, carrying only one allele of *Pfn2*, and was completely missing in *Pfn2* ko embryos (Fig 2.16 B), as expected in a complete ko model.

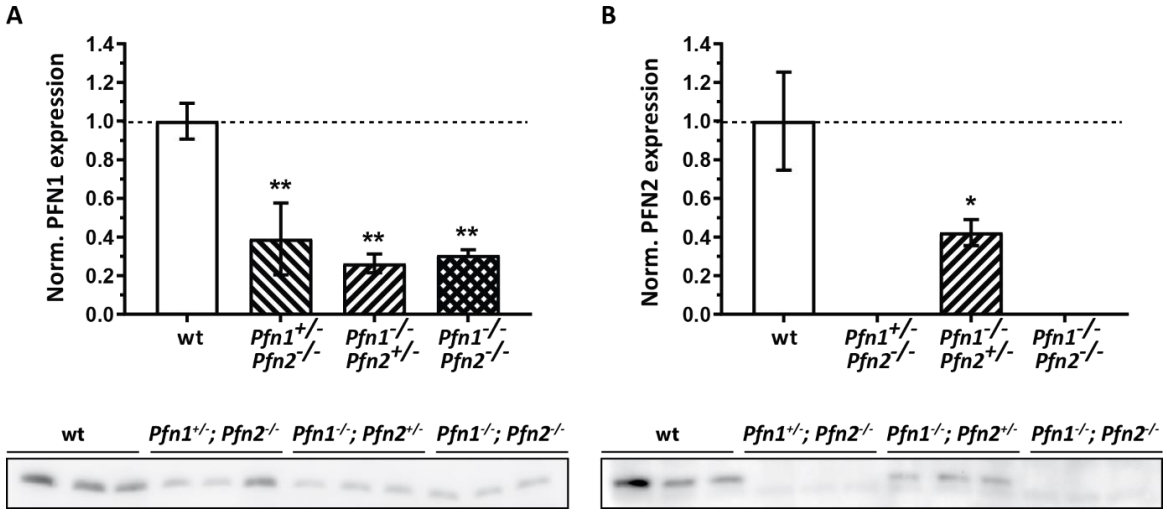

Figure 2.16 **| PFN1 and PFN2 protein expression in E11.5 mutant embryos reflects the genotype. Top.** Normalized relative quantification graphs of PFN1 (**A**) and PFN2 (**B**) protein levels of E11.5 embryo heads from different genotypes. **Top A.** The PFN1 protein signals from mutant embryos were normalized to the wt. PFN1 levels were reduced to 39 % in *Pfn1*$^{+/-}$*;Pfn2*$^{-/-}$ (*Pfn1-flx;Nes*-Cre) embryos (P=0.010), expressing only one allele of *Pfn1*; while *Pfn1*$^{-/-}$*;Pfn2*$^{+/-}$(P=0.003) and *Pfn1*$^{-/-}$*;Pfn2*$^{-/-}$ (*Pfn1-flx;Nes*-Cre) embryos (P=0.005), not expressing any *Pfn1* allele, have even lower PFN1 levels. The residual PFN1 signal still visible in *Pfn1* ko embryos derives from the contribution of the other tissues which are part of the embryo head. **Top B.** PFN2 protein signals from mutant embryos were normalized to the wt. PFN2 levels were reduced to 42 % in *Pfn1*$^{-/-}$*;Pfn2*$^{+/-}$ (*Pfn1-flx;Nes*-Cre) embryos (P=0.036), expressing only a single allele of *Pfn2*; while no PFN2 expression was detected in *Pfn1*$^{+/-}$*;Pfn2*$^{-/-}$ and *Pfn1*$^{-/-}$*;Pfn2*$^{-/}$ (*Pfn1-flx;Nes*-Cre) embryos, not containing any allele of *Pfn2*. **Bottom.** Below the graphs are shown the western blots for PFN1 (**A**) and PFN2 (**B**). n=3 embryos per genotype. Error bars represent s.e.m. One-way ANOVA - Dunnett's test, *P≤0.05, **P≤0.01.

2.2.3 Morphological and histological studies of profilin mutant embryos

At E11.5 the *Pfn1*$^{-/-}$*;Pfn2*$^{-/-}$ double ko embryos were not distinguishable from wt littermates in their external appreance (Fig 2.17 A). At later developmental stages, E14.5 (Fig 2.17 B) and E16.5 (Fig 2.17 C)., the head was smaller in size and at E16.5 the cerebral cortex had a translucent appearance, suggesting a defect in cortical development. *Pfn1*$^{-/-}$*;Pfn2*$^{-/-}$ double ko embryos did not show any other obvious alteration and no difference was observed in their body size compared to wildtypes.

Figure 2.17 | **wt and *Pfn1*$^{-/-}$;*Pfn2*$^{-/-}$ (*Pfn1-flx;Nes*-Cre) mutant embryos at different developmental stages.** Bright field images of wt and *Pfn1*$^{-/-}$;*Pfn2*$^{-/-}$ embryos at **A.** E11.5, **B.** E14.5 and **C.** E16.5. Scale bar: 2 mm.

2.3.4 PFN1 and PFN2 have distinct roles in brain development and in the formation of the cortical layers

Coronal and sagittal sections from the embryos were stained with hematoxylin and eosin (H&E) for histological analysis and with antibodies against specific proteins in order to obtain information regarding the functions of PFN1 and PFN2 during embryonic development.

Analysis of the embryos at E11.5

Sagittal H&E sections from E11.5 *Pfn1*$^{-/-}$;*Pfn2*$^{-/-}$ embryos were compared to sections from wt littermates, matching as many body structures as possible. As observed in figure 2.18, at E11.5 the development of the double mutant embryo was not visibly altered compared to wildtype; in fact, forebrain, midbrain and hindbrain vesicles were clearly observed also in *Pfn1*$^{-/-}$;*Pfn2*$^{-/-}$ embryos.

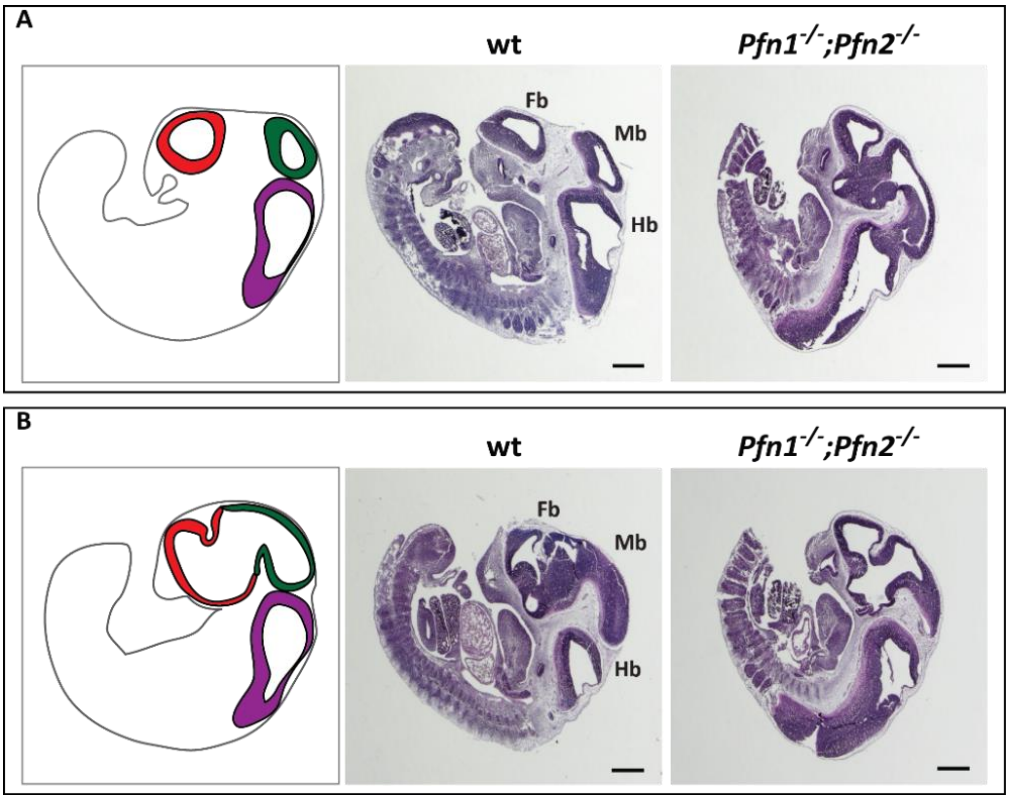

Figure 2.18 **| Sagittal sections of E11.5 wt and *Pfn1*$^{-/-}$;*Pfn2*$^{-/-}$ (*Pfn1-flx;Nes*-Cre) embryos stained with H&E. A-B (left).** Schematic representations of two different section planes of the entire embryo. **A-B (right).** Corresponding embryonic H&E stained sections. In the wt image different brain regions are indicated: Fb, forebrain (red in A-C); Mb, midbrain (green in A-C); Hb, hindbrain (violet in A-C). Scale bar: 1 mm.

Analysis of the embryos at E14.5

Since no morphological alteration could be detected at E11.5 in *Pfn1*$^{-/-}$;*Pfn2*$^{-/-}$ embryos, detailed studies were performed at later stages of development. In addition to the double mutant, also intermediate genotypes expressing a single allele of either *Pfn1* or *Pfn2* were analyzed.

Sagittal sections from wt, *Pfn1*$^{+/-}$;*Pfn2*$^{-/-}$, *Pfn1*$^{-/-}$;*Pfn2*$^{+/-}$ and *Pfn1*$^{-/-}$;*Pfn2*$^{-/-}$ embryos at E14.5 were stained with hematoxylin and eosin (Fig 2.19). Comparable sections were chosen based on topographic array of oral cavities and craniofacial features. Relevant structures (forebrain, midbrain and hindbrain) are labeled in the schemes for orientation and to facilitate comparison.

Compared to the development and morphology of E14.5 control brain (Fig 2.19 A-I), the brain structure of *Pfn1*$^{+/-}$;*Pfn2*$^{-/-}$ embryos (Fig 2.19 A-II), with only one *Pfn1* allele, was not altered. Interestingly, the structure of the forebrain appeared compromised, instead, in *Pfn1*$^{-/-}$;*Pfn2*$^{+/-}$ embryos (Fig 2.19 A-III) expressing a single allele of *Pfn2*, with the cortical layers in the isocortex being not fully established (Fig 2.19 B, compare I and III). All brain structures, forebrain, midbrain and hindbrain, were impaired in *Pfn1*$^{-/-}$; *Pfn2*$^{-/-}$ double ko embryos (Fig 2.19 A-IV).

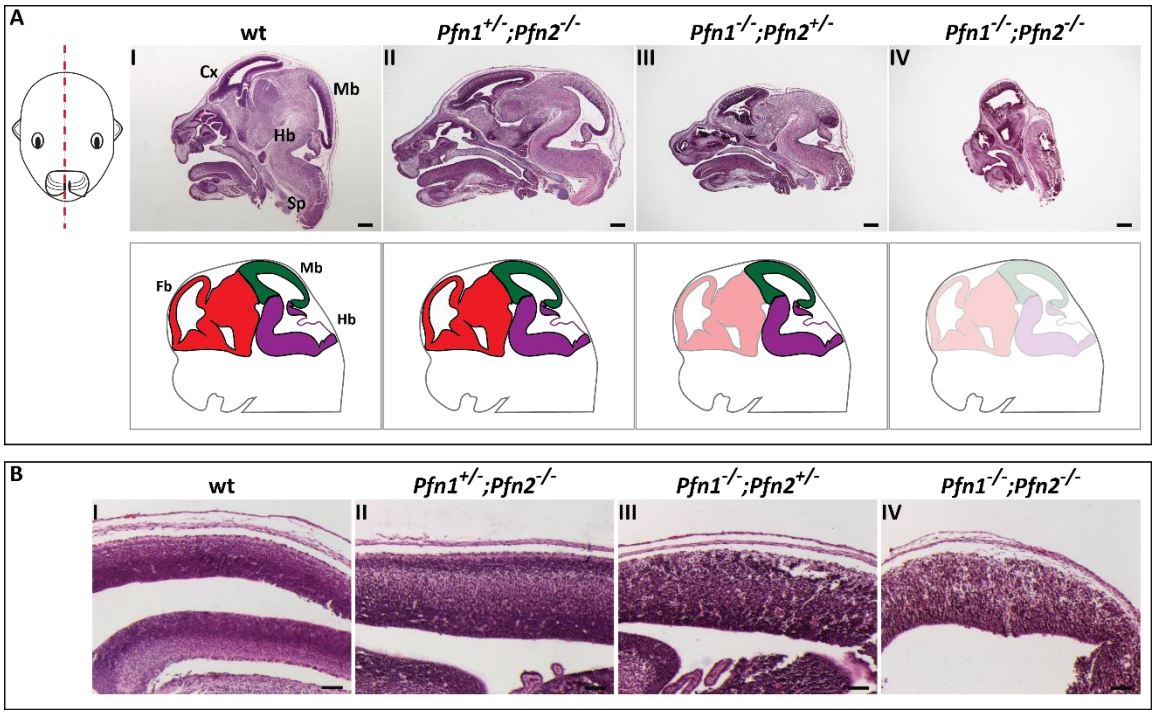

Figure 2.19 | **Sagittal sections of E14.5 embryo heads stained with H&E. A (top-left).** Schematic position of the section plane used for the comparison between different genotypes. **A (top-right).** H&E stained sections from four different genotypes. **A (bottom-right).** Schematic representations of the CNS regions found in the genotypes, specified on top: transparency indicates reduction or loss of the region. *Pfn1*$^{-/-}$;*Pfn2*$^{-/-}$ (*Pfn1-flx;Nes*-Cre) embryos heads showed severe morphological malformation, none of the different brain regions was recognizable and the whole head appeared compressed and collapsed**,** due to the absence of the internal brain structures (**A-IV**). In the wt image different brain regions are indicated: Cx, cortex; Fb, forebrain; Mb: midbrain; Hb, Hindbrain; Sp, spinal cord. Scale bar: 1 mm. **B.** Higher magnification of the anterior cortical region, also defined in the text as isocortex. Scale bar: 200 µm.

For confirmation, the morphology of E14.5 *Pfn1*$^{-/-}$;*Pfn2*$^{-/-}$ double mutant embryos was compared to controls also in coronal sections (Supplementary Fig 7.2). And the severe

impairment in the formation of all the three main brain regions (forebrain, midbrain and hindbrain) was confirmed.

Analysis of the embryos at E16.5

Morphological studies were extended to E16.5 embryonic heads. Sagittal (Fig 2.20) and coronal (Supplementary Fig 7.3) sections from control and mutant heads were compared to study the evolution of the developmental defects. Comparable sections were chosen with the same approach as for E14.5 studies.

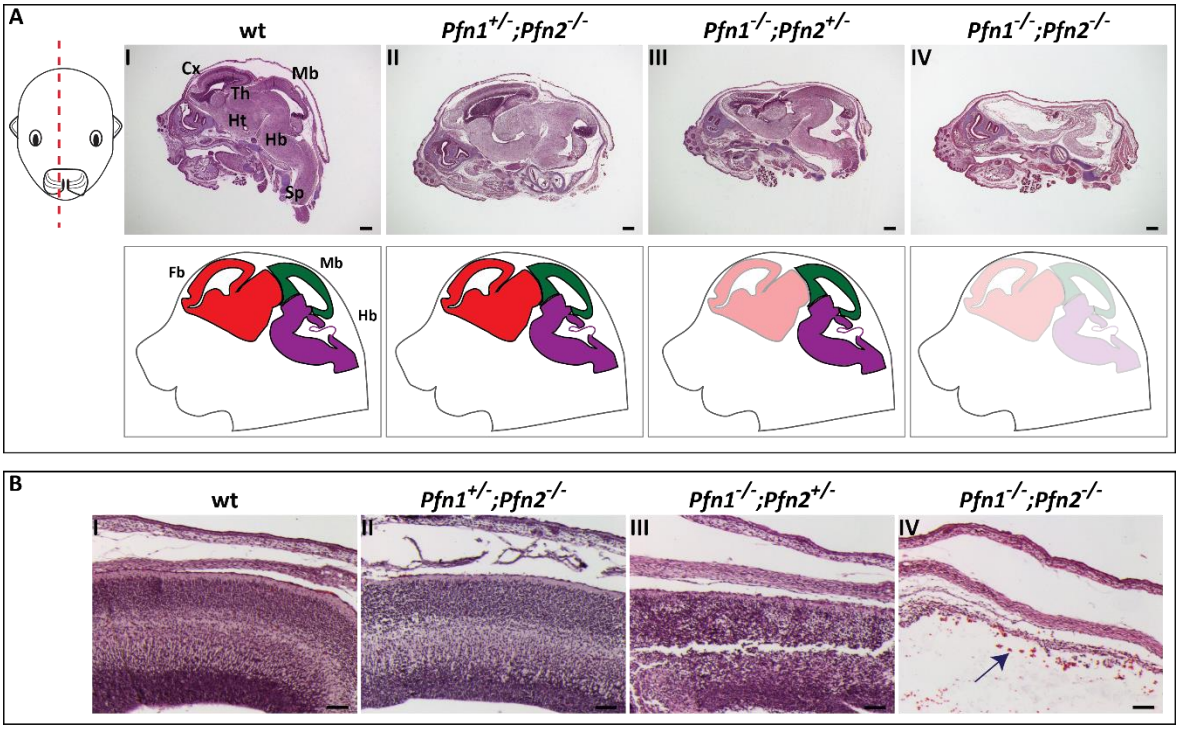

Figure 2.20 | **Sagittal sections of E16.5 embryo heads stained with H&E. A (top-left).** Schematic position of the section plane used for the comparison between different genotypes. **A (top-right).** H&E stained sections from four different genotypes. **A (bottom-right).** Schematic representations of the CNS regions found in the genotypes, specified on top: transparency indicates reduction or loss of the region. *Pfn1*$^{-/-}$*;Pfn2*$^{-/-}$ (*Pfn1-flx;Nes*-Cre) embryo heads showed severe morphological malformation, none of the different brain regions was recognizable (**A-IV**). In the wt image different brain regions are indicated: Cx, cortex; Fb, forebrain; Mb, midbrain; Hb, Hindbrain; Th, thalamus; Ht, hypothalamus; Sp, spinal cord. Scale bar: 1 mm. **B.** Higher magnification of the anterior cortical region, also defined in the text as isocortex. In *Pfn1*$^{-/-}$*;Pfn2*$^{-/-}$ (*Pfn1-flx;Nes*-Cre) embryos, the arrow points to the region where the isocortex should have been located (**B-IV**). Scale bar: 200 µm.

Similarly to E14.5, the brain structure of E16.5 *Pfn1*$^{+/-}$;*Pfn2*$^{-/-}$ embryos (Fig 2.20 A-I), expressing a single *Pfn1* allele, was comparable to controls and not altered (small differences are due to a not perfect sagittal cut). In the *Pfn1*$^{-/-}$;*Pfn2*$^{+/-}$ (Fig 2.20 A-III) and *Pfn1*$^{-/-}$;*Pfn2*$^{-/-}$ (Fig 2.20 A-IV) brains the defects which could already be observed at E14.5 became more evident. The structure of the prosencephalon in *Pfn1*$^{-/-}$;*Pfn2*$^{+/-}$ embryos, expressing a single *Pfn2* allele, was collapsed and smaller in size (Fig 2.20 A-III), and cells were not aligning in the typical layered structure of the isocortex as in control animals (Fig 2.20 B, compare I and III). In the *Pfn1*$^{-/-}$;*Pfn2*$^{-/-}$ double mutant embryos the brain structure was completely missing leaving an empty cavity underneath the skull (Fig 2.20 A-IV, and cf. Fig 2.17 C); indeed, no isocortex could be identified (Fig 2.20 B-IV).
Coronal sections, of chosen planes, from wt and *Pfn1*$^{-/-}$;*Pfn2*$^{-/-}$ double mutant E16.5 embryonic heads were also compared for morphology (Supplementary Fig 7.3), confirming the absence of the brain structures in the double mutant.

In conclusion, the expression of one *Pfn1* allele is sufficient to ensure proper brain development; on the contrary, with the expression of one *Pfn2* allele the development of the forebrain, in particular the isocortex, is compromised. Lastly, without any profilin allele no brain structure develops.

2.2.5 Loss of PFN1 or both profilins causes alterations in cell proliferation

The previous morphological studies highlighted a gross defect in brain development of *Pfn1*$^{-/-}$;*Pfn2*$^{-/-}$ double ko embryos. The complete lack of brain tissue observed at E16.5 might be due to impaired cell proliferation or neuronal differentiation during early developmental stages. To distinguish between the two biological processes, the presence of the first differentiated neurons on the pial surface of the brain and cell proliferation in the ventricular zone (VZ) were studied in E11.5 embryos using specific markers.

ß-III tubulin is a widely used neuronal marker. It is a tubulin involved in differentiation of neuronal cell types; its expression accumulates in cell bodies, dendrites, axons and axonal terminations of mature and immature neurons (Roskams *et al.*, 1998; Lee *et al*, 1990).

Histone H3 is one of the five histone proteins involved in chromatin structure of eukaryotic cells. Phosphorylation of serine in position 10 on H3 (pH3) is coupled to chromosome condensation during mitosis and therefore commonly serves as a proliferation marker (Kim *et al.*, 2017; Elmaci *et al.*, 2018).

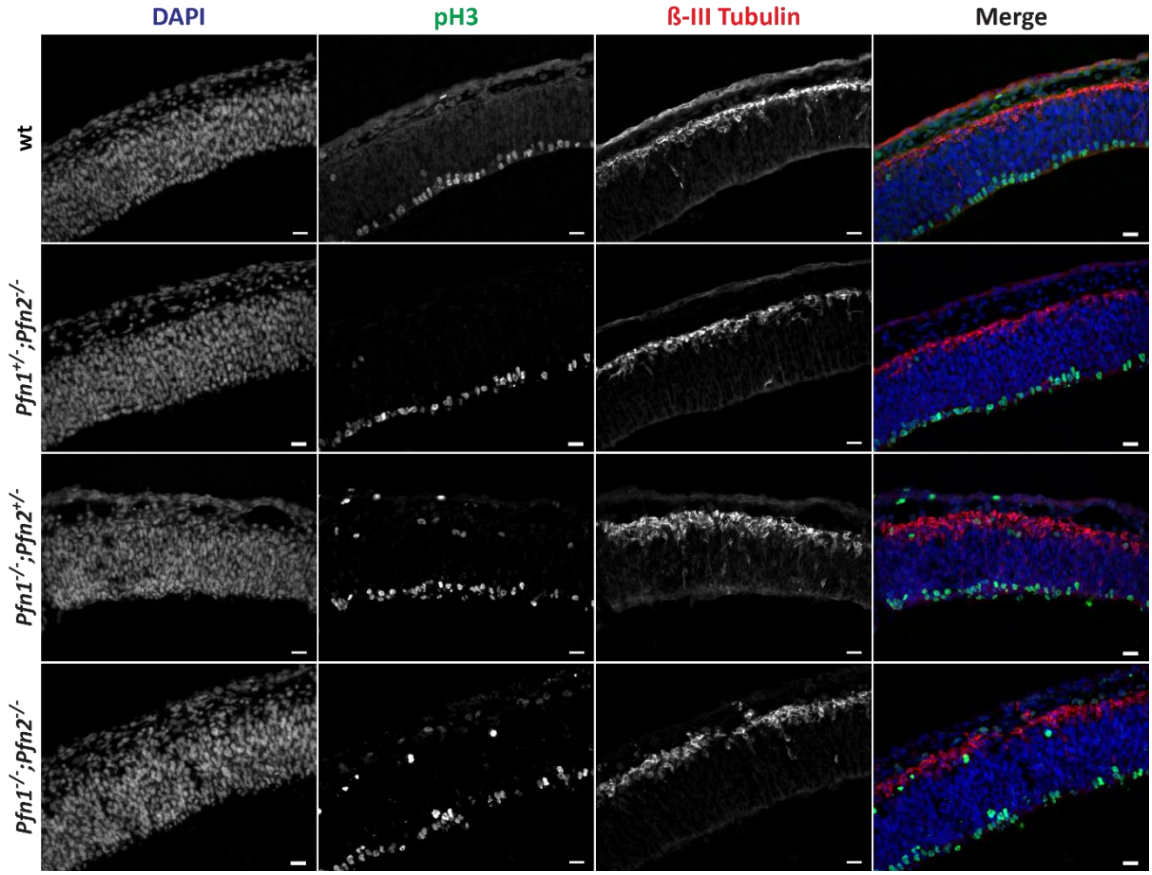

Figure 2.21 **| Altered VZ organization in the forebrain of *Pfn1*$^{-/-}$;*Pfn2*$^{-/-}$ (*Pfn1-flx;Nes*-Cre) E11.5 embryos.** Immunofluorescence staining on matched cryo-sections from wt, *Pfn1*$^{+/-}$;*Pfn2*$^{-/-}$, *Pfn1*$^{-/-}$;*Pfn2*$^{+/-}$ and *Pfn1*$^{-/-}$;*Pfn2*$^{-/-}$ embryos. In the merge picture: in blue is shown the DAPI staining, in green pH3 and in red ß-III Tubulin. The VZ of wt and *Pfn1*$^{+/-}$;*Pfn2*$^{-/-}$ embryos is composed by a layer of pH3+ cells linearly organized. Contrarily, in the VZ of *Pfn1*$^{-/-}$;*Pfn2*$^{+/-}$ and *Pfn1*$^{-/-}$;*Pfn2*$^{-/-}$ embryos, where PFN1 is not expressed, misalignment is observed, as well as ectopic pH3 expression. Scale bar: 20 µm.

Immunofluorescence staining of ß-III tubulin and pH3 was performed on cryo-sections from wt, *Pfn1*$^{+/-}$;*Pfn2*$^{-/-}$, *Pfn1*$^{-/-}$;*Pfn2*$^{+/-}$ and *Pfn1*$^{-/-}$;*Pfn2*$^{-/-}$ embryos at the developmental stage E11.5 (Supplementary Fig 7.4). From each embryo two different regions were analyzed in detail: the pallium located in the forebrain (Fig. 2.21), which later gives rise to the cortical structures; and the superior colliculus, lying on the roof of the midbrain (Supplementary Fig 7.5).

In the forebrain no difference was observed in the ß-III tubulin staining. In both wt and mutant embryos a layer of newly differentiated ß-III tubulin-positive neurons could be found in the mantle zone of the pallium. Instead, in the VZ of the pallium an alteration could be detected in the pH3 staining. In control and *Pfn1*$^{+/-}$;*Pfn2*$^{-/-}$ embryos a single layer of well-ordered and aligned pH3-positive cells was visible, whereas in *Pfn1* ko embryos (*Pfn1*$^{-/-}$;*Pfn2*$^{+/-}$ and *Pfn1*$^{-/-}$;*Pfn2*$^{-/-}$) pH3-positive cells were not linearly organized and were ectopically expressed in other layers (Fig 2.21). The increased pH3-positive cell number and their ectopic expression was more pronounced in in *Pfn1*$^{-/-}$;*Pfn2*$^{-/-}$ double ko embryos.

A quantitative analysis showed that the number of pH3-positive cells is significantly higher in *Pfn1*$^{-/-}$;*Pfn2*$^{-/-}$ double ko embryos (Fig 2.22 A). Indeed, the majority of cells, in double ko embryos, appeared to have condensed chromatin, while in control embryos a significant number of cells with polarized, segregating chromosomes was detected, as shown by the quantitative analysis of mitotic figures (2.22 B). In wt control embryos, 19.4 % of pH3-positive cells in the VZ showed segregating chromosomes, while in *Pfn1*$^{-/-}$;*Pfn2*$^{-/-}$ embryos only 9.5 % were counted.

The same result was observed in the VZ of the superior colliculus in the roof of the midbrain. Also, in this region, the number of pH3-positive cells was significantly higher in *Pfn1*$^{-/-}$;*Pfn2*$^{-/-}$ double ko embryos (Fig 2.23 A). Moreover, in control embryos 17.5 % of pH3-positive cells in the VZ displayed segregating chromosomes, while in *Pfn1*$^{-/-}$;*Pfn2*$^{-/-}$ double ko embryos only 10.8 % were found (2.23 B).

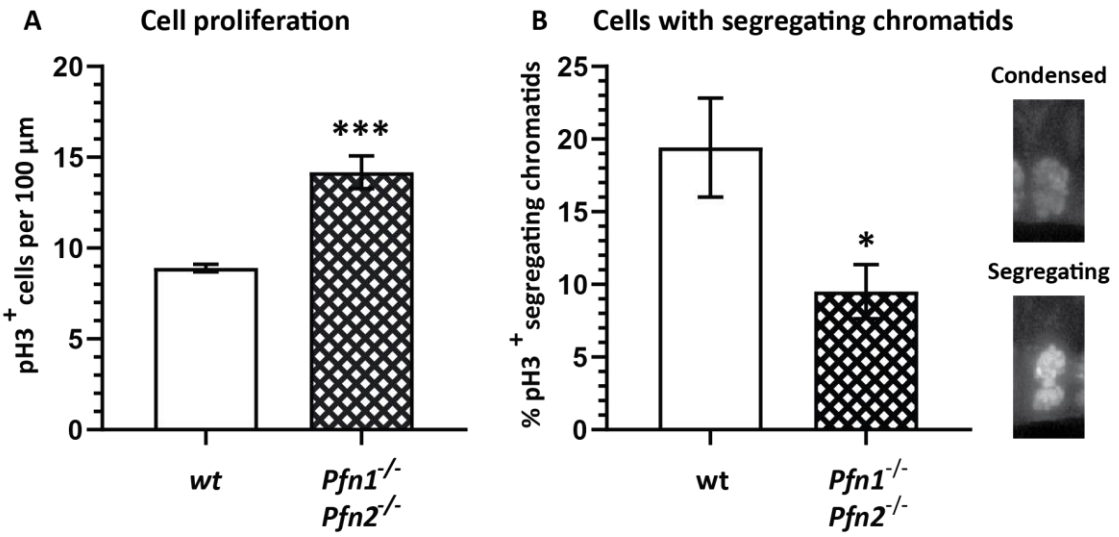

Figure 2.22 |**Increased cell proliferation and altered cell cycle progression in the forebrain of *Pfn1*$^{-/-}$;*Pfn2*$^{-/-}$ (*Pfn1-flx;Nes*-Cre) embryos. A.** In the VZ of the forebrain the density of pH3+ cells (n. cells/100 µm) is increased in *Pfn1*$^{-/-}$;*Pfn2*$^{-/-}$ (14.17 ± 0.89) compared to wt (8.91 ± 0.20) embryos (P<0.001). **B.** The percentage of pH3+ cells with segregating chromatids is decreased in *Pfn1*$^{-/-}$;*Pfn2*$^{-/-}$ (9.5 ± 1.87) compared to wt (19.42 ± 3.40) embryos (P=0.016). On the right, sample images of condensed (top) and segregating (bottom) chromatids are shown. n=3 embryos per genotype. Error bars represent s.e.m. Two-tailed t-test, *P≤0.05, ***P≤0.001

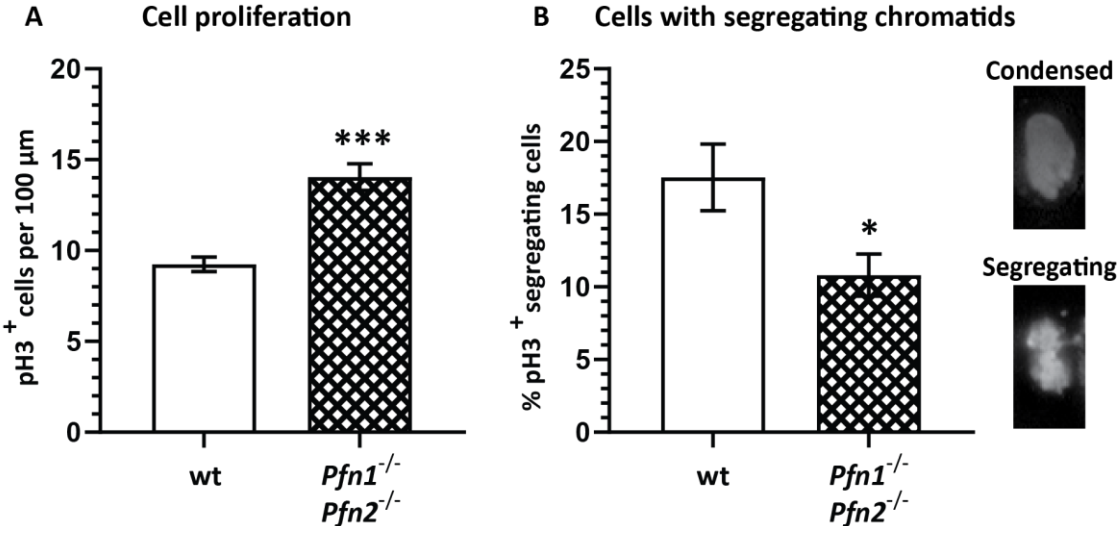

Figure 2.23 | **Increased cell proliferation and altered cell cycle progression in the midbrain of *Pfn1*$^{-/-}$;*Pfn2*$^{-/-}$ (*Pfn1-flx;Nes*-Cre) embryos. A.** In the VZ of the midbrain the density of pH3+ cells (n. cells/100 µm) is increased in *Pfn1*$^{-/-}$;*Pfn2*$^{-/-}$ (14.05 ± 0.73) compared to wt (9.50 ± 0.40) embryos (P<0.001). **B.** The percentage of pH3+ cells with segregating chromatids is decreased in *Pfn1*$^{-/-}$;*Pfn2*$^{-/-}$ (10.81 ± 1.45) compared to wt (17.52 ± 2.29) embryos (P=0.021). On the right, sample images of condensed (top) and segregating (bottom) chromatids are shown. n=3 embryos per genotype. Error bars represent s.e.m. Two-tailed t-test, *P≤0.05, ***P≤0.001.

Additionally, phosphorylated H3 levels were measured in total protein extracts obtained from E11.5 embryonic heads of the four genotypes shown in immunofluorescence. In embryos lacking PFN1, and in particular in *Pfn1*$^{-/-}$;*Pfn2*$^{-/-}$ double mutants, a significant increase of pH3 levels was observed (Fig 2.24 A), supporting the data from immunostaining. This result was further strengthened by studying a different marker, the TPX2 microtubule nucleation factor. TPX2 is a major spindle assembly factor required for normal assembly of mitotic spindles, through the activation of the Aurora A kinase (Wei *et al.*, 2015). It is specifically needed in the G2/M cell cycle transition; therefore, it labels cells entering mitosis. The expression of TPX2 was significantly increased in *Pfn1*$^{-/-}$;*Pfn2*$^{-/-}$ double ko embryos and it was also higher in *Pfn1*$^{-/-}$;*Pfn2*$^{+/-}$ embryos (Fig 2.24 B), interestingly the two genotypes lacking PFN1.

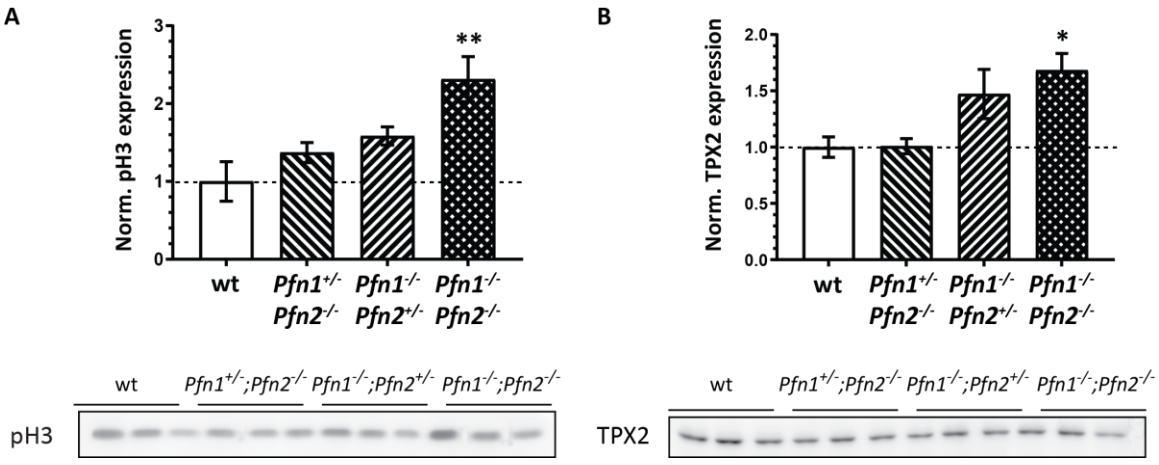

Figure 2.24 | **Increased proliferation in *Pfn1*$^{-/-}$;*Pfn2*$^{-/}$ (*Pfn1-flx;Nes*-Cre) embryos. A.** Normalized relative quantification of pH3 signals from protein extracts of E11.5 embryo heads showed significantly increased levels of histone H3 phosphorylation in *Pfn1*$^{-/-}$;*Pfn2*$^{-/-}$ double mutants (2.31 ± 0.29) compared to wt (1.00 ± 0.25) (P=0.004). Modest but not significant increase was also observed in *Pfn1*$^{+/-}$;*Pfn2*$^{-/-}$(1.37 ± 0.13, P=0.428) and *Pfn1*$^{-/-}$;*Pfn2*$^{+/-}$ (1.58 ± 0.12, P=0.178) embryos. **B.** Normalized relative quantification of TPX2 signals from protein extracts of E11.5 embryo heads showed significantly increased levels of TPX2 in *Pfn1*$^{-/-}$;*Pfn2*$^{-/-}$ double mutants (1.78 ± 0.15) compared to wt (1.00 ± 0.09) (P=0.025). While no difference was detected in *Pfn1*$^{+/-}$;*Pfn2*$^{-/-}$ embryos (1.01 ± 0.07, P=0.999) carrying only one *Pfn1* allele, a modest but not significant increase was detected in *Pfn1*$^{-/-}$;*Pfn2*$^{+/-}$ embryos (1.47 ± 0.22, P=0.114) carrying only one *Pfn2* allele. **Bottom.** Below the graphs are shown the western blots for H3 -pSer10 (**A**) and TPX2 (**B**). n=3 embryos per genotype. Error bars represent s.e.m. One-way ANOVA - Dunnett's test, *P≤0.05, **P≤0.01.

These experiments suggest the presence of an increased number of cells in the G2/M phase of mitosis in *Pfn1*$^{-/-}$;*Pfn2*$^{-/-}$ double ko embryos. Furthermore, in *Pfn1*$^{-/-}$;*Pfn2*$^{-/-}$ double ko embryos and *Pfn1*$^{-/-}$;*Pfn2*$^{+/-}$ embryos, both expressing no PFN1, cells in G2/M phase were observed ectopically in the region comprehended between the VZ and the pial surface or in close proximity to the pial surface (in the neuronal cell layer).

2.2.6 Cell cycle progression is regulated by profilins

The increased number of cells entering mitosis observed in *Pfn1*$^{-/-}$;*Pfn2*$^{-/-}$ double ko embryos could be due to alterations in cell cycle progression.

The entry of eukaryotic cells into mitosis (M phase) is regulated by the activation of the Cdc2 kinase (also called cyclin-dependent kinase 1, CDK1). The activation of this kinase is regulated first by dephosphorylation on threonine 14/tyrosine 15 and subsequently by phosphorylation on threonine 161 (Norbury *et al.*, 1991; Desai *et al.*, 1992). Given the importance of this kinase in the regulation of cell cycle progression, levels of CDK1 phosphorylated on tyrosine 15 (CDK1-pTyr15) were determined by semi-quantitative western blot.

E11.5 brains lacking both profilins showed significantly higher levels of CDK1-pTyr15 (~50 % increase, Fig 2.25 A). Levels of CDK1 phosphorylated on threonine 161 were accordingly reduced by 30 % in double ko embryos, although without reaching statistical significance (Fig 2.25 B). No significant alterations were detected in the other genotypes.

The decreased levels of CDK1 phosphorylated on Thr161 and especially the higher phosphorylation of CDK1 on Thy15 indicate that in *Pfn1*$^{-/-}$;*Pfn2*$^{-/-}$ double ko embryos NPCs are impaired to enter the M phase and progress in the cell cycle.

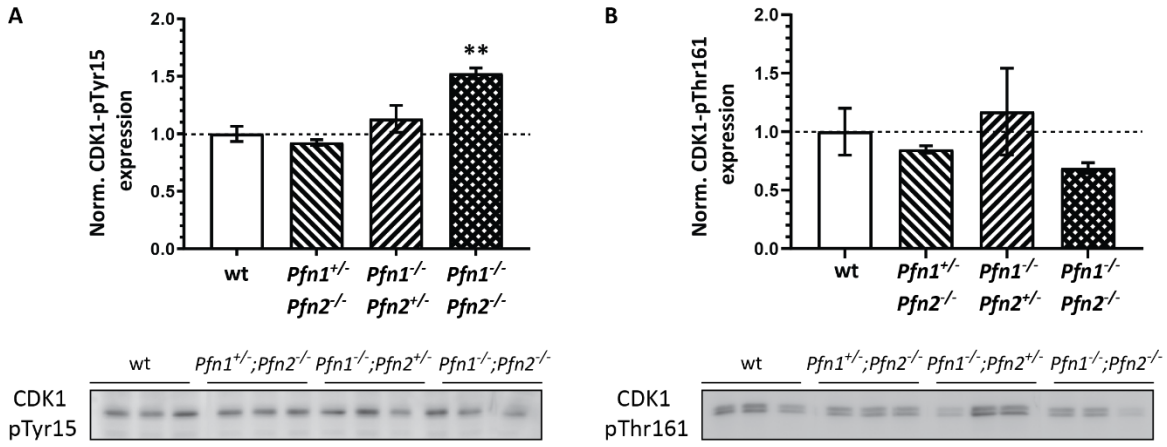

Figure 2.25 | **Cell cycle progression is impaired in *Pfn1*$^{-/-}$;*Pfn2*$^{-/}$ (*Pfn1-flx;Nes*-Cre) embryos. A, B. Top.** Normalized relative quantification graphs of protein levels of the Cdc2-dependent kinase 2 (CDK1) phosphorylated in position Thy15 (CDK1-pThy15, **A**) and Thr161 (CDK1-pThr161, **B**) from different genotypes of E11.5 embryo heads. The CDK1-pThy15 signals showed significantly increased levels of phospho-protein in *Pfn1*$^{-/-}$;*Pfn2*$^{-/-}$(1.53 ± 0.05, P=0.002) embryos, while no change was detected in *Pfn1*$^{+/-}$;*Pfn2*$^{-/-}$ (0.92 ± 0.02, P=0.805) and *Pfn1*$^{-/-}$; *Pfn2*$^{+/-}$ (1.13 ± 0.12, P=0.481) embryos. Conversely, a reduced expression of CDK1-pThr161 was observed in *Pfn1*$^{-/-}$;*Pfn2*$^{-/-}$ (0.69 ± 0.04, P=0.735) embryos. The CDK1-pThr161 signals showed no significant difference in the levels of phospho-protein in *Pfn1*$^{+/-}$;*Pfn2*$^{-/-}$ (0.85 ± 0.03, P=0.935) and *Pfn1*$^{-/-}$;*Pfn2*$^{+/-}$ (1.17 ± 0.37, P=0.0911) embryos. **Bottom.** Below the graphs are shown the western blots for CDK1-pThy15 (**A**) and CDK2-pThr161 (**B**). n=3 embryos per genotype. Error bars represent s.e.m. One-way ANOVA - Dunnett's test, **P≤0.01.

2.3 Functions of profilin 1 and profilin 2 in adult brain

Previous studies performed on *Pfn1* single mutant (*Pfn1*$^{flx/flx}$;*Camk2a-Cre*$^{cre/wt}$) have shown that deletion of *Pfn1* in adult mouse brain did not result in alterations of neither neuronal architecture nor pre-synaptic or post-synaptic physiology. In the same studies it was also demonstrated that PFN1 is dispensable for synapse density and morphology (Görlich *et al.*, 2012). In parallel, studies on *Pfn2* single mutant mice (*Pfn2*$^{-/-}$) have demonstrated the existence of a pre-synaptic function of PFN2 (Pilo Boyl *et al.*, 2007). In contrast to the studies on single mutant mouse models of either *Pfn1* or *Pfn2*, different *in vitro* studies suggested the existence of post-synaptic functions for profilins in spine morphology and dynamics (Ackermann & Matus, 2003;

Lamprecht *et al.*, 2006). These discrepancies suggest that, in the adult brain, a certain degree of functional overlap might exist among the two profilin isoforms, therefore this last section of the work provides an insight on PFN1 and PFN2 functions in the adult forebrain employing the *Pfn1*$^{flx/flx}$*;Pfn2*$^{-/-}$*;Camk2a-Cre*$^{cre/wt}$ double mutant mouse model.

2.3.1 Profilin mutants for the study of the function of the proteins in the adult brain

In *Pfn1*$^{flx/flx}$*;Pfn2*$^{-/-}$*;Camk2a-Cre*$^{cre/wt}$ double ko mouse the deletion of *Pfn1* takes place in the excitatory neurons of cortex and hippocampus starting at ~P18, whereas the deletion of *Pfn2* occurs already in germ line. *Pfn1*$^{flx/flx}$*;Pfn2*$^{-/-}$*;Camk2a-Cre*$^{cre/wt}$ were viable and showed an autistic-like behavior similar to *Pfn2*$^{-/-}$ mice (observations).

The genotypes listed in table 2.3, expressing a different allele dosage of *Pfn1* and *Pfn2*, were analyzed.

Table 2.2 *Pfn1-Pfn2* mutants for the study of profilins function in the adult brain

Genotype	Given name	*Pfn* allele dosage
Pfn1$^{flx/wt}$*;Pfn2*$^{wt/wt}$*;Camk2a-Cre*$^{wt/wt}$	Wt	4 *Pfn* alleles
Pfn1$^{flx/wt}$*;Pfn2*$^{-/-}$*;Camk2a-Cre*$^{cre/wt}$	*Pfn1*$^{+/-}$*;Pfn2*$^{-/-}$	1 *Pfn1* allele
Pfn1$^{flx/flx}$*;Pfn2*$^{+/-}$*;Camk2a-Cre*$^{cre/wt}$	*Pfn1*$^{-/-}$*;Pfn2*$^{+/-}$	1 *Pfn2* allele
Pfn1$^{flx/flx}$*;Pfn2*$^{-/-}$*;Camk2a-Cre*$^{cre/wt}$	*Pfn1*$^{-/-}$*;Pfn2*$^{-/-}$	0 *Pfn* alleles

Since the deletion of *Pfn1* is achieved by a Cre/LoxP system, it was essential to analyze PFN1 loss in the cortex and hippocampus of the mutant mice, these being the tissues where the CAMKIIα is highest expressed.

Total tissue lysates were prepared from wt (*Pfn1*$^{wt/wt}$*;Camk2a-Cre*$^{wt/wt}$) and *Pfn1*$^{-/-}$ (*Pfn1*$^{flx/flx}$*;Camk2a-Cre*$^{cre/wt}$) mice at different ages (P21, P24, P28, P45 and P70) and western blots were performed. The calibrated PFN1 protein levels were normalized against the respective age-matched wildtype (Fig 2.26).

In the cortex of *Pfn1*$^{-/-}$ animals, PFN1 levels were reduced by 25 % at P24 and by 80 % at P28; starting from P45, PFN1 expression was reduced to 10 % and remained stable (Fig 2.26 A). In the hippocampus of *Pfn1*$^{-/-}$ animals, PFN1 protein levels appeared unchanged at P21 but heavily decreased by 84 % at P28, reaching already a stable plateau of expression between P28 and P45 (Fig 2.26 B). The expression of PFN1 in cortex and hippocampus reached a slightly different plateau level possibly because of the different composition of cell types that do not express *Camk2a*, for example inhibitory neurons and glial cells.

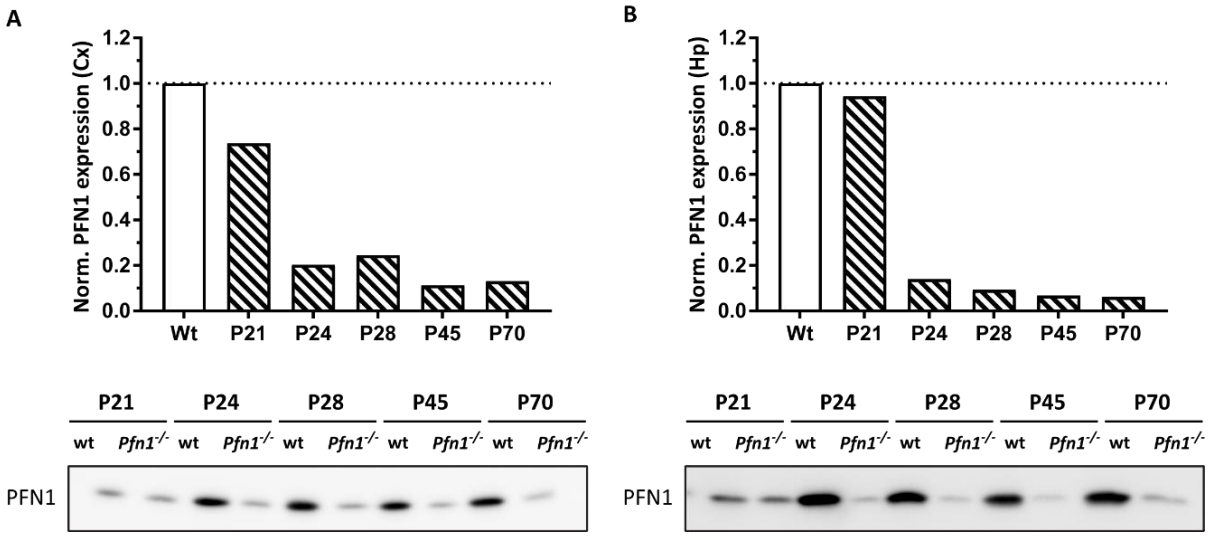

Figure 2.26 **| PFN1 protein deletion in *Pfn1*$^{-/-}$ (*Pfn1-flx;Camk2a-Cre*) mice. A, B. Top.** Quantification of cortical (**A**) and hippocampal (**B**) PFN1 protein levels of conditional *Pfn1*$^{-/-}$ mice compared to age-matched wt mice. Each *Pfn1*$^{-/-}$ sample was normalized to its own age-matched wt, but to facilitate the understanding of the figure only one wt bar is shown. PFN1 protein levels in the cortex of *Pfn1*$^{-/-}$ mice were reduced by 25 % at P21 (0.74), already by 80 % at P24 (0.20) and P28 (0.24), and plateaued at P45 (0.11) as seen by a similar level at P70 (0.13). In the hippocampus of *Pfn1*$^{-/-}$ mice PFN1 protein levels appeared unchanged at P21 (0.94) but were decreased by 84 % at P24 (0.14), and plateaued between P28 (0.09) and P48 (0.07), appearing unchanged at P70 (0.06). PFN1 residual levels appear slightly different in cortex and hippocampus possibly because of the different composition of cell types that do not express CAMKIIα. **Bottom.** Below the graphs are shown the western blots of cortical (**A**) and hippocampal (**B**) samples probed with antibody against PFN1. n=1 sample per genotype.

PFN1 is therefore efficiently deleted from the cortical and hippocampal region of *Pfn1*$^{-/-}$ mice between P28 and P45, consequently all biochemical and morphological

analyses were performed starting with mice aged between P80 - P90 (young) and in P360 (old) animals.

To make sure that both PFN isoforms were lost in double ko mice at the time of the analysis, their expression was evaluated by western blot on total cortical lysates from P80-P90 mice. In figure 2.27 A and B are reported the relative expression levels of PFN1 and PFN2, respectively, in the different mutant mice (*Pfn1*$^{+/-}$*;Pfn2*$^{-/-}$, *Pfn1*$^{-/-}$*;Pfn2*$^{+/-}$ and *Pfn1*$^{-/-}$*;Pfn2*$^{-/-}$) compared to the wildtype.

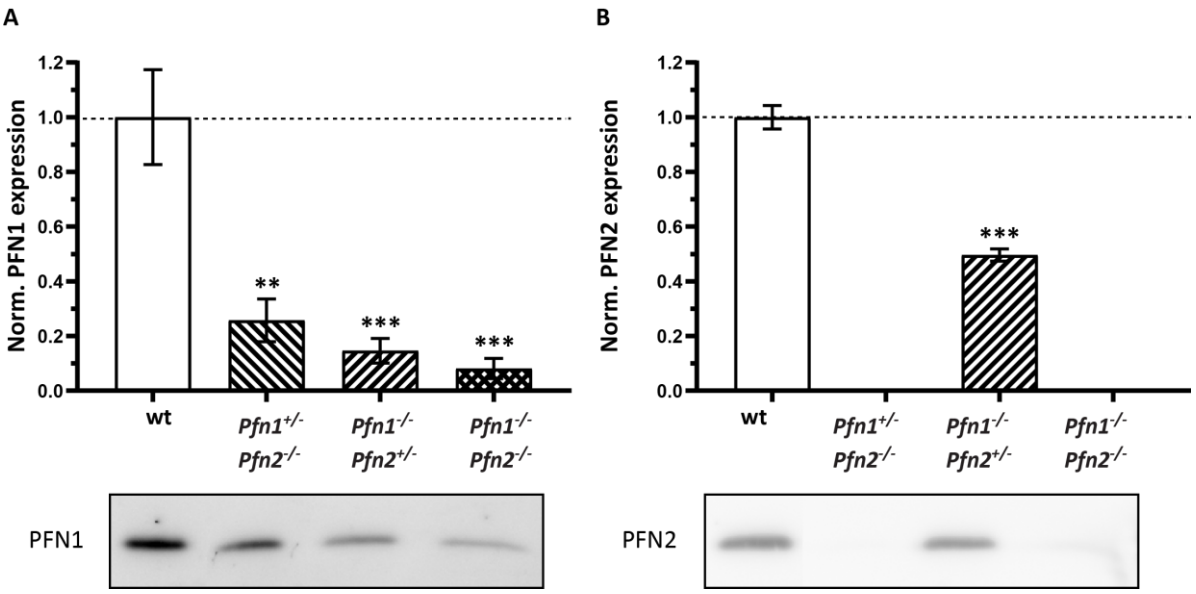

Figure 2.27 **| Reduced PFN1 and PFN2 protein expression in P80-P90 mutant mice. A, B. Top.** Normalized relative quantification graphs of PFN1 (**A**) and PFN2 (**B**) protein levels in the cortex of mice from the indicated genotypes. PFN1 signals from mutant mice were normalized against the wt (1.00 ± 0.24) and a progressive reduction of protein expression was measured in *Pfn1*$^{+/-}$*;Pfn2*$^{-/-}$ (0.25 ± 0.09, P=0.002), *Pfn1*$^{-/-}$*;Pfn2*$^{+/-}$ (0.11 ± 0.05, P<0.001) and *Pfn1*$^{-/-}$*;Pfn2*$^{-/-}$ (*Pfn1-flx;Camk2a-Cre*) (0.08 ± 0.03, P<0.001) mice. PFN2 signals from mutant mice were normalized against the wt (1.00 ± 0.29) and a reduction of protein expression was measured according to the genotype in *Pfn1*$^{+/-}$*;Pfn2*$^{-/-}$ (0.00 ± 0.00), *Pfn1*$^{-/-}$*;Pfn2*$^{+/-}$ (0.50 ± 0.16, P<0.001) and *Pfn1*$^{-/-}$*;Pfn2*$^{-/-}$ (*Pfn1-flx;Camk2a-Cre*) (0.00 ± 0.00) mice. **Bottom.** Below the graphs are shown the western blots for PFN1 (**A**) and PFN2 (**B**). n=3 cortices per genotype. Error bars represent s.e.m. One-way ANOVA - Dunnett's test, **P≤0.01, ***P≤0.001**.**

As expected, PFN1 expression was reduced in *Pfn1*$^{+/-}$*;Pfn2*$^{-/-}$, *Pfn1*$^{-/-}$*;Pfn2*$^{+/-}$ and *Pfn1*$^{-/-}$*;Pfn2*$^{-/-}$ mice. The residual PFN1 signal still visible derives likely from glial cells

and interneurons, which do not express CAMKIIα (Fig 2.27 A). PFN2 expression was halved in *Pfn1*$^{-/-}$;*Pfn2*$^{+/-}$ mice and completely missing in *Pfn2* ko mice (Fig 2.27 B).

In summary, in *Pfn1*$^{-/-}$;*Pfn2*$^{-/-}$ double ko P80-P90 mice, PFN1 expression is lowered to 10 % and is likely missing in all forebrain excitatory neurons, whereas PFN2 is absent.

2.3.2 Impaired actin polymerization and dynamics in *Pfn1*$^{-/-}$;*Pfn2*$^{-/-}$ mice

G-actin in cells is complexed with monomer binding proteins, such as thymosin-beta 4 and profilins. The neuronal deletion of both profilins could leave large amounts of uncomplexed G-actin in the cell, which could lead to spontaneous and not controlled actin filament polymerization. Therefore, it is conceivable that the cell might in turn downregulate actin expression. For this reason, the total actin content was analyzed, by western blotting, in total cortical lysates from *Pfn1*$^{-/-}$;*Pfn2*$^{-/-}$ P80-90 mice. Relative quantification of the total actin showed a 50 % reduction in the *Pfn1-Pfn2* double ko mice (Fig 2.28 A).

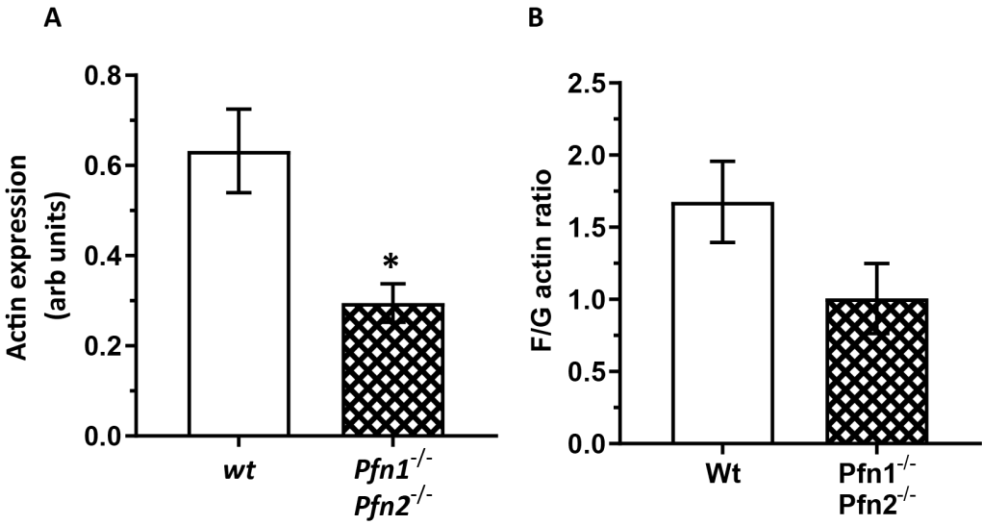

Figure 2.28 **| Loss of actin expression and reduced actin polymerization in *Pfn1*$^{-/-}$;*Pfn2*$^{-/-}$ (*Pfn1-flx;Camk2a-Cre*) cortical tissue. A.** Relative quantification of the actin content in the cortex of *Pfn1*$^{-/-}$;*Pfn2*$^{-/-}$ mice. Total actin was significantly reduced by 50 % in *Pfn1*$^{-/-}$;*Pfn2*$^{-/-}$ (0.29 ± 0.04) cortical lysates compared to wt (0.63 ± 0.09) mice (P=0.014). n=4 cortices per genotype. **B.** Calculation of the F/G-actin ratio in wt (1.67 ± 0.28) and *Pfn1*$^{-/-}$;*Pfn2*$^{-/-}$ (1.01 ± 0.24) cortical lysates revealed a 40 % decrease in the mutant animals (P=0.073). The G-actin levels in the supernatant and F-actin in the pellet fraction were detected by western blotting with an antibody against actin. n=3 cortices per genotype. Error bars represent s.e.m. t-test, *P≤0.05.

The deletion of both profilins in neurons could also likely affect the availability of ATP-G-actin necessary for actin filament growth and, therefore, imbalance the actin polymerization to depolymerization rates, which could result in a reduction of the ratio between F and G actin. In order to investigate changes in the actin polymerization process, two different subcellular fractions were prepared from the cortical region of the brain: a Triton X-100 soluble fraction, containing G-actin and a Triton X-100 insoluble fraction, containing F-actin. Equal volumes were run on an SDS-PAGE and actin levels were identified by western blot. The comparison between wt and *Pfn1*$^{-/-}$*;Pfn2*$^{-/-}$ mice revealed a 40 % reduction of the F/G actin ratio in double mutants, although not significant (Fig 2.28 B).

To investigate the physiological relevance of PFN1 and PFN2 in synaptic actin dynamics, cortical synaptosomes from P80-P90 wt and *Pfn1*$^{-/-}$*;Pfn2*$^{-/-}$ mice were prepared and analyzed. Synaptosomes are a subcellular fraction prepared from specific brain tissues by homogenization followed by density gradient fractionation. Synaptosomes contain the complete pre-synaptic terminal, including mitochondria and synaptic vesicles, along with the post-synaptic terminal. Because all the molecular machinery for the release, uptake and storage of the neurotransmitter remains intact, synaptosomes are considered a good *ex vivo* system to study molecular mechanisms of synaptic transmission (Whittaker, 1993; Nicholls & Sihra, 1986; Harrison *et al.*, 1988; Bai & Witzmann, 2007). Synaptosomes can be stimulated increasing the concentration of external K^+, which induces depolarization in the pre-synaptic terminal mimicking an action potential. In turn, synaptosomes stimulation triggers neurotransmitter release and activates pre-synaptic actin dynamics detectable as changes of the F/G-actin ratio.

Previous studies on cortical synaptosomes showed reduced F/G-actin ratio upon KCl stimulation in *Pfn2*$^{-/-}$ mice compared to wt littermates (Pilo Boyl *et al.*, 2007). Similarly, to these studies, synaptosomes were prepared from cortical tissue of wt and *Pfn1*$^{-/-}$*;Pfn2*$^{-/-}$ mice and were stimulated for 60 seconds with 20 mM KCl. The F/G-actin ratios were then measured in not stimulated (0 s) and stimulated (60 s) synaptosomes,

and the results are shown in the graph in figure 2.29. Under resting conditions (0 s), no significant difference could be observed in the F/G-actin ratio of wt and *Pfn1*$^{-/-}$;*Pfn2*$^{-/-}$ synaptosomes, although a slight reduction was observed in the double ko, in accordance with the reduction detected in total cortex (Fig 2.28 B). Stimulation with KCl for 60 s resulted in a significant increase in the F/G-actin ratio in control but not in double ko synaptosomes, which remained unresponsive (Fig 2.29).

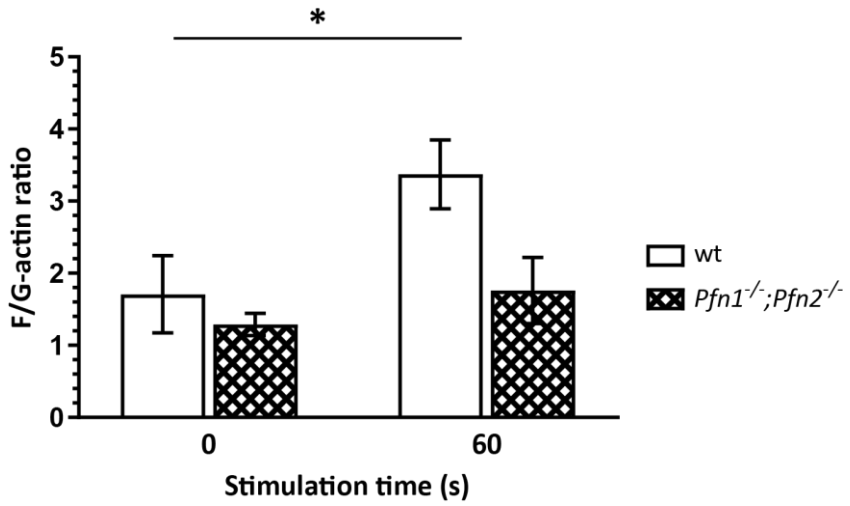

Figure 2.29 **| Impaired actin dynamics in *Pfn1*$^{-/-}$;*Pfn2*$^{-/-}$ (*Pfn1-flx;Camk2α-Cre*) cortical synaptosomes.** F/G-actin ratios were not significantly different in resting cortical synaptosomes (0 sec); after 60 s stimulation with 20 mM KCl the F/G-actin ratio raised by about two-fold in the control (P=0.045), while no significant increase was detected in *Pfn1*$^{-/-}$;*Pfn2*$^{-/-}$ mutant synaptosomes (P=0.999). The G-actin levels in the soluble and F-actin in the insoluble fraction were detected by western blotting with an antibody against actin. n=3 cortices per genotype. Error bars represent s.e.m. One-way ANOVA - Dunnett's test, *P≤0.05.

Lack of F-actin polymerization after stimulation of cortical synaptosomes of *Pfn1*$^{-/-}$;*Pfn2*$^{-/-}$ double ko mice demonstrates that loss of both profilin isoforms leads to impairment of pre-synaptic actin dynamics.

2.3.3 Mild alterations in pre-synaptic but not in the post-synaptic machinery in *Pfn1*$^{-/-}$;*Pfn2*$^{-/-}$ mice.

Loss of actin and impaired actin polymerization dynamics might lead to changes in the pre- or post-synaptic machineries of the neurons. To analyze more in detail proteins

participating in pre-synaptic vesicle exocytosis or being part of the PSD, total cortical lysates were prepared from wt, *Pfn1*$^{+/-}$*;Pfn2*$^{-/-}$, *Pfn1*$^{-/-}$*;Pfn2*$^{+/-}$, and *Pfn1*$^{-/-}$*;Pfn2*$^{-/-}$ mice

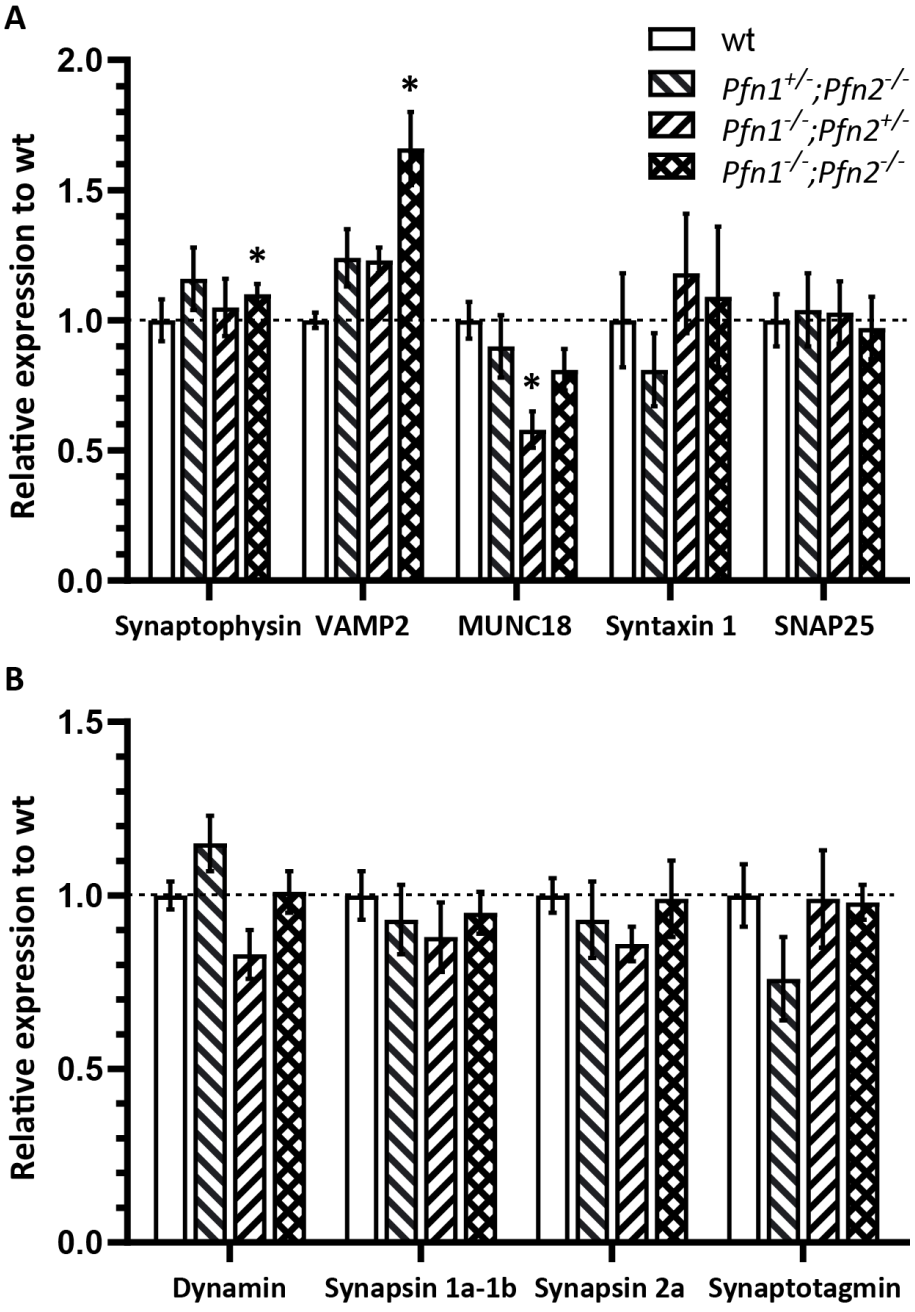

Figure 2.30 **| Loss of both profilins causes an alteration of the expression levels of specific pre-synaptic proteins.** Normalized relative quantification graphs of different pre-synaptic proteins levels in the cortex of mice from the indicated genotypes. In *Pfn1*$^{-/-}$*;Pfn2*$^{-/}$ (*Pfn1-flx;Camk2a-Cre*) mice, it was detected a significant increase in the levels of synaptophysin (P=0.047) and in the levels of VAMP2 (P=0.021), two vesicular proteins that positively regulate vesicle exocytosis. Instead MUNC18, a CAZ protein negatively regulating vesicle exocytosis, was reduced in the absence of PFN1 (P=0.026). No other significant alterations in the pre-synaptic machinery could be detected. n=3 cortices per genotype. Error bars represent s.e.m.*P≤0.05. One-way ANOVA - Dunnett's test, *P≤0.05**.**

aged from P80 to P90. The analysis was extended also to the single profilin allele genotypes, expressing either one *Pfn1* allele or one *Pfn2* allele, with the aim of possibly distinguishing the specific functions of both profilins. First, levels of different pre-synaptic proteins involved in the process of vesicle docking and priming through the formation of the SNARE complex were analyzed. In *Pfn1*$^{-/-}$*;Pfn2*$^{-/-}$ double ko cortices, the levels of two vesicular proteins, synaptophysin and VAMP2, involved in positive regulation of SV exocytosis, were found slightly increased (Fig 2.30). Instead MUNC18 a constituent of the CAZ (cytomatrix active zone), which works as inhibitor of SV exocytosis, was found decreased, strongly correlating with PFN1 loss. Other pre-synaptic proteins involved in different steps of SV exocytosis (synapsin 1a/1b, synapsin 2a, synaptotagmin) or in SV re-uptake (dynamin 1) were not found altered in any mutant genotype (Fig 2.30).

Next, proteins of the PSD were analyzed, and no relevant alteration was found, except for a significant decrease in the levels of GLUR1 in *Pfn1*$^{-/-}$*;Pfn2*$^{+/-}$ mice which was not in agreement with the *Pfn1*$^{-/-}$*;Pfn2*$^{-/-}$ double ko (Fig 2.31).

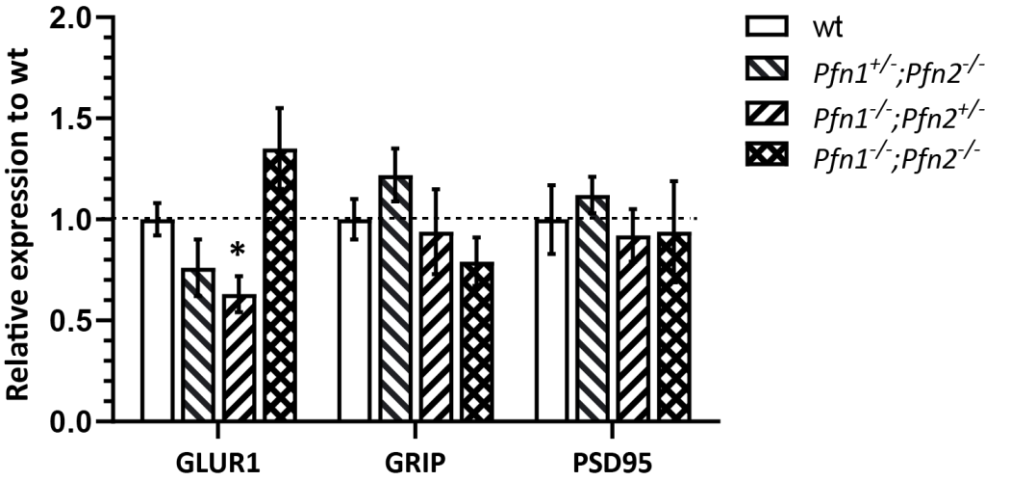

Figure 2.31 **| Post-synaptic machinery is not affected by the loss of both profilins.** Normalized relative quantification graphs of different post-synaptic proteins levels in the cortex of mice from the indicated genotype. No relevant alterations in the post-synaptic machinery could be detected in profilin mutants, except for a decrease in the levels of GLUR1 in Pfn1$^{-/-}$;Pfn2$^{+/-}$ (*Pfn1-flx;Camk2a-Cre*) mice (P=0.035), which was not confirmed in double ko mice. n=3 cortices per genotype. Error bars represent s.e.m. One-way ANOVA - Dunnett's test, *P≤0.05**.**

2.3.4 Cortical organization and layering are disrupted by the loss of PFN2 or both profilin isoforms.

The reduced total actin and F-actin levels as well as the impaired actin dynamics shown in *Pfn1*$^{-/-}$*;Pfn2*$^{-/-}$ double ko mice starting from P80 could affect structural integrity and survival of the neurons at later time points. A convenient brain region to study this possibility is the cortex, where neurons are organized in six distinguishable layers connected by well-established dendritic arborizations (Fig 2.32). Structural losses in this context would lead to alterations in the well-ordered cortical organization and/or in neuronal connectivity.

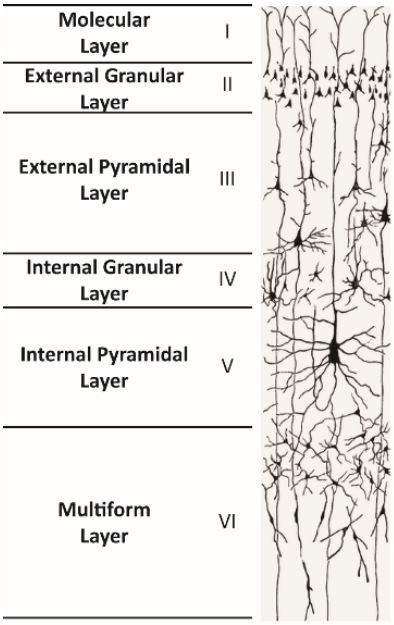

Figure 2.32 **| Schematic representation of the layered cortical structure.** The 6 cortical layers I-VI are composed of different neuronal subtypes. Neurons of the different layers show specific dendritic arborization morphology. Pyramidal excitatory neurons are found in layer III and V.

To analyze the contribution of PFN1 and PFN2 to this structure, Golgi stainings were performed on wt*, Pfn1*$^{+/-}$*;Pfn2*$^{-/-}$, *Pfn1*$^{-/-}$*;Pfn2*$^{+/-}$ and *Pfn1*$^{-/-}$*;Pfn2*$^{-/-}$ animals aged between P80 and P90, approximately 2 months after losing PFN1 in cortical excitatory neurons.

The Golgi staining technique allows to randomly stain neurons with a brownish colour; therefore, it is useful to visualize their complete anatomical features, such as the cell body and the entire dendritic arborization including dendritic spines and possibly the

thin axons. The use of this technique allows to detect alterations in the connectivity of neurons from the different layers and, in part, their density within the layers.

The Golgi staining revealed important changes in the cortical morphology of Pfn*1*$^{+/-}$*;Pfn2*$^{-/-}$ and *Pfn1*$^{-/-}$*;Pfn2*$^{-/-}$ mice, whereas the cortical structure of *Pfn1*$^{-/-}$*;Pfn2*$^{+/-}$ animals, lacking PFN1 but still expressing a single *Pfn2* allele, was not altered compared to controls (Fig. 2.33, Supplementary Fig 7.6). Specifically, a mild alteration could be identified in Pfn*1*$^{+/-}$*;Pfn2*$^{-/-}$ mice, with the cortex appearing less densely populated by neurons compared to the wt control, showing less organized cortical layers, and altered dendritic arborization (Fig 2.33 B).

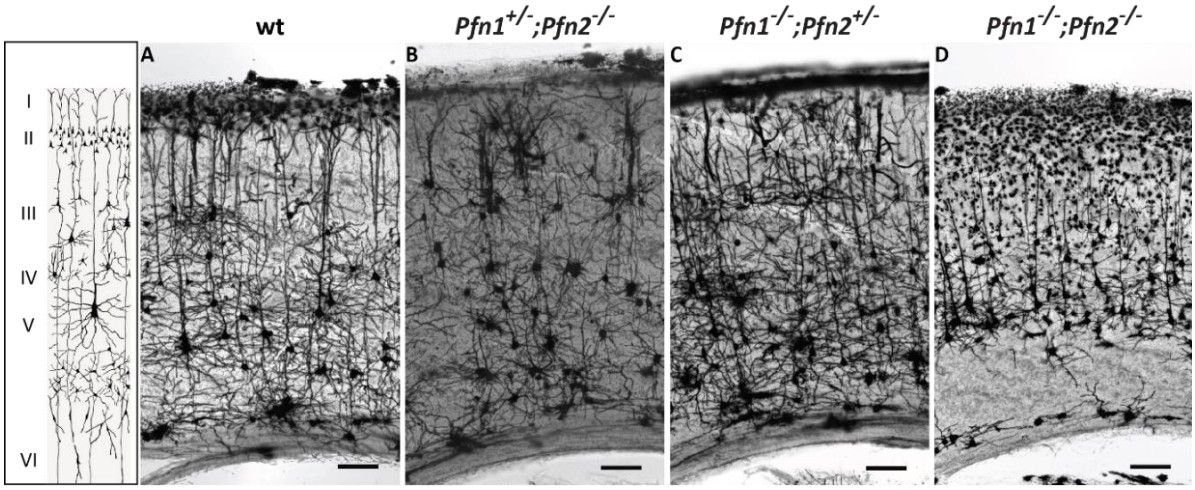

Figure 2.33 **| Altered cortical layering and dendritic arborization in *Pfn1*$^{+/-}$*;Pfn2*$^{-/-}$ and Pfn*1*$^{-/-}$*;Pfn2*$^{-/-}$ (*Pfn1-flx;Camk2a-Cre*) mice.** Sample overview images of the cortex in matched coronal slices from Golgi-stained brains of wt, *Pfn1*$^{+/-}$*;Pfn2*$^{-/-}$, *Pfn1*$^{-/-}$*;Pfn2*$^{+/-}$ and *Pfn1*$^{-/-}$*;Pfn2*$^{-/-}$ P80-P90 mice. The observed defects correlate with the loss of PFN2. Neurons appeared less dense and cortical layers were less organized and defined in Pfn*1*$^{+/-}$*;Pfn2*$^{-/-}$ mice; also, the dendritic arborization appeared simplified (**B**). *Pfn1*$^{-/-}$*;Pfn2*$^{-/-}$ double ko mice showed an even stronger disruption of the cortical structure: layer VI was almost completely missing, apical branches from layer V-IV neurons appeared shorter and less complex. Layers III and II neurons lost completely their dendritic branching and the typical layered cortical organization is barely visible (**D**). Mice with one *Pfn2* allele (**C**) appeared comparable to wt mice (**A**). Scale bar: 100 µm.

Striking and severe impairments were seen in the cortical structure of *Pfn1*$^{-/-}$;*Pfn2*$^{-/-}$ double ko mice (Fig 2.33 D):

- The structure of neurons from layers II-III was completely collapsed, these neurons lost most of their dendritic arborizations (see also Fig 2.34).
- Apical branches from neurons in layers IV and V appeared shorter and less complex compared to control.
- The multiform layer (VI) was almost completely missing.

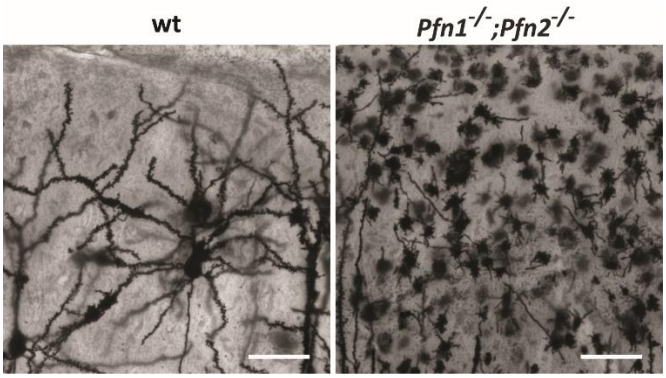

Figure 2.34 **| Collapsed structure of Layer II and III cortical neurons in *Pfn1*$^{-/-}$;*Pfn2*$^{-/-}$ (*Pfn1-flx;Camk2a-Cre*) mice.** Sample images of cortical layer II-III neurons in matched coronal slices from Golgi-stained brains of wt and *Pfn1*$^{-/-}$;*Pfn2*$^{-/-}$ adult P80-P90 mice. *Pfn1*$^{-/-}$;*Pfn2*$^{-/-}$ neurons were branchless and only the cell soma was visible. Scale bar: 40 µm.

The loss of both PFN1 and PFN2 heavily affected the layering of the neurons in the cerebral cortex as well as their branching, with different severity depending on their position: neurons in the top layers (II-III) almost completely lost dendritic arborization (Fig 2.34), neurons in deeper layers (IV-V) showed reduced dendritic length and branching complexity and neurons from layer VI almost totally disappeared (Fig 2.33 D). In addition, while a single *Pfn2* allele completely rescued the double ko phenotype (Fig 2.33 C), the expression of only one *Pfn1* allele was not able to fully rescue the double ko phenotype (Fig 2.33 B): in fact, in the cortex, a disruption of the ordered neuronal layering structure can be observed, as well as a simplified dendritic arborization (see also the next session).

2.3.5 Loss of both profilin isoforms leads to reduced branching complexity of cortical and hippocampal pyramidal neurons

In order to confirm the observation that loss of both profilins was heavily affecting neuronal branching, a quantitative approach to study the dendritic arborization of profilins ko neurons was employed. The random labelling of neurons in the Golgi staining is an advantage, since it allows to trace single neurons in the cortical or hippocampal network in all their anatomical features, including dendritic arborization (Risher *et al.* 2014; Hee Won Kang *et al.*, 2017).

A branching analysis was performed focusing on layer V pyramidal neurons of the cortex, since the morphological features of those neurons are well studied and, although these neurons appeared severely affected in *Pfn1*$^{-/-}$*;Pfn2*$^{-/-}$ double ko mice, the dendritic structures were still visible and quantifiable. The branching analysis was carried out manually and it was performed on the four different genotypes shown in Fig 2.33.

The dendritic tree of a pyramidal neuron is formed by two distinct domains: the basal and the apical dendrites, which descend from the base and the apex of the triangular soma, respectively. Basal and apical dendrites of different orders were traced and analyzed per number and length.

Layer V neurons typically have a single apical primary (1ry) dendrite with secondary (2ry), tertiary (3ry) and quaternary (4ry) branches. The branching analysis on the apical arborization was performed on the length of the unique 1ry branch (Supplementary Fig 7.7) and on the number and length of 2ry and 3ry branches (Fig 2.35). Moreover, in *Pfn1*$^{-/-}$*;Pfn2*$^{-/-}$ double ko neurons no 4ry apical branches were observed (Supplementary Fig 7.8). Since layer V neurons have many basal 1ry dendrites, for the basal arborization the complete analysis was performed only on 1ry and 2ry branches (Fig 2.36), because no 3ry branches were found in *Pfn1*$^{-/-}$*;Pfn2*$^{-/-}$ double ko neurons (Supplementary Fig 7.9).

As shown in figure 2.35, in *Pfn1*$^{-/-}$;*Pfn2*$^{-/-}$ mice the apical dendritic arbor was strongly affected in the number and length of the branches compared to wt controls. Mice lacking PFN2 and with only one functional *Pfn1* allele showed a similar, although intermediate, phenotype to double ko mice. In particular:

- The length of the single apical 1ry dendrite resulted almost halved in *Pfn1*$^{-/-}$;*Pfn2*$^{-/-}$ mice and significantly reduced in *Pfn1*$^{+/-}$;*Pfn2*$^{-/-}$ mice compared to controls (Supplementary Fig 7.7).
- The number of apical 2ry dendrites was found significantly reduced in *Pfn1*$^{-/-}$;*Pfn2*$^{-/-}$ double ko mice and to a lesser extent in *Pfn1*$^{+/-}$;*Pfn2*$^{-/-}$ animals compared to wildtypes (Fig 2.35 A). The length of the apical 2ry dendrites followed a similar trend (Fig 2.35 C).
- Dendrites of 3ry order were also significantly less numerous (Fig 2.35 B) and shorter (Fig 2.35 D) in *Pfn1*$^{-/-}$;*Pfn2*$^{-/-}$ double ko mice as well as in *Pfn1*$^{+/-}$;*Pfn2*$^{-/-}$ mice compared to controls.
- Apical 4ry dendrites were not observed at all in profilin double ko mice and their number was also severely affected in *Pfn1*$^{+/-}$;*Pfn2*$^{-/-}$ mice (Supplementary Fig 7.8).

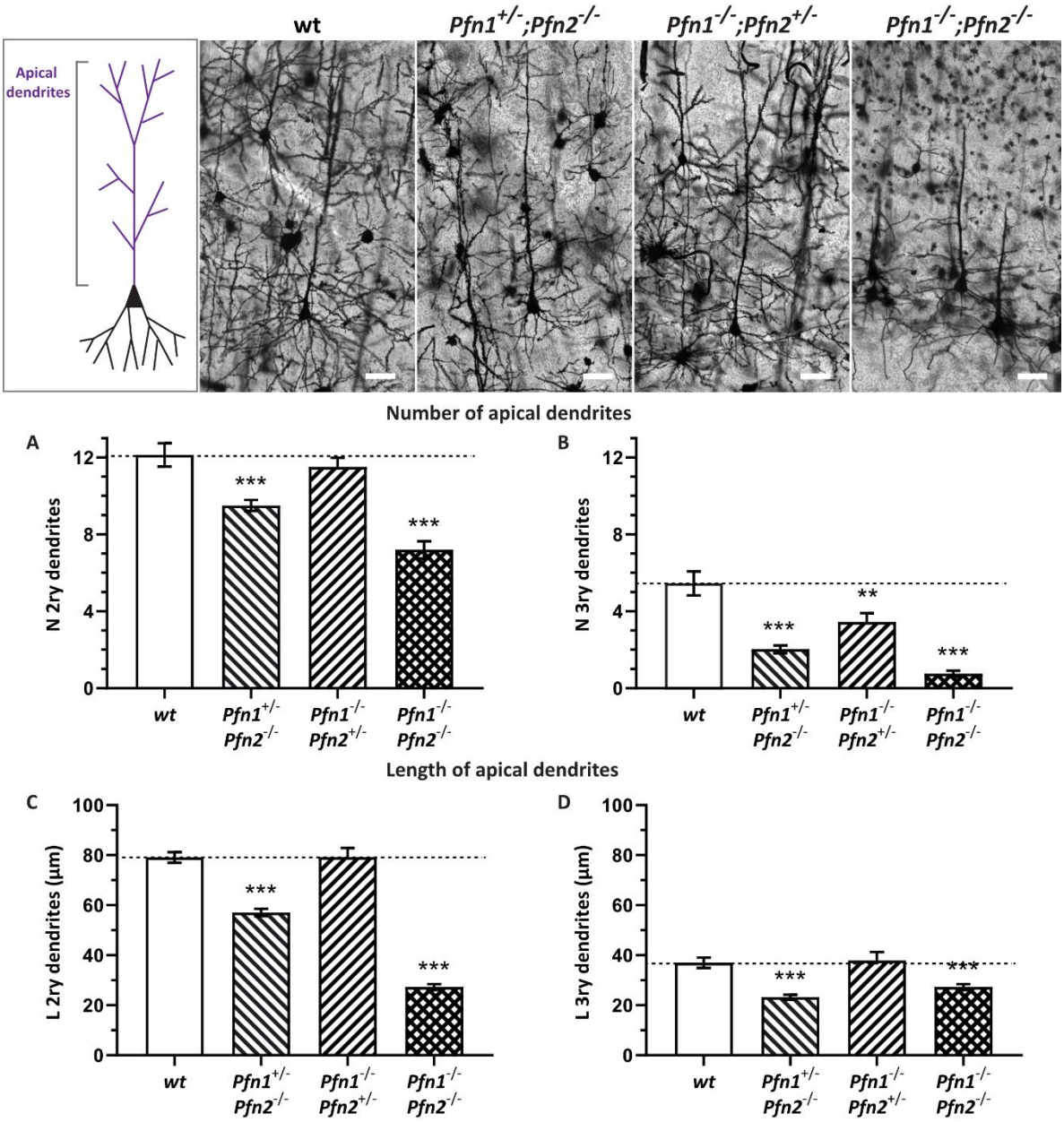

Figure 2.35 **| Layer V cortical pyramidal neurons of *Pfn1*$^{-/-}$;*Pfn2*$^{-/-}$ (*Pfn1-flx;Camk2α-Cre*) mice display reduced apical branching and dendrite length.** On the top, from left to right, a schematic structure of a layer V cortical pyramidal neuron is depicted and then follow high magnification sample images of Golgi stained layer V cortical neurons in coronal brain slices of wt, *Pfn1*$^{+/-}$;*Pfn2*$^{-/-}$, *Pfn1*$^{-/-}$;*Pfn2*$^{+/-}$ and *Pfn1*$^{-/-}$;*Pfn2*$^{-/-}$ P80-P90 mice. Scale bar: 40 µm. **A, B.** Bar graphs representing the average number (N) of 2ry (**A**) and 3ry (**B**) dendritic branches of layer V cortical neurons from control and profilin mutant mice. **C, D.** Bar graphs representing the average length (L) of 2ry (**C**) and 3ry (**D**) dendritic branches of layer V cortical neurons in control and profilin mutant mice. Dotted lines indicate the wt level in each graph. A strong reduction of complexity and length was observed in *Pfn1*$^{-/-}$;*Pfn2*$^{-/-}$ double ko mice and a surprisingly similar phenotype resulted in *Pfn1*$^{+/-}$;*Pfn2*$^{-/-}$ mice, bearing only one *Pfn1* allele. n=2 mice per genotype and a total of 60 cells per genotype were analyzed. Error bars represent s.e.m. One-way ANOVA - Dunnett's test, **P≤0.01, ***P≤0.001.

The analysis of the basal dendrites revealed a similar branching defect in *Pfn1*$^{-/-}$;*Pfn2*$^{-/-}$ double ko mice as well as, with minor severity, in *Pfn1*$^{+/-}$;*Pfn2*$^{-/-}$ mice (Fig 2.36). On the other hand, animals with only one functional copy of *Pfn2* showed only a modest phenotype affecting principally the number of 2ry (Fig 2.36 B) and 3ry branches (Supplementary Fig 7.9). Specifically:

- The number of basal 1ry dendrites was found significantly reduced in *Pfn1*$^{-/-}$;*Pfn2*$^{-/-}$ double ko mice as well as, strikingly similarly, in *Pfn1*$^{+/-}$;*Pfn2*$^{-/-}$ animals (Fig 2.36 A). The length of the basal 1ry dendrites was reduced to almost one third in *Pfn1*$^{-/-}$;*Pfn2*$^{-/-}$ double ko animals compared to controls and was significantly decreased in *Pfn1*$^{+/-}$;*Pfn2*$^{-/-}$ mice. A small, albeit significant, length reduction was also observed in *Pfn1*$^{-/-}$;*Pfn2*$^{+/-}$ mice (Fig 2.36 C).
- Basal 2ry dendrites were severely affected in number (Fig 2.36 B) and length (Fig 2.36 D) in *Pfn1*$^{-/-}$;*Pfn2*$^{-/-}$ double ko mice. Also, in *Pfn1*$^{+/-}$;*Pfn2*$^{-/-}$ mice 2ry dendrites were significantly less numerous (Fig 2.36 B) and shorter (Fig 2.36 D). Interestingly, in the basal arborization, even *Pfn1*$^{-/-}$;*Pfn2*$^{+/-}$ showed an important reduction in the number of 2ry dendrites (Fig 2.36 B).
- Basal 3ry dendrites were not observed at all in *Pfn1*$^{-/-}$;*Pfn2*$^{-/-}$ profilin double ko mice and their number was also severely affected in *Pfn1*$^{+/-}$;*Pfn2*$^{-/-}$ mice, bearing only one *Pfn1* allele. The number of 3ry dendrites was also halved in *Pfn1*$^{-/-}$;*Pfn2*$^{+/-}$ animals, expressing only one *Pfn2* allele, compared to wt (Supplementary Fig 7.9).

Loss of both profilin isoforms affected the dendritic length and resulted in a dramatically reduced branching complexity of pyramidal neurons in layer V of the cortex. Surprisingly, the expression of only one allele of *Pfn2* could in most aspects maintain neuronal morphology comparable to the wt condition, while the expression of one allele of *Pfn1* had only partial rescuing capacity.

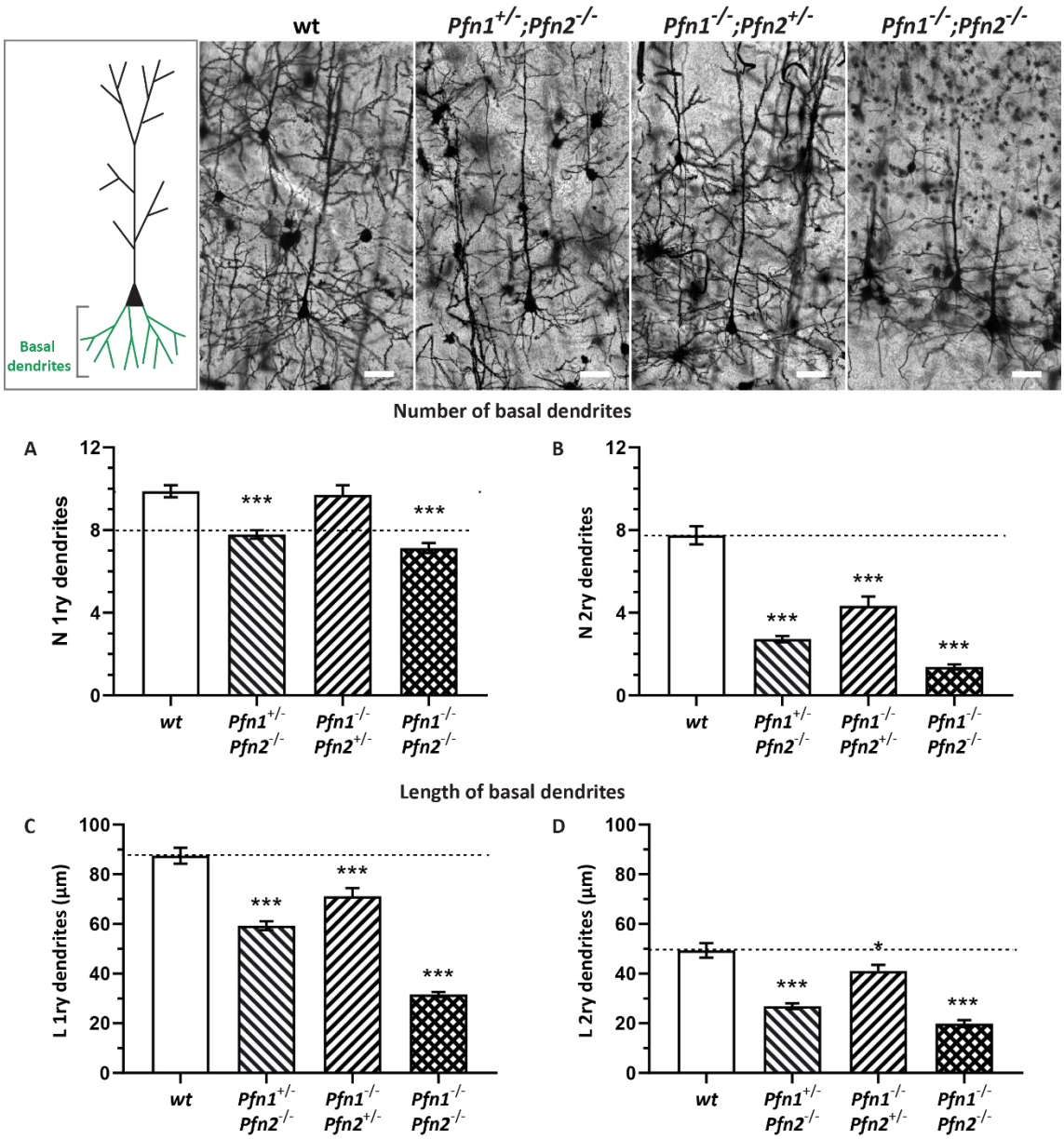

Figure 2.36 **| Layer V cortical pyramidal neurons of *Pfn1*$^{-/-}$;*Pfn2*$^{-/-}$ (*Pfn1-flx;Camk2a-Cre*) mice display reduced basal branching and dendrite length.** On the top, from left to right, a schematic structure of a layer V cortical pyramidal neuron is depicted, and then follow high magnification sample images of Golgi stained layer V cortical neurons in coronal brain slices of wt, *Pfn1*$^{+/-}$;*Pfn2*$^{-/-}$, *Pfn1*$^{-/-}$;*Pfn2*$^{+/-}$ and *Pfn1*$^{-/-}$;*Pfn2*$^{-/-}$ P80-P90 mice. Scale bar: 40 µm. **A, B.** Bar graphs representing the average number (N) of 1ry (**A**) and 2ry (**B**) dendritic branches of layer V cortical neurons in control and profilin mutant mice. **C, D.** Bar graphs representing the average length (L) of 1ry (**C**) and 2ry (**D**) dendritic branches of layer V cortical neurons in control and profilin mutant mice. Dotted lines indicate the wt levels. A strong reduction of complexity was observed in *Pfn1*$^{-/-}$;*Pfn2*$^{-/-}$ double ko mice and a surprisingly similar phenotype resulted in *Pfn1*$^{+/-}$;*Pfn2*$^{-/-}$ mice, bearing only one *Pfn1* allele. Differently from apical dendrites, in basal dendrites an intermediate phenotype was observed also for *Pfn1*$^{-/-}$;*Pfn2*$^{+/-}$ mice, bearing a single *Pfn2* allele. n=2 mice per genotype and a total of 60 cells per genotype were analyzed. Error bars represent s.e.m. One-way ANOVA - Dunnett's test, *P≤0.05, ***P≤0.001**.**

The CA1 region of the hippocampus is also of great interest for higher behavior. Unfortunately, due to the dense apical and basal branching of the wt mice, it was not possible to perform a quantitative analysis in this area. Nevertheless, even just by visual inspection the dendritic complexity of CA1 pyramidal neurons appeared heavily affected in *Pfn1*$^{-/-}$;*Pfn2*$^{-/-}$ double ko mice; in these mice only the 1ry apical and basal branches could be observed, while higher order branches were completely lost (Fig 2.37 D). In *Pfn1*$^{+/-}$;*Pfn2*$^{-/-}$mice was also possible to observe a reduced apical and basal branching complexity compared to wt; in particular both basal and apical branches of higher order appeared affected rather than branches of lower order (Fig 2.37 B). On the contrary, *Pfn1*$^{-/-}$;*Pfn2*$^{+/-}$ animals did not show any visible impairment in the apical and basal branching of CA1 pyramidal neurons, resembling the wildtype condition (Fig 2.37 C) .

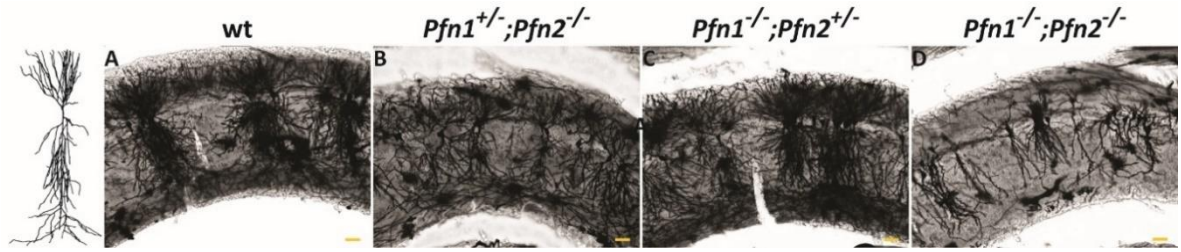

Figure 2.37 **| CA1 pyramidal neurons of *Pfn1*$^{-/-}$;*Pfn2*$^{-/-}$ (*Pfn1-flx;Camk2a-Cre*) mice displayed reduced apical and basal branching complexity.** Schematic representation of a CA1 neuron followed by sample images of the CA1 hippocampal region in matched coronal slices from Golgi-stained brains of wt, *Pfn1*$^{+/-}$;*Pfn2*$^{-/-}$, *Pfn1*$^{-/-}$;*Pfn2*$^{+/-}$ and *Pfn1*$^{-/-}$;*Pfn2*$^{-/-}$ P80-P90 mice. In profilins double ko mice, CA1 pyramidal neurons appeared to have an extremely simplified basal and apical arborization, with 2ry branches being not visible (**D**). Intermediate situation can be observed in mice with one *Pfn1* allele (**B**). Mice with one *Pfn2* allele (**C**) appeared comparable to wt mice (**A**). Scale bar: 40 µm.

In conclusion, loss of both profilins resulted in a dramatic loss in the branching complexity of CA1 pyramidal neurons. Similarly, to the cortical pyramidal neurons, the expression of only one allele of *Pfn2*, but not of *Pfn1*, could maintain the wt morphology.

2.3.6 Deletion of both profilin isoforms reduces pyramidal neurons density in the CA1 hippocampal region

To study whether PFN1 or PFN2 have a role in pyramidal neurons survival, cell density was evaluated in the CA1 hippocampal area of P80-P90 mutant and control mice. Excitatory glutamatergic neurons were labelled with an antibody recognizing neurogranin (NRGN). Neurogranin labels cell bodies and dendrites of glutamatergic neurons and mostly functions in spines, where it sequesters the Ca^{2+} sensor calmodulin, releasing it when phosphorylated by the protein kinase C (Petersen & Gerges, 2013; Zhong & Gerges, 2015).

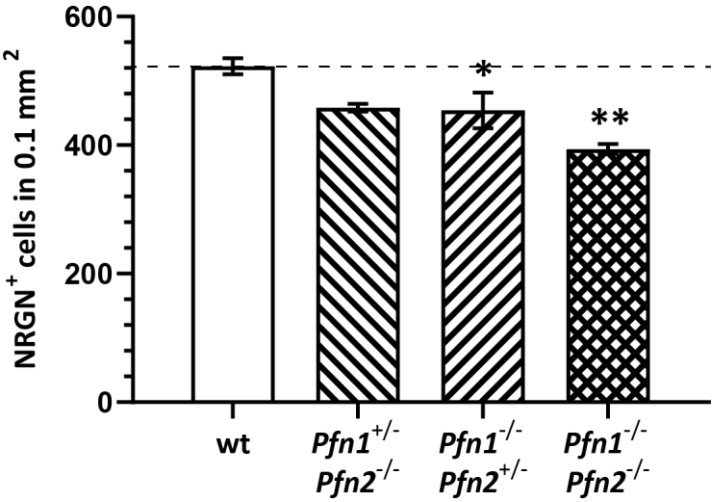

Figure 2.38 **| Loss of PFN1 and PFN2 causes a reduction of glutamatergic neurons density in the hippocampal CA1 region.** Bar graph representing the $NRGN^+$ cell density (n. cells/0.1 mm^2) in the CA1 region of the hippocampus from the different indicated genotypes. A clear significant decrease was observed in *Pfn1*$^{-/-}$;*Pfn2*$^{-/-}$ (*Pfn1-flx;Camk2a-Cre*) double ko (P=0.001), as well as an intermediate reduction in the animals with either one functional *Pfn1* (P=0.052) or *Pfn2* (P=0.040) allele. n=3 mice per genotype, n=3 slices per mouse (left and right hemisphere). Error bars represent s.e.m. One-way ANOVA - Dunnett's test, *P≤0.05, **P≤0.01.

The cell density was evaluated in wt, *Pfn1*$^{+/-}$;*Pfn2*$^{-/-}$, *Pfn1*$^{-/-}$;*Pfn2*$^{+/-}$ and *Pfn1*$^{-/-}$;*Pfn2*$^{-/-}$ mice (Supplementary Fig 7.10 - overview images of NGRN IF stainings) and resulted significantly reduced in *Pfn1*$^{-/-}$;*Pfn2*$^{-/-}$ double ko mice as well as, less strongly, in

animals with only one functional allele of *Pfn1* (*Pfn1*$^{+/-}$;*Pfn2*$^{-/-}$) or *Pfn2* (*Pfn1*$^{-/-}$;*Pfn2*$^{+/-}$), however in the first one without reaching significance (Fig 2.38).

2.3.7 Apoptosis might contribute to cell loss in the hippocampus of *Pfn1*$^{-/-}$;*Pfn2*$^{-/-}$ double ko mice

The decreased number of glutamatergic neurons in the CA1 region of *Pfn1*$^{-/-}$;*Pfn2*$^{-/-}$ double ko mice could be due to apoptosis, caused by the progressive decrease of synaptic transmission consequent to dendrite loss. In order to investigate whether apoptosis contributes to the cell loss observed in the CA1 hippocampal area, co-immunofluorescence staining of NRGN and cleaved caspase 3 (CASP3) was performed on brain sections of wt and *Pfn1*$^{-/-}$;*Pfn2*$^{-/-}$ mice. The cleaved caspase 3 is an enzyme that is only expressed in apoptotic cells. Caspase 3 is synthesized as an inactive pro-enzyme of 34 kDa, which is processed in cells undergoing apoptosis by extrinsic and intrinsic pathways. The cleaved isoform of caspase 3 consists of two subunits (of 17 and 12 kDa), which associate to form the active enzyme. Upon activation, the cleaved caspase 3 proteolytically cleaves and activates other caspases and degrades proteins within the cell (Elmore, 2007).

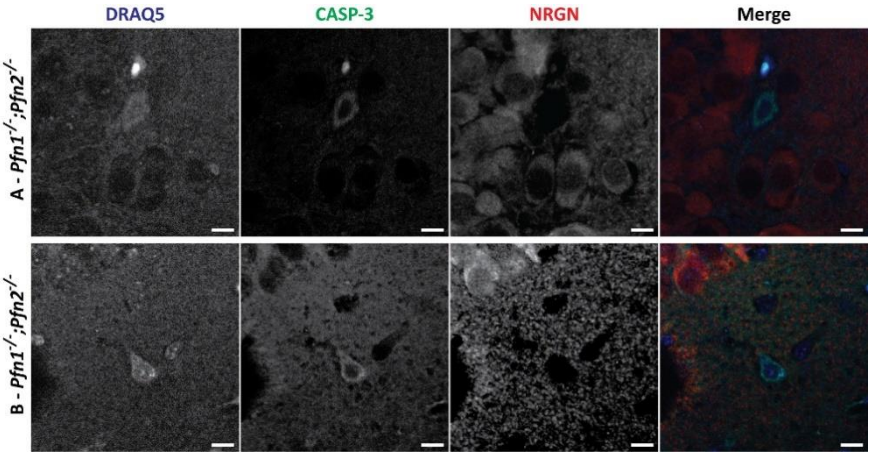

Figure 2.39 **| Apoptosis in the hippocampus of *Pfn1*$^{-/-}$;*Pfn2*$^{-/-}$ (*Pfn1-flx;Camk2a-Cre*) mice**. IF co-staining of NRGN and CASP3 in the CA1 hippocampal region of Pfn1$^{-/-}$;Pfn2$^{-/-}$ mice. Nuclei are labelled with DRAQ5 (blue), CASP3 and NRGN are labelled in green and red, respectively. CASP3^{+} cells were observed within the pyramidal cell layer (**A**) and in the stratum oriens (**B**) of Pfn1$^{-/-}$;Pfn2$^{-/-}$ mice but were negative to NRGN. Scale bars: 5 µm.

A few cells labelled with CASP3 were found in *Pfn1*$^{-/-}$;*Pfn2*$^{-/-}$ mice, whereas in wt mice no apoptotic cell was detected. CASP3^{+} cells found in the pyramidal layer and in the stratum oriens of *Pfn1*$^{-/-}$;*Pfn2*$^{-/-}$ hippocampi might not be glutamatergic neurons, since they were not labeled with neurogranin (Fig 2.39).

2.3.8 Disrupted cortical layering and reduced branching of hippocampal pyramidal neurons in old *Pfn1*$^{-/-}$;*Pfn2*$^{-/-}$ mice

Given the already strong phenotype observed in P80-P90 mice, after two months from the loss of both profilins (reduced complexity of the dendritic arborization of pyramidal neurons), it appeared interesting to study how the phenotype of double ko mice would evolve with aging.

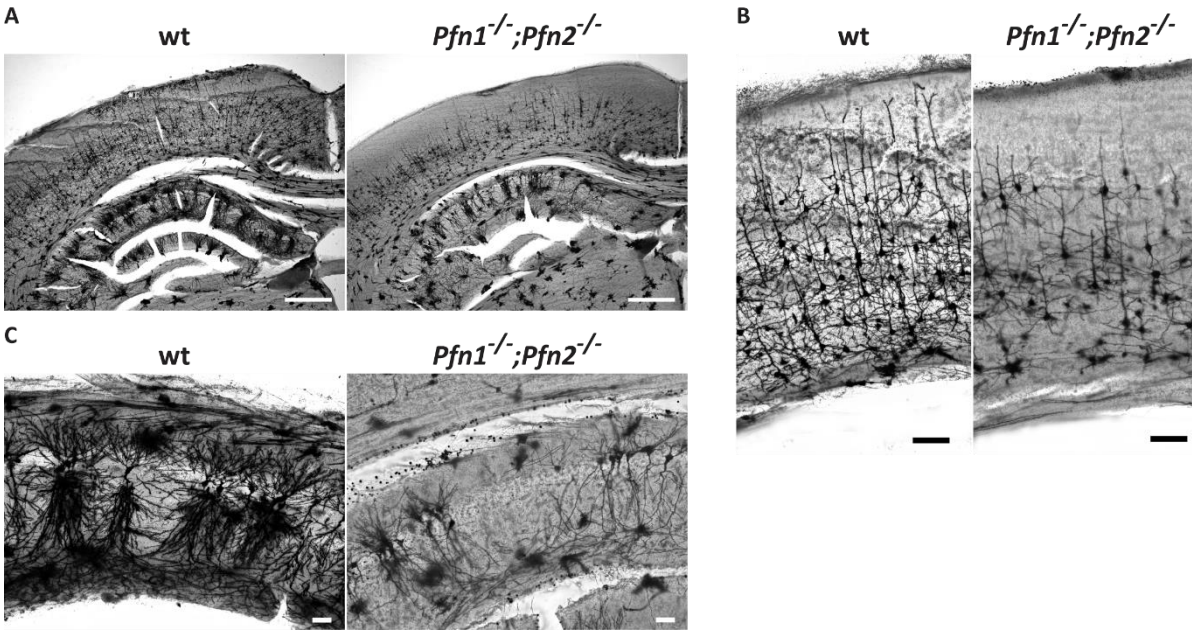

Figure 2.40 **| Disrupted cortical and hippocampal organization in 1-year old *Pfn1*$^{-/-}$;*Pfn2*$^{-/-}$ (*Pfn1-flx;Camk2a-Cre*) mice.** Sample images of the cortico-hippocampal region in Golgi-stained matched coronal brain slices from wt and *Pfn1*$^{-/-}$;*Pfn2*$^{-/-}$ 1-year old mice. An overview of the entire region in one hemisphere (**A**), a magnification of the cortex (**B**), and a magnification of the hippocampal organization (CA1 region) (**C**) are shown. In *Pfn1*$^{-/-}$;*Pfn2*$^{-/-}$ double ko mice cortical layering appeared altered with the upper layers (II-III) lost and cell density strongly reduced in cortex and hippocampus; hippocampal neuronal branching was also evidently affected. Scale bars: 500 μm (**A**); 100 μm (**B**) and 40 μm (**C**).

Double *Pfn* ko mice frequently displayed epileptic seizures (personal observations) and were housed single-caged in order to limit their occurrence. In these conditions they could survive until old age. Therefore, brains from 12 months old wt and *Pfn1*$^{-/-}$;*Pfn2*$^{-/-}$ animals could be examined by Golgi staining.

In *Pfn1*$^{-/-}$;*Pfn2*$^{-/-}$ double ko mice the top layers of the cortex (II and III), which at P80-P90 were occupied by the branchless cell bodies of the neurons, were almost empty having lost most of the cells (Fig 2.40 A - B). The cortical layering was less defined compared to wt (Fig 2.40 B), also due to the reduced cell number. In the CA1 region of the hippocampus, *Pfn1*$^{-/-}$;*Pfn2*$^{-/-}$ pyramidal neurons were very sparse and showed severely reduced branching, indeed only primary basal and apical dendrites could be observed (Fig 2.40 C).

In double ko mice the aging worsened the phenotype of the disrupted cortical organization and the reduced branching complexity of pyramidal neurons observed in younger animals.

Discussion

3.1 A novel molecular pathway in autism spectrum disorder is associated with profilin 2

In the first part of the thesis (chapter 2.1) has been reported evidence suggesting that deficiency of *Pfn2* in mouse could produce an autistic-like phenotype. The autistic-like behavior comprises core (social impairment and repetitive behavior) and comorbid (seizures - communication - motor and coordination deficits) symptoms of ASD. The *Pfn2* ko mouse model recapitulates all hallmarks of autism spectrum disorder, without affecting learning capabilities (Pilo Boyl *et al.*, 2007). As already mentioned in the introduction, it was previously demonstrated that PFN2 is required for fast actin polymerization in the pre-synaptic terminals, in order to restrain glutamatergic vesicles exocytosis during sustained depolarization and to regulate excitatory pre-synaptic physiology (Pilo Boyl *et al.*, 2007). In this work the neuronal acting binding protein profilin 2 was identified as a novel genetic cause for ASD; and it is supported the hypothesis that an increased excitation/inhibition (E/I) ratio in several neuronal circuits can be one cause of autism.

The *PFN2* gene is encoded in a genomic locus, the region 3q25-27, recently linked to autism spectrum disorders (AUTS2) (Auranen *et al.*, 2002). Studies in ASD subjects with Northern European ancestors living in the USA provided an additional linkage of ASD to the 3q25-27 region. The detailed clinical examination of all the family members revealed a broad diagnosis including infantile autism, Asperger syndrome, and developmental dysphasia (Coon *et al.*, 2005). Therefore, given PFN2 role in autistic-like behavior in mice, it was investigated whether gene mutations in *PFN2* could be found in human patients with ASD.

Different parts of the *PFN2* locus (coding regions, exon-intron junctions and partial 3' UTR) were sequenced in affected and healthy subject groups of the Finnish family cohort, but no specific SNV or indel correlating with the autistic syndrome was identified. Even though it was not found a direct link between PFN2 and ASD, it is

possible that ASD-causing mutations are in *PFN2* promoter or intronic regulatory regions. Also, in a recent whole exome sequencing study on USA families with ASD (Iossifov *et al.*, 2014) no single SNV, indel, or CNV was found in the *PFN2* gene and similar results were obtained on a European study group (Thomas Bourgeron, personal communication). Anyway, the heterogeneity of autism symptoms is related to the heterogeneity of the genetic factors that constitute it. Only a minority of ASD can be attributed to a single gene specific mutation or CNVs, therefore it is possible that specific SNP variants of *PFN2* in combination with variants in other genes might prime subjects to the autistic syndrome.

3.1.1 Lack of *Pfn2* produces an autistic-like behavior in the mouse model

ASD-like phenotypes in *Pfn2* ko animals are addressed by performing behavioral assays. Maternal behavior was severely affected in *Pfn2* ko mothers; indeed, the nest building and pup retrieval behaviors were severely compromised. Qualitative and quantitative impairments in social interactions were exhibited by *Pfn2* ko mice, as demonstrated by the altered social approach to the stranger mouse in the 3-chambered test. Social deficits in autism often appear as inappropriate or indiscriminate approaches to strangers; in this regard, the *Pfn2* ko mice were often avoiding nose to nose contacts and were also lacking aggressive intention movements, attack or escape behaviors.

Mice display social communication mechanisms, which could be tested by quantitative measures of ultrasound vocalization (USV) emitted by pups removed from the nest and parental retrieval of the pups (Crawley, 2007). In our *Pfn2* mouse model, the impaired parental retrieval of separated pups and the increased number and monotony of USVs by *Pfn2*$^{-/-}$ pups demonstrated the presence of deficits in communicative interactions. Similarly, to what has already been observed in other mouse models of autism, the elevated pitch of autistic infants cries and the higher intensity of USV calls of pups might be functionally related (Roy *et al.*, 2012; Tsai *et al.,* 2012; Young *et al.*, 2010).

Repetitive and ritualistic behaviors are considered a hallmark for ASD. Furthermore, autistic individuals often maintain rigid habits and frequently show a strong insistence on sameness and resistance to change routine (Frith, 1991; Hollander *et al.*, 2003; Crawley, 2007). *Pfn2*$^{-/-}$ animals showed higher occurrence of stereotyped behaviors, such as circling - jerking - wall leaning. No significant variation was observed in self-grooming and digging, most likely because animals showed a lack of interest in themselves and their surroundings. *Pfn2*$^{-/-}$ animals showed also increased resistance to changes as demonstrated in the Y-maze task. In fact, animals with increased repetitive tendencies usually exhibit in this task a higher number of repetitive entries into the same arm (Favre *et al.*, 2015; Kirsten *et al.*, 2012; Naviaux *et al.*, 2014; Xue *et al.*, 2016), as also demonstrated by *Pfn2*$^{-/-}$ mice.

In humans it was suggested that motor deficits may occur even before communicative or social deficiencies, implying that impaired motor behavior may constitute an ASD feature (Adrien *et al.*, 1993; Baranek 1999; Teitelbaum *et al.*, 2004; Leary & Hill, 1996; Nayate *et al.*, 2005; Fournier *et al.*, 2010). Moreover, motor coordination abnormalities have been reported in mice models for ASD (Crawley, 2007). Accordingly, in our *Pfn2* ko mouse model coordination and motor deficits were also observed.

3.1.2 The autistic-like phenotype of the *Pfn2* ko mouse model is linked to an imbalanced excitation-inhibition (E/I) ratio of neuronal activity

Previously it was shown that the mouse model lacking the actin binding protein PFN2 exhibits an alteration of synaptic activity, due to increased glutamatergic transmission in the cortico-striatal pathway (Pilo Boyl *et al.*, 2007). Similarly, PCs in *Pfn2* ko mutant mice receive increased glutamatergic inputs from parallel fibers (unpublished data). Here it is shown that loss of PFN2 results in increased glutamatergic as well as decreased GABAergic transmission in the Schaffer collaterals. The three mentioned different neuronal circuits mediate social, stereotypic and motor behaviors, which

were found impaired in the *Pfn2* ko mouse model. The *Pfn2* ko mouse model also shows spontaneous audiogenic epileptic seizures, possibly induced by a hypersensitivity to sensory stimuli, implying again increased glutamatergic transmission. Several clinical studies indicate that ASD and epilepsy frequently co-occur specifically, it was observed that epilepsy occurs in 20-25 % of ASD patients (Canitano, 2007). Commonly the prevalence of epilepsy among all children is estimated at 2–3 %, compared to ~30 % in autism (Tuchman & Rapin, 2002). Furthermore, 50-70 % of autistic children have ongoing "sharp spike" activity documented in sleeping EEG or magnetoencephalography recordings (Lewine *et al.*, 1999; Wheless *et al.*, 2002), suggesting that children with ASD have noisy (hyperexcitable) and unstable cortical networks.

The transfer of the information in the brain relies on a functional balance between excitatory and inhibitory networks. At the level of individual neurons, this balance involves the maintenance of the appropriate ratio of excitatory versus inhibitory inputs (Megías *et al.*, 2001; Gao & Penzes, 2015). Glutamatergic synapses excite other glutamatergic neurons and inhibitory neurons, which in turn inhibit excitatory neurons and other GABAergic neurons. Therefore, the maintenance of the circuit E/I ratio is critical for the normal brain development and for its regular functioning (Nelson & Valakh, 2015; Lee *et al.*, 2017).

A widely accepted hypothesis on the etiology of ASD proposes that there is excitatory-inhibitory imbalance in brain neural circuits (Hussman *et al.*, 2001; Rubenstein & Merzenich, 2003). This theory provided a potential explanation for the frequent observation of reduced GABAergic signaling (Cellot & Cherubini, 2014) and decreased density of cortical GABA receptors in the brains of autistic patients as well as their propensity to develop epilepsy (Nelson & Valakh, 2015; Bozzi *et al.*, 2018).

In mouse models, both upregulation and suppression of inhibitory synaptic transmission has been detected (Isshiki *et al.*, 2014). Since inhibition is known to contribute to sharpening the selectivity of excitatory responses in many brain areas (Nelson & Valakh, 2015), the breakdown of inhibitory signaling and/or the increased

excitatory neurotransmission have been proposed to be related to ASD and epilepsy (Bozzi *et al.*, 2018). In the past several mouse models of ASD with an increased E/I ratio, due to either an enhanced glutamatergic or an impaired GABAergic activity, have been studied. The knockout of *Gabarb3* (DeLorey *et al.*, 1998; Sinkkonen *et al.*, 2003), *Cntnap2* (Peñagarikano *et al.*, 2011) and *Fmr1* (Bozzi *et al.*, 2018) represent examples of mouse models of ASD with an impaired GABAergic neurotransmission; on the contrary, knockout mouse models for *Eeif4-bp2* (Gkogkas *et al.*, 2013), *Irsp53* (Chung *et al.*, 2015) and *Syngap1* (Ozkan *et al.*, 2014) show increased glutamatergic neurotransmission. It is interesting to observe that IRSp53 has been proposed as an indirect link to actin within post-synaptic terminals and that SYNGAP1 is a RAS-GTPase activating protein critical for proper synapse function.

On the other side of the spectrum are the autism mouse models with decreased E/I ratio (i.e. *Nrxn1*α - Etherton *et al.*, 2009, *Nlgn3* (R451C) - Tabuchi *et al.*, 2007; *Nlgn3* (R704C) - Etherton *et al.*, 2011, *Shank2* - Schmeisser *et al.*, 2012, *Shank3* - Bozdagi *et al.*, 2010/Peça *et al.*, 2011, and others), which show strong cognitive impairment in addition to the autistic-like phenotype. Recent findings by Filice *et al.* (2016) suggest that the shift of E/I balance towards enhanced inhibition might represent a common feature of some mouse models of ASD that are not necessarily associated with epilepsy comorbidity (Bozzi *et al.*, 2018), but are associated to ID (Nelson & Valakh, 2015). On the contrary, autism with normal or increased intellectual capacity might be associated to increased E/I ratio. This hypothesis suggests that pharmacological treatments leading to restoration of E/I balance might represent an effective therapeutic strategy for ASD-epilepsy comorbidity.

Our mouse model shows that PFN2 contributes to an autistic phenotype by shifting the E/I balance towards an enhanced excitation, at least in the hippocampus. Learning and memory were not affected in the *Pfn2* ko mouse model (Pilo Boyl *et al.*, 2007), suggesting that increased E/I ratio as a cause of ASD is uncoupled from ID.

3.2 Functions of profilins during brain development

The actin cytoskeleton plays crucial roles during brain development and in the establishment of functional neuronal circuits. Alterations in the organization and dynamics of the actin cytoskeleton, due to altered expression patterns of specific ABPs, are linked to various neurodegenerative diseases (Hoogenraad *et al.*, 2004; Maloney & Bamburg 2007).

In the second part of this study, precisely in chapter 2.2, the *Pfn1*$^{flx/del}$*;Pfn2*$^{-/-}$*;Nes-Cre*$^{cre/wt}$ mouse line was used to investigate how lack of PFN1 and PFN2 could affect mouse brain development.

3.2.1 PFN1-specific and PFN2-redundant functions in brain development

The mammalian cortex is a critical brain area responsible for higher brain functions including attention, memory, language, cognition and sensory perception. The cerebral cortex is a particularly demanding structure because of the intricate pattern and interplay of cell proliferation and neuronal migration that is required during its development. The precise assembly of the brain in general, and specifically of the cortex, is an essential step during embryonic development (Mao *et al.*, 2019). Previous publications (Bellenchi *et al.*, 2007; Feng *et al.*, 2000; Pan *et al.*, 2015) and the current study on the *Pfn1*$^{-/-}$*;Pfn2*$^{-/-}$ double ko mouse line provide evidence that proteins affecting actin filament dynamics are valid candidates in diverse neurological and mental disorders, including epilepsy, schizophrenia, autism and ID (Su *et al.*, 2011; Pan *et al.*, 2015; Jayaraman *et al.*, 2018; Mao *et al.*, 2019).

As already discussed in the introduction, PFN1 and PFN2 play different roles during brain development with PFN1 seeming to play a more prominent role, although no single profilin appears to be essential. To dissect any functional overlap between the two isoforms and to find out whether the function of PFN2 during embryonic development was hidden by the presence of PFN1, studies on embryos lacking both profilins or either expressing one allele of *Pfn1* or *Pfn2* were performed. For this

purpose, it was first evaluated the protein expression of PFN1 and PFN2 in mouse brain, from embryonic to adult age. Interestingly, it was shown that PFN1 expression is highest during embryonic brain development and constantly decreases from P1 to reach the lowest levels in adulthood. On the contrary, PFN2 expression steadily increases during brain development reaching its maximum at P7, when synaptogenesis starts. These observations imply that PFN1 is more important for embryonic brain development rather than adult brain physiology; while PFN2 appears to be mostly required during postnatal neuronal development and function.

It is well established that PFN1 and PFN2 are key players in the regulation of actin polymerization. Given the critical importance of the actin cytoskeleton in various cellular functions, particularly neuronal morphology and motility, it is not surprising that genetic ablation of both *Pfn1* and *Pf*n2 genes in the CNS of mice at mid-embryonic developmental stage caused profound alterations in brain structure. Specifically, in *Pfn1*$^{-/-}$;*Pfn2*$^{-/-}$ double ko embryos it was not possible to observe a formed brain underneath the skull at E16.5. This work shows that PFN1 is the only profilin isoform needed and sufficient to maintain a proper brain development, since the expression of only one allele of *Pfn1* completely restored the disrupted brain development observed in the *Pfn1*$^{-/-}$;*Pfn2*$^{-/-}$ double ko animals. On the other hand, the expression of only one allele of *Pfn2* helped little to restore brain development. In conclusion, PFN2 shows only a partial overlapping function with PFN1, probably in sustaining cell proliferation. However, in this study, it was not clarified whether the partial recovery in brain development observed in *Pfn1*$^{-/-}$;*Pfn2*$^{+/-}$ embryos was due to a not sufficient expression of PFN2 during embryonic development or to mostly distinct roles of the two profilin isoforms.

3.2.3 Profilins regulate cell cycle progression during development

The cell cycle of eukaryotic cells can be divided into two major phases: interphase, during which the cell grows and the DNA is duplicated (S-phase); and mitosis (M-phase), where the nucleus and cytoplasm divide. Two gap phases, G1 and G2, are

executed before and after S-phase, respectively. G1 phase is a critical stage, allowing responses to extracellular cues that induce either commitment to finish G1 and enter S-phase or withdrawal from the cell cycle (G0) to embark on a differentiation (post-mitotic) pathway. The end of G1 phase is also involved in the control of DNA integrity before the onset of DNA replication. During G2 phase, the cell checks that the DNA replication is properly performed and controls the genomic integrity before cell division starts. The transition from one phase of the cell cycle to the next is controlled by cyclin–CDK (cyclin-dependent kinase) complexes which ensure that all phases of the cell cycle are processed in the correct order (Dehay *et al.*, 2007).

The entry of eukaryotic cells into mitosis is regulated by Cdc2 kinase (CDK1) activation. The activation of CDK1 is a process controlled by several steps including dephosphorylation of the kinase on Tyr15 and Thr14, cyclin B1 binding and phosphorylation of Thr161 (Atherton-Fessler *et al.*, 1994). However, the first one is the main and critical regulatory step for CDK1 activation and progression into mitosis (Norbury *et al.*, 1991). Specifically, phosphorylation on Tyr15 and Thr14, carried out respectively by Wee1 and Myt1 protein kinases, results in inhibition of CDK1 activity (Wells *et al.*, 1999; McGowan *et al.* 1993), whereas the activation of the CDK1 kinase is caused by dephosphorylation of Tyr15 and Thr14 by the CDC25 class of phosphatases (Atherton-Fessler *et al.*, 1994; Hunter *et al.*, 1995).

In this study the mitotic progression was examined by monitoring the dephosphorylation of CDK1 on Thy15; the higher level of phosphorylation of the CDK1 in mouse embryos lacking *Pfn1* and *Pfn2* was considered a hallmark of a block during the G2/M transition of the cell cycle.

Interestingly, in *Pfn1*$^{-/-}$;*Pfn2*$^{-/-}$ double ko embryos it was also found a higher expression of TPX2, a marker for cells in phase G2/M of the cell cycle, and of phosphorylated H3, a mitotic cell-marker, which together with the presence in the VZ of the double ko embryos of nuclei with preferentially condensed chromatin rather than polarized

segregating chromosomes, further proves the existence of a higher number of cells with delayed or arrested mitotic progression.

Moreover, since embryos with one allele of *Pfn1* resemble the wildtype condition, (with a low expression of TPX2 and pH3) whereas embryos with one allele of *Pfn2* show a similar phenotype to the double ko embryos (with a high expression of TPX2 and pH3), it is conceivable that PFN1 is necessary and sufficient for proper cell proliferation in the developing mouse brain, while PFN2 is dispensable and not capable of compensating PFN1 functions. Further analysis on spindles in the *Pfn1*$^{-/-}$*;Pfn2*$^{-/-}$ double ko and in *Pfn1*$^{+/-}$*;Pfn2*$^{-/-}$ embryos, expressing only one allele of *Pfn1*, is required to confirm that PFN1 in addition to its role during cytokinesis (Böttcher *et al.*,2009) might also have a role in spindle formation. The analysis should be performed on embryos aged between E11.5, when *Pfn1* deletion starts and E14.5, when, as indicated by the H&E stainings the loss of cells is already evident. It would be interesting not only to evaluate the reduction in the proliferation rate at further stages of the development, but also to assess the levels of the Wee kinase, which is degraded with the activation, via dephosphorylation, of the CDK1 kinase (Watanabe *et al.*, 2004; Okamoto & Sagata, 2007).

At early stages of mouse corticogenesis, the neuroepithelial cells mainly adopt symmetric cell division to expand the neuroepithelial plane, thereby promoting enlargement of the ventricle surface. As development proceeds, neuronal stem cells are progressively biased toward asymmetric division, in order to differentiate into progenitor cells and post-mitotic neurons (Lian & Scheen *et al.*, 2015). The actin cytoskeleton participates to the cell cycle progression (Lian & Scheen *et al.*, 2015; Olson *et al.*, 1995; Cappello *et al.*, 2006; Woodhead *et al.*, 2006; Katayama *et al.*, 2011; Ercan-Sencicek *et al.*, 2015). Specifically, actin filaments are essential to set the orientation of the cleavage plane (Cowan & Hyman 2004), regulating in this way the progression through phase M and ensuring the completion of cytokinesis (Heng & Koh, 2010).

Our study elegantly shows the existence of an actin-checkpoint that precedes or accompanies the well-known checkpoint for spindle assembly during G2/M transition. The existence of this actin-checkpoint, which might be evolutionarily conserved, has been already postulated in different organisms. In *Saccharomyces cerevisiae*, a role for actin in the establishment of an oriented spindle, early during cell cycle was identified (Theesfeld *et al.*, 1991). Specifically, a mitotic checkpoint that monitors the integrity of the actin cytoskeleton and delays sister chromatid separation and cytokinesis has been described during yeast fission (Theesfeld *et al.*, 1991). In *Schizosaccharomyces pombe*, cells treated in G2 with latrunculin B, to induce actin depolymerization, showed misoriented spindles and as a consequence delayed entering mitosis (Rupes *et al.*, 2001; Gachet *et al.*, 2001).

Furthermore, in a different study was shown that the mitotic delay is imposed by the stress-activated MAP kinase, which has been reported to function as an actin-checkpoint at the G2/M phase (Gachet *et al.*, 2001). In a study from 2007 a role of actin to regulate mitosis has been postulated in primary mammalian cells (Lee & Song, 2007). Specifically, it was proven that disruption of the actin cytoskeleton, using the actin polymerization inhibitor cytochalasin D, leads to cytokinesis failure due to a defect in the F-actin cable ring at the cleavage furrow; in addition, it was demonstrated that the mammalian primary cells treated with cytochalasin D showed a delayed activation of CDK1, causing a block during cell cycle progression (Lee & Song, 2007 ; Lian *et al.*, 2015).

Diverse mouse models with defective development of the cerebral cortex have shown that, apart from cell migration, cell proliferation and cell cycle progression are critical and determinant steps during development (Woodhead *et al.*, 2006; Bellenchi *et al.*, 2007; Katayama *et al.*, 2011; Lian *et al.*, 2012).

An example of the importance of cytoskeleton in proliferation is provided by FLNA. FLNA as a scaffolding protein, plays an important role in embryonic development by linking adhesion proteins and membrane receptors to the actin cytoskeleton (Lian &

Sheen, 2015). In E15/E18.5 *FlnA* knockout embryos, loss of *FlnA* causes a decrease of the proliferation rate of NPCs and a decline in neuronal progenitor pool size; in this mouse model, the drop in the progenitor population was attributable to a prolonged cell cycle duration, as demonstrated by the increased inhibitory phosphorylation of CDK1 (Lian *et al.*, 2012). Therefore, similarly to our *Pfn1*$^{-/-}$*;Pfn2*$^{-/-}$ double ko embryos, the increased inhibitory phosphorylation on CDK1 would prolong the cell cycle, because of an impairment in actin filament rearrangement (Lian & Sheen, 2015).

3.3 Functions of profilins in the adult brain

In chapter 2.3 of this work the *Pfn1*$^{flx/flx}$*;Pfn2*$^{-/-}$*;Camk2a-Cre*$^{cre/wt}$ mouse model was used to investigate the functions of the two profilin isoforms in adult - already formed - brain circuits. In this double ko line the PFN1 deletion occurs starting from P18 in the forebrain, among others in excitatory neurons of the cortex and hippocampus. *Pfn1*$^{-/-}$*;Pfn2*$^{-/-}$ double ko mice are viable, therefore the analysis was performed on P80-P90 and 1-year old mice.

3.3.1 Profilins functions in the regulation of pyramidal neuron branching

The unique stereotypic architecture of individual neuronal subtypes is fundamental to their ability to integrate into functional neuronal circuits and dictates the extent and quality of information flow across the neural network. Functional integration of neuronal activity is achieved through the projection of elaborately branched dendritic trees into multiple target areas. Neurons develop arbors with branching morphologies that are characteristic for each subtype (Pai & Moore, 2018) and their position in the brain, which then influence the firing pattern of the neuron itself (Dong *et al.*, 2015; Lanoue & Cooper, 2018). Since it is well-known that the dendritic structure and arborization have a profound impact on the processing of neuronal information

(Arikkath, 2012), layer V pyramidal neurons in the cortex and CA1 pyramidal neurons in the hippocampus have been extensively studied in this work. Pyramidal neurons in the cortex and hippocampus have a characteristic morphology with distinct large apical dendritic arbors and shorter basal dendrites. The apical primary dendrite departs from the apex of the triangular soma and in the cortex is directed towards the pial surface, while many basal primary dendrites depart from the base of the soma. Moreover, primary apical and basal dendrites are further ramified (Spruston, 2008).

In this work, it has been shown that loss of both PFNs strongly affects and impairs branching complexity of cortical and hippocampal pyramidal neurons; indeed in the double ko, after less than 2 months from the deletion of both profilins, the structure of pyramidal neurons appears very simplified with only the primary branch left and all higher order branches lost. Pyramidal neurons are usually covered with thousands of dendritic spines, that constitute the postsynaptic site for most excitatory glutamatergic synapses. The number of spines represents a minimum estimate of the number of excitatory synaptic inputs onto a neuron, which varies considerably in different regions and species (Spruston, 2008). *Pfn1*$^{-/-}$*;Pfn2*$^{-/-}$ double ko mice, losing the higher order dendrites, showed only primary branches with not so many visible dendritic spines. From a detailed branching analysis performed on the pyramidal cortical neurons, it resulted that *Pfn1*$^{+/-}$*;Pfn2*$^{-/-}$ mice, only expressing one allele of *Pfn1* and no *Pfn2*, also show a comparably severe reduction of apical and basal branching. Instead, *Pfn1*$^{-/-}$*;Pfn2*$^{+/-}$ mice, expressing only one allele of *Pfn2* and completely lacking *Pfn1*, show only mild reduction of higher order basal and apical dendrites.

Previous *in vitro* studies from Michaelsen showed that the RNAi-mediated knockdown of PFN2 in mature pyramidal neurons affects both the number of dendrites and spine density (Michaelsen *et al.*, 2010). The reduced dendritic complexity and the spine density could be totally rescued by overexpression of PFN2; whereas the expression of exogenous PFN1 could only partially compensate for spine density but not for dendritic complexity. Therefore, in Michaelsen study it was hypothesized a specific

function for PFN2 in stabilizing dendrite architecture and a redundant function of the two profilin isoforms in maintaining dendritic spines (Michaelsen *et al.*, 2010). In accordance, our study seems to confirm, also *in vivo*, that the expression of only one allele of *Pfn2* could sufficiently preserve the dendritic complexity avoiding the massive branching loss observed in *Pfn1*$^{-/-}$;*Pfn2*$^{-/-}$ double ko mice. On the contrary, the expression of only one allele of *Pfn1* was only able to partially compensate for the dendritic loss. And since the loss of PFN1 was evident starting from P28, when the dendritic architecture of the neurons is already formed, our findings seem to indicate that, *in vivo,* PFN2 plays a crucial role in the maintenance of dendritic structure in mature cortical and hippocampal pyramidal neurons, exerting PFN1-indipendent or PFN1-redundant functions. Anyway, current findings do not allow us to say that the maintenance of dendritic arborization can be exclusively attributable to PFN2, since no post-synaptic defect, neither physiological nor behavioral, could be detected in *Pfn2*$^{-/-}$ mice. Moreover, ultrastructural analysis in the stratum radiatum of the CA1 region of *Pfn2*$^{-/-}$ mice revealed unchanged synaptic morphology and density (Pilo Boyl *et al.*, 2007), possibly indicating normal higher order branching. On the other hand, it is important to consider that PFN2 is the highest PFN isoform expressed in the brain. Specifically, PFN2 accounts for the 0.15 % of the total protein of the brain, whereas PFN1 only represents the 0.05 % (Witke *et al.*, 1998). Moreover, PFN2 expression peaks at P7-P14, when the process of synaptogenesis takes place, during which many new synaptic contacts are built and neuronal connectivity is established.

Therefore, it is conceivable that loss of PFN2 alone is only sufficient to induce the dendritic phenotype, without long-term consequences. Or is it possible that the reduced arborization of neurons is evident when no allele of profilins or one allele of *Pfn1* are expressed.

To understand whether the maintenance of the branching and of the dendritic spines on higher order branches is specifically related to *Pfn2* gene function or to a PFN1-PFN2 protein dosage-dependent effect, detailed branching analysis should be

performed on *Pfn2*$^{-/-}$ mice at three months of age and on *Pfn1*$^{-/-}$;*Pfn2*$^{-/-}$ double ko mice at P21-P24, before the loss of PFN1 expression.

Beyond PFNs, also the depletion of other ABPs negatively affect dendritic branching (Lanoue & Cooper, 2019). For example, loss of Cobl, a WH2 nucleation factor which accelerates actin filament formation, disrupts dendrite branching (Gao *et al.*, 1999). Ena/VASP promotes profilin-catalyzed actin polymerization, thereby increasing filopodia activity and enhancing neurite growth and branching (Lanoue & Cooper, 2019; Kalil & Dent, 2014; Lebrand *et al.*, 2004); its loss also disrupts dendrite branching (Gao *et al.*, 1999). ARP2/3 complex activation requires the binding of WASP, a nucleation promoting factor. WASP overexpression in cultured hippocampal neurons results in an increased number of dendritic branches, whereas the block of the WASP-ARP2/3 interaction leads to a reduction in distal branching (Nakamura *et al.*, 2011; Lanoue & Cooper, 2019).

3.3.2 Profilins dosage affects neuronal survival in the CA1 hippocampal region

Pyramidal neuron density was evaluated in the CA1 hippocampal region and was found significantly reduced in profilins double ko mice; a certain degree of reduction was also observed in mice expressing one allele of either *Pfn1* or *Pfn2.*

One of the most studied causes of cell death is apoptosis. In *Pfn1*$^{-/-}$;*Pfn2*$^{-/-}$ double ko hippocampi signs of ongoing apoptosis, expression of cleaved CASP3, were not detected in pyramidal neurons (neurogranin-positive cells), but in cells not expressing neurogranin. In this work, the specific cell-type of the neurogranin-negative cell undergoing apoptosis was not further studied. In conclusion, the exact reasons of pyramidal cell loss are yet to be determined. A possible hypothesis is that the apoptotic non-glutamatergic cells are inhibitory neurons. Interneurons should not be affected by the ko of *Pfn1*, given that PFN1 is deleted only in CAMKIIα-expressing cells, therefore only excitatory neurons of the hippocampus (Minichiello *et al.*, 1999). On

the other hand, PFN2 is expressed in a subset of inhibitory neurons in different brain regions, hippocampus included (Liemersdorf, 2016). Therefore, the observed apoptosis of interneurons in double ko hippocampi could be the result of the loss of PFN2.

An alternative hypothesis is that some other type of cell-death mechanism occurs in excitatory neurons. Following the developmental period, postmitotic neurons are required to be long-lived in order to maintain functional brain circuits. But aberrant neuronal cell death, a phenomenon which contributes to acute and chronic neurodegenerative disease, can occur. In neurodegenerative disorders, several observations support the idea that cell death is only a secondary event and that the loss of synaptic connectivity better reflects the manifestation of the pathological symptoms (Gasic & Nicotera , 2003; Vanderhaeghen & Cheng, 2010). Commonly, when widespread synaptic dysfunction impairs neuronal connectivity, the progressive damage of the neural network is eventually followed by neuronal loss (Gasic & Nicotera , 2003).

Since the actin cytoskeleton plays a crucial role in cell shape and structure, as well as for gap junctions with the nurturing astrocytes, the depletion of PFNs, important regulators of actin filament polymerization, could interfere with the maintenance of a healthy cell shape and with the access to nutrient supply.

Moreover, cell death is, usually, not a “cell autonomous” event but is often triggered by interactions with neighboring neuronal or glial cells. Loss of neurons could occur as a result of loss of synaptic contacts, dendrites, axons or other surrounding neurons. This degeneration can occur to neurons either downstream (anterograde) or upstream (retrograde) of a dead neuron. Thus, anterograde transneuronal degeneration results from loss of synaptic inputs into neurons, while retrograde transneuronal degeneration results from loss of synaptic outputs (Fricker *et al.*, 2018). Therefore, the observed neuronal loss could be the consequence of less synaptic inputs onto the neurons, due to the reduced dendritic branching observed in PFNs double ko mice.

Methods

4.1. Mouse experiments

Mice were socially housed with a standard 12 h light/dark cycle at 22 °C and 50-55% humidity, with free access to water and food pellets. Animals were kept according to European animal welfare regulations. Animal experiments were performed according to LANUV permissions AZ 84-02.04.2013.A223 and AZ 84-02.04.2017.A088.

4.2 Molecular Biology

4.2.1 Genomic DNA extraction from embryos

The developmental role of PFN1 and PFN2 was studied. At this purpose, it was necessary to set precise time mating between the animals, in order to obtain embryos at defined developmental stages. Two females (with the genotype: *Pfn1*$^{flx/flx}$*;Pfn2*$^{+/-}$*;Nes-Cre*$^{wt/wt}$) were placed O/N in a cage with a male (with the genotype: *Pfn1*$^{wt/del}$*;Pfn2*$^{+/-}$*;Nes-Cre*$^{cre/wt}$), and the morning after existence of the mating was determined by presence of a vaginal plug. The day of identification of the vaginal plug was set as E0.5 (number 0.5 of embryonic day of development). Three different developmental stages were analyzed: E11.5 – E14.5 - E16.5. The solutions used for the DNA analysis are listed in chapter 5.2.2.

To determine the genotype of the embryos, 1 mm tail biopsy was used. The tissue was boiled in 1x TENT buffer (80 µl for 1 mm biopsy) for 10 min at 98°C. The proteins of the biopsy were then digested in TENT buffer supplemented with 0.5 µg/µl proteinase K at 55°C O/N. The proteinase K is then inactivated at 98°C for 10 min. The different incubation steps were performed in a PTC100 Thermal Cycler. Later**,** the samples were vortexed and pipetted in order to break the remaining tail fragments, which were then spinned down 2 min at maximum speed. 1 µl of the supernatant was used for the genotyping PCR.

4.2.2 Genomic DNA extraction from mice

Mouse tail biopsies of approximately 3-4 nm were collected from 15-21 days-old pups. The tail biopsy was placed in 1.5 ml Eppendorf with 200 µl of DNA extraction buffer containing 0.5 µg/µl proteinase K. In this buffer the proteins of the tissue were digested O/N at 56°C. After this long incubation time the samples were shortly mixed and half volume (100 µl) of saturated NaCl solution was added. Then, the tubes were shaken vigorously for 1 min and centrifuged at 14000 rpm for 14 min at room temperature (RT). Approximately 200 µl of supernatant was picked up and transferred in a new tube containing ~2.5 volumes (500 µl) of ethanol. The ethanol caused the precipitation of the DNA as a floccule, which was further spinned down at 14000 rpm for 2 min. The supernatant was removed, using a Pasteur pipette, and the pellet was dried out at 37°C for a few minutes. The DNA was resuspended in 200 µl of Milli-Q water by mixing at 37°C for 30 min. For a genotyping PCR 1 µL of this solution was used.

4.2.3 Polymerase chain reaction (PCR)

The PCR is an evolutionary technique, originally developed in 1983 by the American biochemist Kary Mullis. It is used to amplify (make many copies) of small target sections of DNA. This method it is often employed to detect the presence or the absence of a specific gene (Mullis & Falona, 1987).

The denaturation at 94°-98°C of the genomic template for 30 sec-2 min leads to the separation of the dsDNA (double strand DNA) into ssDNA (single strand DNA). Specific sequences of oligonucleotides (~18-25 nucleotide long), also known as primers, have a complementary sequence to the ssDNA templates and therefore can anneal to them for 15-90 sec at the temperature of ~55-65°C. Primers are chosen in pairs, with one being 5´-3´ (sense/forward) direction and the other one 3'-5' (antisense/reverse) direction compared to the DNA template. Once the primers interact to the ssDNA template in presence of the Taq polymerase new fragments of DNA can be

polymerized. The Taq polymerase (isolated from the *archaea bacterium Thermus aquaticus)* is enzyme which elongates the primers in the 5'-3' direction at a temperature ranging from 68°-72°C, by catalyzing the incorporation of free dNTPs (deoxynucleotides) at the 3' – OH of the primer. To allow the taq polymerase to work efficiently, divalent ions are provided by adding $MgCl_2$ in the reaction buffer. The entire process of denaturation, annealing and elongation is repeated for 25-35 cycles, in order to amplify the DNA exponentially. A final extension step of 3-10 min is usually done to ensure that the new fragments of DNA generated are full length. Usually annealing and elongation time and temperature can be adapted in dependence of the melting temperature of the primers and the amplicon size.

In this work of thesis, the PCR was used to determine the genotypes of mouse embryos, pups and adults.

4.2.3.1 The *Pfn1* PCR

The *Pfn1* PCR was used to determine whether embryos and mice had a floxed, deleted, or wildtype allele for *Pfn1*. Specific PCR mix preparation protocol (see table 4.1) and PCR conditions (see table 4.2) were adopted. For the reaction 1 µl of genomic DNA was added to 19 µl of PCR mix.

Table 4.1 - *Pfn1* genotyping PCR mix.

Reagent	Concentration	Amount (µl)
Milli-Q H_2O		11.9
PCR-flexi-buffer (5x)	5x	4
MgCl2 (25 mM)	25 mM	1.2
dNTPs (10 mM)	10 mM	0.4
546/789 (20 µM)	20 µM	0.2
546/752 (20 µM)	20 µM	1
Taq polymerase (5 u/µl)	5 µl	0.3

The couple of primers n.569/n.789 (listed in chapter 5.1.1 – table 5.1) were used in order to amplify a fragment of 306 bp in the *Pfn1*-wt allele and/or a fragment of 370

in the *Pfn1*-floxed allele; instead primers n. 546/n. 789 were employed to identify a fragment of 500 bp in the *Pfn1*-deleted allele.

Table 4.2 – *Pfn1* genotyping PCR conditions.

Temperature	Time	
98 °C	2 min	
96 °C 60 °C 72 °C	30 sec 60 sec 30 sec	35 cycles
72 °C	5 min	

4.2.3.2 The *Pfn2* PCR

In the *Pfn2* PCR the couple of primers (listed in chapter 5.1.1 - table 5.1) n. 229/n.422, identifying the *Pfn2*-wt allele (266 bp) and the couple of primers n.229/n423, identifying the *Pfn2*-ko allele (200 bp), were used. The following PCR mix preparation protocol (see table 4.3) and PCR conditions (see table 4.4) were adopted. For the reaction 1 µl of genomic DNA was added to 19 µl of PCR mix.

Table 4.3 - *Pfn2* genotyping PCR mix.

Reagent	Concentration	Amount (µl)
Milli-Q H_2O		11.1
PCR-flexi-buffer (5x)	5x	4
MgCl2 (25 mM)	25 mM	1.2
dNTPs (10 mM)	10 mM	0.4
229/422 (20 µM)	20 µM	1
229/423 (20 µM)	20 µM	1
Taq polymerase (5 u/µl)	5 µl	0.3

Table 4.4 - *Pfn2* genotyping PCR conditions.

Temperature	Time	
98 °C	2 min	
96 °C 55 °C 72 °C	30 sec 75 sec 30 sec	35 cycles
72 °C	5 min	

4.2.3.3 The *Nes-Cre* PCR

The *Nes-Cre* PCR was used to determine whether the embryos had a Cre recombinase, under the control of the Nestin Cre promoter, inserted in their genome. Specific PCR mix preparation protocol (see table 4.5 - table 5.1) and PCR conditions (see table 4.6) were used.

Primers n. 355/n. 617 (listed in chapter 5.1.1 - table 5.1) were used to amplify a fragment of 450 bp in the *Nestin*-wt allele, whereas the couple of primers n. 355/n.749 was employed to identify a fragment of almost 300 bp in the *Nestin*-cre mutant allele. For the reaction 1 µl of genomic DNA was added to 19 µl of PCR mix.

Table 4.5 – *Nes-Cre* genotyping PCR mix.

Reagent	Concentration	Amount (µl)
Milli-Q H_2O		12.2
PCR-flexi-buffer (5x)	5x	4
MgCl2 (25 mM)	25 mM	1.2
dNTPs (10 mM)	10 mM	0.4
386/618 (20 µM)	20 µM	0.5
386/387 (20 µM)	20 µM	0.5
Taq polymerase (5 u/µl)	5 µl	0.2

Table 4.6 – *Nes-Cre* genotyping PCR conditions.

Temperature	Time	
98 °C	2 min	
96 °C 58 °C 72 °C	30 sec 30 sec 40 sec	30 cycles
72 °C	5 min	

4.2.3.4 The *Camk2a-Cre* PCR

The *Camk2a-Cre* PCR was used to determine whether the mice had a Cre recombinase, under the Camk2a promoter inserted in their genome. Specific PCR mix preparation protocol (see table 4.8) and PCR conditions (see table 4.7) were used. 1 µl of genomic DNA was added to 19 µl of PCR mix.

Primers n. 386/n. 618 (listed in chapter 5.1.1 - table 5.1) were used in order to amplify a fragment of 438 bp in the *Camk2a*-wt allele; the couple of primers n. 386/n.387 were employed to identify a fragment of 800 bp in the *Camk2a*-cre mutant allele.

Table 4.7 – *Camk2a-Cre* genotyping PCR mix.

Reagent	Concentration	Amount (µl)
Milli-Q H_2O		12.2
PCR-flexi-buffer (5x)	5x	4
MgCl2 (25 mM)	25 mM	1.2
dNTPs (10 mM)	10 mM	0.4
386/618 (20 µM)	20 µM	0.5
386/387 (20 µM)	20 µM	0.5
Taq polymerase (5 u/µl)	5 µl	0.2

Table 4.8 – *Camk2a-Cre* genotyping PCR conditions.

Temperature	Time	
98 °C	2 min	
96 °C 58 °C 72 °C	30 sec 30 sec 40 sec	30 cycles
72 °C	5 min	

4.2.4 Agarose Gel electrophoresis

Nucleic acid samples (DNA or RNA) can be visualized using agarose gel electrophoresis, a common technique in molecular biology. In electrophoresis molecules are electrically pushed through the pores of an agarose gel, being separated according to their size. The nucleic acids due to their highly rich composition in phosphate residues become negatively charged. Therefore, when nucleic acid undergoes to an electric field (in the gel electrophoresis apparatus), they run toward the cathode (positive pole). Molecules travel through the pores of the agarose gel at a speed that is inversely related to their length. The gels are prepared with different percentages of agarose (1.5 %-2.5 % agarose in 1x TAE buffer), according to the size of the DNA fragments, which need to be identified. To allow the detection of the samples, ethidium bromide was added to gel solution (3 µl from 10 mg/ml stock solution in 100 ml gel solution). This compound is able to intercalate through the base pairs of the nucleic acid and fluoresces under UV light.

Proper amount of agarose powder was added in boiling 1x TAE, until the powder appeared completely melted and the solution homogenous. Then the gel solution was poured into a running chamber and after it polymerized samples were loaded into the combs. Gels were run at 90V for ~20 min.

Samples from the *Pfn1* (Fig 4.1), *Nes* (Fig 4.2 A) and *Camk2a* PCRs (Fig 4.2 B) were run on a gel of 1.5 % agarose, instead samples from the *Pfn2* PCR (Fig 4.3) were loaded on a 2 % agarose gel.

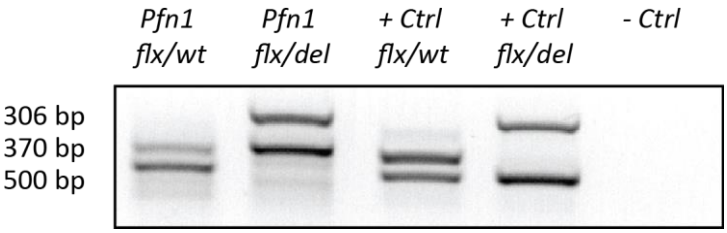

Figure 4.1 **| *Pfn1* genotyping results.** The couple of primers n.569/n.789 was used to amplify a fragment of 306 bp in the *Pfn1*-wt allele and/or a fragment of 370 in the *Pfn1*-floxed allele; the couple of primers n.546/n.789 resulted in a fragment of 500 bp that identifies the deleted allele for *Pfn1*-deleted allele.

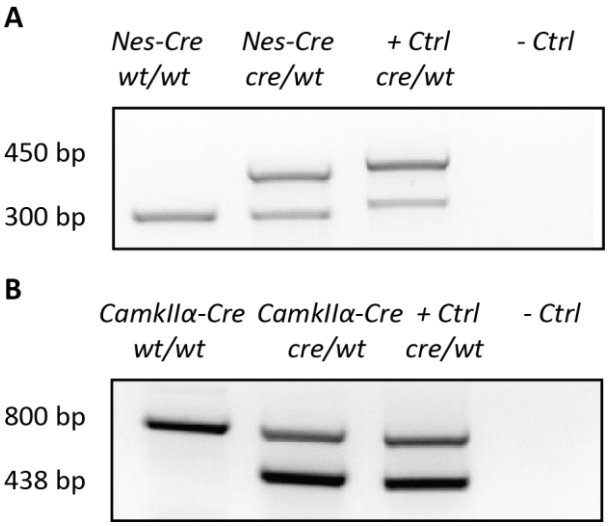

Figure 4.2 **| *Nes-Cre* and *Camk2a-Cre* genotyping results. A. *Nestin-Cre* PCR:** the combination of primers n. 355/n.617 resulted in a wt band for *Nes* of 450 bp; the *Nes-Cre* allele at 300 bp resulted from the combination of primers n.355/n749. **B. *Camk2a-Cre* PCR:** the combination of primers n. 386/n.618 resulted in a wt band for *Camk2a* of 438 bp; the *Camk2a*-cre allele at 800 bp resulted from the combination of primers n.386/n387.

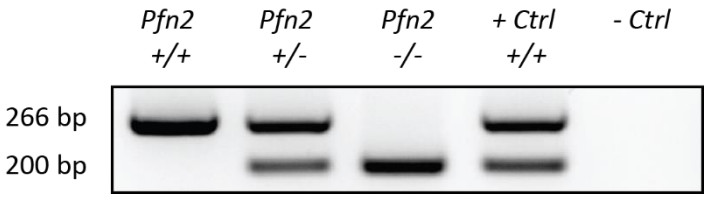

Figure 4.3 **| *Pfn2* genotyping results.** The combination of primers n. 229/n.422 resulted in a Pfn2-wt band of 266 bp. The primers n.229/n423 were used to identify the *Pfn2*-ko allele of 200 bp.

4.3 Biochemistry

4.3.1 Mouse brain tissue dissection

Mice aged between P80-P90 were anesthetized with isoflurane and decapitated. The head was placed on ice and the brain was quickly removed from the skull. After being

washed in ice-cold PBS, the following mouse tissues were dissected: olfactory bulbs, cortex, hippocampus, striatum, midbrain and cerebellum. Tissues were either directly used or stored at -80°C after being frozen in liquid N_2. Solutions used for biochemistry are listed in chapter 5.2.3.

4.3.2 Protein isolation from tissue

Brain tissues (fresh or frozen) placed in a glass/teflon douncer in a solution of 2x SDS loading buffer were electrically homogenized at ~600 rpm. In adult mice, 1 ml of 2x SDS was used for one cortical hemisphere, instead 200 µl for both hippocampi. For embryos of different embryonic ages, different amounts of 2X SDS loading buffer were used depending on the size of the tissue to lyse. The homogenized solution was then transferred on Eppendorf tube and boiled at 99°C for 10 min, vortexing them for 15 sec every 2 min to ensure the lysis and denaturation of the proteins. The lysates, after being settled down at RT, were stored at -20°C.

4.3.2.1 Analysis of the G- and F-actin content from tissue

Half part of a cortical hemisphere was placed in a glass/teflon douncer in 1 ml solution of 1x PHEM buffer supplemented with 1% TritonX-100 and electrically homogenized at ~600 rpm. The PHEM total cortical lysates were ultracentrifugated for 30 min at 100000g. To the 85-90% of the supernatant (900 µl), representing the G-actin fraction, was added 200 µl of 5x SDS loading buffer, in order to reach a 1x SDS final concentration. The remaining 10-15 % of supernatant is discarded to avoid contamination from the pellet fraction, containing F-actin; the remaining part of the supernatant is used to quantify the protein concentration (chapter 4.2.4). The pellet was well dried and then mechanically resuspended in a volume of 1 ml of 1x SDS (equal volume to the initial PHEM buffer solution). The two fractions were then boiled at 99°C for 10 min, vortexing them for 15 sec every 2 min. The lysates, after being settled down at RT, were stored at -20°C. To determine the G-actin and F-actin respective

amounts, equal amounts (5 µg) of the fractions were run on 10 % SDS-PAGE (chapter: 4.2.5) and blotted on a membrane as described in chapter 4.2.6. The western blot against actin was performed (chapter: 4.2.6) and the ratio between F/G actin was evaluated.

4.3.3 Preparation and stimulation of functional synaptosomes

Functional synaptosomes were prepared as described by Nagy and Delgado-Escueta in 1984 (Nagy & Delgado-Escueta, 1984) from P80-P90 mice. The solutions used for synaptosomal preparation are listed in chapter 5.2.3.1. Mouse brain was dissected on ice and one cortical hemisphere was homogenized in ice-cold homogenizing buffer in a glass-Teflon douncer at 250 rpm for 10 to 15 strokes. The homogenized suspension was then transferred in 14 ml snap-cap tube and centrifuged for 10 min at 3000 g at 4°C, to remove nuclei and cell debris. The supernatant, a mixture of cytoplasmic proteins and synaptosomes, was poured into a new snap-cap tube and again centrifuged at 4°C for 15 min at a higher speed (14000 g). The suspension was then transferred into a 14 ml snap-cap tube and spinned for 10 min at 3000 g at 4 °C. The supernatant was transferred into a new 14 ml snap-cap tube and spinned at 14000 g for 12 min at 4 °C. After removing the supernatant, the pellet (composed by the synaptosomal fraction) was carefully (in order to avoid bubbling) resuspended in 450 µl ice-cold Krebs- Ringer buffer and transferred into a 1.5 ml tube. The synaptosomal suspension is gently mixed by inversion with 550 µl Percoll (Sigma - final ~40-45 % v/v). Percoll is composed by colloidal silica particles coated with polyvinylpyrrolidone (PVP), which gives low viscosity. It is a medium used for density gradient separation and it is suitable for cells since it is non-toxic. After centrifugation for 2 min at 16000 g and 4°C, synaptosomes were enriched on the surface of the floating gradient and were collected by aspirating the underlying solution with a 5 ml syringe with a 21G needle. The synaptosomal fraction was carefully resuspended in 1 ml ice-cold Krebs-Ringer buffer and spinned down for 30 sec at 14000 rpm.

The collected synaptosomes were then resuspended in 400 µl of ice-cold Hepes krebs buffer and kept on ice. The protein concentration of the sample was evaluated as mentioned in chapter 4.2.4.

4.3.3.1 Analysis of the G- and F-actin content from synaptosomes

The stimulation of functional cortical synaptosomes was performed at 37°C (the average body temperature) and with KCl. After being quantified the synaptosomal suspension was divided into 100 µg aliquots in Hepes-Krebs buffer and equilibrated for 20 min at 37°C. The samples were stimulated for different time points with 40 mM KCl. The stimulation was stopped by adding to the suspension an equal volume (200 µl) of ice-cold 2x PHEM buffer supplemented with 2 % Triton X-100. PHEM lysates were then processed for the G- and F-actin separation with the McRobbie's assay. The PHEM synaptosomal lysates were centrifuged at 4°C for 10 min at maximum speed. The 80 % of the supernatant (300 µl), representing the G-actin fraction, in order to reach a 1x SDS final concentration. The remaining 20 % of supernatant is discarded to avoid contamination from the pellet fraction, containing F-actin. The pellet was well dried and then resuspended in 1.25 volumes respect to the initial PHEM sample volume of 1x SDS with 0.5 % triton. Samples were denatured (as explained in chapter: 4.2.4) and stored at -20°C. To determine the G-actin and F-actin respective amounts, equal volumes (10 µl) of the fractions were run on 10 % SDS-PAGE (chapter: 4.2.5) and blotted on a membrane as described in chapter 4.2.6. The western blot against actin was performed (chapter: 4.2.6) and the ratio between F/G actin was evaluated.

4.3.4 Protein quantification

Evaluation of protein concentration was obtained by the colorimetric Bradford assay, based on the Bradford dye-method (Bradford, 1976). The Bradford assay is based on the color change of the Coomassie blue brilliant G-250 dye in response to different protein concentration. Coomassie blue brilliant is a dye with a brown color and an

absorbance of 465 nm, which is able to stain the proteins by binding to the basic and aromatic amino acid residues. When the dye reagent complexes with the protein, there is a colour shift from brown to blue and also the absorbance of the bound protein changes to 595 nm. The shift between the excitation and emission absorption is measured by a spectrophotometer, which is calibrated by serial dilutions of a protein (BSA) with a known concentration against a blank (containing only the basic buffer without any protein).

The procedure for the Bradford assay was performed according to the following steps: (i) 4 µl of the sample of interest (tissue lysate for protein extraction or synaptosomal suspension) and 4 µl of the basic buffer (2x SDS lysis buffer, for the preparation of total protein lysates; or Hepes-Krebs buffer, for the isolation of synaptosomes), used as blank, were mixed with 1 µl of 5x SDS loading buffer and boiled at 99°C for 3 min and then cooled down for 5 min. (ii) The sample is then spinned down, in order to collect the condensed liquid, and diluted 10 times by adding 45 µl of Milli-Q water. (iii) 10 µl of total protein lysate or 10 µl of lyses buffer (for the blank) was added to 1 ml of home-made Bradford reagent in a quartz photometer cuvette; the solution was mixed by inversion. (iv) In order to calculate the protein sample concentration in µg/µl, the absorbance value of the blank solution is subtracted from the absorbance value of the sample, which in turn was then divided by the slope of the calibration curve obtained by defined concentration of BSA.

4.3.5 SDS-polyacrylamide gel electrophoresis

SDS-PAGE (SodiumDodecylSulfate (SDS) Polyacrylamide Gel Electrophoresis (PAGE) (Laemmli, 1970) is a routine method used to separate proteins according to their molecular weight. Since proteins separation might be influenced by their tridimensional structure, it is critical to denature (linearize) the tridimensional structure and to negatively charge them. At this purpose proteins were exposed to

high temperatures and treated with SDS, an anionic detergent, and β-Mercaptoethanol, a reducing agent.

Acrylamide gels used in the SDS-PAGE are made up of two different phases. The upper part also known as “stacking gel”, which has a concentration of 4 % acrylamide and a pH of 6.8. The stacking part of the gel with its acidic pH allows to concentrate all the proteins of the different samples within a line between the first and the second portion of the gel. The second part of the gel, called “resolving”, has a pH of 8.8 which allows an optimal migration of the proteins. The percentage of acrylamide in the resolving gel regulates the dimension of the meshes and it was chosen according to the size of the protein of interest; in this work resolving gels of 10 % or 15 % acrylamide were used.

10µg/15µg of the quantified proteins samples were loaded on the gel, together with 5 µl of See Blue Plus2 Pre-Stained Molecular Weight Standard (Invitrogen). Later the gel was mounted in a running chamber (BioRad) submerged in a 1x running buffer solution and exposed to a current. The samples ran at constant voltage of 80 V in the stacking part of the gel. Once samples entered in the resolving gel the voltage was raised to 140 V. The electrophoresis was stopped when the bromophenol blue front ran out from the bottom of the gel.

4.3.6 Western blot

Western blot analysis allowed the detection of specific proteins in a mixture of proteins within a sample. Proteins were separated according to their molecular weight in an SDS-PAGE and later were transferred onto polyvinylidene difluoride (PVDF) membrane (Towbin *et al.*, 1979). Proteins of interest were then specifically labelled and detected on the membrane by using specific antibodies.

4.3.6.1 Submerged transfer

A submerged transfer was performed to move proteins from an acrylamide gel onto a PVDF membrane. In this technique is prepared a “transfer sandwich” made up by a sponge pad, two 3mm Whatman papers, the acrylamide gel, the PVDF membrane (previously activated in methanol), two more 3 mm Whatman papers and a new sponge pad. The so formed “transfer sandwich” is placed into a chamber (western blotting transfer system - BioRad) connected to a current and filled up with cold 1x transfer buffer. The voltage of 110 V for 1h or 20 V O/N was applied to the chamber, allowing the transfer of the proteins on the PVDF membrane. During the procedure to prevent the overheating of the system, the transfer buffer is kept cold by inserting ice-package in the chamber or by moving the transfer apparatus in a 4°C room.

4.3.6.2 Enhanced chemiluminescence detection reaction

After blotting procedure, the membrane was quickly rinsed in 1x NCP and treated for 30 min at RT with blocking solution, which allows to block the unspecific binding sites on the membrane. To detect distinct proteins on the PVDF membrane the O/N incubation at 4°C with specific primary antibodies (see chapter 5.4.1 - table 5.2), diluted in blocking solution, was performed. Afterwards, membrane was washed 3 times for 15 min at RT with 1x NCP, in order to remove the unbound primary antibody. The membrane was then incubated for 1 h at RT with the appropriate (mouse or rabbit) secondary antibody conjugated to the horseradish peroxidase (HRP) diluted 1:2000 in blocking solution. The membrane is again rinsed three times in 1x NCP for 10 min at RT. The membrane was incubated for ~1 min into a 1:1/ ECL solution A: ECL solution B and a signal proportional to the amount of antibody, which reflect the amount of protein, was obtained. HRP is an enzyme which catalyzes the oxidation of the luminol (contained in the ECL solution A) in presence of H_2O_2 (contained in the ECL solution B). Upon oxidation, luminol emitted a light signal at 450 nm, which could be

measured by a luminescent image analyzer with a CCD camera (LAS 4000 mini - GE Healthcare).

4.3.6.3 Densitometric analysis of western blots

The signal emitted from the ECL reaction is proportional to the amount of primary antibody bound on the membrane and therefore to the amount of protein. The software Multi Gauge V3.0 (Fujifilm Life Science) was used to quantify the signal intensity from the protein. For each genotype three or four protein samples from different mice were used and the same samples were also loaded on different membranes to confirm the obtained result.

4.3.6.4 Coomassie staining of the membrane

The value obtained from the quantification of the ECL band of the protein of interest were normalized to minimize the effect from experimental variation or unequal sample loading or transfer. The normalization can occur against proteins which are stably expressed in the lysate tissue (like GAPDH or γ-tubulin) or against total protein amount. The expression of a protein used as a standard can vary a lot according to the tissue and to the developmental stage or the age of the mouse. In order to normalize properly the amount of protein of interest against the total protein on the PVDF membrane, a Coomassie staining on the membrane was performed.

The membrane was incubated in a Coomassie staining solution for ~10 min on a shaker at RT. Membrane then was then rinsed on a shaker at RT with a destaining solution for ~3 min . Membranes were dried and a picture acquired by scan. The total proteins were measured by Multi Gauge, as shown in figure 4.4 To normalize, once the signal from a specific antibody was obtained, it was divided to the respective total protein signal from the Coomassie staining.

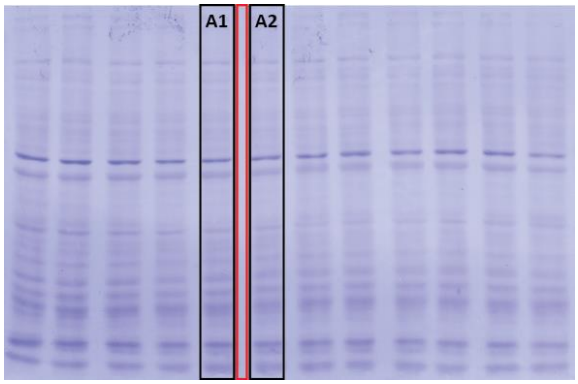

Figure 4.4 **| Coomassie stained PVDF membrane.** Example PVDF membrane stained with Coomassie. Multi Gauge software was used to specifically select the area of each lane of proteins (e.g. lanes A1 and A2). An area, displayed in red, in between the lanes was also chosen as background. The densitometric analysis was performed in order to obtain the total amount of protein probed on the membrane. To obtain the normalization, the signal from the antibody was divided to the total protein signal from its respective lane.

4.4 Histology

4.4.1 Dissection and fixation of mouse embryos

Mouse embryos were carefully dissected at different embryonic stages. E11.5 embryos were entirely processed, while only the head was dissected from E14.5 and E16.5 embryos. Embryos were then cleaned by residual blood and hairs in PBS and prepared for the paraffin- or the cryo-embedding. In chapter 5.2.4 the composition of the histological solutions is indicated. For the histological steps during paraffin and cryo-embedding, depending on the size of the embryo (due to its developmental stage), different amounts of solutions or incubation time were used (shorter incubation time for E11.5 embryos). If not differently specified, the incubations were performed by placing the embryos in tubes on a shaker.

After being dissected the specimens were fixed at 4°C – O/N in a 4 % PFA solution. Fixative slowly penetrate in the embryo, causing chemical and physical changes that harden and preserve the tissue from the subsequent processing steps. The treatment with fixative occurred as soon as possible after dissection to avoid morphological

distortion and damage due to: (i) tissue drying artefacts; (ii) self-digestion of cells and tissues; (iii) decomposition of the tissue by microorganisms.

The day after the embryos were washed from the PFA in 1x PBS, 3 times for 30 min each at 4°C.

4.4.2 Paraffin embedding of mouse embryos

Paraffin is hydrophobic, therefore before penetration of the wax is important to remove all the water from the sample. The dehydration of the embryo was achieved by incubating it in a series of increasing concentration of ethanol solutions and finally in pure absolute ethanol. Since ethanol is soluble in water, with dehydration process of the water is progressively replaced by ethanol. Progressive dehydration steps are summarized here:

Solution	Number of washes	Incubation time	Temperature
Ethanol 50 %	2	30 min	4°C
Ethanol 70 %	3	1 h + O/N	4°C
Ethanol 85 %	2	30 min	RT
Ethanol 96 %	2 – 3	30 min - 1h	RT
Ethanol 100	2 - 3	30 min - 1h	RT

At this step of the protocol the water was removed from the sample. Since paraffin wax and water are not miscible, it was essential to exchange the ethanol in the tissues with the xylene (which is soluble in both water and wax as well). During this process, known as clearing, because the sample acquire a clear-transparent appearance, also the adipose tissue was removed since could constitute a barrier to wax filtration.
Embryos were transferred into glass vials and treated with different dilutions of ethanol-xylene mix and pure xylene; the following steps were performed under the chemical hood:

Solution	Number of washes	Time of incubation	Temperature
EtOH 100 %: Xylene (1:1)	2	30 min	RT
EtOH 100 %: Xylene (1:2)	2	30 min	RT
Xylene	3	30 min	RT

The embryo was now ready for the paraffin wax infiltration. Paraffin is solid at RT and can be used only after being melted O/N at 60°C.

The embryo was left O/N in paraffin at 60°C. The following day two more paraffin changes were done after 30 min of incubation. The embryo was properly orientated according to the desired cutting plane and embedded into a mold with fresh paraffin. The dried embryo-paraffin block was attached on an embedding cassette with melt paraffin. The block was fixed on the microtome (Leica) and prepared for slicing. The thickness of the cut sections is 6 µm.

The cut ribbons were placed on a layer of 10 % EtOH onto super frost slides and transferred to a heating plate at 35°C. Slides were left on the heating plate until the sections were completely stretched and the paraffin had turned white. Slices were left to dry O/N at 37°C and were finally stored at RT. This step is particularly important, since not properly dried slices will not deparaffinize sufficiently with xylene and won't be able to be stained consistently and properly.

4.4.3 Cryo-embedding of mouse embryo

The sucrose cryo-protected tissue freezing method was used to prepare E11.5 embryos for cryo-sectioning. The freezing can cause the distortion of the tissue due to ice crystals which break cell membranes and produces holes within cells and extracellular matrix (this is known as "Swiss Cheese" effect). The basic strategies to prevent crystals formation during freezing are: (i) rapid freezing, in this way water does not have time to form crystals and remains in a vitreous form that does not expand when solidified; (ii) use cryo-protectants that disrupt interactions between water molecules. Cryo-preservation help to prevent ice crystals formation in tissues

when water freezes and therefore expands. In this protocol, the purpose of treating embryos with sucrose is to cryo-preserve tissues.

The embryo was fixed with PFA 4 % prior to cryo-preservation, because sucrose solutions above 10 % are hypertonic and cause water to flow out of cells causing tissue distortion and shrinkage. After fixation the embryo was properly washed in 1x PBS, as previously explained. The incubation of the embryo within the sucrose solutions (15 % and 30 %) occurred at 4° and with a gentle nutation to avoid bubbles. When placed into the new and freshly prepared sucrose solution the embryo was swimming on the top of it, the incubation was stopped only when the embryo sank to the bottom of the tube. The cryo-preservation started with incubation in 15 % sucrose solution and continued with different gradients of 15 % : 30 % sucrose solution ((i) 2:1 15 % sucrose : 30 % sucrose; (ii) 1:1 15 % sucrose : 30 % sucrose; and (iii) 1:2 15 % sucrose : 30 % sucrose). The gradient 15 % : 30 % sucrose solution was discarded and replaced with 30 % sucrose solution, the incubation lasted until the embryo dropped to the bottom of the tube and thereafter O/N.

A container with finely crushed dry ice was prepared. A thin layer of Tissue-Tek OTC was laid at the bottom of a labeled mold and after lying and orienting the E11.5 embryo was carefully covered with other Tissue-Tek OCT solution. Due to the close proximity of the crashed dry ice, the embryo was frozen within a couple of minutes (~5 min). The frozen sample were then placed in an aluminum foil sealed bag below the fine crushed dry ice for 30 min. The sample could be stored at -80°C for a long time.

The embryo was sliced at the cryostat at a temperature of -25°C. The slices, 25 µm thick, were lied on super frost slides and dried in the air for 15 min before being stored at -80°C.

4.4.4 Vibratome cutting of adult mouse brain for IF

P80-P90 mouse brains used for IF were taken out from the skull, briefly washed in PBS and then fixed in 4 % PFA for at least 48 hours at 4°C on the rotating wheal, to crosslink the proteins. The brains were then washed in 1X PBS for 3 times, 30 min each at 4°C. Sagittal sections of a thickness of 25 µm were prepared at a Leica Vibratome VT 1200S. A razor blade, parallel to the positioned brain, was inserted into the machine. The brains were embedded in 6 % low melting agarose, in order to have a complete cut of the slice and to not damage the brain structure. The agarose was removed from the slices at the end of the cutting procedure, to avoid auto fluorescence problems. To obtain coronal slices**,** the cerebellum was cut out and the brain block (embedded in agarose) was glued on the surface of the vibratome tray. The sections were collected with a brush in 24-well plates containing cold 1X PBS supplemented with 0.1 % of sodium azide. The wells were wrapped in plastic and aluminum foil and then stored at 4°C

4.4.5 Staining procedures

Different types of stainings were performed on embryonic or adult brain tissues. In the following chapter the different staining procedures are described.

4.4.5.1 Hematoxylin & Eosin (H&E) staining on paraffin sections

Before treating slices for H&E the removal of paraffin and re-hydration of the slices constitute a critical step to obtain an accurate staining. The de-paraffination and re-hydration took place with the following steps under the chemical hood:

Solution	Number of washes	Time of incubation
Xylene	2	5 min
Ethanol 100 %	1	Dipping
Ethanol 100 %	1	5 min

Ethanol 96 %	1	5 min
Ethanol 75 %	1	5 min
Ethanol 50 %	1	5 min
MilliQ - H_2O	2	10 min

The use of graded percentage of alcohols to hydrate or dehydrate (later) was done to minimize the shrinkage-distortion of cells and tissues section during replacement of alcohol or water.

Hematoxylin and eosin stainings are the most used one in histopathology and histochemistry laboratories because they provide an overview of tissue structure. Hematoxylin has a dark blue purple colour and stains the chromatin (nuclear material) or the DNA within the nucleus. Hematoxylin is a natural dye extracted from the logwood tree (in Mexico and Central America), which does not have staining ability unless it is oxidized to hematin. Hematin can stain only when it is combined to a metallic ion (mordant), which act as a bridge between the stain and the tissue, enabling staining to take place. The colour of the staining reaction depends on the type of mordant used, in our case the positively charged potassium alum/ammonium-hematein complex combines with the negatively charged phosphatase of nuclear DNA forming the typical blue purple colour of the Mayer's hematoxylin. Unlike hematoxylin, eosin Y is an n orange-pink synthetic dye derived from fluorescein, which reacts unspecifically with eosinophilic molecules in the cytoplasm, connective tissue and collagen (Fischer *et al.*, 2006; Avwioro *et al.,* 2011). It was preferred to use and alcohol-based eosin since it is chemically more stable, and it does not contain any impurities (such as water-soluble salts), which may interfere with dye uptake from the section.

For a successful result is important to have in the staining jar a proper volume of staining and washing solutions, at this purpose it is good practice to not completely fill all the spots of the jar with microscope slides. The incubation time for the two dye-

solutions were regulated according to the amount of cytoplasm of the tissue (shorter incubation time in E11.5 compared to E14.5 and E16.5).

After re-hydration slides were incubated for 3 to 5 min in a staining jar containing Mayer's hematoxylin under agitation. The reaction of the dye was then stopped by rinsing the slides one by one under tap water (pH 8.0 – 37°C). The treatment of the slides with an alkaline solution (in our case tap water) turned the stain of the nuclei from red to the typical blue colour of the hematoxylin, this process is also known as blueing.

Slides were then stained with eosin Y for 15-20 min under agitation. Since an alcohol-based formulation of eosin was used, sections could be rinsed from the excess of eosin and dehydrated at the same time with 2 changes in 96 % Ethanol (1 min each). Last dehydration step was done in 100 % ethanol. The rinses with ethanol were always performed on a shaker, in order to obtain a differential staining on the sections. Sections were then cleared in xylene twice for 2 min on a shaker. At the end, 3 drops of mounting medium (entellan) were put on each slide and a glass coverslip was glued on it.

4.4.5.2 Immunofluorescence (IF)

One way to study localization and function of the endogenous proteins in a tissue is to label them with the use of a specific primary antibody against the protein of interest and a secondary fluorescent labelled antibody directed towards the primary one. During the staining and also afterwards the slices were protected from light. IFs were performed either on cryo-sections from E11.5 embryo or on vibratome brain sections from adult mice. In chapter 5.2.4.3 the solutions used during IF experiments are indicated.

4.4.5.2.1 IF on cryo-sections

In immunofluorescences on cryo-sections, unless otherwise stated, all the steps were performed at RT and the washing steps were always done in a staining jar on a shaker, to ensure a proper amount of washing solution.

The slices, stored at -80°C, were thawed for approximately 5 min. Slices were fixed once more with 4 % PFA (for 2 min in a staining jar) and twice washed with 1x TBS to remove the formaldehyde solution. Sections were permeabilized and blocked for non-specific binding sites for 2 hours with blocking solution (300 µl per section) directly on the slide in wet chamber. The blocking solution was replaced by 250 µl primary antibody solution and was incubated O/N at 4°C. Several primary antibodies can be applied together, in the same mix solution (see chapter 5.4.2 – table 5.3). The day after, the unbound primary antibody was washed out 3 times for 15 min in 1x TBS-T. Slices were incubated with the specific secondary antibody (see chapter 5.4.3 – table 5.4) solution for 1 h. The secondary antibody was washed out with 3 washing steps of 10 min in TBS-T. Sections were incubated with the DNA intercalating dye DAPI (1:5000 from 10 ng/ml stock solution) for 5 minutes. Lastly, slides were washed three times for 5 minutes with TBS and were mounted with mowiol mounting medium containing 5 % of antifading reagent n-propyl-gallate (NPG). The slides were left in the dark O/N to dry and then imaged at the wide field fluorescence microscope (Zeiss Axiophot).

4.4.5.2.2 IF on vibratome sections

Coronal brain slices from different genotypes (wt and mutants) were observed with a stereomicroscope and matched, in order to analyze the same plane. Unless otherwise stated, all the steps were performed at RT. The chosen sections were transferred to 24-well plates, they were fixed once more with 4 % PFA and washed 3 times for 5 min with PBS in order to bring away the fixative. The auto-fluoresce from the slices was quenched with 1 h treatment with 50 mM NH_4Cl, then after acidic ammonium chloride treatment the slices were washed 3 times for 10 min with PBS to adjust the pH.

Non-specific binding sites for antibodies were blocked by incubation for 4 h or O/N at 4°C with a blocking solution. The composition of the blocking solution changes according to the affinity of the antibody for the protein of interest, to the thickness of the section and according to the level of exposure of the antigen of the protein. For example, the type and amount of serum (in our case 5-10 % NGS) was low when the affinity of the antibody is not elevated and was increased when the antibody has a high background. Instead the concentration of DMSO, an aprotic solvent with the ability to enhance the permeability of lipid membranes (Notman *et al.*, 2006), was higher (2 %) when sections are thicker and when the antigen is not easily accessible to the antibody. At the end of the incubation blocking solution was replaced by O/N incubation at 4°C with a mixture of combined primary antibodies solution (see chapter 5.4.2 – table 5.3). On the next day, the unbound antibody was washed away with 3 rinses of 15 min. Thereafter, the incubation of the secondary antibody (see chapter 5.4.3 – table 5.4). could start. This secondary antibody incubation last 1 to 2 h, depending on the efficiency of the primary antibody. The solution of antibody was then washed away 3 times for 10 min each. To visualize the nuclei of the cells two different DNA-intercalating dyes with different excitation wavelengths were used, DRAQ5 and DAPI. Sections were incubated first with DRAQ5 (1:1000) and later with DAPI (1:5000) for 30 min and 5 min, respectively, since the latter has a higher efficiency for DNA binding. The left DNA dye was washed out 3 times with TBS, 10 min each. Sections were then transferred, using a brush, on a microscope slide and mounted with mowiol mounting media (same as above). Immunofluorescence images were taken using the LSM 510 Meta confocal microscope.

4.4.6 Golgi staining

Golgi staining technique, based on neurons silver nitrate impregnation, was developed by Camillo Golgi (1873) and further refined by Santiago Ramon y Cajal. This technique was useful to provide extensive knowledge of the anatomy of the neural tissue. In this work the FD Rapid GolgiStain kit (FD NeuroTechnologies), based on the original Golgi-

Cox method, was used. According to Golgi-Cox method the impregnation of the tissue in potassium dichromate and silver nitrate, leads to a micro-crystallization of silver chromate in some neurons generating a brownish color. The Golgi-cox method comprises the following three steps: (i) specimen impregnation (with mercury chloride - $HgCl_2$ instead of silver nitrate, potassium chloride - K_2CrO_4 and potassium dichromate - $K_2Cr_2O_7$), (ii) tissue protection and (iii) color development. The technique allows to randomly stains neurons and to visualize the anatomical features in neurons, such as dendritic arborization and branching and dendritic spines. The random stain of neurons is an advantage since it allows to trace single and specific neurons in the cortical or hippocampal network (Risher *et al.* 2014; Hee Won Kang *et al.*, 2017).

4.4.6.1 Golgi staining procedure

The technique has several advantages compared to fluorescent based methods. It allows an easy imaging of the samples at a bright field microscope, and samples can be stored and used for a longer period (from months to year). However, the analysis is extremely time-consuming since the information that can be extrapolated and studied from even a small set of data constitute a large amount.

During the processing it was important to protect the sample from the light. It was also critical to control the temperature steps of the procedure (4°C or RT), in fact the overheating of the tissue could cause a weak tissue impregnation of the different solutions.

Equal volumes of solution A and B were mixed 24 hours prior to use and left unstained in the dark, in order to produce the impregnation solution. The day after brains were harvest from a P85/P90 and P360 mice, quickly washed in MIlliQ-H_2O to remove blood or residual hairs and incubated in 10 ml of impregnation solution each, O/N in the dark at RT. The impregnation solution was replaced the day after and left for 15 days or 18 days in younger (P80-P90) and older (P360) mice, respectively. After incubation in solution A and B the brains lost their pinkish and soft appearance and became whitish-

yellowish and turgid, then brains were transferred into snap-cap filled with 10 ml of washing solution (solution C) and gently shaked at 4°C in the dark for 72 hours or 84 hours for younger (P80-P90) and older (P360) mice, respectively; solution C was replaced after the first 24 hours of incubation with some fresh one. It is recommended to not leave the brains longer in solution C, otherwise the tissue structure becomes fragile.

250 µl thick coronal slices were cut in PBS using a vibratome and transferred onto gelatin-coated microscope slides (chapter: 4.3.6.2). Solution C was used to stretch the slice on the slide; the excess of solution C was aspirated, and sections were dried at RT - O/N. On the next day slices were placed into a glass staining jar and rinsed in MilliQ-H_2O twice 2 min each. In the meantime, fresh staining solution was prepared by mixing 1 part of solution D, 1 part of solution E and two parts of MilliQ-H_2O (140 ml in total). In this staining solution slices were incubated for 10 min on a shaker at RT and rinsed in MilliQ-H_2O twice, 4 min each. Sections were then dehydrated in 50 %, 75 %, 95 % and absolute ethanol for 1 min each on a shaker. The slices were cleared in xylene three times, 4 min each, and mounted with Entellan. Sections were dried O/N under the hood and images acquired in brightfield mode.

4.4.6.2 Preparation of gelatin-coated slides

Golgi sections were placed on gelatin coated slides to ensure their holding during the staining procedure.

Microscopes slides were coated with a chrome alum gelatin solution. Gelatin was dissolved in MilliQ water heated to 60 ºC, the chromium potassium sulfate was added to the solution, turning it from a transparent to a pale blue colour. Microscope slides were dipped into warm gelatin solution (60°C) and then air-dried O/N at RT. The slides were stored in a dust-free container at RT.

4.4.6.3 Branching analysis

Golgi staining pictures were acquired in bright field mode at a Zeiss axiophote microscope. To analyze the morphology of pyramidal neurons of the layer V of the motor cortex, Z-stack pictures with 20x and 40x objects were taken. Apical dendrites of 1ry, 2ry, 3ry orders and basal dendritic branches of 1ry, 2ry, 3ry were analyzed per number and length. The analysis was blind and performed by manual counting. The obtained data were transferred into an excel sheet and statistical analysis were performed with GraphPad Prism 8.0.

4.5 Electrophysiology

Depending on the scientific question that was posed two different kinds of recordings were performed in order to characterize the electrophysiological properties of *Pfn2*$^{-/-}$ mice: extracellular field recordings and patch clamp recordings. Solutions for electrophysiological recordings are indicated in chapter 5.2.5

4.5.1 Acute hippocampal slice preparation and electrophysiological setup

Acute hippocampal slices were prepared from P15-P21 animals. Mice were anesthetized with isoflurane and decapitated. Brains were removed from the skulls and transferred into ice-cold ACSF gassed with carbogen (95 % O_2 / 5 % CO_2) for 1 min. The two hippocampi were dissected and transversally sliced (400 µm) with a vibratome (Leica VT1200S) in chilled and carbogened ACSF. Slices were then equilibrated in chambers containing ACSF continuously gassed with carbogen for 30 min at 32 °C and subsequently stored at RT in ACSF.

For all the experiments the hippocampal slices were placed on PDL-coated glass coverslips in the recording chamber. All recordings were done at RT in a recording chamber continuously perfused with carbogened ACSF, if needed drugs were added

to the ACSF. Recordings were obtained using 2-4 MΩ borosilicate glass electrodes (Science Products GB150TF- 8P) equipped with chloride coated silver wires and filled with different types of solutions, depending on recording performed. All electrophysiological data were acquired using a Multiclamp 700B amplifier (Axon Instruments) and digitized on a Digita 1322A (Axon Instruments) controlled by the software pCLAMP 9.2.

4.5.2 Electrophysiology field recordings

Extracellular field recordings are a way to characterize the functionality of basic synaptic transmission. These recordings are performed in current-clamp mode that analyzes how the membrane potential of the cell varies in response to an injected current and to specific drugs; in this approach, current pulses are injected into the cell to determine the membrane resistance and therefore its behavior.

In this study extracellular field recordings were carried in the CA3-CA1 synapse of the hippocampus. In detail, Shaffer collaterals were activated via a stimulation electrode and post-synaptic responses were recorded in the stratum radiatum (dendritic level) of the CA1 region. The stimulation and the recording electrode are both filled with ACSF. The stimulation in the Shaffer collaterals causes a depolarization in the fibers and the generation of APs, which in turn result in a pre-synaptic glutamate release and in the activation of the post-synaptic receptors. The influx of ions, due to the opening of glutamate receptors, cause the depolarization of the post-synaptic membrane and the generation of EPSPs in the CA1 region.

To analyze excitatory synaptic transmission the extracellular ACSF was supplemented with 100 µm of PTX, a blocker of $GABA_A$ receptors.

To prevent recurrent spontaneous excitation, fEPSP were recorded in acute hippocampal brain slices disconnecting the Shaffer collaterals with a cut between the CA1/CA3 region. Shaffer collaterals were then stimulated in the CA3 region and synaptic responses were recorded in the stratum radiatum of the CA1 region, using glass microelectrodes filled with ACSF. Before starting the real experiment, free

recordings were taken for 20 min until fEPSP reached a stable baseline. For each slide (one experiment) 20 fEPSP were averaged to reduce the electrical noise. All data were analyzed using Clampfit 10.2 (Molecular Devices), a custom written Matlab routine (MathWorks) and GraphPad Prism 5 (GraphPad Software). Values are given as means ± SEM.

4.5.2.1 Input-Output (I-O) curves

The input is the amplitude of the fiber volley, which represents the strength of the AP arriving from the Schaffer collaterals; whereas the output is defined as the slope of the resulting fEPSP. In the resulting I-O graphs fiber volley amplitudes of 0.05, 0.1, 0.15, 0.2 and 0.25 mV were evoked and the resulting fEPSC plotted.

4.5.2.2 Paired-Pulse-Facilitation (PPF)

With paired pulse facilitation the pre-synaptic neurotransmitter release was analyzed. For PPF experiments, Schaffer collaterals were stimulated twice for 0.2 ms with a stimulus interval of 40 ms and fEPSP were recorded in CA1 region. The ratio of the slope of the second to the first EPSP was calculated and defined as PPR.

4.5.3 Whole cell recordings

Intracellular recordings are performed in order to study the behavior and the current flow through synaptic membranes of single cells, according to the whole-cell patch clamp method invented by Erwin Naher and Bert Sakmann (Hamill et al., 1981). The glass recording electrode is filled with a specific internal solution that mimics the intracellular ion-concentration and that is modified according to the specific experiment which is performed. The fine glass pipette is guided towards the soma of the CA1 pyramidal cell by constantly applying a pressure which cause an outflow of internal solution to prevent the obstruction of the pipette with tissue fragments. When the pipette is near enough to the cell, a light pressure on the membrane of the

cell is visible. At this point, a mild suction is applied and the cell-attached configuration is achieved, which is characterized by the formation of the gigaseal (high resistance seal between the pipette and the membrane). Short pulses of suctions are applied to disrupt the cell membrane and to reach the whole-cell configuration, in this configuration the intracellular space of the patch cell is connected to and mixes with the intracellular solution of the pipette.

In this work patch clamp recordings in whole cell configuration were performed on the pyramidal cells of the CA1 region. Cells were visualized using differential interference contrast camera on an upright microscope (Olympus, BX51WI).

Once the whole cell configuration was obtained, a test pulse of -5mV was applied to the cell and only cells with an input resistance lower than 20 MΩ were analyzed.

In voltage-clamp mode the current flow through the membrane and therefore the membrane channels features of excitatory cells were measured, at this purpose the membrane voltage of the cell was held at a defined value (-70 mV). The membrane potential was monitored and whenever it changed the amplifier injected the amount of current which was necessary to keep the system at the desired holding potential, therefore the amount of current that is needed to compensate the changes is analyzed.

4.5.3.1 Miniature excitatory post-synaptic current recordings (mEPSC)

mEPSC were recorded from CA1 pyramidal neurons in acute hippocampal slices at a holding potential of -70 mV for at least 10 min and analyzing 2 minutes (~120 events) in the middle region of the recording. The intracellular solution used had the following composition (in mM): 150 Cs-gluconate, 8 NaCl, 2 MgATP, 2 $MgCl_2$, 10 HEPES, 0.2 EGTA and 5 QX-314 (pH 7.2 - 290 mOsM/L). To record mEPSC, ACSF was supplemented with PTX (100 µM) to block $GABA_A$ receptors, TTX (0.2 µM) to block action potentials and trichlormethiazide (TCM, 250 µM) to increase mEPSC frequency. For the statistical analysis 120 mEPSC events were analyzed with a custom written MATLAB routine (MathWorks).

4.5.3.2 Miniature inhibitory post-synaptic current recordings (mIPSC)

mIPSCs were recorded from CA1 pyramidal neurons at -70 mV holding potential for 10 minutes and analyzing 2 minutes (~120 events) in the middle region of the recording. The intracellular solution used contained a high chloride concentration, the composition of the solution was the following (in mM): 90 CsCl, 20 Cs-gluconate, 8 NaCl, 2 $MgCl_2$, 10 HEPES, 1 EGTA, and 2 QX-314, pH 7.2 (290 mOsM/L). To isolate mIPSCs, ASCF was additionally supplemented with NBQX (10 µM) to block AMPA and KA receptors and TTX (0.2 µM) to block action potentials. mIPSCs events were analyzed with a custom written MATLAB routine (MathWorks).

4.5.3.3 Evoked IPSCs

IPSCs were recorded as described above in section 4.4.3.2. IPSC were evoked with a stimulation electrode placed ~100 µm away from the soma of the recorded pyramidal cell. The position of the stimulation electrode was adjusted such that, the smallest stimulus (5 pA) elicited a current smaller than 40 pA. Paired pulse ratio (PPR) was determined as the ratio of the IPSC amplitude of the second pulse to the IPSC amplitude of the first pulse, with an inter-stimulus interval of 50 ms.

4.6 Behavioral analysis of *Pfn2* animals

The *Pfn2* ko (*Pfn2*$^{-/-}$) mouse model was previously described (Pilo Boyl *et al*, 2007); these mice were employed in behavioral tests and electrophysiological analysis. All mice used in the experiments were littermates generated by crossing heterozygous parents. Mice were socially housed with a standard 12 h light/dark cycle at 22 °C and 50-55 % humidity, with free access to water and food pellets. All experiments were performed according to EU regulations (Licenses n. 19/2005-B and AZ 84-02.04.2013.A233).

Male mice between 3 to 5 months old were used in behavioral experiments, except where differently specified.

4.6.1 Maternal behavior

Pregnant females were single-housed a week before delivery. Litter survival was assessed at P10. In a second approach, pregnant female and male were left together to allow cross-fostering.

For the study of maternal behavior and pup retrieval the following procedure was realized: P5 pups from *Pfn2*$^{-/-}$ and wt control females were dispersed in the cage and time for retrieval of the first pup and of the entire litter was scored up to 30 min.

4.6.2 Social interaction

To evaluate social interaction the test chamber was built according to (Moy *et al*, 2007) (Fig 4.5).

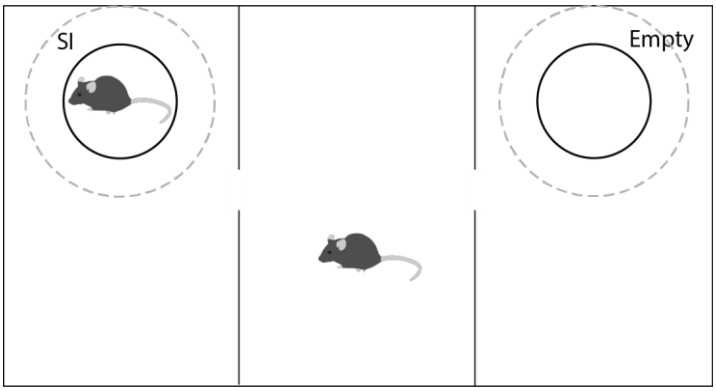

Figure 4.5 **| Scheme of the testing apparatus for 3-chambered test maze.** Dashed circles delimit the SI (Social Interaction) zone hosting a novel juvenile mouse; whereas the Empty zone is localized on the opposite part of the apparatus. The approach of the test mouse to the SI or Empty zone was evaluated for social behavior quantification.

The experiment was made of two trials of 10 min each. During the first trial, the test animal was allowed to explore a tripartite chamber containing two empty cages in the outer compartments. Whereas, during the second trial, the social interaction (SI) zone contained a stranger juvenile mouse; the behavior of the test animal toward the SI or Empty zone was analyzed.

4.6.3 Stereotypic and repetitive behavior

Mice were transferred into a novel cage and the presence of different repetitive behaviors was analyzed. Self-grooming, digging, jerking, circling, and wall-leaning behaviors were scored as number of events in 300 sec.

4.6.4 Y-maze

A three-armed maze, with the shape of the letter Y, was used to measure exploratory behaviors in rodents. The mouse was placed in a maze formed by three arms with a length of 35 cm and 5 cm width, oriented at an angle of 120° (Fig 4.6).

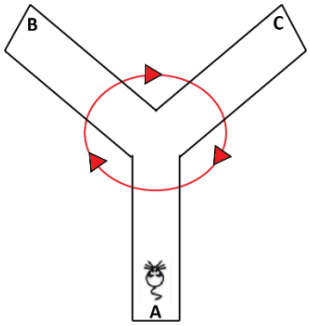

Figure 4.6 **| Scheme of the testing apparatus for Y-maze.** Schematic illustration showing an example of a correct alternation in the Y-maze test.

Mice were allowed to freely explore the Y maze for 5 min and percent of SPA (spontaneous alternation) and SAR (same arm return) was calculated in relation to total arm entries.

4.6.5 Ultrasound vocalizations

USVs were measured in P5-P9 male and female pups (Branchi *et al.*, 2001). Pups were singularly taken from the mother and placed away from littermates in a soundproof chamber at RT, this type of chamber could attenuate the external noise. The sound attenuating chamber was placed under a condenser ultrasound microphone (Avisoft Bioacoustics CM16/CMPA) connected to an UltraSoundGate 116Hb. The obtained data were collected for 300 sec with the Avisoft Recorder 2.76 in 16-bit format. Analysis of USVs was performed using the Avisoft SASLab Pro software (Avisoft

Bioacoustics, Berlin DE). The low frequency (<70-75 MHz) long calls (>20 ms) and the call trains (series of calls with a regular spacing of 150±10 ms) were manually scored.

4.6.6 Motor performance

RotaRod

The rotarod consists of a circular rod turning at a constant or increasing speed (Bohlen *et al.*, 2009). Animals placed on the rotating rod try to remain on it, rather than fall onto a platform just below. The rotarod test is widely used to generally assess motor performance in rats and mice; indeed, the test measure the ability of the mouse to maintain itself on the rod.

An automated apparatus (TSE Systems, Germany) was used to test young (2.5-5 months) and older (5.5-8 months) mice. On the first day, mice were placed on the rotarod and exposed to a constant speed (3 rpm) protocol for 4 sequential trials of 300 sec each, with inter-trial interval of 1 h 30 min. Afterwards, for five consecutive days mice were exposed to incremental rotation speed paradigm (3 to 30 rpm) for 300 sec, three times a day with inter-trial interval of 1 h 30 min. The best performance of the day was selected for every single mouse to assess motor ability, coordination and learning.

Hanging test

Mice were hanged with the forelegs to a thin metal bar and stay time was measured.

Grip test

A grip strength meter (Harvard Apparatus) was used to test muscle strength of the animals. Mice were allowed to grab a metal grid with the forepaws only or with all 4 paws and were gently and constantly pulled by the tail until they lost the grip. The pulling strength was measured in Newton. Three measurements were taken for each mouse and the average was used for statistical purposes.

Material

5.1 Mouse lines

Line	Reference
Pfn2$^{-/-}$	Pilo Boyl *et al.* 2007
Pfn1$^{flx/del}$;*Pfn2*$^{-/-}$;*Nes-Cre*$^{cre/wt}$	This work
Pfn1$^{flx/flx}$;*Pfn2*$^{-/-}$;*Camk2a-Cre*$^{cre/wt}$	This work

5.1.1 Oligonucleotides for genotyping PCRs

Table 5.1 - Oligonucleotides for genotyping PCRs

Primer (Number - Witke lab archive)	Sequence (5'-3' direction)
Pfn1-flx1 for (546)	TGG AGC GGA TCC AGC GAA GG
Pfn1-flx1 rev (789)	CGG CTT GGC TGC GTG AG
Pfn1-del2 as (752)	CAT GGT CCT AAA GTC TGG
Pfn2-for (229)	GTC TTG GTC TTT GTA ATG GGA AAA G
NestP2wt-rev (422)	CAA TGC TGG AGT ACA CAA GG
NestLacZ-rev (423)	CTG CAA GGC GAT TAA GTT GG
NesPr1 (s) (355)	CGC TTC CGC TGG GTC ACT GTC G
NesPr2 (as) (617)	TGC AGG CCG CCT CGA TGG
Cre4 (as) (749)	ATC GAC CGG TAA TGC AGG
MP90 (s) (386)	GGA CCT GGA TGC TGA CGA AG'
MP80 (as) (387)	CGC ATA ACC AGT GAA ACA GCA T
aCamkII-1 (as) (618)	ATG TGT CAG CGC CTA ACT CTG

5.2 Solutions and buffers

5.2.1 General solutions

Solution	Reagent	Concentration
Paraformaldehyde (PFA) 4 % - pH 7.4 (100 ml)	PBS 1x Formaldehyde	100 ml 4 g
PBS 10x - pH 7.4	NaCl Na_2HPO_4	1.5 M 162 mM

	NaH_2PO_4	38 mM
TBS 10x	Tris-HCl (pH 7.4)	400 mM
	NaCl	1.5 M

5.2.2 Solutions for the analysis of nucleic acids

Solution	Reagent	Concentration
DNA extraction buffer	Tris-HCl (pH 7.4)	50 mM
	NaCl	100 mM
	EDTA	5 mM
	SDS (20 %)	1 %
	Proteinase K	0.5 µg/µl
DNA loading buffer (100 ml)	Sucrose	40 %
	SDS	0.5 %
	Bromophenol blue	0.25 %
	TE buffer	to 100 ml
Proteinase K (10 mg/ml)	Proteinase K	
	MilliQ-H_2O	
Saturated NaCl (100 ml)	NaCl	~36 g
	MilliQ	Up to 100 ml
TE buffer	Tris-HCl (pH 8.0)	100 mM
	EDTA	1 mM
TAE buffer 50x – pH 8.3	Tris-HCl (pH 8.3)	2 M
	Acetic acid	57.1 ml
	EDTA (pH 8.0)	0.05 M
TENT buffer	Tris-HCl (pH 8.3)	20 mM
	EDTA	0.1 mM
	Tween-20	1 %
	Triton-X-100	0.2 %

5.2.3 Solutions for biochemistry

Solution	Reagent	Concentration
Coomassie destaining solution 40 %	Methanol	40 %
	Acetic acid	10 %
Coomassie destaining solution 20 %	Methanol	20 %
	Acetic acid	10 %

Coomassie staining solution	Methanol Acetic acid Coomassie Brilliant Blue R250	50 % 10 % 0.1 %
ECL solution A	Tris-HCl (pH 8.5) Luminol p-hydroxy-coumarin stock	0.1 M 2 % 0.05 %
ECL solution B	Tris-HCl (pH 8.5) H_2O_2 (30 %)	0.1 M 0.03 %
F-G actin separation buffer	Triton®X-100 PHEM	2 % 2x
p-hydroxy-coumarin stock solution	p-Coumaric Acid in DMSO	90 mM
Luminol stock solution	Luminol in DMSO	250 mM
Membrane blocking solution	NCP Milk powder (non-fat) or BSA	1x 5 %
NCP 10x (pH 8-8.4)	NaCl 1 Tris base Tween-20	1.47 M 0.4 M 0.05 %
PHEM buffer 10x (pH 6.9)	PIPES HEPES EGTA MgCl	600 mM 250 mM 100 mM 20 mM
Polyacrylamide resolving gel 10 % (50 ml for 7 gels)	Milli-Q H_2O 30 % Acrylamide (1:38) 2 M Tris/HCl pH 8.8 20 % SDS 10 % APS TEMED	23.3 ml 16.7 ml 9.5 ml 250 µl 320 µl 25 µl
Polyacrylamide resolving gel 15 % (50 ml for 7 gels)	Milli-Q H_2O 30 % Acrylamide (1:38) 2 M Tris/HCl pH 8.8 20 % SDS 10 % APS TEMED	15 ml 25.0 ml 9.5 ml 250 µl 320 µl 25 µl

Polyacrylamide resolving gel 3.8% (30 ml for 7 gels)	Milli-Q H_2O	18 ml
	30 % Acrylamide (1:38)	3.9 ml
	0.5 M Tris/HCl pH 6.8	7.5 ml
	20 % SDS	150 µl
	10 % APS	180 µl
	TEMED	14 µl
SDS loading buffer 5x	Tris-HCl (pH 6.8)	110 mM
	Glycerol	20%
	SDS	3.8%
	β-mercaptoethanol	8 %
	Bromophenol Blue	0.03 % (w/v)
SDS running buffer 10x	Tris base	0.25 M
	Glycine	1.92 M
	SDS (20 %)	1 %
Transfer buffer	Tris base	25 mM
	Glycine	192 mM
	Methanol	20 %

5.2.3.1 Solutions for synaptosomal preparation

Solution	Reagent	Concentration
Hepes-Krebs buffer	NaCl	147 mM
	KCl	3 mM
	Glucose	10 mM
	$MgSO_4$	1 mM
	$CaCl_2$	1 mM
	Hepes pH	20 mM
Homogenizing buffer	Sucrose	0.32
	EDTA	1 mM
	BSA	1 mg/ml
	HEPES pH 7.4	5 mM
Krebs-Ringer buffer	NaCl	140 mM
	KCl	5 mM
	Glucose	5 mM
	EDTA	1 mM
	HEPES pH 7.4	10 nM

5.2.4 Solutions for histological analysis

5.2.4.1 Prepared solutions for paraffin- cryo- and Golgi- method

Solution	Reagent	Concentration
Chrome alum solution (500 ml)	Gelatin type A $KCr(SO_4)_2$ Milli-Q H_2O	1.5 g 0.25 g 500 ml
EtOH 50 %-75 %-85 %-96 %	Ethanol Milli-Q H_2O	Different %
Sucrose 15 % (4°C - 100 ml)	Sucrose 1X PBS	15 g Up to 100 ml
Sucrose 30 % (4°C - 100 ml)	Sucrose 1X PBS	30 g Up to 100 ml

5.2.4.2 Commercial solutions for paraffin- cryo- and Golgi- method

Reagent	Supplier
Eosin Y	Sigma
Entellan	Merck
FD Rapid GolgiStain kit	FD NeuroTechnologies
Mayer's hemalum solution	Merck
Paraffin supplemented with DMSO	Sigma
Tissue-Tek O.C.T. Compound	Sakura
Entellan	Merck

5.2.4.3 Prepared solutions for stainings

Solution	Reagent	Concentration
Autofluorescence quenching solution	Ammonium chloride (NH4Cl)	50 mM
DAPI stock solution		10 ng/ml
DAPI staining solution	DAPI (in TBS-T)	1:5000
Draq5 staining solution	Draq5 (in TBS-T)	1:2000

IF Primary Antibody solution (cryo-section)		
IF Primary Antibody solution (vibratome sections)	IF Blocking solution Primary antibody (IAb)	1x Depending on the Ab
IF Secondary Antibody solution (cryo-sections)		
IF Secondary Antibody solution (vibratome sections)	IF Blocking solution Secondary antibody (IIAb)	1x Depending on the Ab
IF Blocking solution (cryo-sections)	NGS (Normal Goat Serum) DMSO Triton-X-100 TBS-T	5 % 2 % 0.5 % 1x
IF Blocking solution (vibratome sections)	NGS DMSO TBS-T	2-10 % 1-2 % 1x
Mowiol mounting media	Mowiol Tris-HCl pH 8.5 n-propyl-gallate (NPG) 1,4-diazabicyclo[2,2,2]octane (DABCO) p-phenyl-endiamine (PDD)	 20 % 5 % 2.5 % 0.25 %
TBS-T	Triton X-100 TBS	0.2 % 1x

5.2.5 Solutions for electrophysiology

Solution	**Reagent**	**Concentration**
Artificial cerebrospinal fluid (ACSF) – pH 7.3-7.4 315–325 mOsm/L	NaCl KCl $MgSO_4.7H_2O$ NaH_2PO_4 $NaHCO_3$ $CaCl_2$ Glucose	130 mM 2.75 mM 1.43 mM 1.1 mM 28.8 mM 2.5 mM 11 mM

Intracellular Solution (pH 7.2 – 290 mOSm/L)	Cs-Gluconate	150 mM
	HEPES	10 mM
	$MgCl_2$	2 mM
	MgATP	2 mM
	EGTA	0.2 mM
	QX-314	5 mM
	NaCl	8 mM
High-Chloride Intracellular Solution (pH 7.2 – 290 mOSm/L)	CsCl	90 mM
	Cs-Gluconate	20 mM
	HEPES	10 mM
	$MgCl_2$	2 mM
	EGTA	1 mM
	QX-314	2 mM
	NaCl	8 mM
Pharmacological Drugs	NBQX	10 µM
	PTX	100 µM
	TCM	250 µM
	TTX	0.2 µM

5.3 Commercial solutions, chemicals and reagents

5.3.1 Solid chemicals

Reagent	**Supplier**
Agarose	Biozym
Ammonium persulfate (APS)	Sigma-Aldrich
Bovine serum albumin (BSA)	Pan Biotech
Bromophenol blue	Bio-Rad
$CaCl_2 \cdot 2H_20$	Sigma-Aldrich
Coomassie Brilliant Blue R-250	AppliChem
CsCl	Sigma-Aldrich
CsOH	Sigma-Aldrich
CNQX	Tocris
D(+)-Glucose	Sigma-Aldrich

D(+)-Sucrose	VWR
EDTA	AppliChem
EGTA	Sigma-Aldrich
Gelatin Type A	Merck
Gluconate	Sigma-Aldrich
HEPES	Sigma-Aldrich
KCl	Sigma-Aldrich
$KCr(SO_4)_2$	Merck
Luminol	Sigma-Aldrich
$MgCl_2 \cdot 6H_20$	AppliChem
$MgSO_4 \cdot 7H_20$	AppliChem
Milk powder (non-fat)	Roth
n-propyl-gallate (NPG)	Sigma-Aldrich
NaCl	Th. Geyer
NaH_2PO_4	AppliChem
$NAHCO_3$	AppliChem
NaN_3	Merck
NBQX	Bio Trend
Paraffin, low-melting	Merck
Picrotoxin (PTX)	Sigma-Aldrich
Poly-D-Lysine	Sigma-Aldrich
Proteinase K	Sigma-Aldrich
QX-314	Tocris
Trichlormethiazide (TCM)	Sigma-Aldrich
Tetrodotoxin (TTX)	Bio Trend
Tris base	Sigma-Aldrich

5.3.2 Liquid chemicals

Reagent	Supplier
β-mercaptoethanol	Sigma-Aldrich
Acetic acid glacial	VWR
Acrylamide (30 %)	Merck
Bradford reagent	Witke Lab
Dimethyl sulfoxide (DMSO)	Sigma-Aldrich
dNTPs	Promega
Ethanol	Sigma-Aldrich
Ethidium bromide (1 %)	VWR
Glycine	Roth
Go-*Taq* polymerase	Promega
HEPES	Life Technologies
Hydrochloric acid (HCl) (37 %)	VWR
Isopropanol	VWR
Methanol	VWR
$MgCl_2$	Promega
Mowiol 4-88	Roth
Nitrogen	German-Cryo
Normal goat serum (NGS)	Vector Laboratories
PCR-flexi-buffer (5x)	Promega
PIPES	Roth
Sodium dodecyl sulfate (SDS)	AppliChem
TEMED	VWR
Triton-X 100	Roche
Tween-20	Sigma-Aldrich
Xylene	Roth

5.3.3 Markers

Reagent	Supplier
1 kb Plus DNA Ladder	Invitrogen
SeaBlue Plus2 Pre-Stained Standard	Invitrogen

5.4 Antibodies

5.4.1 Primary antibodies for WB

Unless stated otherwise, all antibodies for western blot were diluted in 5 % milk powder in 1x NCP and were incubated O/N at 4°C.

Table 5.2 - Primary antibodies for WB.

Antigen	Host species	Dilution	Manufacturer
Actin (C4)	Mouse	1:5000	MP Biomedicals
pCDK2(Thy15)	Rabbit	(BSA)	Cell Signaling
pCDK2(Thr161)	Rabbit	(BSA)	Cell Signaling
Dynamin 1 (KG43)	Rabbit	1:1000	Witke Lab
pH3(Ser 10)	Rabbit	(BSA)	Millipore
MUNC18	Mouse	1:1000	BD Transduction
α-PFN1 (p1T)	Rabbit	1:500	Witke Lab
α-PFN2 (3003)	Rabbit	1:500	Witke Lab
PSD95	Mouse	1:500	Upstate Cell Signaling
PSD95	Rabbit	1:500	Synaptic Systems
SNAP25	Rabbit	1:1000	Sigma-Aldrich
Synapsin 1	Rabbit	1:1000	Millipore
Synapsin 2A	Mouse	1:500	BD Transduction
Synaptophysin	Mouse	1:1000	Sigma-Aldrich
Synaptotagmin 1	Rabbit	1:1000	Synaptic Systems
Syntaxin 1			
VAMP2	Rabbit	1:1000	Synaptic Systems

Tpx2	Rabbit	1:500	Gruss Lab
γ-tubulin	Rabbit	1:1000	Sigma-Aldrich

5.4.2 Primary antibodies for IF

Table 5.3 - Primary antibodies for IF.

Antigen	Host species	Dilution	Manufacturer
Cleaved Caspase3 (Asp175) Alexa 488 conjugate	Rabbit	IF 1:50	Millipore
GFAP	Mouse	IF 1:500	Millipore
pH3(Ser10)	Rabbit	IF 1:500	Millipore
Iba1	Rabbit	IF 1:750	WAKO Chemicals
NRGN	Rabbit	IF 1:500	Proteintech
s100β	Rabbit	IF 1:1000	Abcam
β3-tubulin	Mouse	IF 1:1000	Promega

5.4.3 Secondary antibodies

All secondary antibodies for western blot were diluted 1:2000 in 5 % milk powder in 1x NCP and were incubated 2 hours at RT.

Table 5.4 - Secondary antibodies for WB & IF.

Antigen species	Conjugate	Host species	Dilution	Supplier
Mouse	HRP	Goat	WB 1:2000	Jackson ImmunoResearch
Rabbit	HRP	Goat	WB 1:2000	Jackson ImmunoResearch
Mouse	Alexa-488	Goat	IF 1:500	Life Technologies
Mouse	Alexa-555	Goat	IF 1:500	Life Technologies
Rabbit	Alexa-488	Goat	IF 1:500	Life Technologies
Rabbit	Alexa-555	Goat	IF 1:500	Life Technologies

5.4.3 Dyes reagents and staining solutions

Dye	Dilution	Supplier
DAPI	1:5000	Sigma-Aldrich
Draq5	1:1000	Abcam

5.5 Equipment and Software

5.5.1 Equipment for electrophysiology

Equipment	Supplier	Model/Version
Amplifier	Axon Instruments	Muticlamp 700B
Digitizer	Axon Instruments	Digidata 1322A
Electrodes	Science Products	GB150TF-8P
Vibratome	Leica	VT1200S

5.5.2 Software

Software	Supplier	Version
Clampfit	Axon Instruments	10.2
Custom written matlab routine	MathWorks	
Image J	NIH	1.45s
Multi Gauge	Fujifilm	V3.0
Prism	GraphPad	8

References

Ackermann, M., & Matus, A. (2003). Activity-induced targeting of profilin and stabilization of dendritic spine morphology. *Nature neuroscience*, *6*(11), 1194–1200. https://doi.org/10.1038/nn1135

Adrien, J. L., Lenoir, P., Martineau, J., Perrot, A., Hameury, L., Larmande, C., et al. (1993). Blind ratings of early symptoms of autism based upon family home movies. Journal of the American Academy of Child and Adolescent Psychiatry, 32(3), 617–626.

Andersen, P. *et al.* (2007) *The Hippocampus Book*. New York: Oxford University Press. doi: 10.1093/acprof:oso/9780195100273.001.0001.

Ahuja, R., Pinyol, R., Reichenbach, N., Custer, L., Klingensmith, J., Kessels, M. M., & Qualmann, B. (2007). Cordon-bleu is an actin nucleation factor and controls neuronal morphology. *Cell*, *131*(2), 337–350. https://doi.org/10.1016/j.cell.2007.08.030

Alkam, D., Feldman, E. Z., Singh, A., & Kiaei, M. (2017). Profilin1 biology and its mutation, actin(g) in disease. *Cellular and molecular life sciences : CMLS*, *74*(6), 967–981. https://doi.org/10.1007/s00018-016-2372-1

American Psychiatric Association (2013) Diagnostic and Statistical Manual of Mental Disorders, Fifth Edition DSM-5. Arlington, VA: American Psychiatric Association

Arasada, R., Gloss, A., Tunggal, B., Joseph, J. M., Rieger, D., Mondal, S., Faix, J., Schleicher, M., & Noegel, A. A. (2007). Profilin isoforms in Dictyostelium discoideum. *Biochimica et biophysica acta*, *1773*(5), 631–641. https://doi.org/10.1016/j.bbamcr.2007.03.009

Archer, S. J., Vinson, V. K., Pollard, T. D., & Torchia, D. A. (1994). Elucidation of the poly-L-proline binding site in Acanthamoeba profilin I by NMR spectroscopy. *FEBS letters*, *337*(2), 145–151. https://doi.org/10.1016/0014-5793(94)80262-9

Arikkath J. (2012). Molecular mechanisms of dendrite morphogenesis. *Frontiers in cellular neuroscience*, *6*, 61. https://doi.org/10.3389/fncel.2012.00061

Ascher, P., & Nowak, L. (1988). The role of divalent cations in the N-methyl-D-aspartate responses of mouse central neurones in culture. *The Journal of physiology*, *399*, 247–266. https://doi.org/10.1113/jphysiol.1988.sp017078

Atherton-Fessler, S., Liu, F., Gabrielli, B., Lee, M. S., Peng, C. Y., & Piwnica-Worms, H. (1994). Cell cycle regulation of the p34cdc2 inhibitory kinases. *Molecular biology of the cell*, *5*(9), 989–1001. https://doi.org/10.1091/mbc.5.9.989

Atladóttir, H. O., Thorsen, P., Schendel, D. E., Østergaard, L., Lemcke, S., & Parner, E. T. (2010). Association of hospitalization for infection in childhood with diagnosis of autism spectrum disorders: a Danish cohort study. *Archives of pediatrics & adolescent medicine*, *164*(5), 470–477. https://doi.org/10.1001/archpediatrics.2010.9

Auranen M, Vanhala R, Varilo T, Ayers K, Kempas E, Ylisaukko-Oja T, Sinsheimer JS, Peltonen L & Järvelä I (2002). A genomewide screen for autism-spectrum disorders: evidence for a major susceptibility locus on chromosome 3q25-27. *Am. J. Hum. Genet.* 71: 777–90

Avwioro G. (2011) Histochemical uses of haematoxylin – a review. JPCS. 2011;1:24–34.

Bai, F., & Witzmann, F. A. (2007). Synaptosome proteomics. *Sub-cellular biochemistry*, *43*, 77–98. https://doi.org/10.1007/978-1-4020-5943-8_6

Baranek, G. T. (1999). Autism during infancy: a retrospective video analysis of sensory-motor and social behaviors at 9–12 months of age. Journal of Autism and Developmental Disorders, 29(3), 213–224.

Barber, M., & Pierani, A. (2016). Tangential migration of glutamatergic neurons and cortical patterning during development: Lessons from Cajal-Retzius cells. *Developmental neurobiology*, *76*(8), 847–881. https://doi.org/10.1002/dneu.22363

Baron-Cohen, S., Wheelwright, S., Skinner, R., Martin, J., & Clubley, E. (2001). The autism-spectrum quotient (AQ): evidence from Asperger syndrome/high-functioning autism, males and females, scientists and mathematicians. *Journal of autism and developmental disorders*, *31*(1), 5–17. https://doi.org/10.1023/a:1005653411471

Barry, M. F., & Ziff, E. B. (2002). Receptor trafficking and the plasticity of excitatory synapses. *Current opinion in neurobiology*, *12*(3), 279–286. https://doi.org/10.1016/s0959-4388(02)00329-x

Behnen, M., Murk, K., Kursula, P., Cappallo-Obermann, H., Rothkegel, M., Kierszenbaum, A. L., & Kirchhoff, C. (2009). Testis-expressed profilins 3 and 4 show distinct functional characteristics and localize in the acroplaxome-manchette complex in spermatids. *BMC cell biology*, *10*, 34. https://doi.org/10.1186/1471-2121-10-34

Bellenchi, G. C., Gurniak, C. B., Perlas, E., Middei, S., Ammassari-Teule, M., & Witke, W. (2007). N-cofilin is associated with neuronal migration disorders and cell cycle control in the cerebral cortex. *Genes & development*, *21*(18), 2347–2357. https://doi.org/10.1101/gad.434307

Betancur C. (2011). Etiological heterogeneity in autism spectrum disorders: more than 100 genetic and genomic disorders and still counting. *Brain research*, *1380*, 42–77. https://doi.org/10.1016/j.brainres.2010.11.078

Bilder, D. A., Bakian, A. V., Viskochil, J., Clark, E. A., Botts, E. L., Smith, K. R., Pimentel, R., McMahon, W. M., & Coon, H. (2013). Maternal prenatal weight gain and autism spectrum disorders. *Pediatrics*, *132*(5), e1276–e1283. https://doi.org/10.1542/peds.2013-1188

Bir, S. C., Ambekar, S., Kukreja, S., & Nanda, A. (2015). Julius Caesar Arantius (Giulio Cesare Aranzi, 1530-1589) and the hippocampus of the human brain: history behind the discovery. *Journal of neurosurgery*, *122*(4), 971–975. https://doi.org/10.3171/2014.11.JNS132402

Birbach A. (2008). Profilin, a multi-modal regulator of neuronal plasticity. *BioEssays : news and reviews in molecular, cellular and developmental biology*, *30*(10), 994–1002. https://doi.org/10.1002/bies.20822

Bittel DC, Kibiryeva N & Butler MG (2006). Expression of 4 genes between chromosome 15 breakpoints 1 and 2 and behavioral outcomes in Prader-Willi syndrome. *Pediatrics* 118: e1276-83

Blasco, R., Cole, N. B., & Moss, B. (1991). Sequence analysis, expression, and deletion of a vaccinia virus gene encoding a homolog of profilin, a eukaryotic actin-binding protein. *Journal of virology*, *65*(9), 4598–4608.

Bloom, O., Evergren, E., Tomilin, N., Kjaerulff, O., Löw, P., Brodin, L., Pieribone, V. A., Greengard, P., & Shupliakov, O. (2003). Colocalization of synapsin and actin during synaptic vesicle recycling. *The Journal of cell biology*, *161*(4), 737–747. https://doi.org/10.1083/jcb.200212140

Bohlen, M., Cameron, A., Metten, P., Crabbe, J. C., & Wahlsten, D. (2009). Calibration of rotational acceleration for the rotarod test of rodent motor coordination. *Journal of neuroscience methods*, *178*(1), 10–14. https://doi.org/10.1016/j.jneumeth.2008.11.001

Bormann, J., & Feigenspan, A. (1995). GABAC receptors. *Trends in neurosciences*, *18*(12), 515–519. https://doi.org/10.1016/0166-2236(95)98370-e

Böttcher, R. T., Wiesner, S., Braun, A., Wimmer, R., Berna, A., Elad, N., Medalia, O., Pfeifer, A., Aszódi, A., Costell, M., & Fässler, R. (2009). Profilin 1 is required for abscission during late cytokinesis of chondrocytes. *The EMBO journal*, *28*(8), 1157–1169. https://doi.org/10.1038/emboj.2009.58

Bowerman, M., Anderson, C. L., Beauvais, A., Boyl, P. P., Witke, W., & Kothary, R. (2009). SMN, profilin IIa and plastin 3: a link between the deregulation of actin dynamics and SMA pathogenesis. *Molecular and cellular neurosciences*, *42*(1), 66–74. https://doi.org/10.1016/j.mcn.2009.05.009

Bowerman, M., Beauvais, A., Anderson, C. L., & Kothary, R. (2010). Rho-kinase inactivation prolongs survival of an intermediate SMA mouse model. *Human molecular genetics*, *19*(8), 1468–1478. https://doi.org/10.1093/hmg/ddq021

Bourgeron T. (2015). From the genetic architecture to synaptic plasticity in autism spectrum disorder. *Nature reviews. Neuroscience*, *16*(9), 551–563. https://doi.org/10.1038/nrn3992

Bourgeron T. (2016). Current knowledge on the genetics of autism and propositions for future research. *Comptes rendus biologies*, *339*(7-8), 300–307. https://doi.org/10.1016/j.crvi.2016.05.004

Bozdagi, O., Sakurai, T., Papapetrou, D., Wang, X., Dickstein, D. L., Takahashi, N., Kajiwara, Y., Yang, M., Katz, A. M., Scattoni, M. L., Harris, M. J., Saxena, R., Silverman, J. L., Crawley, J. N., Zhou, Q., Hof, P. R., & Buxbaum, J. D. (2010). Haploinsufficiency of the autism-associated Shank3 gene leads to deficits in synaptic function, social interaction, and social communication. *Molecular autism*, *1*(1), 15. https://doi.org/10.1186/2040-2392-1-15

Bozzi, Y., Provenzano, G., & Casarosa, S. (2018). Neurobiological bases of autism-epilepsy comorbidity: a focus on excitation/inhibition imbalance. *The European journal of neuroscience*, *47*(6), 534–548. https://doi.org/10.1111/ejn.13595

Bradford M. M. (1976). A rapid and sensitive method for the quantitation of microgram quantities of protein utilizing the principle of protein-dye binding. *Analytical biochemistry*, *72*, 248–254. https://doi.org/10.1006/abio.1976.9999

Bradke, F., & Dotti, C. G. (1999). The role of local actin instability in axon formation. *Science (New York, N.Y.)*, *283*(5409), 1931–1934. https://doi.org/10.1126/science.283.5409.1931

Branchi, I., Santucci, D., & Alleva, E. (2001). Ultrasonic vocalisation emitted by infant rodents: a tool for assessment of neurobehavioural development. *Behavioural brain research*, *125*(1-2), 49–56. https://doi.org/10.1016/s0166-4328(01)00277-7

Braun, A., Aszódi, A., Hellebrand, H., Berna, A., Fässler, R., & Brandau, O. (2002). Genomic organization of profilin-III and evidence for a transcript expressed exclusively in testis. *Gene*, *283*(1-2), 219–225. https://doi.org/10.1016/s0378-1119(01)00855-1

Burgin, K. E., Waxham, M. N., Rickling, S., Westgate, S. A., Mobley, W. C., & Kelly, P. T. (1990). In situ hybridization histochemistry of Ca2+/calmodulin-dependent protein kinase in developing rat brain. *The Journal of neuroscience : the official journal of the Society for Neuroscience*, *10*(6), 1788–1798. https://doi.org/10.1523/JNEUROSCI.10-06-01788.1990

Buss, F., Temm-Grove, C., Henning, S., & Jockusch, B. M. (1992). Distribution of profilin in fibroblasts correlates with the presence of highly dynamic actin filaments. *Cell motility and the cytoskeleton*, *22*(1), 51–61. https://doi.org/10.1002/cm.970220106

Butler-Cole, C., Wagner, M. J., Da Silva, M., Brown, G. D., Burke, R. D., & Upton, C. (2007). An ectromelia virus profilin homolog interacts with cellular tropomyosin and viral A-type inclusion protein. *Virology journal*, *4*, 76. https://doi.org/10.1186/1743-422X-4-76

Campellone, K. G., & Welch, M. D. (2010). A nucleator arms race: cellular control of actin assembly. *Nature reviews. Molecular cell biology*, *11*(4), 237–251. https://doi.org/10.1038/nrm2867

Canitano R. (2007). Epilepsy in autism spectrum disorders. *European child & adolescent psychiatry*, *16*(1), 61–66. https://doi.org/10.1007/s00787-006-0563-2

Cappello, S., Attardo, A., Wu, X., Iwasato, T., Itohara, S., Wilsch-Bräuninger, M., Eilken, H. M., Rieger, M. A., Schroeder, T. T., Huttner, W. B., Brakebusch, C., & Götz, M. (2006). The Rho-GTPase cdc42 regulates neural progenitor fate at the apical surface. *Nature neuroscience*, *9*(9), 1099–1107. https://doi.org/10.1038/nn1744

Carlsson, L., Nyström, L. E., Sundkvist, I., Markey, F., & Lindberg, U. (1977). Actin polymerizability is influenced by profilin, a low molecular weight protein in non-muscle cells. *Journal of molecular biology*, *115*(3), 465–483. https://doi.org/10.1016/0022-2836(77)90166-8

Cellot, G., & Cherubini, E. (2014). GABAergic signaling as therapeutic target for autism spectrum disorders. *Frontiers in pediatrics*, *2*, 70. https://doi.org/10.3389/fped.2014.00070

Chang, Y., Wang, R., Barot, S., & Weiss, D. S. (1996). Stoichiometry of a recombinant GABAA receptor. *The Journal of neuroscience : the official journal of the Society for Neuroscience*, *16*(17), 5415–5424. https://doi.org/10.1523/JNEUROSCI.16-17-05415.1996

Chang, Y. C., Cole, T. B., & Costa, L. G. (2017). Behavioral Phenotyping for Autism Spectrum Disorders in Mice. *Current protocols in toxicology*, *72*, 11.22.1–11.22.21. https://doi.org/10.1002/cptx.19

Cheng, Y. J., Zhu, Z. X., Zhou, J. S., Hu, Z. Q., Zhang, J. P., Cai, Q. P., & Wang, L. H. (2015). Silencing profilin-1 inhibits gastric cancer progression via integrin β1/focal adhesion kinase pathway modulation. *World journal of gastroenterology*, *21*(8), 2323–2335. https://doi.org/10.3748/wjg.v21.i8.2323

Chesarone, M. A., & Goode, B. L. (2009). Actin nucleation and elongation factors: mechanisms and interplay. *Current opinion in cell biology*, *21*(1), 28–37. https://doi.org/10.1016/j.ceb.2008.12.001

Christensen, J., Grønborg, T. K., Sørensen, M. J., Schendel, D., Parner, E. T., Pedersen, L. H., & Vestergaard, M. (2013). Prenatal valproate exposure and risk of autism spectrum disorders and childhood autism. *JAMA*, *309*(16), 1696–1703. https://doi.org/10.1001/jama.2013.2270

Chung W, Choi SY, Lee E, Park H, Kang J, Park H, Choi Y, Lee D, Park S-G, Kim R, Cho YS, Choi J, Kim M-H, Lee JW, Lee S, Rhim I, Jung MW, Kim D, Bae YC & Kim E (2015). Social deficits in IRSp53 mutant mice improved by NMDAR and mGluR5 suppression. *Nat. Neurosci.* 18: 435–43

Cingolani, L. A., & Goda, Y. (2008). Actin in action: the interplay between the actin cytoskeleton and synaptic efficacy. *Nature reviews. Neuroscience*, *9*(5), 344–356. https://doi.org/10.1038/nrn2373

Cooley, L., Verheyen, E., & Ayers, K. (1992). chickadee encodes a profilin required for intercellular cytoplasm transport during Drosophila oogenesis. *Cell*, *69*(1), 173–184. https://doi.org/10.1016/0092-8674(92)90128-y

Coon H, Matsunami N, Stevens J, Miller J, Pingree C, Camp NJ, Thomas A, Krasny L, Lainhart J, Leppert MF & McMahon W (2005). Evidence for linkage on chromosome 3q25-27 in a large autism extended pedigree. *Hum. Hered.* 60: 220–6

Courchesne, E., & Pierce, K. (2005). Brain overgrowth in autism during a critical time in development: implications for frontal pyramidal neuron and interneuron development and connectivity. *International journal of developmental neuroscience : the official journal of the International Society for Developmental Neuroscience*, *23*(2-3), 153–170. https://doi.org/10.1016/j.ijdevneu.2005.01.003

Couteaux R. and M. Pecot-Dechavassine. (1970) Vesicles synaptiques et poches au niveau des "zones actives" de la jonction neuromusculaire. Comptes Rend. Acad. Sci. (Paris) Ser D 271: 2346-2349.

Cowan, C. R., & Hyman, A. A. (2004). Asymmetric cell division in C. elegans: cortical polarity and spindle positioning. *Annual review of cell and developmental biology*, *20*, 427–453. https://doi.org/10.1146/annurev.cellbio.19.111301.113823lo

Crawley JN (2007). Mouse behavioral assays relevant to the symptoms of autism. *Brain Pathol.* 17: 448–59

Da Silva, J. S., Medina, M., Zuliani, C., Di Nardo, A., Witke, W., & Dotti, C. G. (2003). RhoA/ROCK regulation of neuritogenesis via profilin IIa-mediated control of actin stability. *The Journal of cell biology*, *162*(7), 1267–1279. https://doi.org/10.1083/jcb.200304021

Das, T., Bae, Y. H., Wells, A., & Roy, P. (2009). Profilin-1 overexpression upregulates PTEN and suppresses AKT activation in breast cancer cells. *Journal of cellular physiology*, *218*(2), 436–443. https://doi.org/10.1002/jcp.21618

De Rubeis, S., Pasciuto, E., Li, K. W., Fernández, E., Di Marino, D., Buzzi, A., Ostroff, L. E., Klann, E., Zwartkruis, F. J., Komiyama, N. H., Grant, S. G., Poujol, C., Choquet, D., Achsel, T., Posthuma, D., Smit, A. B., & Bagni, C. (2013). CYFIP1 coordinates mRNA translation and cytoskeleton remodeling to ensure proper dendritic spine formation. *Neuron*, *79*(6), 1169–1182. https://doi.org/10.1016/j.neuron.2013.06.039

De Rubeis, S., & Buxbaum, J. D. (2015). Genetics and genomics of autism spectrum disorder: embracing complexity. *Human molecular genetics*, *24*(R1), R24–R31. https://doi.org/10.1093/hmg/ddv273

Dehay, C., & Kennedy, H. (2007). Cell-cycle control and cortical development. *Nature reviews. Neuroscience*, *8*(6), 438–450. https://doi.org/10.1038/nrn2097

DeLorey TM, Handforth A, Anagnostaras SG, Homanics GE, Minassian BA, Asatourian A, Fanselow MS, Delgado-Escueta A, Ellison GD & Olsen RW (1998). Mice lacking the beta3 subunit of the GABAA receptor have the epilepsy phenotype and many of the behavioral characteristics of Angelman syndrome. *J. Neurosci.* 18: 8505–14

Desai, D., Gu, Y., & Morgan, D. O. (1992). Activation of human cyclin-dependent kinases in vitro. *Molecular biology of the cell*, *3*(5), 571–582. https://doi.org/10.1091/mbc.3.5.571

Deshmukh, S. S., & Knierim, J. J. (2012). Hippocampus. *Wiley interdisciplinary reviews. Cognitive science*, *3*(2), 231–251. https://doi.org/10.1002/wcs.1164

Di Nardo, A., Gareus, R., Kwiatkowski, D., & Witke, W. (2000). Alternative splicing of the mouse profilin II gene generates functionally different profilin isoforms. *Journal of cell science*, *113 Pt 21*, 3795–3803.

Dillon, C., & Goda, Y. (2005). The actin cytoskeleton: integrating form and function at the synapse. *Annual review of neuroscience*, *28*, 25–55. https://doi.org/10.1146/annurev.neuro.28.061604.135757

Ding, Z., Bae, Y. H., & Roy, P. (2012). Molecular insights on context-specific role of profilin-1 in cell migration. *Cell adhesion & migration*, *6*(5), 442–449. https://doi.org/10.4161/cam.21832

Dominguez R. (2004). Actin-binding proteins--a unifying hypothesis. *Trends in biochemical sciences*, *29*(11), 572–578. https://doi.org/10.1016/j.tibs.2004.09.004

Dominguez, R., & Holmes, K. C. (2011). Actin structure and function. *Annual review of biophysics*, *40*, 169–186. https://doi.org/10.1146/annurev-biophys-042910-155359

Domke, T., Federau, T., Schlüter, K., Giehl, K., Valenta, R., Schomburg, D., & Jockusch, B. M. (1997). Birch pollen profilin: structural organization and interaction with poly-(L-proline) peptides as revealed by NMR. *FEBS letters*, *411*(2-3), 291–295. https://doi.org/10.1016/s0014-5793(97)00719-9

Dong, X., Shen, K., & Bülow, H. E. (2015). Intrinsic and extrinsic mechanisms of dendritic morphogenesis. *Annual review of physiology*, *77*, 271–300. https://doi.org/10.1146/annurev-physiol-021014-071746

dos Remedios, C. G., Chhabra, D., Kekic, M., Dedova, I. V., Tsubakihara, M., Berry, D. A., & Nosworthy, N. J. (2003). Actin binding proteins: regulation of cytoskeletal microfilaments. *Physiological reviews*, *83*(2), 433–473. https://doi.org/10.1152/physrev.00026.2002

Doyle, C. A., & McDougle, C. J. (2012). Pharmacologic treatments for the behavioral symptoms associated with autism spectrum disorders across the lifespan. *Dialogues in clinical neuroscience*, *14*(3), 263–279.

Elmaci, İ., Altinoz, M. A., Sari, R., & Bolukbasi, F. H. (2018). Phosphorylated Histone H3 (PHH3) as a Novel Cell Proliferation Marker and Prognosticator for Meningeal Tumors: A Short Review. *Applied immunohistochemistry & molecular morphology : AIMM*, *26*(9), 627–631. https://doi.org/10.1097/PAI.0000000000000499

Elmore S. (2007). Apoptosis: a review of programmed cell death. *Toxicologic pathology*, *35*(4), 495–516. https://doi.org/10.1080/01926230701320337

Emptage, N., Bliss, T. V., & Fine, A. (1999). Single synaptic events evoke NMDA receptor-mediated release of calcium from internal stores in hippocampal dendritic spines. *Neuron*, *22*(1), 115–124. https://doi.org/10.1016/s0896-6273(00)80683-2

Epsztein, Jérôme & Represa, Alfonso & Crépel, Valérie. (2017). Role of Kainate Receptors in Glutamatergic Synaptic Transmission: Implications for Acute and Chronic Seizure Generation. 10.1016/B978-0-12-809324-5.00077-8.

Ercan-Sencicek, A. G., Jambi, S., Franjic, D., Nishimura, S., Li, M., El-Fishawy, P., Morgan, T. M., Sanders, S. J., Bilguvar, K., Suri, M., Johnson, M. H., Gupta, A. R., Yuksel, Z., Mane, S., Grigorenko, E., Picciotto, M., Alberts, A. S., Gunel, M., Šestan, N., & State, M. W. (2015). Homozygous loss of DIAPH1 is a novel cause of microcephaly in humans. *European journal of human genetics : EJHG*, *23*(2), 165–172. https://doi.org/10.1038/ejhg.2014.82

Etherton, M. R., Blaiss, C. A., Powell, C. M., & Südhof, T. C. (2009). Mouse neurexin-1alpha deletion causes correlated electrophysiological and behavioral changes consistent with cognitive impairments. *Proceedings of the National Academy of Sciences of the United States of America*, *106*(42), 17998–18003. https://doi.org/10.1073/pnas.0910297106

Etherton, M. R., Tabuchi, K., Sharma, M., Ko, J., & Südhof, T. C. (2011). An autism-associated point mutation in the neuroligin cytoplasmic tail selectively impairs AMPA receptor-mediated synaptic transmission in hippocampus. *The EMBO journal*, *30*(14), 2908–2919. https://doi.org/10.1038/emboj.2011.182

Evergren, E., Benfenati, F., & Shupliakov, O. (2007). The synapsin cycle: a view from the synaptic endocytic zone. *Journal of neuroscience research*, *85*(12), 2648–2656. https://doi.org/10.1002/jnr.21176

Farrar, S. J., Whiting, P. J., Bonnert, T. P., & McKernan, R. M. (1999). Stoichiometry of a ligand-gated ion channel determined by fluorescence energy transfer. *The Journal of biological chemistry*, *274*(15), 10100–10104. https://doi.org/10.1074/jbc.274.15.10100

Favre, M. R., La Mendola, D., Meystre, J., Christodoulou, D., Cochrane, M. J., Markram, H., & Markram, K. (2015). Predictable enriched environment prevents development of hyper-emotionality in the VPA rat model of autism. *Frontiers in neuroscience*, *9*, 127. https://doi.org/10.3389/fnins.2015.00127

Fedorov, A. A., Ball, T., Mahoney, N. M., Valenta, R., & Almo, S. C. (1997). The molecular basis for allergen cross-reactivity: crystal structure and IgE-epitope mapping of birch pollen profilin. *Structure (London, England : 1993)*, *5*(1), 33–45. https://doi.org/10.1016/s0969-2126(97)00164-0

Feng, Y., Olson, E. C., Stukenberg, P. T., Flanagan, L. A., Kirschner, M. W., & Walsh, C. A. (2000). LIS1 regulates CNS lamination by interacting with mNudE, a central component of the centrosome. *Neuron*, *28*(3), 665–679. https://doi.org/10.1016/s0896-6273(00)00145-8

Filice, F., Vörckel, K.J., Sungur, A.Ö., Wöhr, M. & Schwaller, B. (2016) Reduction in parvalbumin expression not loss of the parvalbumin-expressing GABA interneuron subpopulation in genetic parvalbumin and shank mouse models of autism. *Mol. Brain*, 9, 10. doi: 10.1186/s13041-016-0192-8.

Finlay, B. L., & Darlington, R. B. (1995). Linked regularities in the development and evolution of mammalian brains. *Science (New York, N.Y.)*, *268*(5217), 1578–1584. https://doi.org/10.1126/science.7777856

Fischer, A. H., Jacobson, K. A., Rose, J., & Zeller, R. (2008). Hematoxylin and eosin staining of tissue and cell sections. *CSH protocols*, *2008*, pdb.prot4986. https://doi.org/10.1101/pdb.prot4986

Fournier KA, Hass CJ, Naik SK, Lodha N & Cauraugh JH (2010). Motor coordination in autism spectrum disorders: A synthesis and meta-analysis. *J. Autism Dev. Disord.* 40: 1227–1240

Fricker, M., Tolkovsky, A. M., Borutaite, V., Coleman, M., & Brown, G. C. (2018). Neuronal Cell Death. *Physiological reviews*, *98*(2), 813–880. https://doi.org/10.1152/physrev.00011.2017
Frith, U. (Ed.). (1991). Autism and Asperger syndrome. Cambridge University Press. https://doi.org/10.1017/CBO9780511526770

Fukushima N. (2011) Microtubules in the Nervous System. In: Nixon R., Yuan A. (eds) Cytoskeleton of the Nervous System. Advances in Neurobiology, vol 3. Springer, New York, NY

Gachet, Y., Tournier, S., Millar, J. B., & Hyams, J. S. (2001). A MAP kinase-dependent actin checkpoint ensures proper spindle orientation in fission yeast. *Nature*, *412*(6844), 352–355. https://doi.org/10.1038/35085604

Gao, F. B., Brenman, J. E., Jan, L. Y., & Jan, Y. N. (1999). Genes regulating dendritic outgrowth, branching, and routing in Drosophila. *Genes & development*, *13*(19), 2549–2561. https://doi.org/10.1101/gad.13.19.2549

Gao, R., & Penzes, P. (2015). Common mechanisms of excitatory and inhibitory imbalance in schizophrenia and autism spectrum disorders. *Current molecular medicine*, *15*(2), 146–167. https://doi.org/10.2174/1566524015666150303003028

Gareus, R., Di Nardo, A., Rybin, V., & Witke, W. (2006). Mouse profilin 2 regulates endocytosis and competes with SH3 ligand binding to dynamin 1. *The Journal of biological chemistry*, *281*(5), 2803–2811. https://doi.org/10.1074/jbc.M503528200

Gasic, G. P., & Nicotera, P. (2003). To die or to sleep, perhaps to dream. *Toxicology letters*, *139*(2-3), 221–227. https://doi.org/10.1016/s0378-4274(02)00487-3

Germain, N., Banda, E., & Grabel, L. (2010). Embryonic stem cell neurogenesis and neural specification. *Journal of cellular biochemistry*, *111*(3), 535–542. https://doi.org/10.1002/jcb.22747

Gertler, F. B., Niebuhr, K., Reinhard, M., Wehland, J., & Soriano, P. (1996). Mena, a relative of VASP and Drosophila Enabled, is implicated in the control of microfilament dynamics. *Cell*, *87*(2), 227–239. https://doi.org/10.1016/s0092-8674(00)81341-0

Ghashghaei, H. T., Lai, C., & Anton, E. S. (2007). Neuronal migration in the adult brain: are we there yet?. *Nature reviews. Neuroscience*, *8*(2), 141–151. https://doi.org/10.1038/nrn2074

Gieselmann, R., Kwiatkowski, D. J., Janmey, P. A., & Witke, W. (1995). Distinct biochemical characteristics of the two human profilin isoforms. *European journal of biochemistry*, *229*(3), 621–628. https://doi.org/10.1111/j.1432-1033.1995.tb20506.x

Giesemann, T., Schwarz, G., Nawrotzki, R., Berhörster, K., Rothkegel, M., Schlüter, K., Schrader, N., Schindelin, H., Mendel, R. R., Kirsch, J., & Jockusch, B. M. (2003). Complex formation between the postsynaptic scaffolding protein gephyrin, profilin, and Mena: a possible link to the microfilament system. *The Journal of neuroscience : the official journal of the Society for Neuroscience*, *23*(23), 8330–8339. https://doi.org/10.1523/JNEUROSCI.23-23-08330.2003

Gillberg C. (1991). The treatment of epilepsy in autism. *Journal of autism and developmental disorders*, *21*(1), 61–77. https://doi.org/10.1007/bf02206998

Gillberg C, Coleman M. (2000). *The Biology of the Autistic Syndromes*. 3rd ed. London, UK: Mac Keith Press, Distributed by Cambridge University Press

Gillberg, C., Billstedt, E., Sundh, V., & Gillberg, I. C. (2010). Mortality in autism: a prospective longitudinal community-based study. *Journal of autism and developmental disorders*, *40*(3), 352–357. https://doi.org/10.1007/s10803-009-0883-4

Gkogkas CG, Khoutorsky A, Ran I, Rampakakis E, Nevarko T, Weatherill DB, Vasuta C, Yee S, Truitt M, Dallaire P, Major F, Lasko P, Ruggero D, Nader K, Lacaille JC & Sonenberg N (2013). Autism-related deficits via dysregulated eIF4E-dependent translational control. *Nature* 493: 371–377

Görlich, A., Zimmermann, A. M., Schober, D., Böttcher, R. T., Sassoè-Pognetto, M., Friauf, E., Witke, W., & Rust, M. B. (2012). Preserved morphology and physiology of excitatory synapses in profilin1-deficient mice. *PloS one*, *7*(1), e30068. https://doi.org/10.1371/journal.pone.0030068

Greengard, P., Benfenati, F., & Valtorta, F. (1994). Synapsin I, an actin-binding protein regulating synaptic vesicle traffic in the nerve terminal. *Advances in second messenger and phosphoprotein research*, *29*, 31–45. https://doi.org/10.1016/s1040-7952(06)80005-4

Griswold, A. J., Ma, D., Cukier, H. N., Nations, L. D., Schmidt, M. A., Chung, R. H., Jaworski, J. M., Salyakina, D., Konidari, I., Whitehead, P. L., Wright, H. H., Abramson, R. K., Williams, S. M., Menon, R., Martin, E. R., Haines, J. L., Gilbert, J. R., Cuccaro, M. L., & Pericak-Vance, M. A. (2012). Evaluation of copy number variations reveals novel candidate genes in autism spectrum disorder-associated pathways. *Human molecular genetics*, *21*(15), 3513–3523. https://doi.org/10.1093/hmg/dds164

Gunning, P. W., Hardeman, E. C., Lappalainen, P., & Mulvihill, D. P. (2015). Tropomyosin - master regulator of actin filament function in the cytoskeleton. *Journal of cell science*, *128*(16), 2965–2974. https://doi.org/10.1242/jcs.172502

Gurniak, C. B., Perlas, E., & Witke, W. (2005). The actin depolymerizing factor n-cofilin is essential for neural tube morphogenesis and neural crest cell migration. *Developmental biology*, *278*(1), 231–241. https://doi.org/10.1016/j.ydbio.2004.11.010

Haikarainen, T., Chen, W. Q., Lubec, G., & Kursula, P. (2009). Structure, modifications and ligand-binding properties of rat profilin 2a. *Acta crystallographica. Section D, Biological crystallography*, *65*(Pt 4), 303–311. https://doi.org/10.1107/S0907444909000699

Hamill, O. P., Marty, A., Neher, E., Sakmann, B., & Sigworth, F. J. (1981). Improved patch-clamp techniques for high-resolution current recording from cells and cell-free membrane patches. *Pflugers Archiv : European journal of physiology*, *391*(2), 85–100. https://doi.org/10.1007/bf00656997

Harrison, S. M., Jarvie, P. E., & Dunkley, P. R. (1988). A rapid Percoll gradient procedure for isolation of synaptosomes directly from an S1 fraction: viability of subcellular fractions. *Brain research*, *441*(1-2), 72–80. https://doi.org/10.1016/0006-8993(88)91384-4

Haugwitz, M., Noegel, A. A., Rieger, D., Lottspeich, F., & Schleicher, M. (1991). Dictyostelium discoideum contains two profilin isoforms that differ in structure and function. *Journal of cell science*, *100 (Pt 3)*, 481–489.

Heng, Y. W., & Koh, C. G. (2010). Actin cytoskeleton dynamics and the cell division cycle. *The international journal of biochemistry & cell biology*, *42*(10), 1622–1633. https://doi.org/10.1016/j.biocel.2010.04.007

Hinton, V. J., Brown, W. T., Wisniewski, K., & Rudelli, R. D. (1991). Analysis of neocortex in three males with the fragile X syndrome. *American journal of medical genetics*, *41*(3), 289–294. https://doi.org/10.1002/ajmg.1320410306

Hirvikoski T, Mittendorfer-Rutz E, Boman M, Larsson H, Lichtenstein P & Bölte S (2016). Premature mortality in autism spectrum disorder. *Br. J. Psychiatry* 208: 232–8

Hoogenraad, C. C., Akhmanova, A., Galjart, N., & De Zeeuw, C. I. (2004). LIMK1 and CLIP-115: linking cytoskeletal defects to Williams syndrome. *BioEssays : news and reviews in molecular, cellular and developmental biology*, *26*(2), 141–150. https://doi.org/10.1002/bies.10402

Hollander, E., Novotny, S., Hanratty, M., Yaffe, R., DeCaria, C. M., Aronowitz, B. R., & Mosovich, S. (2003). Oxytocin infusion reduces repetitive behaviors in adults with autistic and Asperger's disorders. *Neuropsychopharmacology : official publication of the American College of Neuropsychopharmacology*, *28*(1), 193–198. https://doi.org/10.1038/sj.npp.1300021

Hollmann, M., & Heinemann, S. (1994). Cloned glutamate receptors. *Annual review of neuroscience*, *17*, 31–108. https://doi.org/10.1146/annurev.ne.17.030194.000335

Honoré, B., Madsen, P., Andersen, A. H., & Leffers, H. (1993). Cloning and expression of a novel human profilin variant, profilin II. *FEBS letters*, *330*(2), 151–155. https://doi.org/10.1016/0014-5793(93)80262-s

Hu, E., Chen, Z., Fredrickson, T., & Zhu, Y. (2001). Molecular cloning and characterization of profilin-3: a novel cytoskeleton-associated gene expressed in rat kidney and testes. *Experimental nephrology*, *9*(4), 265–274. https://doi.org/10.1159/000052621

Huguet, G., Ey, E., & Bourgeron, T. (2013). The genetic landscapes of autism spectrum disorders. *Annual review of genomics and human genetics*, *14*, 191–213. https://doi.org/10.1146/annurev-genom-091212-153431

Hunter T. (1995). Protein kinases and phosphatases: the yin and yang of protein phosphorylation and signaling. *Cell*, *80*(2), 225–236. https://doi.org/10.1016/0092-8674(95)90405-0

Hussey, P. J., Ketelaar, T., & Deeks, M. J. (2006). Control of the actin cytoskeleton in plant cell growth. *Annual review of plant biology*, *57*, 109–125. https://doi.org/10.1146/annurev.arplant.57.032905.105206

Hussman J. P. (2001). Suppressed GABAergic inhibition as a common factor in suspected etiologies of autism. *Journal of autism and developmental disorders*, *31*(2), 247–248. https://doi.org/10.1023/a:1010715619091

Iossifov I, O'Roak BJ, Sanders SJ, Ronemus M, Krumm N, Levy D, Stessman H a., Witherspoon KT, Vives L, Patterson KE, Smith JD, Paeper B, Nickerson D a., Dea J, Dong S, Gonzalez LE, Mandell JD, Mane SM, Murtha MT, Sullivan C a., et al (2014). The contribution of de novo coding mutations to autism spectrum disorder. *Nature* 515: 216–221

Ingram JL, Peckham SM, Tisdale B, Rodier PM (2000) Prenatal exposure of rats to valproic acid reproduces the cerebellar anomalies associated with autism. *Neurotoxicol Teratol* 22:319–324.

Isshiki, M., Tanaka, S., Kuriu, T., Tabuchi, K., Takumi, T., & Okabe, S. (2014). Enhanced synapse remodelling as a common phenotype in mouse models of autism. *Nature communications*, *5*, 4742. https://doi.org/10.1038/ncomms5742

Jamain, S., Quach, H., Betancur, C., Råstam, M., Colineaux, C., Gillberg, I. C., Soderstrom, H., Giros, B., Leboyer, M., Gillberg, C., Bourgeron, T., & Paris Autism Research International Sibpair Study (2003). Mutations of the X-linked genes encoding neuroligins NLGN3 and NLGN4 are associated with autism. *Nature genetics*, *34*(1), 27–29. https://doi.org/10.1038/ng1136

Janke, J., Schlüter, K., Jandrig, B., Theile, M., Kölble, K., Arnold, W., Grinstein, E., Schwartz, A., Estevéz-Schwarz, L., Schlag, P. M., Jockusch, B. M., & Scherneck, S. (2000). Suppression of tumorigenicity in breast cancer cells by the microfilament protein profilin 1. *The Journal of experimental medicine*, *191*(10), 1675–1686. https://doi.org/10.1084/jem.191.10.1675

Jayaraman, D., Bae, B. I., & Walsh, C. A. (2018). The Genetics of Primary Microcephaly. *Annual review of genomics and human genetics*, *19*, 177–200. https://doi.org/10.1146/annurev-genom-083117-021441

Jockusch, B. M., Murk, K., & Rothkegel, M. (2007). The profile of profilins. *Reviews of physiology, biochemistry and pharmacology*, *159*, 131–149. https://doi.org/10.1007/112_2007_704

Johnson, J. W., & Ascher, P. (1987). Glycine potentiates the NMDA response in cultured mouse brain neurons. *Nature*, *325*(6104), 529–531. https://doi.org/10.1038/325529a0

Johnston, D., & Wu, S. M. (1995). *Foundations of cellular neurophysiology*. Cambridge, Mass: MIT Press.

Jones, K. A., Borowsky, B., Tamm, J. A., Craig, D. A., Durkin, M. M., Dai, M., Yao, W. J., Johnson, M., Gunwaldsen, C., Huang, L. Y., Tang, C., Shen, Q., Salon, J. A., Morse, K., Laz, T., Smith, K. E., Nagarathnam, D., Noble, S. A., Branchek, T. A., & Gerald, C. (1998). GABA(B) receptors function as a heteromeric assembly of the subunits GABA(B)R1 and GABA(B)R2. *Nature*, *396*(6712), 674–679. https://doi.org/10.1038/25348

Just, M. A., Cherkassky, V. L., Keller, T. A., Kana, R. K., & Minshew, N. J. (2007). Functional and anatomical cortical underconnectivity in autism: evidence from an FMRI study of an executive

function task and corpus callosum morphometry. *Cerebral cortex (New York, N.Y. : 1991)*, *17*(4), 951–961. https://doi.org/10.1093/cercor/bhl006

Kaiser, D. A., Goldschmidt-Clermont, P. J., Levine, B. A., & Pollard, T. D. (1989). Characterization of renatured profilin purified by urea elution from poly-L-proline agarose columns. *Cell motility and the cytoskeleton*, *14*(2), 251–262. https://doi.org/10.1002/cm.970140211

Kalil, K., & Dent, E. W. (2014). Branch management: mechanisms of axon branching in the developing vertebrate CNS. *Nature reviews. Neuroscience*, *15*(1), 7–18. https://doi.org/10.1038/nrn3650

Kandasamy, M. K., McKinney, E. C., & Meagher, R. B. (2002). Plant profilin isovariants are distinctly regulated in vegetative and reproductive tissues. *Cell motility and the cytoskeleton*, *52*(1), 22–32. https://doi.org/10.1002/cm.10029

Kandel, E. R. *et al.* (2012) *Principles of Neural Science*. 5th edn. McGraw-Hill.

Kang HW, Kim HK, Moon BH, Lee SJ, Lee SJ, Rhyu IJ (2017). Comprehensive Review of Golgi Staining Methods for Nervous Tissue. *Applied Microscopy 47(2): 63-69.* https://doi.org/10.9729/AM.2017.47.2.63

Kanner, L. (1943). Autistic disturbances of affective contact. Pathology 217–250.

Katayama, K., Melendez, J., Baumann, J. M., Leslie, J. R., Chauhan, B. K., Nemkul, N., Lang, R. A., Kuan, C. Y., Zheng, Y., & Yoshida, Y. (2011). Loss of RhoA in neural progenitor cells causes the disruption of adherens junctions and hyperproliferation. *Proceedings of the National Academy of Sciences of the United States of America*, *108*(18), 7607–7612. https://doi.org/10.1073/pnas.1101347108

Keinänen, K., Wisden, W., Sommer, B., Werner, P., Herb, A., Verdoorn, T. A., Sakmann, B., & Seeburg, P. H. (1990). A family of AMPA-selective glutamate receptors. *Science (New York, N.Y.)*, *249*(4968), 556–560. https://doi.org/10.1126/science.2166337

Kelleher, J. F., Atkinson, S. J., & Pollard, T. D. (1995). Sequences, structural models, and cellular localization of the actin-related proteins Arp2 and Arp3 from Acanthamoeba. *The Journal of cell biology*, *131*(2), 385–397. https://doi.org/10.1083/jcb.131.2.385

Kilpinen, H., Ylisaukko-Oja, T., Hennah, W., Palo, O. M., Varilo, T., Vanhala, R., Nieminen-von Wendt, T., von Wendt, L., Paunio, T., & Peltonen, L. (2008). Association of DISC1 with autism and Asperger syndrome. *Molecular psychiatry*, *13*(2), 187–196. https://doi.org/10.1038/sj.mp.4002031

Kim, J. Y., Jeong, H. S., Chung, T., Kim, M., Lee, J. H., Jung, W. H., & Koo, J. S. (2017). The value of phosphohistone H3 as a proliferation marker for evaluating invasive breast cancers: A comparative study with Ki67. *Oncotarget*, *8*(39), 65064–65076. https://doi.org/10.18632/oncotarget.17775

Kim S. K. (2015). Recent update of autism spectrum disorders. *Korean journal of pediatrics*, *58*(1), 8–14. https://doi.org/10.3345/kjp.2015.58.1.8

Kirkpatrick, B., Xu, L., Cascella, N., Ozeki, Y., Sawa, A., & Roberts, R. C. (2006). DISC1 immunoreactivity at the light and ultrastructural level in the human neocortex. *The Journal of comparative neurology*, *497*(3), 436–450. https://doi.org/10.1002/cne.21007

Kirsch, J., Langosch, D., Prior, P., Littauer, U. Z., Schmitt, B., & Betz, H. (1991). The 93-kDa glycine receptor-associated protein binds to tubulin. *The Journal of biological chemistry*, *266*(33), 22242–22245.

Kirsten, T. B., Chaves-Kirsten, G. P., Chaible, L. M., Silva, A. C., Martins, D. O., Britto, L. R., Dagli, M. L., Torrão, A. S., Palermo-Neto, J., & Bernardi, M. M. (2012). Hypoactivity of the central dopaminergic system and autistic-like behavior induced by a single early prenatal exposure to lipopolysaccharide. *Journal of neuroscience research*, *90*(10), 1903–1912. https://doi.org/10.1002/jnr.23089

Kleckner, N. W., & Dingledine, R. (1988). Requirement for glycine in activation of NMDA-receptors expressed in Xenopus oocytes. *Science (New York, N.Y.)*, *241*(4867), 835–837. https://doi.org/10.1126/science.2841759

Kleijer, K., Huguet, G., Tastet, J., Bourgeron, T., & Burbach, J. (2017). Anatomy and Cell Biology of Autism Spectrum Disorder: Lessons from Human Genetics. *Advances in anatomy, embryology, and cell biology*, *224*, 1–25. https://doi.org/10.1007/978-3-319-52498-6_1

Kneussel, M., Hermann, A., Kirsch, J., & Betz, H. (1999). Hydrophobic interactions mediate binding of the glycine receptor beta-subunit to gephyrin. *Journal of neurochemistry*, *72*(3), 1323–1326. https://doi.org/10.1046/j.1471-4159.1999.0721323.x

Koganezawa, N., Hanamura, K., Sekino, Y., & Shirao, T. (2017). The role of drebrin in dendritic spines. *Molecular and cellular neurosciences*, *84*, 85–92. https://doi.org/10.1016/j.mcn.2017.01.004

Kim S. K. (2015). Recent update of autism spectrum disorders. *Korean journal of pediatrics*, *58*(1), 8–14. https://doi.org/10.3345/kjp.2015.58.1.8

Kovar D.R. and Pollard T.D. (2004). Insertional assembly of actin filament barbed ends in association with formins produces piconewton forces. Pnas 101 (41) 14725-14730.

Kovar, D. R., Harris, E. S., Mahaffy, R., Higgs, H. N., & Pollard, T. D. (2006). Control of the assembly of ATP- and ADP-actin by formins and profilin. *Cell*, *124*(2), 423–435. https://doi.org/10.1016/j.cell.2005.11.038

Kron, S. J., Drubin, D. G., Botstein, D., & Spudich, J. A. (1992). Yeast actin filaments display ATP-dependent sliding movement over surfaces coated with rabbit muscle myosin. *Proceedings of the National Academy of Sciences of the United States of America*, *89*(10), 4466–4470. https://doi.org/10.1073/pnas.89.10.4466

Kullmann, J. A., Neumeyer, A., Gurniak, C. B., Friauf, E., Witke, W., & Rust, M. B. (2011). Profilin1 is required for glial cell adhesion and radial migration of cerebellar granule neurons. *EMBO reports*, *13*(1), 75–82. https://doi.org/10.1038/embor.2011.211

Kullmann, J. A., Neumeyer, A., Wickertsheim, I., Böttcher, R. T., Costell, M., Deitmer, J. W., Witke, W., Friauf, E., & Rust, M. B. (2012). Purkinje cell loss and motor coordination defects in profilin1 mutant mice. *Neuroscience*, *223*, 355–364. https://doi.org/10.1016/j.neuroscience.2012.07.055

Kunda P., Craig, G., Dominguez V., and Baum B. (2003). Abi, Sra1, and Kette Control the Stability and Localization of SCAR/WAVE to Regulate the Formation of Actin-Based Protrusions. Curr. Biol. 13, 1867–1875.

Laemmli U. K. (1970). Cleavage of structural proteins during the assembly of the head of bacteriophage T4. Nature, 227(5259), 680–685. https://doi.org/10.1038/227680a0

Lainiola, M., Procaccini, C., & Linden, A. M. (2014). mGluR3 knockout mice show a working memory defect and an enhanced response to MK-801 in the T- and Y-maze cognitive tests. *Behavioural brain research*, *266*, 94–103. https://doi.org/10.1016/j.bbr.2014.03.008

Lambrechts, A., Verschelde, J. L., Jonckheere, V., Goethals, M., Vandekerckhove, J., & Ampe, C. (1997). The mammalian profilin isoforms display complementary affinities for PIP2 and proline-rich sequences. *The EMBO journal*, *16*(3), 484–494. https://doi.org/10.1093/emboj/16.3.484

Lambrechts, A., Braun, A., Jonckheere, V., Aszodi, A., Lanier, L. M., Robbens, J., Van Colen, I., Vandekerckhove, J., Fässler, R., & Ampe, C. (2000). Profilin II is alternatively spliced, resulting in profilin isoforms that are differentially expressed and have distinct biochemical properties. *Molecular and cellular biology*, *20*(21), 8209–8219. https://doi.org/10.1128/mcb.20.21.8209-8219.2000

Lambrechts, A., Jonckheere, V., Dewitte, D., Vandekerckhove, J., & Ampe, C. (2002). Mutational analysis of human profilin I reveals a second PI(4,5)-P2 binding site neighbouring the poly(L-proline) binding site. *BMC biochemistry*, *3*, 12. https://doi.org/10.1186/1471-2091-3-12

Lamprecht, R., Farb, C. R., Rodrigues, S. M., & LeDoux, J. E. (2006). Fear conditioning drives profilin into amygdala dendritic spines. *Nature neuroscience*, *9*(4), 481–483. https://doi.org/10.1038/nn1672

Landis, D. M., Hall, A. K., Weinstein, L. A., & Reese, T. S. (1988). The organization of cytoplasm at the presynaptic active zone of a central nervous system synapse. *Neuron*, *1*(3), 201–209. https://doi.org/10.1016/0896-6273(88)90140-7

Lanoue, V., & Cooper, H. M. (2019). Branching mechanisms shaping dendrite architecture. *Developmental biology*, *451*(1), 16–24. https://doi.org/10.1016/j.ydbio.2018.12.005

Lassing, I., & Lindberg, U. (1985). Specific interaction between phosphatidylinositol 4,5-bisphosphate and profilactin. *Nature*, *314*(6010), 472–474. https://doi.org/10.1038/314472a0

Leary, M. R., & Hill, D. A. (1996). Moving on: autism and movement disturbance. Mental Retardation, 34(1), 39–53.

Leblond CS, Heinrich J, Delorme R, Proepper C, Betancur C, Huguet G, Konyukh M, Chaste P, Ey E, Rastam M, Anckarsäter H, Nygren G, Gillberg IC, Melke J, Toro R, Regnault B, Fauchereau F, Mercati O, Lemière N, Skuse D, et al (2012). Genetic and functional analyses of SHANK2 mutations suggest a multiple hit model of autism spectrum disorders. *PLoS Genet.*8:

Lebrand, C., Dent, E. W., Strasser, G. A., Lanier, L. M., Krause, M., Svitkina, T. M., Borisy, G. G., & Gertler, F. B. (2004). Critical role of Ena/VASP proteins for filopodia formation in neurons and in function downstream of netrin-1. *Neuron*, *42*(1), 37–49. https://doi.org/10.1016/s0896-6273(04)00108-4

Lee, M. K., Tuttle, J. B., Rebhun, L. I., Cleveland, D. W., & Frankfurter, A. (1990). The expression and posttranslational modification of a neuron-specific beta-tubulin isotype during chick embryogenesis. *Cell motility and the cytoskeleton*, *17*(2), 118–132. https://doi.org/10.1002/cm.970170207

Lee, K., & Song, K. (2007). Actin dysfunction activates ERK1/2 and delays entry into mitosis in mammalian cells. *Cell cycle (Georgetown, Tex.)*, *6*(12), 1487–1495.

Lee E, Lee J & Kim E (2017). Excitation/Inhibition Imbalance in Animal Models of Autism Spectrum Disorders. *Biol. Psychiatry* 81: 838–847 Lewine *et al.*, 1999

Lester, R. A., & Jahr, C. E. (1992). NMDA channel behavior depends on agonist affinity. *The Journal of neuroscience : the official journal of the Society for Neuroscience*, *12*(2), 635–643. https://doi.org/10.1523/JNEUROSCI.12-02-00635.1992

Lewine, J. D., Andrews, R., Chez, M., Patil, A. A., Devinsky, O., Smith, M., Kanner, A., Davis, J. T., Funke, M., Jones, G., Chong, B., Provencal, S., Weisend, M., Lee, R. R., & Orrison, W. W., Jr (1999). Magnetoencephalographic patterns of epileptiform activity in children with regressive autism spectrum disorders. *Pediatrics*, *104*(3 Pt 1), 405–418. https://doi.org/10.1542/peds.104.3.405

Lian, G., Lu, J., Hu, J., Zhang, J., Cross, S. H., Ferland, R. J., & Sheen, V. L. (2012). Filamin a regulates neural progenitor proliferation and cortical size through Wee1-dependent Cdk1 phosphorylation. *The Journal of neuroscience : the official journal of the Society for Neuroscience*, *32*(22), 7672–7684. https://doi.org/10.1523/JNEUROSCI.0894-12.2012

Lian, G., & Sheen, V. L. (2015). Cytoskeletal proteins in cortical development and disease: actin associated proteins in periventricular heterotopia. *Frontiers in cellular neuroscience*, *9*, 99. https://doi.org/10.3389/fncel.2015.00099

Liemersdorf, C. (2016), Neuronal Systems Potentially Involved in Autism Spectrum Disorder. Doctorate dissertation.

Liu, X. B., & Murray, K. D. (2012). Neuronal excitability and calcium/calmodulin-dependent protein kinase type II: location, location, location. *Epilepsia*, *53 Suppl 1*, 45–52. https://doi.org/10.1111/j.1528-1167.2012.03474.x

Lomaga, M. A., Henderson, J. T., Elia, A. J., Robertson, J., Noyce, R. S., Yeh, W. C., & Mak, T. W. (2000). Tumor necrosis factor receptor-associated factor 6 (TRAF6) deficiency results in exencephaly and is required for apoptosis within the developing CNS. *The Journal of neuroscience : the official journal of the Society for Neuroscience*, *20*(19), 7384–7393. https://doi.org/10.1523/JNEUROSCI.20-19-07384.2000

Loveland, K. A., Pearson, D. A., Tunali-Kotoski, B., Ortegon, J., & Gibbs, M. C. (2001). Judgments of social appropriateness by children and adolescents with autism. *Journal of autism and developmental disorders*, *31*(4), 367–376. https://doi.org/10.1023/a:1010608518060

Machesky, L. M., Goldschmidt-Clermont, P. J., & Pollard, T. D. (1990). The affinities of human platelet and Acanthamoeba profilin isoforms for polyphosphoinositides account for their relative abilities to inhibit phospholipase C. *Cell regulation*, *1*(12), 937–950. https://doi.org/10.1091/mbc.1.12.937

Machesky, L. M., Atkinson, S. J., Ampe, C., Vandekerckhove, J., & Pollard, T. D. (1994). Purification of a cortical complex containing two unconventional actins from Acanthamoeba by affinity chromatography on profilin-agarose. *The Journal of cell biology*, *127*(1), 107–115. https://doi.org/10.1083/jcb.127.1.107

Maloney, M. T., & Bamburg, J. R. (2007). Cofilin-mediated neurodegeneration in Alzheimer's disease and other amyloidopathies. *Molecular neurobiology*, *35*(1), 21–44. https://doi.org/10.1007/bf02700622

Mammoto, A., Sasaki, T., Asakura, T., Hotta, I., Imamura, H., Takahashi, K., Matsuura, Y., Shirao, T., & Takai, Y. (1998). Interactions of drebrin and gephyrin with profilin. *Biochemical and biophysical research communications*, *243*(1), 86–89. https://doi.org/10.1006/bbrc.1997.8068

Mao, R., Deng, R., Wei, Y., Han, L., Meng, Y., Xie, W., & Jia, Z. (2019). LIMK1 and LIMK2 regulate cortical development through affecting neural progenitor cell proliferation and migration. *Molecular brain*, *12*(1), 67. https://doi.org/10.1186/s13041-019-0487-7

McCollum, D., Feoktistova, A., Morphew, M., Balasubramanian, M., & Gould, K. L. (1996). The Schizosaccharomyces pombe actin-related protein, Arp3, is a component of the cortical actin cytoskeleton and interacts with profilin. *The EMBO journal*, *15*(23), 6438–6446.

McGowan, C. H., & Russell, P. (1993). Human Wee1 kinase inhibits cell division by phosphorylating p34cdc2 exclusively on Tyr15. *The EMBO journal*, *12*(1), 75–85.

Megías, M., Emri, Z., Freund, T. F., & Gulyás, A. I. (2001). Total number and distribution of inhibitory and excitatory synapses on hippocampal CA1 pyramidal cells. *Neuroscience*, *102*(3), 527–540. https://doi.org/10.1016/s0306-4522(00)00496-6

Metzler, W. J., Constantine, K. L., Friedrichs, M. S., Bell, A. J., Ernst, E. G., Lavoie, T. B., & Mueller, L. (1993). Characterization of the three-dimensional solution structure of human profilin: 1H, 13C, and 15N NMR assignments and global folding pattern. *Biochemistry*, *32*(50), 13818–13829. https://doi.org/10.1021/bi00213a010

Meyer, G., Kirsch, J., Betz, H., & Langosch, D. (1995). Identification of a gephyrin binding motif on the glycine receptor beta subunit. *Neuron*, *15*(3), 563–572. https://doi.org/10.1016/0896-6273(95)90145-0

Michaelsen, K., Murk, K., Zagrebelsky, M., Dreznjak, A., Jockusch, B. M., Rothkegel, M., & Korte, M. (2010). Fine-tuning of neuronal architecture requires two profilin isoforms. *Proceedings of the National Academy of Sciences of the United States of America*, *107*(36), 15780–15785. https://doi.org/10.1073/pnas.1004406107

Michaelsen-Preusse, K., Zessin, S., Grigoryan, G., Scharkowski, F., Feuge, J., Remus, A., & Korte, M. (2016). Neuronal profilins in health and disease: Relevance for spine plasticity and Fragile X syndrome. *Proceedings of the National Academy of Sciences of the United States of America*, *113*(12), 3365–3370. https://doi.org/10.1073/pnas.1516697113

Miki, H., Suetsugu, S., & Takenawa, T. (1998). WAVE, a novel WASP-family protein involved in actin reorganization induced by Rac. *The EMBO journal*, *17*(23), 6932–6941. https://doi.org/10.1093/emboj/17.23.6932

Miles, J. H., Takahashi, T. N., Bagby, S., Sahota, P. K., Vaslow, D. F., Wang, C. H., Hillman, R. E., & Farmer, J. E. (2005). Essential versus complex autism: definition of fundamental prognostic subtypes. *American journal of medical genetics. Part A*, *135*(2), 171–180. https://doi.org/10.1002/ajmg.a.30590

Minichiello, L., Korte, M., Wolfer, D., Kühn, R., Unsicker, K., Cestari, V., Rossi-Arnaud, C., Lipp, H. P., Bonhoeffer, T., & Klein, R. (1999). Essential role for TrkB receptors in hippocampus-mediated learning. *Neuron*, *24*(2), 401–414. https://doi.org/10.1016/s0896-6273(00)80853-3

Miyagi, Y., Yamashita, T., Fukaya, M., Sonoda, T., Okuno, T., Yamada, K., Watanabe, M., Nagashima, Y., Aoki, I., Okuda, K., Mishina, M., & Kawamoto, S. (2002). Delphilin: a novel PDZ and formin homology domain-containing protein that synaptically colocalizes and interacts with glutamate receptor delta 2 subunit. *The Journal of neuroscience : the official journal of the Society for Neuroscience*, *22*(3), 803–814. https://doi.org/10.1523/JNEUROSCI.22-03-00803.2002

Moy, S. S., Nadler, J. J., Young, N. B., Perez, A., Holloway, L. P., Barbaro, R. P., Barbaro, J. R., Wilson, L. M., Threadgill, D. W., Lauder, J. M., Magnuson, T. R., & Crawley, J. N. (2007). Mouse behavioral tasks relevant to autism: phenotypes of 10 inbred strains. *Behavioural brain research*, *176*(1), 4–20. https://doi.org/10.1016/j.bbr.2006.07.030

Muhle, Rebecca & Trentacoste, Stephanie & Rapin, Isabelle. (2004). The genetics of autism. Pediatrics. 113. e472-86. 10.1542/peds.113.5.e472.

Mullins, R. D., Heuser, J. A., & Pollard, T. D. (1998). The interaction of Arp2/3 complex with actin: nucleation, high affinity pointed end capping, and formation of branching networks of filaments. *Proceedings of the National Academy of Sciences of the United States of America*, *95*(11), 6181–6186. https://doi.org/10.1073/pnas.95.11.6181

Mullis, K. B., & Faloona, F. A. (1987). Specific synthesis of DNA in vitro via a polymerase-catalyzed chain reaction. *Methods in enzymology*, *155*, 335–350. https://doi.org/10.1016/0076-6879(87)55023-6

Nagy, A., & Delgado-Escueta, A. V. (1984). Rapid preparation of synaptosomes from mammalian brain using nontoxic isoosmotic gradient material (Percoll). *Journal of neurochemistry*, *43*(4), 1114–1123. https://doi.org/10.1111/j.1471-4159.1984.tb12851.x

Nakamura, Y., Wood, C. L., Patton, A. P., Jaafari, N., Henley, J. M., Mellor, J. R., & Hanley, J. G. (2011). PICK1 inhibition of the Arp2/3 complex controls dendritic spine size and synaptic plasticity. *The EMBO journal*, *30*(4), 719–730. https://doi.org/10.1038/emboj.2010.357

Napoli, I., Mercaldo, V., Boyl, P. P., Eleuteri, B., Zalfa, F., De Rubeis, S., Di Marino, D., Mohr, E., Massimi, M., Falconi, M., Witke, W., Costa-Mattioli, M., Sonenberg, N., Achsel, T., & Bagni, C. (2008). The fragile X syndrome protein represses activity-dependent translation through CYFIP1, a new 4E-BP. *Cell*, *134*(6), 1042–1054. https://doi.org/10.1016/j.cell.2008.07.031

Nassar, N., Dixon, G., Bourke, J., Bower, C., Glasson, E., de Klerk, N., & Leonard, H. (2009). Autism spectrum disorders in young children: effect of changes in diagnostic practices. *International journal of epidemiology*, *38*(5), 1245–1254. https://doi.org/10.1093/ije/dyp260

Naviaux, J. C., Schuchbauer, M. A., Li, K., Wang, L., Risbrough, V. B., Powell, S. B., & Naviaux, R. K. (2014). Reversal of autism-like behaviors and metabolism in adult mice with single-dose antipurinergic therapy. *Translational psychiatry*, *4*(6), e400. https://doi.org/10.1038/tp.2014.33

Nayate, A., Bradshaw, J. L., & Rinehart, N. J. (2005). Autism and Asperger's disorder: are they movement disorders involving the cerebellum and/or basal ganglia? Brain Research Bulletin, 67(4), 327–334.

Nelson SB & Valakh V (2015). Excitatory/Inhibitory Balance and Circuit Homeostasis in Autism Spectrum Disorders. *Neuron* 87: 684–698

Neves, G., Cooke, S. F., & Bliss, T. V. (2008). Synaptic plasticity, memory and the hippocampus: a neural network approach to causality. *Nature reviews. Neuroscience*, *9*(1), 65–75. https://doi.org/10.1038/nrn2303

Neuhoff, H., Sassoè-Pognetto, M., Panzanelli, P., Maas, C., Witke, W., & Kneussel, M. (2005). The actin-binding protein profilin I is localized at synaptic sites in an activity-regulated manner. *The European journal of neuroscience*, *21*(1), 15–25. https://doi.org/10.1111/j.1460-9568.2004.03814.x

Nicholls, D., Sihra, T. Synaptosomes possess an exocytotic pool of glutamate. *Nature* 321, 772–773 (1986). https://doi.org/10.1038/321772a0

Nimchinsky, E. A., Sabatini, B. L., & Svoboda, K. (2002). Structure and function of dendritic spines. *Annual review of physiology*, *64*, 313–353. https://doi.org/10.1146/annurev.physiol.64.081501.160008

Niswender, C. M., & Conn, P. J. (2010). Metabotropic glutamate receptors: physiology, pharmacology, and disease. *Annual review of pharmacology and toxicology*, *50*, 295–322. https://doi.org/10.1146/annurev.pharmtox.011008.145533

Nodelman, I. M., Bowman, G. D., Lindberg, U., & Schutt, C. E. (1999). X-ray structure determination of human profilin II: A comparative structural analysis of human profilins. *Journal of molecular biology*, *294*(5), 1271–1285. https://doi.org/10.1006/jmbi.1999.3318

Norbury, C., Blow, J., & Nurse, P. (1991). Regulatory phosphorylation of the p34cdc2 protein kinase in vertebrates. *The EMBO journal*, *10*(11), 3321–3329.

Notman, R., Noro, M., O'Malley, B., & Anwar, J. (2006). Molecular basis for dimethylsulfoxide (DMSO) action on lipid membranes. *Journal of the American Chemical Society*, *128*(43), 13982–13983. https://doi.org/10.1021/ja063363t

Nowak, L., Bregestovski, P., Ascher, P., Herbet, A., & Prochiantz, A. (1984). Magnesium gates glutamate-activated channels in mouse central neurones. *Nature*, *307*(5950), 462–465. https://doi.org/10.1038/307462a0

Obermann, H., Raabe, I., Balvers, M., Brunswig, B., Schulze, W., & Kirchhoff, C. (2005). Novel testis-expressed profilin IV associated with acrosome biogenesis and spermatid elongation. *Molecular human reproduction*, *11*(1), 53–64. https://doi.org/10.1093/molehr/gah132

Okamoto, K., Nagai, T., Miyawaki, A., & Hayashi, Y. (2004). Rapid and persistent modulation of actin dynamics regulates postsynaptic reorganization underlying bidirectional plasticity. *Nature neuroscience*, *7*(10), 1104–1112. https://doi.org/10.1038/nn1311

Okamoto, K., & Sagata, N. (2007). Mechanism for inactivation of the mitotic inhibitory kinase Wee1 at M phase. *Proceedings of the National Academy of Sciences of the United States of America*, *104*(10), 3753–3758. https://doi.org/10.1073/pnas.0607357104

Olson, M. F., Ashworth, A., & Hall, A. (1995). An essential role for Rho, Rac, and Cdc42 GTPases in cell cycle progression through G1. *Science (New York, N.Y.)*, *269*(5228), 1270–1272. https://doi.org/10.1126/science.7652575

Ozaki, K., Sugino, H., Hasegawa, T., Takahashi, S., & Hatano, S. (1983). Isolation and characterization of Physarum profilin. *Journal of biochemistry*, *93*(1), 295–298. https://doi.org/10.1093/oxfordjournals.jbchem.a134167

Ozkan, E. D., Creson, T. K., Kramár, E. A., Rojas, C., Seese, R. R., Babyan, A. H., Shi, Y., Lucero, R., Xu, X., Noebels, J. L., Miller, C. A., Lynch, G., & Rumbaugh, G. (2014). Reduced cognition in Syngap1 mutants is caused by isolated damage within developing forebrain excitatory neurons. *Neuron*, *82*(6), 1317–1333. https://doi.org/10.1016/j.neuron.2014.05.015

Pai, Y. J., & Moore, A. W. (2018). Dendritic actin delivery service. *The Journal of cell biology*, *217*(10), 3325–3326. https://doi.org/10.1083/jcb.201808095

Pan, X., Chang, X., Leung, C., Zhou, Z., Cao, F., Xie, W., & Jia, Z. (2015). PAK1 regulates cortical development via promoting neuronal migration and progenitor cell proliferation. *Molecular brain*, *8*, 36. https://doi.org/10.1186/s13041-015-0124-z

Pantaloni, D., Carlier, M. F., Coué, M., Lal, A. A., Brenner, S. L., & Korn, E. D. (1984). The critical concentration of actin in the presence of ATP increases with the number concentration of filaments and approaches the critical concentration of actin.ADP. *The Journal of biological chemistry*, *259*(10), 6274–6283.

Pantaloni, D., & Carlier, M. F. (1993). How profilin promotes actin filament assembly in the presence of thymosin beta 4. *Cell*, *75*(5), 1007–1014. https://doi.org/10.1016/0092-8674(93)90544-z

Pantaloni, D., Le Clainche, C., & Carlier, M. F. (2001). Mechanism of actin-based motility. *Science (New York, N.Y.)*, *292*(5521), 1502–1506. https://doi.org/10.1126/science.1059975

Parner, E. T., Schendel, D. E., & Thorsen, P. (2008). Autism prevalence trends over time in Denmark: changes in prevalence and age at diagnosis. *Archives of pediatrics & adolescent medicine*, *162*(12), 1150–1156. https://doi.org/10.1001/archpedi.162.12.1150

Pearson, A. M., Baksa, K., Rämet, M., Protas, M., McKee, M., Brown, D., & Ezekowitz, R. A. (2003). Identification of cytoskeletal regulatory proteins required for efficient phagocytosis in Drosophila. *Microbes and infection*, *5*(10), 815–824. https://doi.org/10.1016/s1286-4579(03)00157-6

Peça J, Feliciano C, Ting JT, Wang W, Wells MF, Venkatraman TN, Lascola CD, Fu Z & Feng G (2011). Shank3 mutant mice display autistic-like behaviours and striatal dysfunction. *Nature* 472: 437–42

Peñagarikano O, Abrahams BS, Herman EI, Winden KD, Gdalyahu A, Dong H, Sonnenblick LI, Gruver R, Almajano J, Bragin A, Golshani P, Trachtenberg JT, Peles E & Geschwind DH (2011). Absence of CNTNAP2 leads to epilepsy, neuronal migration abnormalities, and core autism-related deficits. *Cell* 147: 235–46

Petersen, A., & Gerges, N. Z. (2015). Neurogranin regulates CaM dynamics at dendritic spines. *Scientific reports*, *5*, 11135. https://doi.org/10.1038/srep11135

Pilo Boyl P, Di Nardo A, Mulle C, Sassoè-Pognetto M, Panzanelli P, Mele A, Kneussel M, Costantini V, Perlas E, Massimi M, Vara H, Giustetto M & Witke W (2007). Profilin2 contributes to synaptic vesicle exocytosis, neuronal excitability, and novelty-seeking behavior. *EMBO J.* 26: 2991–3002 Q

Pinto, D., Delaby, E., Merico, D., Barbosa, M., Merikangas, A., Klei, L., Thiruvahindrapuram, B., Xu, X., Ziman, R., Wang, Z., Vorstman, J. A., Thompson, A., Regan, R., Pilorge, M., Pellecchia, G., Pagnamenta, A. T., Oliveira, B., Marshall, C. R., Magalhaes, T. R., Lowe, J. K., … Scherer, S. W. (2014). Convergence of genes and cellular pathways dysregulated in autism spectrum disorders. *American journal of human genetics*, *94*(5), 677–694. https://doi.org/10.1016/j.ajhg.2014.03.018

Polet, D., Lambrechts, A., Ono, K., Mah, A., Peelman, F., Vandekerckhove, J., Baillie, D. L., Ampe, C., & Ono, S. (2006). Caenorhabditis elegans expresses three functional profilins in a tissue-specific manner. *Cell motility and the cytoskeleton*, *63*(1), 14–28. https://doi.org/10.1002/cm.20102

Pollard, T. D., Blanchoin, L., & Mullins, R. D. (2000). Molecular mechanisms controlling actin filament dynamics in nonmuscle cells. *Annual review of biophysics and biomolecular structure*, *29*, 545–576. https://doi.org/10.1146/annurev.biophys.29.1.545

Pollard, T. D., & Borisy, G. G. (2003). Cellular motility driven by assembly and disassembly of actin filaments. *Cell*, *112*(4), 453–465. https://doi.org/10.1016/s0092-8674(03)00120-x

Pollard, T. D., & Cooper, J. A. (2009). Actin, a central player in cell shape and movement. *Science (New York, N.Y.)*, *326*(5957), 1208–1212. https://doi.org/10.1126/science.1175862

Pollard T. D. (2016). Actin and Actin-Binding Proteins. *Cold Spring Harbor perspectives in biology*, *8*(8), a018226. https://doi.org/10.1101/cshperspect.a018226

Prakash, N., & Wurst, W. (2006). Genetic networks controlling the development of midbrain dopaminergic neurons. *The Journal of physiology*, *575*(Pt 2), 403–410. https://doi.org/10.1113/jphysiol.2006.113464

Pring, M., Weber, A., & Bubb, M. R. (1992). Profilin-actin complexes directly elongate actin filaments at the barbed end. *Biochemistry*, *31*(6), 1827–1836. https://doi.org/10.1021/bi00121a035

Purves D, Augustine GJ, Fitzpatrick D, et al., editors. Neuroscience. 2nd edition. Sunderland (MA): Sinauer Associates; 2001. Available from: https://www.ncbi.nlm.nih.gov/books/NBK10799/

Raghunathan, V., Mowery, P., Rozycki, M., Lindberg, U., & Schutt, C. (1992). Structural changes in profilin accompany its binding to phosphatidylinositol, 4,5-bisphosphate. *FEBS letters*, *297*(1-2), 46–50. https://doi.org/10.1016/0014-5793(92)80324-a

Ramming, M., Kins, S., Werner, N., Hermann, A., Betz, H., & Kirsch, J. (2000). Diversity and phylogeny of gephyrin: tissue-specific splice variants, gene structure, and sequence similarities to molybdenum cofactor-synthesizing and cytoskeleton-associated proteins. *Proceedings of the National Academy of Sciences of the United States of America*, *97*(18), 10266–10271. https://doi.org/10.1073/pnas.97.18.10266

Reichstein, E., & Korn, E. D. (1979). Acanthamoeba profilin. A protein of low molecular weight from Acanpthamoeba castellanii that inhibits actin nucleation. *The Journal of biological chemistry*, *254*(13), 6174–6179.

Reinhard, M., Giehl, K., Abel, K., Haffner, C., Jarchau, T., Hoppe, V., Jockusch, B. M., & Walter, U. (1995). The proline-rich focal adhesion and microfilament protein VASP is a ligand for profilins. *The EMBO journal*, *14*(8), 1583–1589.

Risher, W. C., Ustunkaya, T., Singh Alvarado, J., & Eroglu, C. (2014). Rapid Golgi analysis method for efficient and unbiased classification of dendritic spines. *PloS one*, *9*(9), e107591. https://doi.org/10.1371/journal.pone.0107591

Ronald, A., & Hoekstra, R. A. (2011). Autism spectrum disorders and autistic traits: a decade of new twin studies. *American journal of medical genetics. Part B, Neuropsychiatric genetics : the official publication of the International Society of Psychiatric Genetics*, *156B*(3), 255–274. https://doi.org/10.1002/ajmg.b.31159

Rosenmund, C., & Stevens, C. F. (1996). Definition of the readily releasable pool of vesicles at hippocampal synapses. *Neuron*, *16*(6), 1197–1207. https://doi.org/10.1016/s0896-6273(00)80146-4

Rosenmund, C., Stern-Bach, Y., & Stevens, C. F. (1998). The tetrameric structure of a glutamate receptor channel. *Science (New York, N.Y.)*, *280*(5369), 1596–1599. https://doi.org/10.1126/science.280.5369.1596

Roskams, A. J., Cai, X., & Ronnett, G. V. (1998). Expression of neuron-specific beta-III tubulin during olfactory neurogenesis in the embryonic and adult rat. *Neuroscience*, *83*(1), 191–200. https://doi.org/10.1016/s0306-4522(97)00344-8

Roy, S., Watkins, N., & Heck, D. (2012). Comprehensive analysis of ultrasonic vocalizations in a mouse model of fragile X syndrome reveals limited, call type specific deficits. PloS one, 7(9), e44816. https://doi.org/10.1371/journal.pone.0044816

Rubenstein JLR & Merzenich MM (2003). Model of autism: increased ratio of excitation/inhibition in key neural systems. Genes. Brain. Behav. 2: 255–67

Rudelli, R. D., Brown, W. T., Wisniewski, K., Jenkins, E. C., Laure-Kamionowska, M., Connell, F., & Wisniewski, H. M. (1985). Adult fragile X syndrome. Clinico-neuropathologic findings. *Acta neuropathologica*, *67*(3-4), 289–295. https://doi.org/10.1007/bf00687814

Rutter, M., & Schopler, E. (1987). Autism and pervasive developmental disorders: concepts and diagnostic issues. *Journal of autism and developmental disorders*, *17*(2), 159–186. https://doi.org/10.1007/bf01495054

Sankaranarayanan, S., Atluri, P. P., & Ryan, T. A. (2003). Actin has a molecular scaffolding, not propulsive, role in presynaptic function. *Nature neuroscience*, *6*(2), 127–135. https://doi.org/10.1038/nn1002

Scattoni, M. L., Crawley, J., & Ricceri, L. (2009). Ultrasonic vocalizations: a tool for behavioural phenotyping of mouse models of neurodevelopmental disorders. *Neuroscience and biobehavioral reviews*, *33*(4), 508–515. https://doi.org/10.1016/j.neubiorev.2008.08.003

Schlüter, K., Jockusch, B. M., & Rothkegel, M. (1997). Profilins as regulators of actin dynamics. *Biochimica et biophysica acta*, *1359*(2), 97–109. https://doi.org/10.1016/s0167-4889(97)00100-6

Schmeisser MJ, Ey E, Wegener S, Bockmann J, Stempel a V, Kuebler A, Janssen A-L, Udvardi PT, Shiban E, Spilker C, Balschun D, Skryabin B V, Dieck ST, Smalla K-H, Montag D, Leblond CS, Faure P, Torquet N, Le Sourd A-M, Toro R, et al (2012). Autistic-like behaviours and hyperactivity in mice lacking ProSAP1/Shank2. *Nature* 486: 256–60

Schutt, C. E., Lindberg, U., Myslik, J., & Strauss, N. (1989). Molecular packing in profilin: actin crystals and its implications. *Journal of molecular biology*, *209*(4), 735–746. https://doi.org/10.1016/0022-2836(89)90603-7

Schutt, C. E., Myslik, J. C., Rozycki, M. D., Goonesekere, N. C., & Lindberg, U. (1993). The structure of crystalline profilin-beta-actin. *Nature*, *365*(6449), 810–816. https://doi.org/10.1038/365810a0

Scoville, W. B., & Milner, B. (2000). Loss of recent memory after bilateral hippocampal lesions. 1957. *The Journal of neuropsychiatry and clinical neurosciences*, *12*(1), 103–113. https://doi.org/10.1176/jnp.12.1.103

Sept, D., & McCammon, J. A. (2001). Thermodynamics and kinetics of actin filament nucleation. *Biophysical journal*, *81*(2), 667–674. https://doi.org/10.1016/S0006-3495(01)75731-1

Sheng, M., & Hoogenraad, C. C. (2007). The postsynaptic architecture of excitatory synapses: a more quantitative view. *Annual review of biochemistry*, *76*, 823–847. https://doi.org/10.1146/annurev.biochem.76.060805.160029

Shupliakov, O., Bloom, O., Gustafsson, J. S., Kjaerulff, O., Low, P., Tomilin, N., Pieribone, V. A., Greengard, P., & Brodin, L. (2002). Impaired recycling of synaptic vesicles after acute perturbation of the presynaptic actin cytoskeleton. *Proceedings of the National Academy of Sciences of the United States of America*, *99*(22), 14476–14481. https://doi.org/10.1073/pnas.212381799

Silverman JL, Yang M, Lord C, Crawley JN. Behavioural phenotyping assays for mouse models of autism. *Nat Rev Neurosci*. 2010;11(7):490–502. doi:10.1038/nrn2851

Sinkkonen, S. T., Homanics, G. E., & Korpi, E. R. (2003). Mouse models of Angelman syndrome, a neurodevelopmental disorder, display different brain regional GABA(A) receptor alterations. *Neuroscience letters*, *340*(3), 205–208. https://doi.org/10.1016/s0304-3940(03)00123-x

Skare, P., & Karlsson, R. (2002). Evidence for two interaction regions for phosphatidylinositol(4,5)-bisphosphate on mammalian profilin I. *FEBS letters*, *522*(1-3), 119–124. https://doi.org/10.1016/s0014-5793(02)02913-7

Skefos J, Cummings C, Enzer K, Holiday J, Weed K, Levy E, Yuce T, Kemper T & Bauman M (2014). Regional alterations in Purkinje cell density in patients with autism. *PLoS One* 9: 1–12

Somboonwiwat, K., Supungul, P., Rimphanitchayakit, V., Aoki, T., Hirono, I., & Tassanakajon, A. (2006). Differentially expressed genes in hemocytes of Vibrio harveyi-challenged shrimp Penaeus monodon. *Journal of biochemistry and molecular biology*, *39*(1), 26–36. https://doi.org/10.5483/bmbrep.2006.39.1.026

Spruston N. (2008). Pyramidal neurons: dendritic structure and synaptic integration. *Nature reviews. Neuroscience*, *9*(3), 206–221. https://doi.org/10.1038/nrn2286

Su, S. C., & Tsai, L. H. (2011). Cyclin-dependent kinases in brain development and disease. *Annual review of cell and developmental biology*, *27*, 465–491. https://doi.org/10.1146/annurev-cellbio-092910-154023

Südhof T. C. (2008). Neuroligins and neurexins link synaptic function to cognitive disease. *Nature*, *455*(7215), 903–911. https://doi.org/10.1038/nature07456

Südhof, T. C., & Rizo, J. (2011). Synaptic vesicle exocytosis. *Cold Spring Harbor perspectives in biology*, *3*(12), a005637. https://doi.org/10.1101/cshperspect.a005637

Suetsugu, S., Miki, H., & Takenawa, T. (1998). The essential role of profilin in the assembly of actin for microspike formation. *The EMBO journal*, *17*(22), 6516–6526. https://doi.org/10.1093/emboj/17.22.6516

Tabuchi, K., Blundell, J., Etherton, M. R., Hammer, R. E., Liu, X., Powell, C. M., & Südhof, T. C. (2007). A neuroligin-3 mutation implicated in autism increases inhibitory synaptic transmission in mice. *Science (New York, N.Y.)*, *318*(5847), 71–76. https://doi.org/10.1126/science.1146221

Tanaka, M., Sasaki, H., Kino, I., Sugimura, T., & Terada, M. (1992). Genes preferentially expressed in embryo stomach are predominantly expressed in gastric cancer. *Cancer research*, *52*(12), 3372–3377.

Teitelbaum, O., Benton, T., Shah, P. K., Prince, A., Kelly, J. L., & Teitelbaum, P. (2004). Eshkol-Wachman movement notation in diagnosis: the early detection ofAsperger's syndrome. Proceedings of the National Academy of Sciences USA, 101(32), 11909–11914.

Thorn, K. S., Christensen, H. E., Shigeta, R., Huddler, D., Shalaby, L., Lindberg, U., Chua, N. H., & Schutt, C. E. (1997). The crystal structure of a major allergen from plants. *Structure (London, England : 1993)*, *5*(1), 19–32. https://doi.org/10.1016/s0969-2126(97)00163-9

Tilney, L. G., Bonder, E. M., Coluccio, L. M., & Mooseker, M. S. (1983). Actin from Thyone sperm assembles on only one end of an actin filament: a behavior regulated by profilin. *The Journal of cell biology*, *97*(1), 112–124. https://doi.org/10.1083/jcb.97.1.112

Tobacman, L. S., Brenner, S. L., & Korn, E. D. (1983). Effect of Acanthamoeba profilin on the pre-steady state kinetics of actin polymerization and on the concentration of F-actin at steady state. *The Journal of biological chemistry*, *258*(14), 8806–8812.

Towbin, H., Staehelin, T., & Gordon, J. (1992). Electrophoretic transfer of proteins from polyacrylamide gels to nitrocellulose sheets: procedure and some applications. 1979. *Biotechnology (Reading, Mass.)*, *24*, 145–149.

Tronche, F., Kellendonk, C., Kretz, O., Gass, P., Anlag, K., Orban, P. C., Bock, R., Klein, R., & Schütz, G. (1999). Disruption of the glucocorticoid receptor gene in the nervous system results in reduced anxiety. *Nature genetics*, *23*(1), 99–103. https://doi.org/10.1038/12703

Tsai PT, Hull C, Chu Y, Greene-Colozzi E, Sadowski AR, Leech JM, Steinberg J, Crawley JN, Regehr WG & Sahin M (2012) "Autistic-like behaviour and cerebellar dysfunction in Purkinje cell Tsc1 mutant mice." *Nature* 488: 647–51U

Tuchman, R., & Rapin, I. (2002). Epilepsy in autism. *The Lancet. Neurology*, *1*(6), 352–358. https://doi.org/10.1016/s1474-4422(02)00160-6

Valenta, R., Ferreira, F., Grote, M., Swoboda, I., Vrtala, S., Duchêne, M., Deviller, P., Meagher, R. B., McKinney, E., & Heberle-Bors, E. (1993). Identification of profilin as an actin-binding protein in higher plants. *The Journal of biological chemistry*, *268*(30), 22777–22781.

Vanderhaeghen, P., & Cheng, H. J. (2010). Guidance molecules in axon pruning and cell death. *Cold Spring Harbor perspectives in biology*, *2*(6), a001859. https://doi.org/10.1101/cshperspect.a001859

Varghese, M., Keshav, N., Jacot-Descombes, S., Warda, T., Wicinski, B., Dickstein, D. L., Harony-Nicolas, H., De Rubeis, S., Drapeau, E., Buxbaum, J. D., & Hof, P. R. (2017). Autism spectrum disorder: neuropathology and animal models. *Acta neuropathologica*, *134*(4), 537–566. https://doi.org/10.1007/s00401-017-1736-4

Vinson, V. K., Archer, S. J., Lattman, E. E., Pollard, T. D., & Torchia, D. A. (1993). Three-dimensional solution structure of Acanthamoeba profilin-I. *The Journal of cell biology*, *122*(6), 1277–1283. https://doi.org/10.1083/jcb.122.6.1277

Vorstman, J. A., van Daalen, E., Jalali, G. R., Schmidt, E. R., Pasterkamp, R. J., de Jonge, M., Hennekam, E. A., Janson, E., Staal, W. G., van der Zwaag, B., Burbach, J. P., Kahn, R. S., Emanuel, B. S., van Engeland, H., & Ophoff, R. A. (2011). A double hit implicates DIAPH3 as an autism risk gene. *Molecular psychiatry*, *16*(4), 442–451. https://doi.org/10.1038/mp.2010.26

Wang, X., Kibschull, M., Laue, M. M., Lichte, B., Petrasch-Parwez, E., & Kilimann, M. W. (1999). Aczonin, a 550-kD putative scaffolding protein of presynaptic active zones, shares homology regions with Rim and Bassoon and binds profilin. *The Journal of cell biology*, *147*(1), 151–162. https://doi.org/10.1083/jcb.147.1.151

Watanabe, N., Madaule, P., Reid, T., Ishizaki, T., Watanabe, G., Kakizuka, A., Saito, Y., Nakao, K., Jockusch, B. M., & Narumiya, S. (1997). p140mDia, a mammalian homolog of Drosophila diaphanous, is a target protein for Rho small GTPase and is a ligand for profilin. *The EMBO journal*, *16*(11), 3044–3056. https://doi.org/10.1093/emboj/16.11.3044

Watanabe, N., Arai, H., Nishihara, Y., Taniguchi, M., Watanabe, N., Hunter, T., & Osada, H. (2004). M-phase kinases induce phospho-dependent ubiquitination of somatic Wee1 by SCFbeta-TrCP. *Proceedings of the National Academy of Sciences of the United States of America*, *101*(13), 4419–4424. https://doi.org/10.1073/pnas.0307700101

Wei, J. H., Zhang, Z. C., Wynn, R. M., & Seemann, J. (2015). GM130 Regulates Golgi-Derived Spindle Assembly by Activating TPX2 and Capturing Microtubules. *Cell*, *162*(2), 287–299. https://doi.org/10.1016/j.cell.2015.06.014

Wells, N. J., Watanabe, N., Tokusumi, T., Jiang, W., Verdecia, M. A., & Hunter, T. (1999). The C-terminal domain of the Cdc2 inhibitory kinase Myt1 interacts with Cdc2 complexes and is required for inhibition of G(2)/M progression. *Journal of cell science*, *112 (Pt 19)*, 3361–3371.

Wheless, J. W., & Kim, H. L. (2002). Adolescent seizures and epilepsy syndromes. *Epilepsia*, *43 Suppl 3*, 33–52. https://doi.org/10.1046/j.1528-1157.43.s.3.12.x

Whiting P. J. (1999). The GABA-A receptor gene family: new targets for therapeutic intervention. *Neurochemistry international*, *34*(5), 387–390. https://doi.org/10.1016/s0197-0186(99)00048-0

Whittaker V. P. (1993). Thirty years of synaptosome research. *Journal of neurocytology*, *22*(9), 735–742. https://doi.org/10.1007/bf01181319

Wilkes, D. E., & Otto, J. J. (2000). Molecular cloning of profilin from Tetrahymena thermophila. *Gene*, *246*(1-2), 295–301. https://doi.org/10.1016/s0378-1119(00)00097-4

Wilkes, D. E., & Otto, J. J. (2003). Profilin functions in cytokinesis, nuclear positioning, and stomatogenesis in Tetrahymena thermophila. *The Journal of eukaryotic microbiology*, *50*(4), 252–262. https://doi.org/10.1111/j.1550-7408.2003.tb00130.x

Winder, S. J., & Ayscough, K. R. (2005). Actin-binding proteins. *Journal of cell science*, *118*(Pt 4), 651–654. https://doi.org/10.1242/jcs.01670

Witke, W., Podtelejnikov, A. V., Di Nardo, A., Sutherland, J. D., Gurniak, C. B., Dotti, C., & Mann, M. (1998). In mouse brain profilin I and profilin II associate with regulators of the endocytic pathway and actin assembly. *The EMBO journal*, *17*(4), 967–976. https://doi.org/10.1093/emboj/17.4.967

Witke, W., Sutherland, J. D., Sharpe, A., Arai, M., & Kwiatkowski, D. J. (2001). Profilin I is essential for cell survival and cell division in early mouse development. *Proceedings of the National Academy of Sciences of the United States of America*, *98*(7), 3832–3836. https://doi.org/10.1073/pnas.051515498

Witke W. (2004). The role of profilin complexes in cell motility and other cellular processes. *Trends in cell biology*, *14*(8), 461–469. https://doi.org/10.1016/j.tcb.2004.07.003

Witte, H., & Bradke, F. (2008). The role of the cytoskeleton during neuronal polarization. *Current opinion in neurobiology*, *18*(5), 479–487. https://doi.org/10.1016/j.conb.2008.09.019

Wolven, A. K., Belmont, L. D., Mahoney, N. M., Almo, S. C., & Drubin, D. G. (2000). In vivo importance of actin nucleotide exchange catalyzed by profilin. *The Journal of cell biology*, *150*(4), 895–904. https://doi.org/10.1083/jcb.150.4.895

Woodhead, G. J., Mutch, C. A., Olson, E. C., & Chenn, A. (2006). Cell-autonomous beta-catenin signaling regulates cortical precursor proliferation. *The Journal of neuroscience : the official journal of the Society for Neuroscience*, *26*(48), 12620–12630. https://doi.org/10.1523/JNEUROSCI.3180-06.2006

Xue, R., Lei, S., Xia, Z. Y., Wu, Y., Meng, Q., Zhan, L., Su, W., Liu, H., Xu, J., Liu, Z., Zhou, B., & Xia, Z. (2016). Selective inhibition of PTEN preserves ischaemic post-conditioning cardioprotection in STZ-induced Type 1 diabetic rats: role of the PI3K/Akt and JAK2/STAT3 pathways. *Clinical science (London, England : 1979)*, *130*(5), 377–392. https://doi.org/10.1042/CS20150496

Yano, H., Ninan, I., Zhang, H., Milner, T. A., Arancio, O., & Chao, M. V. (2006). BDNF-mediated neurotransmission relies upon a myosin VI motor complex. *Nature neuroscience*, *9*(8), 1009–1018. https://doi.org/10.1038/nn1730

Young, D. M., Schenk, A. K., Yang, S. B., Jan, Y. N., & Jan, L. Y. (2010). Altered ultrasonic vocalizations in a tuberous sclerosis mouse model of autism. *Proceedings of the National Academy of Sciences of the United States of America*, *107*(24), 11074–11079. https://doi.org/10.1073/pnas.1005620107

Zerbo, O., Iosif, A. M., Walker, C., Ozonoff, S., Hansen, R. L., & Hertz-Picciotto, I. (2013). Is maternal influenza or fever during pregnancy associated with autism or developmental delays? Results from the CHARGE (CHildhood Autism Risks from Genetics and Environment) study. *Journal of autism and developmental disorders*, *43*(1), 25–33. https://doi.org/10.1007/s10803-012-1540-x

Zhong, L., & Gerges, N. Z. (2012). Neurogranin targets calmodulin and lowers the threshold for the induction of long-term potentiation. *PloS one*, *7*(7), e41275. https://doi.org/10.1371/journal.pone.0041275

Zimmerman, L., Parr, B., Lendahl, U., Cunningham, M., McKay, R., Gavin, B., Mann, J., Vassileva, G., & McMahon, A. (1994). Independent regulatory elements in the nestin gene direct transgene expression to neural stem cells or muscle precursors. *Neuron*, *12*(1), 11–24. https://doi.org/10.1016/0896-6273(94)90148-1

Zoidakis, J., Makridakis, M., Zerefos, P. G., Bitsika, V., Esteban, S., Frantzi, M., Stravodimos, K., Anagnou, N. P., Roubelakis, M. G., Sanchez-Carbayo, M., & Vlahou, A. (2012). Profilin 1 is a potential biomarker for bladder cancer aggressiveness. *Molecular & cellular proteomics : MCP*, *11*(4), M111.009449. https://doi.org/10.1074/mcp.M111.009449

Zou, L., Jaramillo, M., Whaley, D., Wells, A., Panchapakesa, V., Das, T., & Roy, P. (2007). Profilin-1 is a negative regulator of mammary carcinoma aggressiveness. *British journal of cancer*, *97*(10), 1361–1371. https://doi.org/10.1038/sj.bjc.6604038

Appendix

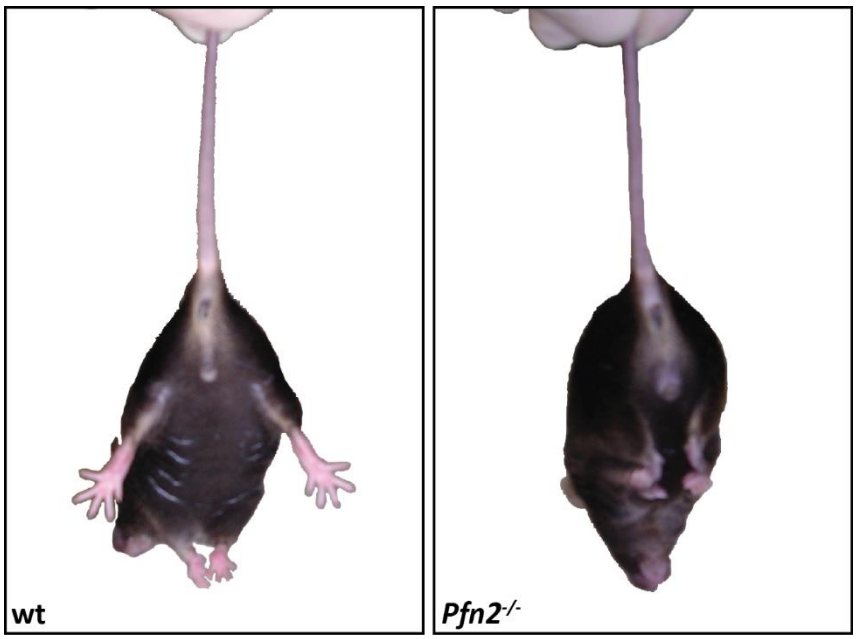

Supplementary figure 7.1 **| *Pfn2*$^{-/-}$ mice show hind legs clasping.** *Pfn2*$^{-/-}$ mice show from very early age (P10) the characteristic coordination deficit of clamping their hind legs when picked up by the tail instead of spreading them out.

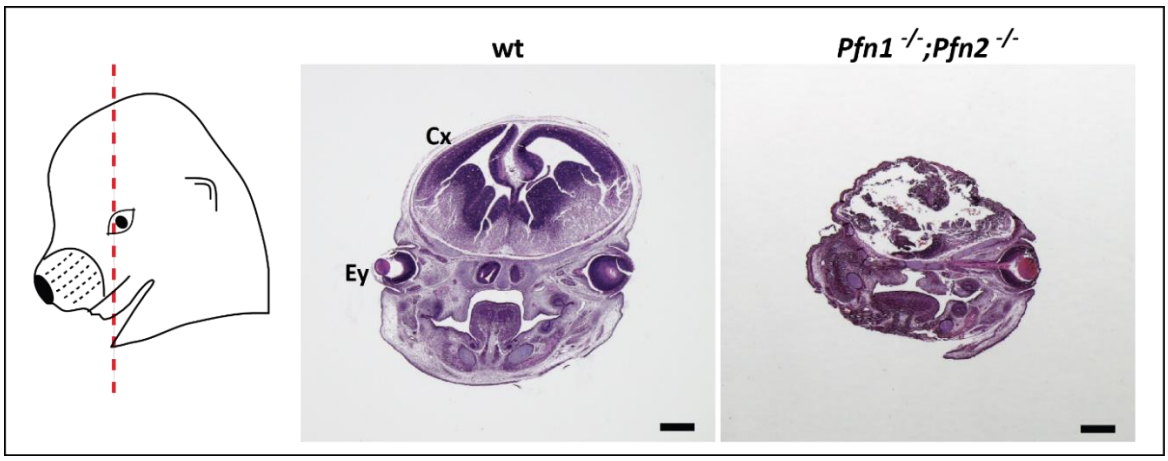

Supplementary figure 7.2 **| Coronal sections of E14.5 wt and *Pfn1*$^{-/-}$*;Pfn2*$^{-/-}$ (*Pfn1-flx;Nes-Cre*) embryo heads stained with H&E.** On the left, it is shown the schematic position of the section plane used for the comparison between the genotypes. On the right, H&E stained sections are shown. *Pfn1*$^{-/-}$*;Pfn2*$^{-/-}$ embryos showed severe morphological malformation, none of the different brain regions was precisely recognizable. In the wt image different brain regions are indicated: Cx, cortex; Ey, eye. Scale bar: 1mm.

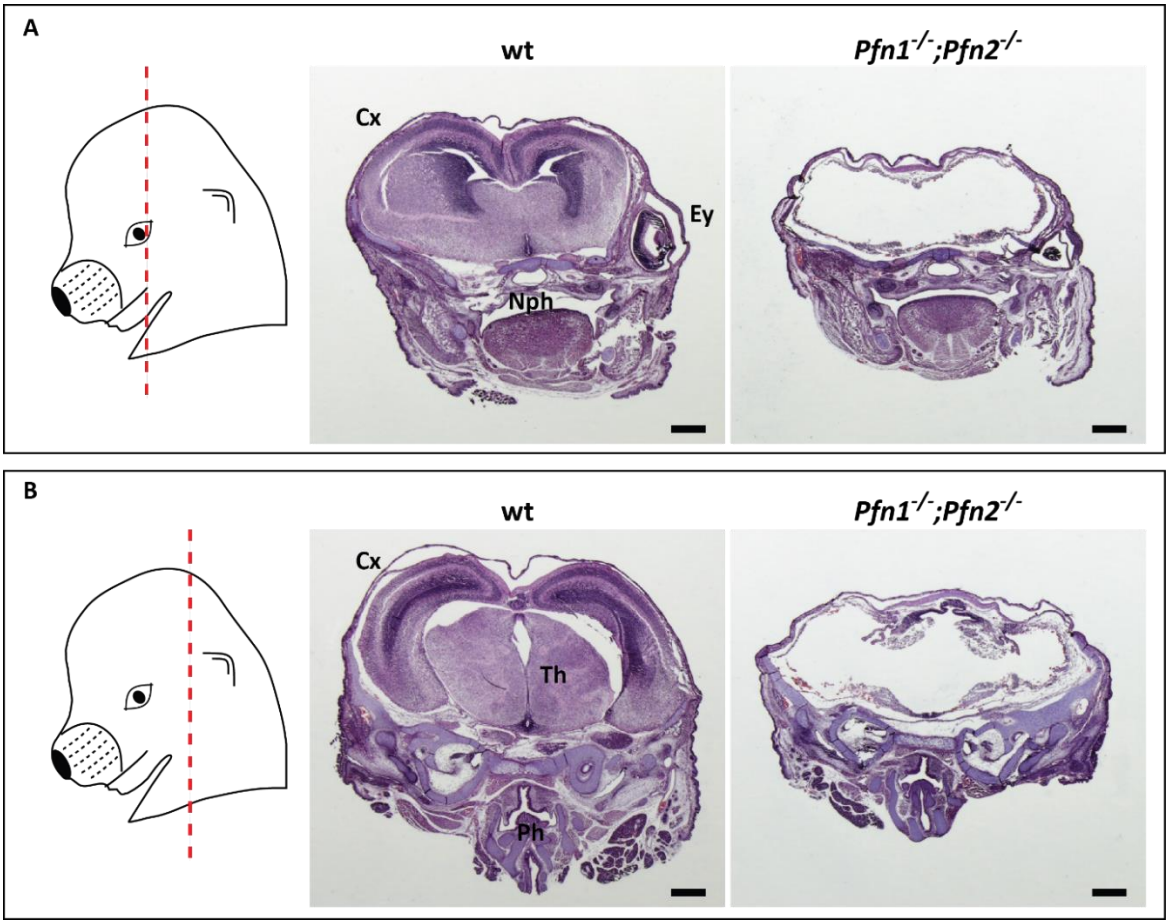

Supplementary figure 7.3 **| Coronal sections of E16.5 wt and *Pfn1*$^{-/-}$;*Pfn2*$^{-/-}$ (*Pfn1-flx;Nes-Cre*) embryo heads stained with H&E. A.** On the left, it is shown the schematic position of the more anterior section plane used for the comparison. On the right, H&E stained control and *Pfn* double ko sections are shown. **B.** On the left, it is shown the schematic position of the more posterior section plane used for the comparison. On the right, H&E stained control and *Pfn* double ko sections are shown. *Pfn1*$^{-/-}$;*Pfn2*$^{-/-}$ embryos showed severe morphological malformation, all brain structures were completely lost. In the wt image different brain regions are indicated: Cx, cortex; Ey, eye; Nph, nasopharynx; Th, thalamus; Ph, pharynx. Scale bar: 1mm.

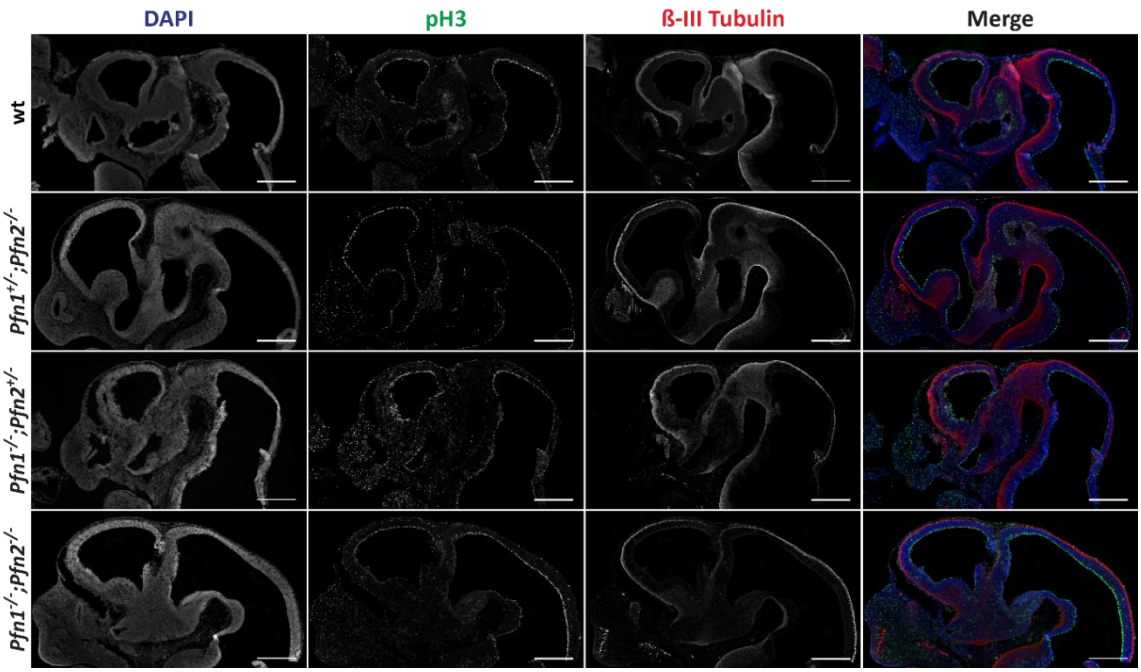

Supplementary figure 7.4 **| Overview of the radial glia and neuronal populations in the forebrain-midbrain region of E11.5 embryos.** pH3 (RG) and β-III tubulin (neurons) immunofluorescence staining on matched cryo-sections from wt, *Pfn1*$^{+/-}$*;Pfn2*$^{-/-}$, *Pfn1*$^{-/-}$*;Pfn2*$^{+/-}$ and *Pfn1*$^{-/-}$*;Pfn2*$^{-/-}$ (*Pfn1-flx;Nes-Cre*) embryos. In the merge picture: in blue is shown the DAPI staining, in green pH3 and in red ß-III Tubulin. Scale bar: 100 µm.

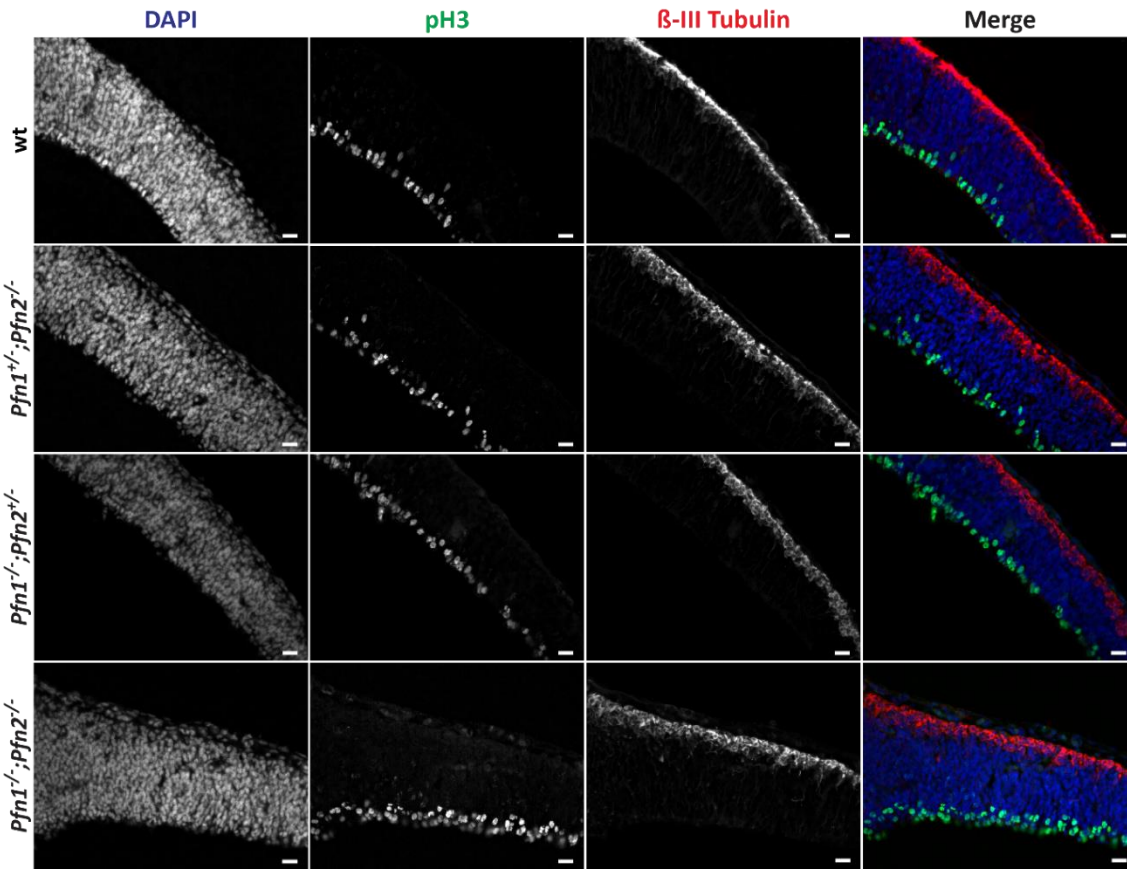

Supplementary figure 7.5 **| Altered VZ organization in the midbrain of *Pfn1*$^{-/-}$;*Pfn2*$^{-/-}$ (*Pfn1-flx;Nes-Cre*) E11.5 embryos.** Immunofluorescence staining on matched cryo-sections from wt, *Pfn1*$^{+/-}$;*Pfn2*$^{-/-}$, *Pfn1*$^{-/-}$;*Pfn2*$^{+/-}$ and *Pfn1*$^{-/-}$;*Pfn2*$^{-/-}$ red ß-III Tubulin. The VZ of wt and *Pfn1*$^{+/-}$;*Pfn2*$^{-/-}$ embryos is composed by a layer of pH3+ cells linearly organized. Contrarily, in the VZ of *Pfn1*$^{-/-}$;*Pfn2*$^{+/-}$ and *Pfn1*$^{-/-}$;*Pfn2*$^{-/-}$ embryos, where PFN1 is not expressed, pH3+ cells misalignment is observed. Scale bar: 20 µm.

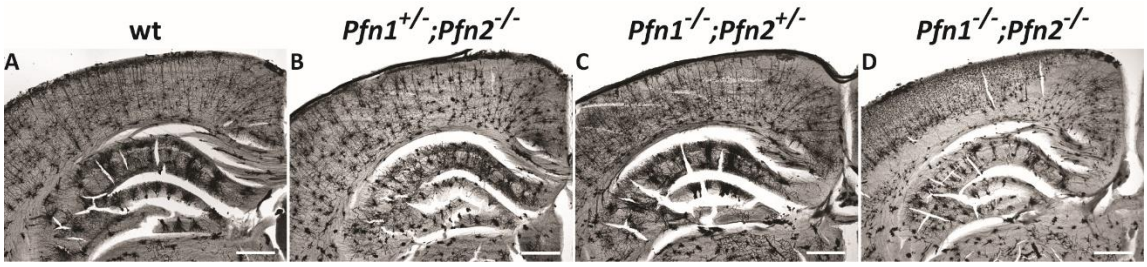

Supplementary figure 7.6 **| Altered cortical and hippocampal organization in P80-P90 *Pfn1*$^{-/-}$;*Pfn2*$^{-/-}$ (*Pfn1-flx;Camk2a-Cre*) mice.** Sample overview images of the cortico-hippocampal region in matched coronal slices from Golgi-stained brains of P80-P90 wt, *Pfn1*$^{+/-}$;*Pfn2*$^{-/-}$, *Pfn1*$^{-/-}$;*Pfn2*$^{+/-}$ and *Pfn1*$^{-/-}$;*Pfn2*$^{-/-}$ mice. Cortical and CA1 hippocampal regions are heavily altered in their organization in *Pfn1*$^{-/-}$; *Pfn2*$^{-/-}$ mice (**D**). Pfn*1*$^{+/-}$;*Pfn2*$^{-/-}$ mice also show a certain degree of impairment, with reduced neuronal density and simplified dendritic arborizations (**B**). *Pfn1*$^{-/-}$;*Pfn2*$^{+/-}$ mice (**C**) show a cortical and hippocampal organization similar to the wt condition (**A**). Scale bar: 500 µm.

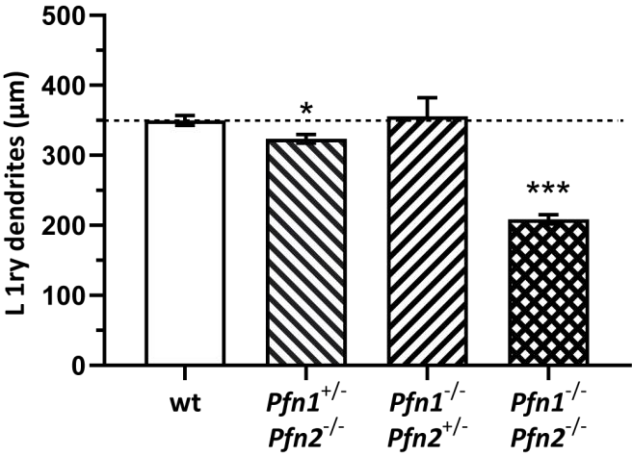

Supplementary figure 7.7 **| Layer V cortical pyramidal neurons of *Pfn1*$^{-/-}$;*Pfn2*$^{-/-}$ (*Pfn1-flx;Camk2a-Cre*) mice displayed reduced length of apical 1ry dendritic branches.** Bar graph representing the average length (L) of 1ry apical dendrites of layer V cortical neurons in control and profilin mutant mice. The length of 1ry apical dendritic branches was halved in *Pfn1*$^{-/-}$;*Pfn2*$^{-/-}$ double ko mice (P<0.001); a modest reduction in length was also observed in *Pfn1*$^{+/-}$;*Pfn2*$^{-/-}$ mice (P=0.041), bearing only one *Pfn1* allele. The dotted line indicates the wt level. n=2 mice per genotype and a total of 60 cells per genotype were analyzed. Error bars represent s.e.m. One-way ANOVA - Dunnett's test, *P≤0.05, ***P≤0.001**.**

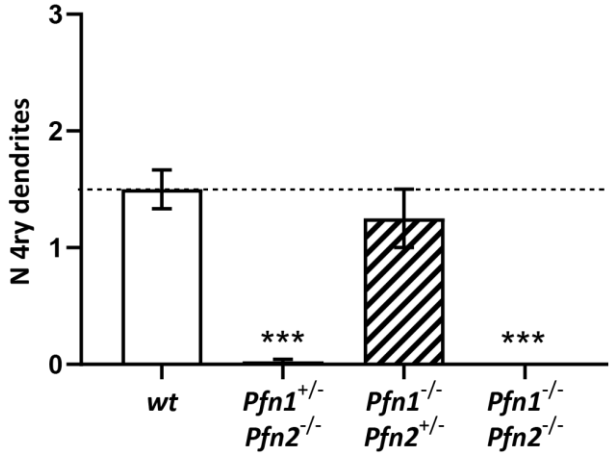

Supplementary figure 7.8 **| Layer V cortical pyramidal neurons of *Pfn1*$^{-/-}$;*Pfn2*$^{-/-}$ (*Pfn1-flx;Camk2a-Cre*) mice displayed no apical 4ry dendritic branches.** Bar graph representing the average number (N) of 4ry apical dendritic branches of layer V cortical neurons of control and profilin mutant mice. The dotted line indicates the wt level. A strong reduction of complexity was observed in *Pfn1*$^{-/-}$;*Pfn2*$^{-/-}$ mice, indeed no 4ry apical branch was observed. A surprisingly similar impairment was also observed in *Pfn1*$^{+/-}$;*Pfn2*$^{-/-}$ mice, bearing only one *Pfn1* allele. n=2 mice per genotype and a total of 60 cells per genotype were analyzed. Error bars represent s.e.m. One-way ANOVA - Dunnett's test, ***P≤0.001**.**

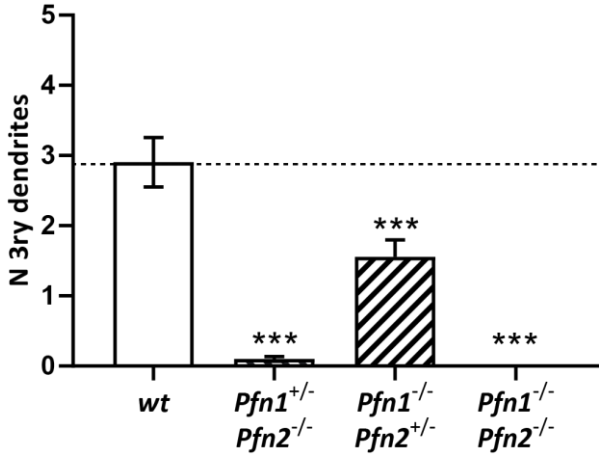

Supplementary figure 7.9 **| Layer V cortical pyramidal neurons of *Pfn1*$^{-/-}$;*Pfn2*$^{-/-}$ (*Pfn1-flx;Camk2a-Cre*) mice displayed no basal 3ry dendritic branches.** Bar graph representing the average number (N) of basal 3ry dendritic branches in layer V cortical neurons of control and profilin mutant mice. The dotted line indicates the wt level. In *Pfn1*$^{-/-}$;*Pfn2*$^{-/-}$ mice no basal 3ry branch was observed. A surprisingly similar impairment was also observed in *Pfn1*$^{+/-}$;*Pfn2*$^{-/-}$ mice, bearing only one *Pfn1* allele. A significant reduction was also observed in *Pfn1*$^{-/-}$;*Pfn2*$^{+/-}$ mice, bearing only one *Pfn2* allele. n=2 mice per genotype and a total of 60 cells per genotype were analyzed. Error bars represent s.e.m. One-way ANOVA - Dunnett's test, ***P≤0.001**.**

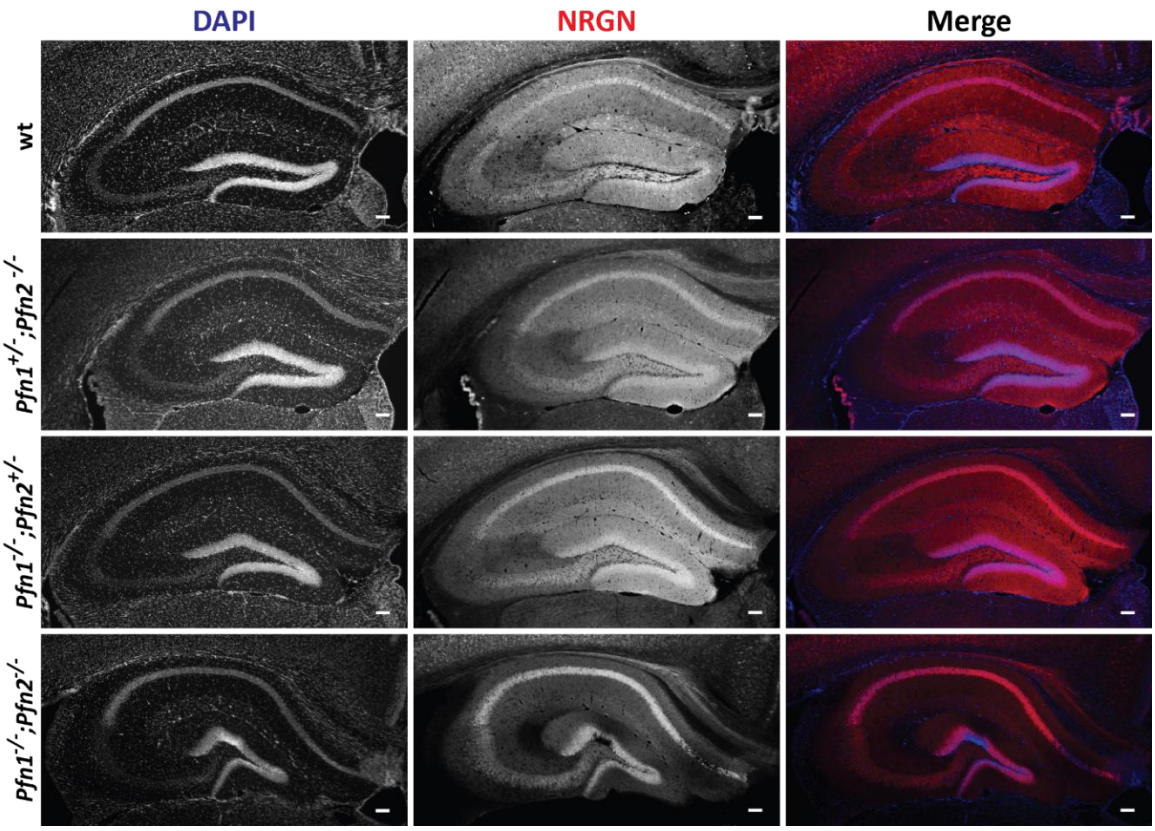

Supplementary figure 7.10 **| Overview images of the hippocampus in immunofluorescence stainings against neurogranin on P80-P90 *Pfn* mutants.** Immunofluorescence staining of NRGN (red) on coronal brain slices from wt, *Pfn1*$^{+/-}$;*Pfn2*$^{-/-}$, *Pfn1*$^{-/-}$;*Pfn2*$^{+/-}$ and *Pfn1*$^{-/-}$;*Pfn2*$^{-/-}$ (*Pfn1-flx;Camk2a-Cre*) P80-P90 mice. Nuclei are stained with DAPI (blue). Scale bar: 40 µm.

Acknowledgments

I would like to thank my supervisor Prof. Dr. Walter Witke for giving me the opportunity start my PhD thesis in his lab, for trusting me and for his professional and personal support during these years.

I am really thankful to Prof. Dr. Valentin Stein for supporting and helping me with the electrophysiological studies and for the important training and knowledge acquired and received in his lab.

Moreover, I would like to thank Dr. Pietro Pilo Boyl, for his suggestions and for his guide during my studies and also for the critical discussions.

The nice friendly atmosphere in the AG Stein and the intense professional atmosphere was really fruitful for my spirit and my mind. I want to say thanks to the AG Witke for the helpful atmosphere of the lab and for always being ready to discuss experiments. Thanks to Gerda and Melly for their professional support. Thanks to Melly and Ilkin for their friendship, and also to Michael, Stefanie and Carina for our parties, funny moments and girl-nights!

Questa tesi è il frutto non solo di un lavoro di ricerca, ma è soprattutto il risultato di un percorso di crescita personale che mi ha permesso di essere più "resistente agli urti" e mi ha reso finalmente consapevole di me stessa e delle mie potenzialità.

Un caro ringraziamento va agli Ammappen, la mia "seconda famiglia di Bonn", vi ringrazio per le serate in compagnia e per le risate e per aver reso questo posto una casa lontana da casa per tutti noi. Ringrazio Giulia ed Eli per le nostre chiacchierate che mi hanno permesso spesso di sfogarmi, di sopravvivere alla lontananza da casa e di conoscervi.
Un ringraziamento all'amico Peppe per avermi pazientemente salvato ogni volta che con il mio pc combinavo un disastro!

Ringrazio mia Madre per non avermi fatto pesare la lontananza, quando aveva più bisogno di me. La ringrazio per il suo affetto e per aver trovato il modo di venirmi incontro, anche se siamo distanti per carattere. Ti voglio bene e ti ringrazio per permettere di comprenderci e di starci vicino.
Ringrazio mio Fratello, perché anche se entrambi parliamo poco ha sempre fatto ciò che mi aspettassi da un fratello, cioè farmi sentire accolta. Ringrazio la sua famiglia (Cate, Alessia ed ora il piccolo Lorenzo) per aver trascorso insieme dei momenti di gioia (tra cucina e risate) a casa loro. Ringrazio la mia piccola kartoffelina Alessia per le giornate di gioco fino allo sfinimento.

Ringrazio le mie Sorelle, per essere state vicino a mia a madre e per avermi in questo modo permesso di poter lavorare lontano da casa. Le ringrazio perché anche se, ognuna in modo diverso e su cose diverse sono delle gran testarde, hanno un unico grande cuore buono.

Per ultimo non per importanza, voglio ringraziare colui che nel tempo è diventato mio marito ed il compagno di questa mia vita. Claudio, grazie per avermi sopportato quando mi lamentavo, grazie per avermi aiutato a smettere di lamentarmi. Ma soprattutto grazie per avermi continuamente spronato a combattere per me stessa ed a credere in me stessa. Ti ringrazio e ti ricambio per l'amore che ogni giorno mi rinnovi e che mi offri in maniera incondizionata. Grazie per essere Tu la mia Casa.

SCIENTIFIC PUBLICATION

- L. Speranza, A. Chambery, M. Di Domenico, M. Crispino, V. Severino, F. Volpicelli, M. Leopoldo, G.C. Bellenchi, U. di Porzio, C. Perrone-Capano. The serotonin receptor 7 promotes neurite outgrowth via ERK and Cdk5 signaling pathways. Neuropharmacol. 67, 155-167 (2013).